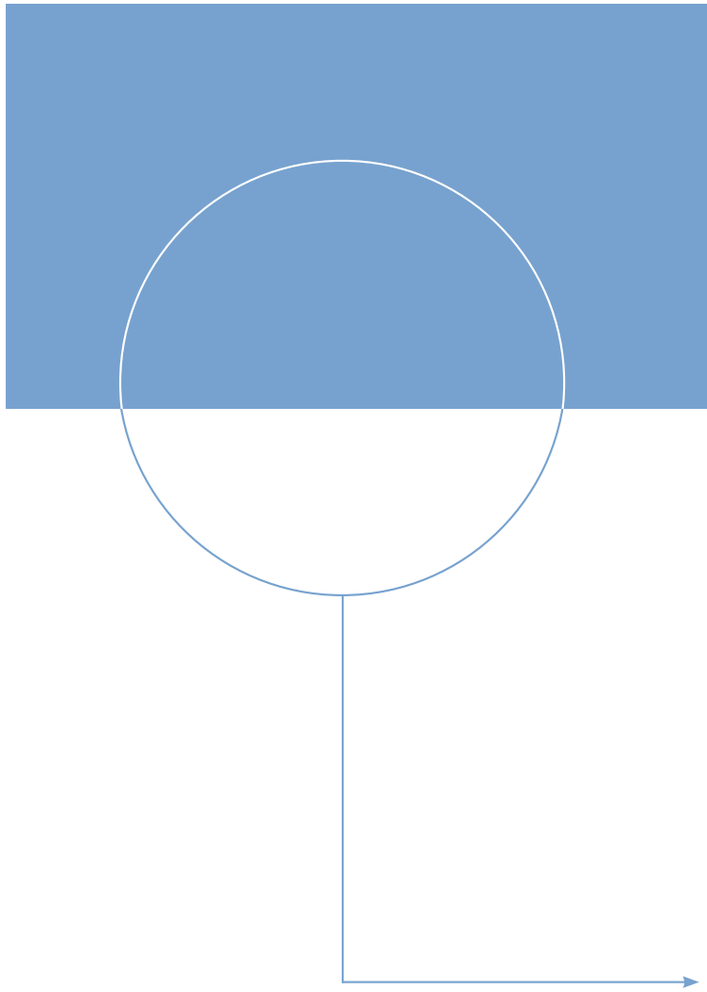

Master's thesis

2021

Thomas Christiansen

NTNU
Norwegian University of
Science and Technology
Faculty of Information Technology and Electrical
Engineering
Department of Mathematical Sciences

Thomas Christiansen

Traveling Wave Solutions for the Hunter-Saxton Equation

June 2021

NTNU
Norwegian University of
Science and Technology

NTNU
Norwegian University of
Science and Technology

NTNU

Norwegian University of
Science and Technology

Traveling Wave Solutions for the Hunter-Saxton Equation

Thomas Christiansen

Master of Science in: Applied Physics and Mathematics
Submission date: June 2021
Supervisor: Helge Holden, IMF
Co-supervisor: Katrin Grunert, IMF
Susanne Solem, NMBU

Norwegian University of Science and Technology
Department of Mathematical Sciences

Abstract

In this thesis we study traveling wave solutions of the Hunter-Saxton equation. We employ a gluing formalism which allows us to glue together two local, classical traveling wave solutions along a curve in order to produce a weak composite traveling wave in a larger region, provided certain requirements are met. Using these requirements we are able to classify all possible weak traveling waves. Of particular interest are cuspons and stumpons. For the Hunter-Saxton equation these tend asymptotically to $\pm\infty$. Then we augment the Hunter-Saxton equation by an energy equation, in order to derive additional conditions that need to be satisfied by weak, conservative traveling waves. In particular this severely limits the possible waves, and we are only left with cuspons as candidates for nontrivial weak, conservative traveling waves. We analyze cuspons in greater detail, and derive a system of ODEs which needs to be satisfied when following the solutions along characteristics. This is used to give a formal physical explanation to why none of the other weak traveling waves are conservative.

Moreover we present an already existing algorithm for approximating conservative solutions to the integrated formulation of Hunter-Saxton equation, and we point out why the current formulation of this algorithm is inadequate in the setting of conservative traveling waves. To overcome the met obstacles, we introduce a modified algorithm, which is based on the differentiated formulation of the Hunter-Saxton equation rather than the integrated one. As a result we obtain more flexibility in the mesh construction, and we adapt a moving mesh in order to simulate conservative traveling waves. Then we show by a few examples how the newly introduced algorithm perform. Finally we give a plausible explanation to the cause of the observed discrepancies between the numerical approximation and the true solution.

Sammendrag

I denne oppgaven studerer vi vandrende bølgeløsninger til Hunter-Saxton likningen. Vi benytter en lime-formalisme som lar oss lime sammen to klassiske vandrende løsninger langs en kurve. Dette lar oss konstruere svake sammensatte vandrende bølger, som er gyldige i et større område så lenge visse kriterier er oppfylt. Ved å bruke disse betingelsene er vi i stand til å klassifisere alle mulige svake vandrende bølger. Blant disse er "cuspons" og "stumpons" av spesiell interesse. Disse går asymptotisk til $\pm\infty$. Videre legger vi til en ekstra energilikning, som benyttes for å utlede ekstra betingelser som må være oppfylt for svake konservative vandrende bølger. Det viser seg at disse betingelsene utelukker mesteparten av de svake løsningene, bortsett fra "cuspons". Videre studerer vi "cuspons" i mer detalj, og utleder et ODE-system som må være tilfredsstilt for løsninger langs karakteristikker. Dette systemet anvendes så til å gi en formell fysisk forklaring på hvorfor ingen av de andre svake bølgene klassifiseres som konservative.

Videre i oppgaven presenterer vi en allerede eksisterende algoritme, som kan brukes til å approksimere konservative løsninger til den integrerte Hunter-Saxton likningen. Vi poengterer hvorfor den nåværende formuleringen av denne algoritmen er utilpass for å simulere konservative vandrende bølger. For å håndtere dette introduserer vi en modifisert algoritme, som istedenfor er basert på den differensierte formuleringen av Hunter-Saxton likningen. Dette fører til at vi får mer fleksibilitet når vi skal konstruere en numerisk grid. Vi benytter en grid som beveger seg for å være i bedre stand til å simulerer konservative vandrende bølger. Deretter tester vi ut algoritmen på noen eksempler. Vi gir en mulig formell forklaring på hvorfor vi observerer avvik mellom den numeriske approksimasjonen og den faktiske løsningen for konservative vandrende bølger.

Preface

This thesis is the conclusion of my master's degree in Industrial Mathematics within the Applied Physics and Mathematics study programme at the Norwegian University of Science and Technology (NTNU). In the thesis I have used much of the knowledge acquired during the course of my degree, especially knowledge about hyperbolic conservation laws and numerical theory concerned about numerical solutions of partial differential equations. I have also learned much about mathematical topics I knew little or nothing about prior to this thesis; e.g. completely integrable partial differential equations and Radon measures to mention a few.

The thesis is slightly divided into three parts, the first part is about the underlying physics of the equation studied, and was motivated by the desire to use some of the physics I got acquainted with during my degree. The second part is more analytical in nature, and concerns the analysis of traveling waves for the Hunter-Saxton equation. The final part is devoted to numerics, and in particular how to simulate such traveling waves. This division also reflect well upon the diversity of courses I have taken during my degree.

I will like to thank my main supervisor Helge Holden for teaching me a lot about analysis of partial differential equations and introducing me to the wonderful world of hyperbolic conservation laws which is a topic I have become very fond of. I also would like to thank my co-supervisor Susanne Solem for valuable discussions and valuable suggestions during my thesis. Finally I would like to give a very special thanks to my co-supervisor Katrin Grunert for excellent supervision and proofreading. Without her help numerous more mistakes would have been present in this thesis. Her support of my work this semester has been invaluable.

Thomas Christiansen
Trondheim
June 2021

Contents

1 Introduction

The Hunter-Saxton equation commonly appear in the literature on the form

$$u_t + uu_x = \frac{1}{4}\Big(\int_{-\infty}^{x} u_x^2 \, dx - \int_{x}^{\infty} u_x^2 \, dx \Big),$$

also referred to as the integrated Hunter-Saxton equation. The Hunter-Saxton equation was introduced by Hunter and Saxton in [HS91] as an asymptotic model describing wave propagation in nematic liquid crystals. In that context $u = u(x,t)$ is a suitable scaled perturbation of the director field from a constant equilibrium angle, while x is a spatial variable in a reference frame moving with a linearized velocity, while t is a slow time variable.

The equation has been subject to much research, due to some of its remarkable properties. We do not try to give an exhaustive literature review here, rather just a brief presentation of some of the papers used in the development of this thesis. In [HZ94] it was shown by Hunter and Zheng that the equation is bi-variational, bi-hamiltonian, completely integrable, and that classical solutions satisfy an infinite number of conservation laws. It was shown already in the paper [HS91] that classical solutions cease to exist, due to the phenomenon of wave breaking, and that weak solutions are not unique. In the paper [HZ95] by Hunter and Zheng the notions of conservative and dissipative solutions were introduced. These are two natural classes of more restrictive weak solutions. Well-posedness of the Cauchy problem to the Hunter-Saxton equation in the case of dissipative and conservative solutions has been discussed in numerous articles. Zhang and Zheng established in [ZZ00] global existence and uniqueness of dissipative and conservative solutions on $(0,\infty) \times (0,\infty)$ for the case of compactly supported initial data $u_{0,x}$ in $L^2(\mathbb{R})$. Here they employed Young measures and mollification techniques. Bressan and Constantin gave in [BC05] an alternative proof for dissipative solutions which extended the result obtained by Zhang and Zheng, to global existence of dissipative solutions without the assumption about compactly supported initial data. Moreover they also constructed a continuous semigroup of weak, dissipative solutions and derived an explicit representation formula for dissipative solutions. Furthermore in [BC05] a new distance functional was introduced, which renders the semigroup Lipschitz continuous, and hence establishes uniqueness and continuous dependence on initial data for the Cauchy problem. Dafermos gave a new short proof of uniqueness of dissipative solutions to the Cauchy problem using the generalized method of characteristics in [Daf11]. A Lipshitz continuous semigroup for weak, conservative solutions was constructed by Bressan et al. in [BHR10]. In [GHR15] Grunert et al. introduced the notion of α-dissipative solutions for the two component Camassa-Holm equation, acting as a continuous interpolation between conservative and dissipative solutions. This notion was later considered by Grunert and Nordli in [GN18] for the two-component Hunter-Saxton equation, which is a generalization of the Hunter-Saxton equation.

Bressan and Constantin introduced in [BC05] a transformation of variables that transformed the Hunter-Saxton equation into a system of linear ordinary differential equations taking values in a Banach space, where singularities which form upon wave breaking were removed. A related but much more complicated transformation of variables can be performed for the Camassa-Holm equation, this has been done by Holden and Raynaud in [HR07]. Bressan et al. introduced in [BHR10] a Lipschitz metric for measuring the difference between conservative solutions of the Hunter-Saxton equation. The distance introduced has at most an exponential growth in time. Carillo et al. introduced a new metric in [CGH19], where they could bound the difference between two conservative solution by a quadratic bound in time. The Euler-Lagrange formalism discussed in these aforementioned papers will be used here in this thesis. In this thesis the main concern is not about well-posedness, but rather about traveling wave solutions of the Hunter-Saxton equation.

1.1 Objective

The main objectives of this thesis have been three-folded:

- Find all weak traveling wave solutions of the Hunter-Saxton equation.
- Find all weak, conservative traveling wave solutions of the Hunter-Saxton equation.
- Find/modify a numerical method to visualize the traveling wave solutions of the Hunter-Saxton equation.

In particular the gluing formalism introduced by Reigstad and Grunert in [GR20] has been central for studying the first two objectives. The algorithm introduced by Grunert et al. in [GNS21] has been central when concerned about the final objective. The algorithm has been modified, and adapted to a moving reference frame in order to simulate conservative traveling wave solutions of the Hunter-Saxton equation.

1.2 Main results

The main results in this thesis can be shortly summarized as follows:

- There exist no bounded weak traveling waves, except from the trivial wave. It is shown that one can glue together two local, classical traveling waves to construct cuspons and other kinds of waves. This is provided that for the resulting composite traveling wave the derivative becomes unbounded at the gluing point, and the derivative is monotone on either side of the gluing point. The composite weak wave, u, becomes asymptotically unbounded. A maximum of two gluing points is possible, which allows for the construction of stumpons.
- The only possible weak, conservative traveling waves are cuspons and the trivial wave.
- For cuspons wave breaking occurs at the cusp singularity for every time. Moreover the cusp singularity jumps metaphorically speaking from characteristic to characteristic. At every time, t, wave breaking occurs at a single point in Eulerian and Lagrangian coordinates.

For precise statements about these results, the reader is referred to Theorem 4.1 and Theorem 5.1 for the two first statements, and Lemma 5.2 and Lemma 5.4 for the final statement. Notice that we have only shown that wave breaking occurring at $t = 0$ happens at a single point in Lagrangian coordinates, but the result can be extended. Moreover a modified algorithm for simulating conservative traveling waves of the Hunter-Saxton equation is introduced in Chapter 7. The algorithm relies on a moving reference frame, i.e., moving grid points, and one must handle fictitious boundary conditions that arise. For details the reader is referred to Subsection 7.3.

1.3 Outline of thesis

The Hunter-Saxton Equation was derived as an asymptotic model for nematic liquid crystals, where one neglect viscous effects, compared to inertia. This is reflected upon in Chapter 2 of this thesis, where we outline the classical Oseen-Frank static theory, and the Ericksen-Leslie continuum description of Liquid crystals, before we introduce some assumptions leading to the nonlinear variational wave equation. Then we perform an asymptotic expansion to derive the Hunter-Saxton equation.
In the next chapter, Chapter 3, typical properties of the Hunter-Saxton equation are discussed. An example illustrating the difference between conservative and dissipative solutions is considered. Various notions of solutions are introduced, and in particular that of conservative and dissipative solutions. The Euler-Lagrange formalism is presented.
In Chapter 4 we first consider classical traveling waves for the Hunter-Saxton equation. Then we introduce the gluing formalism, which we use to derive conditions that need to be satisfied for weak traveling waves of the Hunter-Saxton equation. We exhaust all possible weak traveling waves satisfying the imposed conditions. In particular this leads to one of the main statements of this thesis. The various possible weak traveling waves are sketched.

Chapter 5 takes the idea in Chapter 4 one step further, and considers what additional requirements that are imposed on conservative traveling waves to the Hunter-Saxton equation. Here we apply the gluing formalism to an energy equation. We combine the conditions derived for the energy equation with those derived for the Hunter-Saxton equation. This leads to the second main statement of the thesis. Furthermore we consider how the cusp singularity for cuspons evolves as time progresses. Moreover we show that wave breaking occurs at all times, and the point where wave breaking occurs jumps from characteristic to characteristic as time evolves.
Chapter 6 is devoted to numerics and in particular the introduction of an already existing numerical algorithm for conservative solutions of the Hunter-Saxton equation. A CFL-type condition is introduced in order to prevent wave breaking from occurring during a single time step for the numerical algorithm. The algorithm is first applied to the example considered in Chapter 3, and then we apply it to truncated initial data resembling the typical initial data for a conservative traveling wave. In particular the formulation of the algorithm is found to be inadequate for conservative traveling waves.
In Chapter 7 we consider the gluing formalism applied to linear solutions of the Hunter-Saxton equation. We show that we can glue together such linear solutions to construct a conservative continuous and piecewise linear solution of the Hunter-Saxton equation, provided the gluing points move along characteristics. Then the Lagrangian system for the differentiated Hunter-Saxton equation is derived formally. The explicit solution for the resulting ODE system is used in a modified algorithm. This modified algorithm is introduced to overcome the obstacles met in Chapter 6. The algorithm is first presented for a fixed mesh, and then for a mesh with moving grid points. The chapter ends with applications of the algorithm to conservative traveling waves and stumpons.
In Chapter 8 we summarize, and conclude, before suggesting possible future work.

2 Physical derivation

In this section we describe the underlying physical phenomenon which the Hunter-Saxton equation is an asymptotic model for. In particular we describe briefly what a liquid crystal is, and give a brief overview of the continuum theory for liquid crystals based on the Ericksen-Leslie model. This model describes the hydrodynamic flow of a nematic liquid crystal. The Ericksen-Leslie equations are based on an extension of the static equilibrium theory, hence we first present the static theory and then move onto the dynamical equilibrium theory. Moreover we apply calculus of variations to derive the nonlinear variational wave equation, and do a formal asymptotic expansion to derive the Hunter-Saxton equation.

In physics one typically operates with three states of matter: gas, liquid, and solid. By varying the pressure and temperature a phase transition can be induced between the states. For some organic substances however, there are intermediate states in between that of a liquid and a solid, which are referred to as mesophases. Such mesophases enjoy mixed properties of both the liquid and the solid phase. A solid state is characterized by strongly bounded atoms, in a rigid orientation. That is, molecules in a solid state are constrained to point only in certain directions, and stay at certain positions. The geometry of a solid can vary significantly, it can be completely irregular like that of a glass, or form an ordered lattice such as for metals. The ordered lattice is often referred to as a crystalline configuration. The identifying feature of a liquid phase on the other hand is that molecules are free to flow. The liquid state is completely isotropic so there exist no correlation between the positions of the centers of mass of the various molecules, nor are there any orientational ordering of the molecules.

A liquid crystal as the name suggests is a substance in a mesophase, inheriting crystalline properties, while flowing like a liquid. One can view liquid crystals as fluids made up of long rigid molecules, with an average orientation that describes the local direction of the medium. The ordering of the molecules in a liquid crystal can vary greatly, depending on the geometric and physical features of the underlying molecules. A variety of classes of liquid crystals have been introduced, distinguished by the amount of ordering observed in the liquid crystal. We give a rough summary of some of the characteristic features of the three most common liquid crystal phases: the nematic-, the cholesteric-, and the smectic liquid crystal phase.

- **Nematic phase**: This mesophase consists of elongated molecules. Due to the geometry, the long axis of neighbouring molecules tend to align, but there is no correlation in their positions. This alignment of the long axes causes a macroscopic order in the molecular orientation as illustrated in Figure 1. While we have macroscopic order, the centers of mass of the molecules are free to flow like a liquid. The nematic phase is the liquid crystal phase which is closest to being in the liquid phase. Thus we expect this phase to have more similarities with the liquid phase than other liquid crystal phases.

- **Cholesteric phase**: This phase is similar to the nematic phase in the sense that the long axes of molecules tend to orient themselves locally in the same direction, while the positions of the molecules are not correlated. The cholesteric phase differs from the nematic phase in that the director varies in a regular pattern throughout the medium. The geometry of the molecules cause a helical configuration of the long axes. The director which describes the average orientation of the long axis will twist around a common axis. Cholesteric phases consist of molecules tending to have the same alignment within a helical structure, but varies regularly between different helices with a given periodicity distance $p/2$. That is the director varies in a periodic fashion, where a full rotation of the director axis occurs after a period p, known as the pitch. But the director is invariant under reflections, so the pattern as shown in Figure 2 is repeated after a period of $p/2$.

- **Smectic phase**: In this phase the molecules are ordered in layers, and inside each of these layers the molecules may float around freely, however they cannot move freely between different layers. Within the layers, the molecules have a preferred orientation along a

Figure 1: The figure illustrates the orientational ordering within a nematic liquid crystal. The elongated molecules tend to align their long axes, while flowing like a liquid, but there is no positional correlation between the molecules.

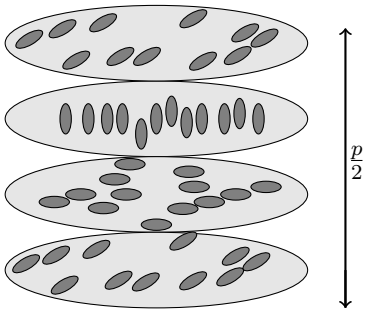

Figure 2: Illustrates the helices a cholesteric organize in, the director, i.e. average molecular alignment varies with each helical structure. The pattern is repeated after $\frac{p}{2}$.

common local director. Smectic liquid crystals are therefore examples of liquid crystals with both positional and orientational molecular ordering. It is common to distinguish between different types of smectic liquid crystals depending on how the molecules orient themselves within the layers. Figure 3 shows two types of smectic mesophases. In Figure 3a we see an example of the smectic A phase, where the average molecular orientation is perpendicular to the layer interface. The layers are shown by dashed lines. Figure 3b depicts an instant of the smectic C phase, where the alignment is tilted compared to the vertical.

2.1 Continuum theory for nematic liquid crystals

For the rest of the present paper, we will only consider the nematic phase. This phase is characterized by the long-axes of the elongated molecules aligning along a preferred direction. This preferred direction will in general fluctuate throughout the medium. In an ideal nematic liquid crystal, all molecules will be aligned along a common direction, however typically there are external influences leading to nontrivial configurations. One such effect is thermal excitation which causes individual molecules to not be perfectly aligned. Typically to describe nematic liquid crystals one needs to predescribe two linearly independent vector fields and an order parameter.

1. One vector field describing the fluid flow, i.e. a local velocity field $v(x,t)$

(a) Smectic A. **(b)** Smectic C.

Figure 3: Illustrates the smectic mesophase. In the smectic A phase, the molecules align themselves in layers which are perpendicular to the layer interface. In the smectic C phase, the molecules align themselves in a tilted orientation compared to the vertical. Here with an angle θ.

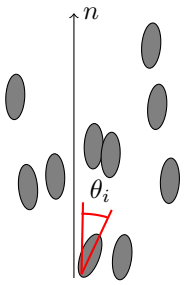

Figure 4: The director n, representing the average molecular alignment in an uniaxial nematic, together with a schematic representation of molecules. In addition we have a local degree of orientation along the director, here indicated by an angle θ_i. This represents the tilted angle from the director for a particular molecule.

2. One vector field to describe the mean local molecular alignment of the rod-like molecules, which we denote by n. This vector field is called the director.

3. An order parameter S, giving the local degree of orientation

To model nematic liquid crystals it is essential to obtain the equation governing the evolution of the director field describing the average molecular alignment in some ball B. The alternative is to study the dynamics of each individual molecule in the liquid crystal, leading to an intractable task. The molecules in nematics are able to rotate about their long axes, and there seem to be no preferred arrangement of the two ends of a molecule, thus the sign of the director has no physical significance. In mathematical terms this means that the director n is invariant under the transformation $n \to -n$. Moreover the magnitude of n is of no impotance, and for convenience we take n to be a unit vector. In particular $n : \Omega \times (0, T) \to \mathbb{S}^2$, that is a map from space-time to the unit sphere $\mathbb{S}^2 := \{x \in \mathbb{R}^3 \text{ s.t } |x| = 1\}$. Here $\Omega \subseteq \mathbb{R}^3$ is the volume occupied by the liquid crystal.
The order parameter $S(\vec{x})$ gives the local degree of orientation, which often is described in terms of the 2^{nd} Legendre polynomial. However the order parameter can be defined in terms of higher-order Legendre polynomials if one desires higher accuracy. Extreme cases of the order parameter are

- $S = 1$ - indicate perfect alignment along the director
- $S = 0$ - no orientation (isotropic)
- $S = -\frac{1}{2}$ - perfect alignment perpendicular to the director

The quantities used in the continuum description thus far only apply to uniaxial nematics (only one preferred axis). There exist biaxial nematics, which consist of molecules having shapes such that it is required to use two director fields n_1 and n_2 and two scalar order parameters S_1 and S_2 to describe the static theory. We will however assume uniaxiality and make the usual simplifying assumption of the order parameter S being a constant. Figure 4 shows the director field n and the local degree of orientation indicated by an angle θ_i.

2.1.1 Oseen-Frank static theory

The uniaxiality assumption results in rotational symmetry. The assumption is commonly made as it simplifies the analysis and contains the most important class of liquid crystals. If we assume that once the average molecular alignment is known at a point x, it varies slowly from point to point, then we can describe the response of a liquid crystal to deformations using continuum elasticity theory. A common starting point for the continuum description for nematic liquid crystals is to assume that there is a free energy density, w, representing the locally stored

energy associated with distortions of the uniform equilibrium alignment of the director. This takes the form

$$w = w(n, \nabla n).$$

Fluctuations in the director field n are mainly due to thermodynamical forces caused by elastic deformations in the form of bending, twisting and splay. These effects are accounted for in the famous Oseen-Frank energy functional as we will see. The total elastic/potential energy in a sample volume $V \subseteq \Omega$ of the liquid crystal is then given by the elastic energy functional

$$W(n) := \int_V w(n(\vec{x}, t), \nabla n(\vec{x}, t)) d\vec{x}. \tag{2.1}$$

A liquid crystal in a completely relaxed configuration, i.e., in the absence of forces is said to be in natural orientation. The elastic energy is determined up to an arbitrary constant $c \in \mathbb{R}$. We choose this constant in such a way, that the elastic energy density is zero in a natural orientation. The elastic energy density $w(\cdot, \cdot)$ is minimal in such an orientation, as a physical system takes on equilibrium positions where the potential energy is minimized. Therefore we require w to be a positive semidefinite function, that is,

$$w(n, \nabla n) \geq 0, \tag{2.2}$$

for all possible molecular alignments $n \in \mathbb{S}^2$. Moreover as nematic liquid crystals lack polarity, we have the invariance $n \to -n$, hence we require

$$w(n, \nabla n) = w(-n, -\nabla n), \tag{2.3}$$

i.e., w is an even function. Moreover we have a third constraint which needs to be satisfied by the free energy density. We require frame indifference, that is the free energy density must be the same when described in any two reference frames. This is more commonly referred to as Galilean invariance. One can also separate into a constraint of material symmetry, such that w is required to satisfy 4 conditions as in [HP18]. Either way we require that

$$w(n, \nabla n) = w(Qn, Q \nabla n Q^T) \tag{2.4}$$

for any orthogonal matrix with $\det(Q) = \pm 1$.
In a given microscopic region of a liquid crystal there is a preferred axis along which molecules orient themselves as shown in Figure 4. We want to determine how much energy it will take to deform this orientation. We assume that the free energy density is a quadratic function of the curvature strains that can occur. This leads to the so-called Oseen-Frank energy. Deformations relative to orientations of molecules away from equilibrium positions are called curvature strains, while the restoring forces which arise to oppose the deformations, are called curvature stresses. The curvature strains can be mainly split into splay, twist, and bend strains as mentioned. The different geometrical effects these have are shown in Figure 5. Splay is strain that causes a fan-shaped outspreading of the molecules from the original direction, bending is a change in the molecular direction, while twisting corresponds to a rotation of the director in a plane parallel to the rotation axis. The Oseen-Frank free energy density for nematics and cholestrics, takes the form

$$\begin{aligned} w(n, \nabla n) = \frac{\alpha}{2} \underbrace{(\nabla \cdot n)^2}_{\text{Splay}} + \frac{\beta}{2} \underbrace{(n \cdot \nabla \times n)^2}_{\text{Twist}} + \frac{\gamma}{2} \underbrace{|n \times (\nabla \times n)|^2}_{\text{Bend}} \\ + \frac{(\beta + \eta)}{2} \underbrace{\left((\mathrm{Tr}(\nabla n)^2 - (\nabla \cdot n)^2 \right)}_{\text{Saddle-Splay}}. \end{aligned} \tag{2.5}$$

Here α, β and γ are coefficients which correlate to the splay, twist, and bend of the director field, respectively. The coefficients α, β, γ, and η sometimes go under the name Frank's elasticity coefficients in the literature. Their values are tabulated for many liquid crystals. We say the

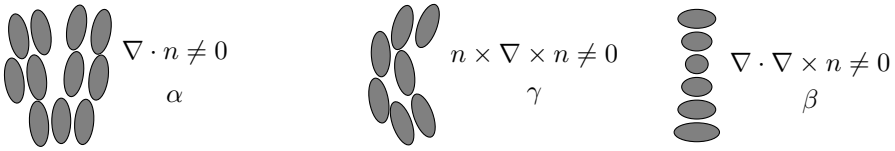

(a) Illustration of splay **(b)** Illustration of bending **(c)** Illustration of twist

Figure 5: The three types of elastic distortions (curvature strains) of the director field considered in the Oseen-Frank density.

motion consist of pure splay waves if the term involving the splay is the only nonzero term, and similar for twist and bend.
Considering in particular the integral of the last term and rewriting it using the identity

$$(\mathrm{Tr}(\nabla n)^2) - (\nabla \cdot n)^2 = \nabla \cdot \Big((\nabla n)n - (\nabla \cdot n)n \Big),$$

it becomes, by applying the divergence theorem,

$$(\beta + \eta) \int_\Omega \left(\nabla \cdot \Big((\nabla n)n - (\nabla \cdot n)n \Big) \right) dx = \int_{\partial\Omega} \Big((\nabla n)n - (\cdot \nabla)n \Big) \cdot \nu' dx,$$

and we see its value only depends on the director field at the boundary $\partial\Omega$. Here ν' is the outward pointing unit normal on the boundary. Hence if the trace $n|_{\partial\Omega}$ is predescribed this term can be completely neglected, as this corresponds to a null Lagrangian. That means that the corresponding Euler-Lagrange equations for the functional consisting solely of this term vanish identically, so it yields no contribution to the Euler-Lagrange equations. The form taken by the Oseen-Frank free energy density is not arbitrary, it has been shown as noted in [HP18] that if one restricts the free energy density w to at most be a quadratic function of the gradient ∇n and $n \in C^1(\Omega; \mathbb{S}^2)$, then w can only be frame indifferent if it takes on the particular form (2.5).
Now if we impose the nonnegativity constraint (2.2) on the Oseen-Frank free energy (2.5), we can derive the Ericksen inequalities stating that

$$\begin{aligned} \alpha \geq 0, \quad \beta \geq 0, \quad \gamma \geq 0, \\ \beta \geq |\eta|, \qquad 2\alpha \geq \beta + \eta \geq 0. \end{aligned}$$

These are necessary and sufficient to ensure a lower bound on the free energy density, in particular we have that $w(n, \nabla n) \geq c_0 |\nabla n|^2$ for all director fields n and some positive constant $c_0 > 0$. If the elasticity coefficients are unknown one often resorts to the so-called one constant approximation. Under very special physical situations it may occur that the elasticity is isotropic, then this one-constant approximation reflects the physical situation. In general however the elasticity coefficients differ significantly. Either way one sets the coefficient for the splay, twist, and bend to be equal and $\eta = 0$. Combining this with the identity

$$|\nabla n|^2 = (\nabla \cdot n)^2 + (n \cdot \nabla \times n)^2 + |n \times (\nabla \times n)|^2 + ([\mathrm{Tr}(\nabla n)]^2 - (\nabla \cdot n)^2),$$

one obtains that the total free energy within the liquid crystal reduces to

$$W(n) = \frac{\alpha}{2} \int_\Omega |\nabla n|^2 dx,$$

which is the energy functional for harmonic maps, i.e., the common Dirichlet energy. It is independent of n and only depends on the gradient.

A well-known principle from physics is the principle of minimum energy. This is essentially a restatement of the second law of thermodynamics, and states that for a closed system, the

internal energy will decrease and approach a minimum at equilibrium. Therefore it is of interest to consider the minimization of the energy functional (2.1). That is, one considers the following minimization problem

$$\min_n W(n) = \int_\Omega w(n, \nabla n) dx,$$
$$n|_{\partial\Omega} = n_D,$$

subject to the constraint $|n| = 1$, where n_D is some given boundary data for the director field. A review of some results are found in [Bal17]. Here we assume that the director is known a priori at the boundary. This is called strong anchoring. We have neglected other common external forces such as electric and magnetic fields, which are present in common applications of liquid crystals. The most common modern application of liquid crystals is in LCD (liquid-crystal display) screens. In such cases strong anchoring is often inappropriate, since strong applied electromagnetic fields result in torques which typically overcome the boundary anchoring. Then one needs to introduce weak anchoring in the form of a penalty term of the free energy at the boundary. The total free energy functional then takes the form

$$\hat{W}[n] = \int_\Omega \Big(W_{OF} + W_E + W_M \Big) dx + \int_{\partial\Omega} W_P \, ds, \tag{2.6}$$

where W_{OF} is the Oseen-Frank energy, W_E and W_M are the bulk energy density due to electric and magnetic fields, respectively, and W_P is the penalty term. A nice account for these effects is given in [Aur15]. One looks for equilibrium solutions for the director field n by looking for stationary points of the functional (2.6). This amounts to considering variations of the director configuration of the form

$$n_\epsilon = n + \epsilon\phi,$$

for a smooth vector ϕ and a small parameter ϵ. This vector is chosen in such a way, that if we have strong anchoring, n_ϵ satisfies the boundary condition for any ϵ. For a given ϕ, n_ϵ yields a path of configurations of the director parameterized by ϵ. We say n is an equilibrium configuration with respect to the functional if the first variation vanishes for all smooth vectors ϕ. That is, if

$$\frac{\partial}{\partial\epsilon}\hat{W}[n + \epsilon\phi]|_{\epsilon=0} = 0,$$

for all ϕ.

2.1.2 Classical Ericksen-Leslie theory

It is not necessary to use the full machinery of the Ericksen-Leslie formalism [WXL13] to derive the equation of interest in this thesis. However it is enlightening to see under what assumptions the Ericksen-Leslie continuum description reduces to the setting we consider here. We thus give a quick overview of the theory, without digging into the rather complicated constitute relations. As done in [Les92] and [Ste14] one can derive required constitute relations for the governing dynamical equations by considering the typical balance equations of continuum physics: mass conservation, balance of linear momentum, and balance of angular momentum. We introduce the material derivative or so-called Lagrange derivative by

$$\frac{D}{Dt} = \frac{\partial}{\partial t} + v \cdot \nabla.$$

Then we can state the three balance laws governing the dynamics of nematic liquid crystals as

$$\frac{D}{Dt}\rho = 0, \tag{2.7a}$$

$$\rho\frac{D}{Dt}v + q\frac{D^2}{Dt^2}n\cdot\nabla n = \rho f + g\cdot\nabla n + \nabla\cdot T, \tag{2.7b}$$

$$q\frac{D^2}{Dt^2}n + \lambda n = g + \hat{g} - \frac{\partial W}{\partial n} + \nabla\cdot\frac{\partial W}{\partial(\nabla n)}. \tag{2.7c}$$

Here $v \in \mathbb{R}^3$ is the velocity field of the liquid crystal flow, $f \in \mathbb{R}^3$ is the vector of external forces, while $g \in \mathbb{R}^3$ is the vector of generalized forces. $q > 0$ is the inertial material constant. Moreover λ is a Langrange multiplier associated with the constraint (2.8b). T is the full stress tensor consisting of a term involving the pressure p of the liquid and also a viscous stress tensor $\hat{T} \in \mathbb{R}^{3\times 3}$. To determine an explicit expression for the stress tensor and the viscous stress tensor, Leslie introduced in [Les92] a rate of work hypothesis. One considers the rate at which forces and moments do work on a sample volume V of a nematic liquid crystal, and postulate that this is absorbed into changes in the the stored internal energy or the kinetic energy, or that the work will be lost due to viscous dissipation. One considers the resulting strong form which reads

$$T = -pI - \rho\frac{\partial W}{\partial(\nabla n)}\nabla n + \hat{T},$$

where $\hat{T}$ consists of 6 terms, all proportional to different viscosity coefficients μ_i for $i \in \{1,\dots,6\}$. There are constraints on these coefficients, but we will not go into that here. Finally $\hat{g}$ is also a vector dependent on the viscosity of the fluid. We assume incompressible fluid flow in the nematic liquid crystal. Otherwise the free energy density representing the internally stored energy of deformations of the director field would not only be a function of n and ∇n, as postulated by Frank-Oseen in (2.5). If we had considered a compressible fluid, we would have to include the density ρ of the fluid and possibly variations in density, i.e., $w = w(n, \nabla n, \rho, \nabla\rho)$. We will assume constant density ρ in the nematic liquid crystal. Thus the mass conservation reduces to the typical incompressiblity condition. Hence leading to two constraints

$$\nabla\cdot v = 0 \quad \text{in } \Omega, \tag{2.8a}$$

$$|n| = 1. \tag{2.8b}$$

The second constraint results from n being a map to the unit sphere.

Now the two equations (2.7b) - (2.7c) plus the two constraints (2.8a)-(2.8b) yield 8 equations in 8 unknowns. The unknowns are the 3 components of v and n, in addition to the two Lagrange multipliers λ and p. As noted in [HZ95] there are two extreme cases of time-dependent solutions.

- $q = 0$: Here viscous effects dominate the inertia. The evolution of the director field is governed by a gradient-flow parabolic PDE, and this is typically the most physically significant regime.
- The opposite borderline case is letting inertia dominate viscosity (we neglect viscosity), this amounts to setting $\hat{T} = 0$ and $\hat{g} = 0$. The director field will in such a case satisfy a hyperbolic PDE, which can be derived from a constrained variational principle.

We will now introduce three simplifying assumptions: we specialize to stationary flow, assume vanishing viscosity, and that there are no external forces acting on the liquid crystal. Postulating stationary flow means that the material derivatives reduce to usual partial derivatives with respect to time. This way we exclusively focuses on the dynamics of the director field. The equations for linear and angular momentum reduce to

$$qn_{tt}\cdot\nabla n + \nabla\cdot(pI - \rho\frac{\partial W}{\partial(\nabla n)}\nabla n) = 0, \tag{2.9a}$$

$$qn_{tt} + \lambda n + \frac{\partial W}{\partial n} - \nabla\cdot\frac{\partial W}{\partial(\nabla n)} = 0. \tag{2.9b}$$

Now we can take the inner product with n in (2.9b) and use the constraint $|n|^2 = 1$ to eliminate the Lagrange multiplier λ. In particular we obtain by an integration by parts in time for the first term that λ is given by

$$\lambda = -qn_t \cdot n_t + n \cdot \frac{\partial w}{\partial n} + \sum_{j,i} \Big(\partial_j n_i \frac{\partial w}{\partial(\partial_j n_i)} - \partial_j (n_i \frac{\partial w}{\partial(\partial_j n_i)}) \Big). \tag{2.10}$$

Equations (2.9a) and (2.10) describe the governing equations for the dynamics of the director field $n = n(\vec{x}, t)$. If we keep our assumptions, but allow for a nonzero viscosity, the vector $\hat{g}$ will also yield a contribution, which manifest itself as a term $\hat{\gamma} n_t$ in (2.9b). This is a lower order damping term, which is not expected to smooth out singularities. If one sets the term $qn_{tt} \cdot \nabla = 0$ one obtains precisely the same equations as considered in [HS91], and the reason we have this term in the first place is that we have already done some additional manipulations to recast the conservation of linear momentum on the more convenient formulation (2.7b).

We will now apply Hamiltonian's principle of classical mechanics [Chp2, [GSP14]], which describe the motion of a conservative system. Let the system be described by N generalized coordinates $q_1, ..., q_N$ with Lagrangian

$$\mathcal{L} = \mathcal{L}(q_1, .., q_N, q_{1,t}, ..., q_{N,t}, t),$$

depending explicitly on the generalized coordinates, their time derivatives, and time t. Here by generalized coordinates we mean coordinates where we have incorporated holonomic constraints, i.e., used the holonomic constraint to remove dependent variables. Therefore $\{q_j\}$ are independent coordinates. The Hamiltonian principle states that the evolution of the system between times t_0 to t_1 is given by a path in the configuration spaces, which is such that the time integral of the Lagrangian is stationary. That is,

$$\delta \int_{t_0}^{t_1} \mathcal{L}(q_1, .., q_n, q_{1,t}, ..., q_{n,t}, t)\, dt = 0,$$

where δ denotes the first variation operator. Then we observe that (2.9b) can be written as the Euler-Lagrange equation of the following action functional (the action functional is defined as the time integral of the Lagrangian function $\mathcal{L}$)

$$A[n] = \int_{t_0}^{t_1} \int_\Omega \Big(\frac{1}{2} q |n_t|^2 - \frac{1}{2} \lambda |n|^2 - W(n, \nabla n) \Big) dx dt.$$

That is, considering variations of the director field of the form $n_\epsilon = n + \epsilon\phi$, with ϕ having compact support, a computation of the first variation yields

$$\begin{aligned}
\delta \int_{t_0}^{t_1} \mathcal{L}\, dt &= \frac{\partial}{\partial \epsilon}|_{\epsilon=0} \int_{t_0}^{t_1} \int_\Omega \Big(\frac{1}{2} [q(n_t + \epsilon\phi_t) \cdot (n_t + \epsilon\phi_t) - \lambda(n + \epsilon\phi) \cdot (n + \epsilon\phi)] \\
&\qquad - W(n + \epsilon\phi, \nabla n + \epsilon \nabla\phi) \Big) dx dt \\
&= \int_{t_0}^{t_1} \int_\Omega \Big(q(n_t + \epsilon\phi_t) \cdot \phi_t - \lambda(n + \epsilon\phi) \cdot \phi - \frac{\partial W}{\partial n}\phi - \frac{\partial W}{\partial(\nabla n)} \nabla\phi \Big) dx dt |_{\epsilon=0} \\
&= \int_{t_0}^{t_1} \int_\Omega \Big(- qn_{tt} - \lambda n - \frac{\partial W}{\partial n} + \nabla \cdot \frac{\partial W}{\partial(\nabla n)} \Big) \phi\, dx\, dt\,.
\end{aligned}$$

Here we have integrated by parts and used that ϕ is compactly supported in $\Omega \times (t_0, t_1)$ so the boundary terms vanish. For this to vanish for all such functions, the integrand must vanish, which leads to (2.9b).

2.2 Deriving the Hunter-Saxton equation

Now we will restrict ourselves to the bend-splay geometry in one spatial dimension only, then the director field takes the form

$$n(x,t) = (\cos(\psi(x,t)), \sin(\psi(x,t)), 0).$$

Here $\psi(x,t)$ is the angle between the x axis and the director field. Now ignoring the saddle-splay term in the Frank-Oseen free energy density (2.5), and inserting for this form of director field we obtain

$$\begin{aligned} w(n, \nabla n) &= \frac{1}{2}\Big(\alpha(\nabla \cdot n)^2 + \beta(n \cdot \nabla \times n)^2 + \gamma|n \times (\nabla \times n)|^2\Big) \\ &= \frac{1}{2}(\alpha \sin^2(\psi) + \gamma \cos^2(\psi))(\psi_x)^2. \end{aligned}$$

In particular we see that there is no twist. If $\psi_x \neq 0$ the internal energy will be minimized either for $\psi = 2\pi k$, representing no splay, or $\psi = (2k + \frac{1}{2})\pi$, representing no bending, for k being an integer. What minimum the system takes, depends on the relative magnitude between the splay and bend coefficient. Typically one introduces a wave speed

$$c^2(\psi) = \alpha \sin^2(\psi(x,t)) + \gamma \cos^2(\psi(x,t)),$$

and the resulting Frank-Oseen potential density become $\frac{1}{2}c^2(\psi)(\psi_x)^2$. As a short recap, the first term describes the potential energy density due to splay, while the second explains the potential energy density due to bending. When

- $\psi = 0$: The director field is aligned parallel to the direction field and we have pure bending waves.
- $\psi = \frac{\pi}{2}$: The director field is aligned perpendicular to the director field representing pure splay waves.

We will assume that the domain of the liquid crystal is infinite and that there is no energy dissipation (no viscosity), we also assume absence of electromagnetic fields. If we take as kinetic energy

$$\mathbb{K} = \frac{1}{2}\int_{\mathbb{R}} q|n_t|^2 dx,$$

the energy associated with rotational moment of inertia of the director field, we notice that $n_t = (-\sin(\psi(x,t))\psi_t, \cos(\psi(x,t))\psi_t)$. Hence $\frac{1}{2}|n_t|^2 = \frac{1}{2}\psi_t^2$ will be our nondimensionalized kinetic energy density. Then since the Lagrangian functional of a mechanical system is given as the kinetic energy minus the potential energy it takes the particular form

$$\mathcal{L}(n, \nabla n) = \mathbb{K} - W[n, \nabla n] = \frac{1}{2}\int_{\mathbb{R}} \left[q(\psi_t)^2 - c^2(\psi)(\psi_x)^2\right] dx.$$

Notice this is of the same form as the Lagrangian used to derive the angular momentum equation from Hamilton's principle, except now we have eliminated the Lagrange multiplier. We again apply Hamilton's principle and look for stationary solutions with respect to the time integral of

the Lagrangian. We take a small parameter ϵ and a compactly supported ϕ, yielding

$$\begin{aligned}
0 &= \frac{\partial}{\partial\epsilon}|_{\epsilon=0} \int_{t_0}^{t_1} \mathcal{L}(\psi+\epsilon\phi, \nabla\psi+\epsilon\nabla\phi)\, dt \\
&= \int_{t_0}^{t_1}\int_{\mathbb{R}} \frac{\partial}{\partial\epsilon}\Big(q(\psi_t+\epsilon\phi_t)\cdot(\psi_t+\epsilon\phi_t) - c^2(\psi+\epsilon\phi)(\psi_x+\epsilon\phi_x)\cdot(\psi_x+\epsilon\phi_x)\Big)\, dx\, dt\,|_{\epsilon=0} \\
&= \int_{t_0}^{t_1}\int_{\mathbb{R}} \Big(q(\psi_t+\epsilon\phi_t)\phi_t - c^2(\psi+\epsilon\phi)(\psi_x+\epsilon\phi_x)\phi_x \\
&\qquad\qquad - c(\psi+\epsilon\phi)c'(\psi+\epsilon\phi)(\psi_x+\epsilon\phi_x)^2\phi\Big)|_{\epsilon=0}\, dx\, dt \\
&= \int_{t_0}^{t_1}\int_{\mathbb{R}} \Big(q\psi_t\phi_t - c^2(\psi)\psi_x\phi_x - c(\psi)c'(\psi)\psi_x^2\phi\Big)\, dx\, dt \\
&= \int_{t_0}^{t_1}\int_{\mathbb{R}} (-q\psi_{tt} + c(\psi)(c(\psi)\psi_x)_x)\phi\, dx\, dt,
\end{aligned}$$

by a formal calculation. For this to hold for all such compactly supported functions ϕ we require that the angle ψ satisfy

$$q\psi_{tt} - c(\psi)(c(\psi)\psi_x)_x = 0. \tag{2.11}$$

This equation was introduced by Hunter and Saxton in [HS91] with $q = 1$. And is referred to as the nonlinear variational wave equation, which as we have seen is a simplified model for the director field of nematic liquid crystals.

We want to examine the asymptotic behaviour of this nonlinear variational equation motivated by [HS91]. So we expand around an equilibrium state ψ_0 in a small parameter ϵ and retain only first order terms in the expansion, i.e.,

$$\psi(x,t;\epsilon) = \psi_0 + \epsilon\psi_1(\Theta,\tau) + O(\epsilon^2).$$

Here $\Theta = x - c(\psi_0)t$ and the slow time scale $\tau = \epsilon t$ is the independent variable. We assume the unperturbed wave speed is nonzero, i.e., $c'(\psi_0) \neq 0$. Inserting that into each of the terms in (2.11) yields

$$\begin{aligned}
\psi_{tt} &= \epsilon\Big[c_0^2\psi_{1,\Theta\Theta} - 2\epsilon c_0\psi_{1,\Theta\tau} + \epsilon^2\psi_{1,\tau\tau}\Big] \\
c(\psi)(c(\psi)\psi_x)_x &= \epsilon c_0^2\psi_{1,\Theta\Theta} + \epsilon^2 c_0 c_0'[\psi_1\psi_{1,\Theta}]_\Theta + \epsilon^2 c_0 c_0'\psi_1\psi_{1,\Theta\Theta} + \epsilon^3(c_0')^2\psi_1(\psi_1\psi_{1,\Theta})_\Theta,
\end{aligned}$$

where we have Taylor expanded $c(\psi_0+\epsilon\psi_1+O(\epsilon^2))$ around the equilibrium state and introduced $c_0 = c(\psi_0)$. We neglect the terms proportional to ϵ^3 and require the factors in front of ϵ^2 to vanish, this yields

$$2c_0\psi_{1,\Theta\tau} + c_0c_0'\left([\psi_1\psi_{1,\Theta}]_\Theta + \psi_1\psi_{1,\Theta\Theta}\right) = 0.$$

Dividing by $2c_0$ and adding and subtracting $\frac{c_0'}{2}\psi_{1,\Theta}^2$ now yields

$$(\psi_{1,\tau} + c_0'\psi_1\psi_{1,\Theta})_\Theta = \frac{1}{2}c_0'\psi_{1,\Theta}^2.$$

We introduce $u = c'(\psi_0)\psi_1$, and redefine our spatial and temporal variables $x \to x = \operatorname{sign}(c_0')\Theta$ and $t = \tau$. The resulting equation must be coupled with some initial data, this results finally in

$$(u_t + uu_x)_x = \frac{1}{2}(u_x)^2 \tag{2.12a}$$

$$u|_{t=0} = u_0(x), \tag{2.12b}$$

which is the Cauchy problem for the Hunter-Saxton equation, introduced in [HS91]. The expansion done here, bear some similarities to a two-timing expansion used for weakly nonlinear oscillators for instance, except that we expand around a constant state ψ_0. Notice now that (x,t) are moving spatio-temporal coordinates, which are scaled and synchronized with the wave motion described by the Hunter-Saxton equation. The main motivation for seeking and studying such equations, lies in capturing nonlinear phenomena such as wave-breaking and traveling waves. The Hunter-Saxton equation, is governed by a hyperbolic variational principle as noticed in [HS91]. In particular, this is the Euler-Lagrange equation of the action functional

$$A[u] = \int_{t_0}^{t_1} \int_{\mathbb{R}} \Big(u_t u_x + u u_x^2 \Big) dx dt. \tag{2.13}$$

Yet again computing the first variation, and requiring the time integral of the Lagrangian to be stationary leads to

$$\begin{aligned}
\delta \int_{t_0}^{t_1} \mathcal{L}\, dt &= \int_{t_0}^{t_1} \int_{\mathbb{R}} \frac{\partial}{\partial \epsilon} \Big((u+\epsilon\phi)_t (u+\epsilon\phi)_x + (u+\epsilon\phi)(u+\epsilon\phi)_x^2 \Big) |_{\epsilon=0}\, dx\, dt \\
&= \int_{t_0}^{t_1} \Big(u_t \phi_x + \phi_t u_x + 2 u u_x \phi_x + u_x^2 \phi \Big)\, dx\, dt \\
&= \int_{t_0}^{t_1} \int_{\mathbb{R}} \Big(-2(u_t + u u_x)_x + u_x^2 \Big) \phi\, dx\, dt = 0,
\end{aligned}$$

hence indeed the Hunter-Saxton equation is the Euler-Lagrange equation stemming from this Lagrangian. Here we have assumed that ϕ is supported away from $t = t_0$ and t_1 and that it is compactly supported in the space variable.
It turns out that the Hunter-Saxton equation can be derived as the Euler-Lagrange equation stemming from another nonequivalent action functional. This action functional stems from the high-frequency limit of the Camassa-Holm equation

$$u_t - u_{xxt} + 2\kappa u_x + 3 u u_x - 2 u_x u_{xx} - u u_{xxx} = 0,$$

being a model for wave propagation in a shallow water approximation. We will not go into detail of that derivation here, but it is related to changing variables

$$x \to \epsilon x \qquad t \to \epsilon t,$$

and passing to the limit $\epsilon \downarrow 0$. An exposition on the high-frequency limit is written in [DP98]. Introducing the momentum π and a characteristic coordinate $\xi = z(x,t)$ having inverse $x = X(\xi, t)$, which will be used much in the forthcoming sections, we consider the action functional

$$S[u, \pi, z] = \int_{t_0}^{t_1} \int_{\mathbb{R}} \Big(\frac{1}{2} u_x^2 + \pi (z_t + u z_x) \Big)\, dx\, dt\,.$$

There are three variables associated to this action functional, and we need to compute the first variation with respect to all three and eliminate π and z and their associated derivatives, respectively. Computing the first variation with respect to u first we find

$$\begin{aligned}
0 &= \frac{\delta}{\delta u} S[u, \pi, z] \\
&= \int_{t_0}^{t_1} \int_{\mathbb{R}} \frac{d}{d\epsilon} \Big(\frac{1}{2} ([u+\epsilon\phi]_x)^2 + \pi (z_t + (u+\epsilon\phi) z_x) \Big) |_{\epsilon=0}\, dx\, dt \\
&= \int_{t_0}^{t_1} \int_{\mathbb{R}} (u_x \phi_x + \pi \phi z_x)\, dx\, dt = \int_{t_0}^{t_1} \int_{\mathbb{R}} (-u_{xx} + \pi z_x) \phi\, dx\, dt\,.
\end{aligned}$$

Next computing with respect to π

$$\begin{aligned}0 &= \frac{\delta}{\delta\pi}S[u,\pi,z]\\ &= \int_{t_0}^{t_1}\int_{\mathbb{R}}\frac{d}{d\epsilon}\left(\frac{1}{2}u_x^2+(\pi+\epsilon\phi)(z_t+uz_x)\right)|_{\epsilon=0}\,dx\,dt\\ &= \int_{t_0}^{t_1}\int_{\mathbb{R}}(z_t+uz_x)\phi\,dx\,dt,\end{aligned}$$

and then z we get

$$\begin{aligned}0 &= \frac{\delta}{\delta z}S[u,\pi,z]\\ &= \int_{t_0}^{t_1}\int_{\mathbb{R}}\frac{d}{d\epsilon}\left(\frac{1}{2}u_x^2+\pi([z+\epsilon\phi]_t u[z+\epsilon\phi])\right)dx\,dt\\ &= \int_{t_0}^{t_1}\int_{\mathbb{R}}(\pi\phi_t+u\phi_x\pi)\,dx\,dt = -\int_{t_0}^{t_1}\int_{\mathbb{R}}(\pi_t+(u\pi)_x)\phi\,dx\,dt\end{aligned}$$

Thus the resulting equations are

$$\begin{aligned}u_{xx}-\pi z_x &= 0\\ z_t+uz_x &= 0\\ \pi_t+(u\pi)_x &= 0\end{aligned}$$

eliminating π and z from these equations, using the first equation to write $\pi=\frac{u_{xx}}{z_x}$ and plugging that into the third equation we obtain

$$\pi_t+(u\pi)_x=(\frac{u_{xx}}{z_x})_t+(u\frac{u_{xx}}{z_x})_x=\frac{u_{xxt}}{z_x}-\frac{u_{xx}z_{xt}}{z_x^2}+\frac{(uu_{xx})_x}{z_x}-\frac{uu_{xx}z_{xx}}{z_x^2}=0$$

We multiply both sides by z_x and collect terms involving $\frac{1}{z_x}$ to get

$$\begin{aligned}0 &= u_{xxt}+(uu_{xx})_x-\frac{u_{xx}}{z_x}(\underbrace{z_{xt}+uz_{xx}+u_xz_x}_{(z_t+uz_x)_z=0}-u_xz_x) = u_{xxt}+(uu_{xx})_x+u_xu_{xx}\\ &= (u_t+uu_x)_{xx}-\frac{1}{2}(u_x^2)_x\end{aligned}$$

Now we integrate once with respect to x and set the integration constant to zero, to obtain the Hunter-Saxton equation. Thus the Hunter-Saxton equation on differentiated from, can be derived as the Euler-Lagrange Equation of two distinct nonequivalent action functionals.

3 Properties of the Hunter-Saxton Equation

In this section we want to review some of the properties which the Hunter-Saxton equation enjoys, and introduce various solution concepts, such as the notion of conservative and dissipative solutions. There are several formulations of the Hunter-Saxton equation that appear in the literature, the two most prominent formulations are the differentiated version (2.12a) and the integrated formulation. In this section we will interchange between these. The Cauchy problem for the integrated Hunter-Saxton equation reads

$$u_t + uu_x = \frac{1}{4}\bigg(\int_{-\infty}^{x} u_x^2 dy - \int_{x}^{\infty} u_x^2 dy \bigg), \tag{3.1a}$$

$$u|_{t=0} = u_0(x). \tag{3.1b}$$

One observes that the Hunter-Saxton equation is a nonlocal evolution equation. Moreover it is scale-invariant and nondispersive [HZ94].

By applying the method of characteristics one can show that, $u_x(x,t) \to -\infty$, pointwise in finite time, while the solution itself remains continuous and $\|u_x(\cdot,t)\|_{L^2(\mathbb{R})}$ is finite. This will be elaborated further upon in the next subsection. This is a characteristic feature of the phenomenon of wave breaking. Upon wave breaking, energy concentrates on a set of Lebesgue measure zero. This energy concentration resembles what we physically observe when water surface waves break on a coastline. Wave breaking will occur for solutions to the Cauchy problem (3.1a)-(3.1b) even when the initial data is smooth, provided the initial data is not monotonically increasing. This renders the concept of classical solutions too strong. One can extend smooth solutions past blow up in several distinct ways by resorting to weak solutions. As a consequence weak solutions are not unique. The continuation past wave breaking is concerned with how we treat the energy in the system past blow up. The total energy in the system before wave breaking is given by

$$E[u](t) = \int_{\mathbb{R}} u_x(x,t)^2 dx = \|u_x(\cdot,t)\|^2_{L^2(\mathbb{R})}, \tag{3.2}$$

and some or all of this energy will concentrate upon wave breaking. The energy (3.2) can actually increase for weak solutions, therefore a natural restriction is to enforce it to be nonincreasing past blow up. This restriction is not sufficient to gain uniqueness of the continuation. We need to consider even more restrictive classes of weak solutions. The two most prominent classes are that of a dissipative solutions where the concentrated energy is removed, and that of conservative solutions where the energy E is constant at all times. Regardless of the choice of continuation, it is natural to require the kinetic energy to stay bounded at all times.

Remark 3.1. The requirement that the kinetic energy functional stays bounded, i.e., $u_x(\cdot,t) \in L^2(\mathbb{R})$ for all times $t \geq 0$, already enforces some regularity to solutions u of (3.1a)-(3.1b). This suggests that one might incorporate a reasonable high degree of regularity even for weak solutions to the Cauchy problem.

As noted in [Daf11] in contrast to the inviscid Burgers equation, i,e,

$$u_t + \left(\frac{1}{2}u^2\right)_x = 0,$$

which is precisely the left-hand side of (3.1a), shocks do not form. Breakdown of the Hunter-Saxton equation manifests itself in the formation of cusps rather than shocks. That is, the characteristics focus upon wave breaking, as opposed to colliding. This will be illustrated by an example in Subsection 3.2.
We observed in Section 2 that the Hunter-Saxton equation can be derived as the Euler-Lagrange equation stemming from two distinct nonequivalent action functionals. The existence of two such action functionals and thus also Lagrangians implies the existence of two Hamiltonian

structures. These structures are shown to be compatible in [HZ94]. Introduce the skew-adjoint anti-derivative operator

$$D^{-1}(f)(x) = \frac{1}{2}(\int_{-\infty}^{x} - \int_{x}^{\infty})f(y)dy.$$

Then the first Hamiltonian structure can be expressed as

$$u_t = J_1 \frac{\delta H_1}{\delta u}, \qquad J_1 = u_x D^{-2} - D^{-2} u_x, \qquad H_1[u] = \frac{1}{2}\int_{\mathbb{R}} u_x^2 \, dx,$$

while the second one reads

$$u_t = J_2 \frac{\delta H_2}{\delta u}, \qquad J_2 = D^{-1}, \qquad H_2[u] = \frac{1}{2}\int_{\mathbb{R}} u u_x^2 \, dx \, .$$

Consequently the Hunter-Saxton equation is bi-Hamiltonian, i.e., it can be written as a Hamiltonian differential equation of two compatible Hamiltonian operators. These Hamiltonian structures can be derived from the Lagrangians in Section 2. The notion $\frac{\delta}{\delta u}$ denotes the variation operator with respect to u, just as in Section 2. Moreover the Hunter-Saxton equation is completely integrable. These properties are discussed in greater detail in [HZ94].

Classical solutions to Hunter-Saxton equation will also satisfy an infinite number of conservation laws. Some of the conservation laws are derived in [HS91]. In [HZ94] it is shown that smooth solutions will conserve an infinite number of Hamiltonian functionals, and thus satisfy an infinite number of associated conservation laws. In particular we can employ Noether's theorem [Mar06] to obtain a few of the conservation laws associated with the Hunter-Saxton equation. Noether's theorem states that for every continuous transformation under which the action functional is invariant, there is an associated conservation law. A symmetry of an action functional is defined as a transformation that leaves the action functional invariant, so we are essentially looking for symmetries of action functionals. From Section 2 we know there are two action functionals, but we confine our attention to the functional (2.13). We observe four apparent symmetries: invariance with respect to space translations ($\hat{x} = x + \epsilon, \hat{t} = t, \hat{u} = u$), time translations ($\hat{x} = x, \hat{t} = t + \epsilon, \hat{u} = u$) , scale invariance ($\hat{x} = \epsilon x, \hat{t} = \epsilon t, \hat{u} = u$) and Galilean invariance ($\hat{x} = x + \epsilon t, \hat{t} = t, \hat{u} = u + \epsilon$). Set $v(x,t) = u_x(x,t)$, then these symmetries lead to the following conservation laws, respectively,

$$(v^2)_t + (uv^2)_x = 0, \tag{3.3a}$$

$$(uv^2)_t - (2uvu_t + u_t^2)_x = 0, \tag{3.3b}$$

$$(tuv^2 - xv^2)_t - (xuv^2 + 2tuvu_t + tu_t^2)_x = 0, \tag{3.3c}$$

$$(v - tv^2)_t + (u_t + 2uv - tuv^2)_x = 0. \tag{3.3d}$$

Equation (3.3a) is an energy equation, and conservative solutions satisfy this equation even after blow up. The energy equation and variants of it, will be used extensively in this thesis. In particular it will be used for the classification of conservative traveling waves, and when we consider numerical algorithms for conservative solutions. We will now proceed by discussing what happens for classical solutions of the Hunter-Saxton equation. Then the concept of weak solution is introduced, before we show by an example the difference between a dissipative and a conservative solution, and then define these concepts rigorously.

3.1 Classical solutions of the Hunter-Saxton equation

Consider the initial-value problem for the differentiated Hunter-Saxton equation

$$(u_t + uu_x)_x = \frac{1}{2}u_x^2, \tag{3.4a}$$

$$u|_{t=0} = u_0(x), \tag{3.4b}$$

where we assume that u_0 is a smooth function. Furthermore assume that u is a smooth solution to the Cauchy problem (i.e., a C^2-function, satisfying the equation at least in the classical sense). Then we can apply the method of characteristics. Define a characteristic coordinate ξ such that $x = X(\xi, t)$ and set

$$U(\xi, t) = u(X(\xi, t), t). \tag{3.5}$$

We trace the solution along a characteristic represented by $X(\xi, t)$. Hence $X(\xi, t)$ gives the position of the characteristic emanating from (ξ, t_0), where we for convenience take $t_0 = 0$, so that the characteristic crosses $(\xi, 0)$. $U(\xi, t)$ is the solution to the Cauchy problem along the characteristic. Naturally, we can also interpret U as the velocity of the characteristic. This leads to

$$X_t(\xi, t) = U(X(\xi, t), t), \tag{3.6a}$$
$$X(\xi, 0) = \xi. \tag{3.6b}$$

A direct calculation of the time-derivative of the quantity U yields

$$U_t = \frac{d}{dt} u(X(\xi, t), t) = u_t \circ X + X_t u_x \circ X = (u_t + u u_x) \circ X. \tag{3.7}$$

The change of variable $x = X(\xi, t)$ is done for a fixed time t, and the new independent variable is ξ instead of x. Taking the partial derivative with respect to ξ on both sides of (3.7) results in

$$U_{\xi t} = \Big((u_t + u u_x) \circ X \Big)_x X_\xi.$$

Define a new variable by $w(\xi, t) = X_\xi(\xi, t)$. We observe that $\frac{\partial \xi}{\partial X} = \frac{1}{w}$, provided $X_\xi \neq 0$. Moreover we see immediately using (3.6a) that we have

$$\begin{aligned} w_t = X_{\xi t} &= \frac{d}{d\xi} U(\xi, t) = U_\xi(\xi, t), \\ u_x &= \frac{U_\xi}{X_\xi} = U_\xi \frac{1}{w}. \end{aligned} \tag{3.8}$$

Using the derived relations, the left side of the Hunter-Saxton equation (3.4a) transforms into

$$(u_t + u u_x)_x = U_{\xi t} X_\xi^{-1} = w_{tt} \frac{1}{w}.$$

The right-hand side of (3.4a) transforms into

$$\frac{1}{2} u_x^2 = \frac{1}{2} (U_\xi \frac{1}{w})^2 = \frac{1}{2} (w_t \frac{1}{w})^2.$$

Therefore we obtain a second order ODE for w. To solve this ODE we need two initial conditions. The first part of the initial data is given by differentiating (3.6b) with respect to ξ. Moreover $w_t(\xi, 0) = U_\xi(\xi, 0) = u_0(X(\xi, 0))_\xi = u_0'(\xi)$. Thus the Cauchy problem (3.4a)-(3.4b) transforms into

$$w w_{tt} = \frac{1}{2} (w_t)^2, \tag{3.9a}$$
$$w(\xi, 0) = 1, \tag{3.9b}$$
$$w_t(\xi, 0) = u_0'(\xi), \tag{3.9c}$$

which is a second-order nonlinear initial value problem. A general explicit solution can be found for this problem, in particular we find

$$\begin{aligned} w = X_\xi &= \frac{w_t(\xi, 0)^2 t^2}{4 w(\xi, 0)} + w_t(\xi, 0) t + w(\xi, 0) \\ &= \left(1 + \frac{1}{2} u_0'(\xi) t \right)^2. \end{aligned} \tag{3.10}$$

This shows that X_ξ is nonnegative and that the map $\xi \to X(\xi, t)$ is an absolutely continuous increasing diffeomorphism on the line for each time $t \in [0, t^*)$, where t^* is the first time where $X_\xi(\xi, t^*) = 0$. At time $t = t^*$ we might have $X_\xi(\xi, t) = 0$ for all ξ in an arbitrary interval $\xi \in I \subseteq \mathbb{R}$, and the map is no longer an increasing diffeomorphism. The next theorem yields an explicit formula for smooth solutions of the Hunter-Saxton equation, and an expression for the blow-up time of the spatial derivative. This result is taken from [HS91].

Theorem 3.1 (Blow-up classical)**.** *Every smooth solution to the initial value problem* (3.4a)-(3.4b) *can be expressed implicitly by the system*

$$U(\xi, t) = u_0(\xi) + tg(\xi) + h'(t), \tag{3.11a}$$

$$X(\xi, t) = \xi + u_0(\xi)t + \frac{1}{2}t^2 g(\xi) + h(t), \tag{3.11b}$$

where $g'(\xi) = \frac{1}{2}(u_0'(\xi))^2$ *and* $x = X(\xi, t)$*. Here* h *is an arbitrary function with* $h(0) = h'(0) = 0$*. Suppose the initial data* u_0 *for* (3.4a)-(3.4b) *is not monotonically increasing. Then the smooth solution* $u(x, t)$ *exists in a time interval* $t \in (0, t^*)$*, where*

$$t^* = \frac{2}{\sup_\xi\{-u_0'(\xi)\}}. \tag{3.12}$$

t^* *is the blow-up time, i.e.,* $\inf(u_x) \to -\infty$ *as* t *approaches* t^* *from below.*

Proof. To obtain the implicit solution expression we first expand the parenthesis in (3.10) and integrate with respect ξ. Then we use the relation $X_t = U$ to determine U. The function $h(\cdot)$ and its derivative $h'(\cdot)$ have to be zero at $t = 0$, since we require $U(\xi, 0) = u_0(\xi)$ and $X(\xi, 0) = \xi$. Conversely we can directly check that (3.11a)-(3.11b) satisfy the Hunter-Saxton equation provided we can solve (3.11b) in terms of the characteristic variable ξ. That is, we can invert X to get

$$\xi = X^{-1}(x, t). \tag{3.13}$$

If we want to uniquely determine $h(\cdot)$, and thus get a unique solution to the Cauchy problem (3.4a)-(3.4b), we need to pose an additional boundary condition. Regarding the blow up, by the implicit function theorem, there is a smooth solution to (3.13) if $X_\xi \neq 0$. Using (3.10) we see that this is guaranteed up till time t^* given by the theorem, at time $t = t^*$, X_ξ becomes zero. Moreover by the expression for u_x in (3.8) we get

$$u_x = \frac{w_t}{X_\xi} = \frac{u_0'(\xi)(1 + \frac{1}{2}u_0'(\xi)t)}{(1 + \frac{1}{2}u_0'(\xi)t)^2} = \frac{u_0'(\xi)}{(1 + \frac{1}{2}u_0'(\xi)t)}$$

which tends to $-\infty$ as $t \to t^*$. □

Theorem 3.1 states that every classical solution to the Hunter-Saxton system experiences wave breaking within finite time, provided the initial data u_0 is not monotonically increasing, and we have an explicit expression for the breaking time, t^*. Classical solutions cease to exist at time t^*. We recognize $g(\xi)$ as the initial kinetic energy in the system. For classical solutions this energy is conserved. Characteristics focus upon wave breaking, i.e., approach the same tangent, in contrast to hyperbolic conservation laws where they collide. We can continue the solution beyond wave breaking in various ways, so uniqueness is lost upon wave breaking. All these continuations are weak solutions, which is the topic of the next subsection.

3.2 Weakly admissible solutions of the Hunter-Saxton equation

Several notions of weak solutions to the Hunter-Saxton equation have been introduced in the literature. In [BC05], Bressan and Constantin discuss some weak solution notions. In particular the definitions in [HS91] and [HZ95] are compared. We will however stick with the definition in [Daf11]. As mentioned since it is natural to require the kinetic energy to stay finite at all times we can enforce additional regularity onto weak solutions of the Hunter-Saxton equation, compared to what one typically requires for weak solutions to hyperbolic conservation laws.

Definition 3.1 (Weak solution)**.** A continuous function $u(x,t) \in C(\mathbb{R} \times [0,\infty); \mathbb{R})$ is a weak solution to the Cauchy problem (3.1a) - (3.1b) if the following holds

1. $u(\cdot, t)$ is absolutely continuous on $\mathbb{R}$ for all $t \in [0,\infty)$.
2. $u_x(\cdot, t) \in L^\infty([0,\infty); L^2(\mathbb{R}))$.
3. The Hunter-Saxton equation holds in a distributional sense with $u(x,0) = u_0(x)$, that is

$$\int_0^\infty \int_{\mathbb{R}} \left(\phi_t u + \frac{1}{2}\phi_x u^2 + \frac{1}{4}\phi \left[\int_{-\infty}^x u_x^2 dy - \int_x^\infty u_x^2 dy \right] \right) dx\, dt + \int_{\mathbb{R}} \phi|_{t=0} u_0\, dx = 0.$$

In [HS91] the authors introduced an entropy-like condition, in a similar spirit to what one does for conservation laws. The definition is stated next.

Definition 3.2 (Weakly admissible)**.** A weak solution u to the Cauchy problem for the Hunter-Saxton equation is said to be weakly admissible if

$$(u_x^2)_t + (uu_x^2) \leq 0,$$

holds in the sense of distributions.

This admissibility criterion requires that the total energy (3.2) is a non-increasing function of time, it is based on the transport equation for the energy density $u_x^2\, dx$

$$\underbrace{(u_x^2)_t}_{\text{Rate of change of energy}} + \underbrace{(uu_x^2)_x}_{\text{Energy flux}} = 0.$$

The criterion restricts in particular the appearance of corners in solutions. However it is not strong enough to force uniqueness to the Cauchy problem for the Hunter-Saxton equation. This is illustrated in [HS91] by an explicit example. Which motivates the stronger concepts of dissipative and conservative solutions.

We will now consider an explicit weak solution to the Hunter-Saxton equation where we extend beyond wave breaking. We will use a piecewise C^2 initial data inspired by [Bre16], but now adapted to the skew-symmetric integration operator, rather than the one used in [Bre16]. This is used to illustrate the difference in nature between conservative and dissipative solutions. Now it is important to notice as pointed out in [CGH19], that different formulations of the Hunter-Saxton equation posses different explicit solutions. Hence there will be a difference in the explicit solutions of the Cauchy problem to

$$u_t + uu_x = \frac{1}{2}\int_0^x u_x^2(y,t)dy, \tag{3.14}$$

and (3.1a). But they all formally lead to the same differentiated form of the Hunter-Saxton equation (which is the original form of the system). In (3.14), we essentially consider the accumulated kinetic energy from a fixed origin $x = 0$ up till the point x, while in (3.1a) we consider the kinetic energy accumulated all the way from $-\infty$ up till the point x and subtract all the kinetic energy ahead of that particular point, i.e., from x to ∞.

Example 3.1. We consider the Hunter-Saxton equation with the following piecewise affine initial data

$$u_0(x) = \begin{cases} 0 & \text{if } x < 0 \\ x & \text{if } 0 \leq x < 1 \\ 2 - x & \text{if } 1 \leq x \leq 2 \\ 0 & \text{if } 2 < x \end{cases}.$$

The initial data is shown in the upper part of Figure 6. Here the direction of movement of the different parts of the initial data is indicated by arrows (given by integrating $U_t = \frac{1}{2}(H - \frac{1}{2}K)$, which is shown in the next subsection). The length of the arrows give a rough estimate of the magnitudes of the velocity at the various points. In particular the peak at $x = 1$ moves faster than the part at $x = 0$ and $x = 2$. Therefore the characteristic starting at $x = 1$ will catch up with that starting at $x = 2$, while it will move further and further away from the characteristic starting at $x = 0$. The solution to the Cauchy problem is

$$u(x,t) = \begin{cases} -\frac{t}{2} & \text{if } x < -\frac{t^2}{4} \\ \frac{2x-t}{t+2} & \text{if } -\frac{t^2}{4} \leq x < t+1 \\ \frac{2x-t-4}{t-2} & \text{if } t+1 \leq x \leq 2+\frac{t^2}{4} \\ \frac{t}{2} & \text{if } 2+\frac{t^2}{4} < x \end{cases}, \tag{3.15}$$

which is found by using the Euler-Lagrange formalism introduced in the next subsection. Here we observe that $u_x \to -\infty$ as $t \uparrow 2$ at $x = 3$, thus the solution experiences wave breaking at $(x^*, t^*) = (3, 2)$. This is also the breaking time we expect according to Theorem 3.1.
An alternative way to find the solution is to apply the method of characteristics to find the characteristics emanating from the breakpoints and the solution along these characteristics. Then one can linearly interpolate between the characteristics to find the solution everywhere. That is, for this particular problem one considers the characteristics: $t \to x_0(t)$, $t \to x_1(t)$ and $t \to x_2(t)$ starting at 0, 1 and 2, respectively. In Section 7, we show that the breakpoints will move along characteristics. The method of characteristics yields the following system of ODEs

$$\dot{x}(t) = u(x(t), t), \tag{3.16a}$$

$$\dot{u}(x(t), t) = \frac{1}{4}\left(\int_{-\infty}^{x(t)} u_x^2(y,t)dy - \int_{x(t)}^{\infty} u_x^2(y,t)dy \right), \tag{3.16b}$$

$$\int_{-\infty}^{x(t)} u_x^2(y,t)dy = \int_{-\infty}^{x(0)} u_{0,x}^2(y)dy, \tag{3.16c}$$

with initial data $(x, u)|_{t=0} = (\bar{x}, \bar{u}(\bar{x}))$. Consider for instance the characteristic starting at the origin, $t \to x_0(t)$ then we get

$$\dot{u}(x_0(t), t) = -\frac{1}{2},$$

hence we obtain

$$u(x_0(t), t) = -\frac{t}{2} \qquad \text{and} \qquad x_0(t) = -\frac{t^2}{4}.$$

We observed that $\|u_x(\cdot, t)\|_{L^\infty(\mathbb{R})}$ blows up as $t \uparrow 2$. What happens is that the characteristic $x_1(t) = t + 1$ approaches $x_2(t) = 2 + \frac{t^2}{4}$ as t tends to $t^* = 2$, and they coincide at $t = t^*$. The characteristics are without further ado not uniquely determined past this time. We have a dichotomy to choose from. We can continue the solution past wave breaking with a dissipative solution or a conservative solution. Before wave breaking the conservative and dissipative solutions will coincide. It is first when we extend the solution past blow up, the two solution concepts start to differ.

- **Dissipative solution**: We force the energy to disappear at the fastest possible rate, so after $t > 2$ we continue the solution with decreased energy. The solution in this case becomes

$$u_d(x,t) = \begin{cases} -\frac{t}{2} & \text{if } x \leq -\frac{t^2}{4} \\ \frac{2x-t}{t+2} & \text{if } -\frac{t^2}{4} < x \leq t+1 \\ \frac{t}{2} & \text{if } x \geq t+1 \end{cases} \qquad t > t^* = 2\,.$$

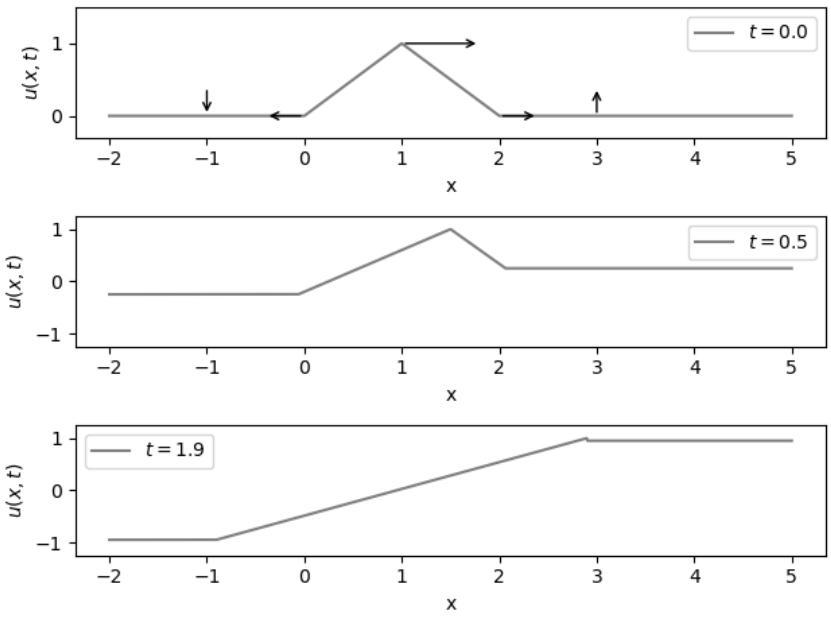

Figure 6: The solution (3.15) at various times before wave breaking.

Figure 7a shows what happens when the two characteristics x_1 and x_2 meet, the part, $u = \frac{2x-t-4}{t-2}$, vanishes. The characteristics are unique forward in time, we cannot however go backward in time for dissipative solutions, as dissipation of energy represents an irreversible process. Following the characteristic $x_1(t) = t + 1$ backward to time $t = t^*$, we do no longer know where we came from. Notice that the initial energy, $E_0 = 2$. After blow-up, continuing with a dissipative solution, the energy is $E = 1$, hence we have lost half of the energy.

- **Conservative solution**: For conservative solutions, there can be infinitely many characteristics originating from or passing through the same point. Taking advantage of the additional energy conservation equation

$$(u_x^2)_t + (uu_x^2)_x = 0,$$

results in the additional integral identity (3.16c). Thus for conservative solutions we require (3.16c) to also hold past wave breaking for any characteristic $t \to x(t)$ starting at $x|_{t=0} = x_0$. Hence we can uniquely trace out characteristics. The conservative solution becomes

$$u_c(x,t) = \begin{cases} -\frac{t}{2} & \text{if } x \leq -\frac{t^2}{4} \\ \frac{2x-t}{t+2} & \text{if } -\frac{t^2}{4} \leq x \leq t+1 \\ \frac{2x-t-4}{t-2} & \text{if } t+1 \leq x \leq 2+\frac{t^2}{4} \\ \frac{t}{2} & \text{if } x \geq 2+\frac{t^2}{4} \end{cases} \qquad t > t^* = 2 \quad .$$

This is precisely the same expression as we had before wave breaking. Some characteristics of the conservative solution are shown in Figure 7b. Here we can follow the characteristics both backward and forward in time.

We will not be too concerned about dissipative solutions in this thesis, but for completeness we define the notion of a dissipative solution. Again we use the same definition as in [Daf11].

Definition 3.3 (Dissipative sol.)**.** A weak solution u to the Cauchy problem (3.1a)-(3.1b) is called a dissipative solution if the following holds

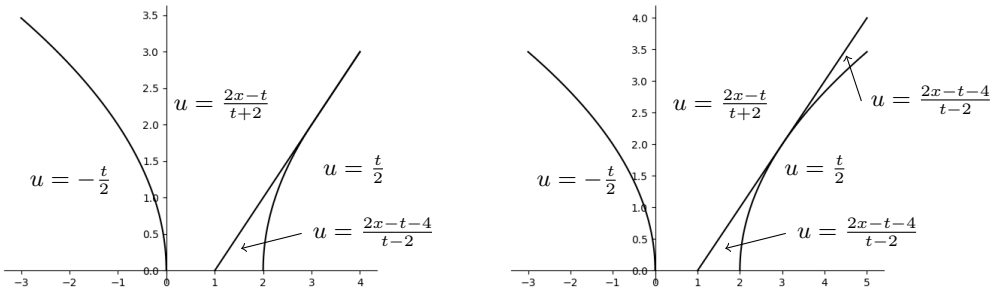

(a) Characteristics for the dissipative solution. **(b)** Characteristics for the conservative solution.

Figure 7: Characteristics for the solution to the example in the dissipative case (a) and the conservative case(b). In the dissipative case, the characteristics are unique forward in time, while in the conservative case there can be infinitely many characteristics passing through the same point (x^*, t^*).

1. The derivative satisfies

$$u_x(x,t) \leq M \quad \text{for } (x,t) \in K,$$

where $K \subseteq \mathbb{R} \times (0,\infty)$ is any compact subset and M is a finite constant.

2. The following convergence holds

$$u_x(\cdot,t) \to u_0'(\cdot) \quad \text{strongly in } L^2(\mathbb{R}),$$

as $t \downarrow 0$.

We postpone the definition of a conservative solution to the next subsection. As observed in the previous example, generally for smooth initial data, the dissipative and conservative solutions will coincide while the solution still is smooth, but they become distinct past blow-up. Dissipation of energy is an irreversible process. Dissipative solutions can therefore only be extended forward in time. Conservation of energy on the other hand is reversible and conservative solutions can be extend both backwards and forwards. In general for continuous and piecewise linear solutions, wave breaking will manifests itself at times where two or more characteristics focus.

Figure 8 shows two characteristics that meet at a point (x^*, t^*). The shaded region is where the energy confined between the characteristics is located, and we see that as $t \uparrow t^*$, the energy is concentrated on a smaller and smaller set, until the two characteristics meet and the energy is thus concentrated at the single point (x^*, t^*). All characteristics emanating from/passing through points in between $(\xi, 0)$ and $(\eta, 0)$ will also focus at this point. Each individually contributing to the energy accumulation. The concentration of energy confined in an interval to a single point (x^*, t^*) upon wave breaking, is how wave breaking manifests itself for continuous, piecewise linear solution. We can also describe what happens to the solution itself upon wave breaking. The slope of a linear segment with negative slope tends to $-\infty$. At the blow up time t^*, the left and right corner of that linear segment collide, and the interval $I(t)$ occupied by the segment shrinks to a single point. At times past wave breaking, the corners move apart again. We will observe in Section 5 that wave breaking manifests itself very differently for cuspons. At wave breaking, the energy density cannot be described by $u_x^2\,dx$, since the energy concentrates at a Lebesgue null set. We will observe in the next subsection, that in general one describes the energy density by a positive Radon measure. Usually this measure is finite, although this is not the case for non-trivial traveling waves of the Hunter-Saxton equation. When the measure

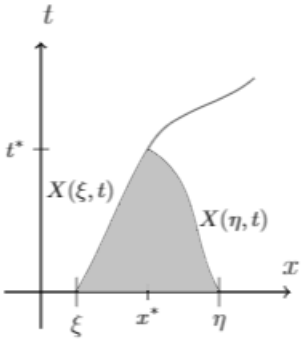

Figure 8: Two characteristics emanating from $(\xi, 0)$ and $(\eta, 0)$ meeting at time $t = t^*$. The energy confined between the two characteristics is located in the gray-shaded region. This energy concentrates at the point (x^*, t^*).

is finite, then the energy remains finite even at wave breaking, this implies that we can describe the energy as the cumulative distribution function of the associated Radon measure. In the case of a dissipative solution, we remove the part of the energy that concentrates and continue the solution with the single characteristics $X(\xi, t)$. This is in contrast to the conservative case, where we again reinsert the concentrated energy into the system.

The focusing of characteristics cause a loss in uniqueness. For $t \in [0, t^*)$, each point on the interval $[\xi, \eta]$ has a unique characteristic emanating from it and as we saw in Section 3.1, X_ξ given by (3.10) is positive. Therefore by the implicit function theorem we can invert $x = X(\xi, t)$ and solve for the characteristic variable ξ. For $t \geq t^*$, we no longer know which characteristic is associated to which starting point, and the time at which this first happens is given by Theorem 3.1. This is where X_ξ becomes zero, and we cannot invert $x = X(\xi', t)$ where $\xi' \in [\xi, \eta]$.

3.3 Eulerian to Lagrangian coordinates

We are interested in constructing conservative solutions to the Hunter-Saxton equation, hence we augment the equation with an energy equation. Smooth conservative solutions of the Hunter-Saxton equation can in Eulerian coordinates be written as solutions to the system

$$u_t + uu_x = \frac{1}{4}\left(\int_{-\infty}^{x} u_x^2 dy - \int_{x}^{\infty} u_x^2 dy \right), \tag{3.17a}$$

$$(u_x^2)_t + (uu_x^2)_x = 0. \tag{3.17b}$$

We want to recast this system to Lagrangian coordinates. We first introduce the characteristics

$$X_t(\xi, t) = u(X(\xi, t), t),$$

and then the Lagrangian velocity U

$$U(\xi, t) = u(X(\xi, t), t).$$

We here consider a particular particle moving along the particle path described by $X(\cdot, \cdot)$, where U denotes its velocity as it propagates along this curve. We also introduce the cumulative Lagrangian energy

$$H(\xi, t) = \int_{-\infty}^{X(\xi,t)} u_x^2(y, t) dy,$$

measuring the energy accumulated up to the characteristic $X(\xi, t)$. We can formally derive the time-evolution of the variables (X, U, H), leading to the Lagrangian system. Computing

formally we find

$$U_t(\xi,t) = \frac{d}{dt}u(X(\xi,t),t) = X_t u_x \circ X + u_t \circ X = \frac{1}{4}\Big(\int_{-\infty}^{X(\xi,t)} u_x^2 dy - \int_{X(\xi,t)}^{\infty} u_x^2 dy\Big)$$
$$= \frac{1}{4}H(\xi,t) + \frac{1}{4}(\int_{-\infty}^{X(\xi,t)} u_x^2 dy - \int_{-\infty}^{\infty} u_x^2 dy) = \frac{1}{2}H - \frac{1}{4}K,$$

where $K = H(\infty,t)$ is time-independent and represents the total cumulative Lagrangian energy. Now due to the energy equation (3.17b) we also formally get

$$H_t = \frac{d}{dt}\int_{-\infty}^{X(\xi,t)} u_x^2(y,t)dy = \int_{-\infty}^{X(\xi,t)} (u_x^2)_t dy + X_t u_x^2 \circ X$$
$$= -\int_{-\infty}^{X(\xi,t)} (uu_x^2)_x dy + (uu_x^2)\circ X = 0.$$

In this formal computation we require u and u_x to be smooth and decay rapidly at infinity. Hence formally (3.17a)-(3.17b) in Eulerian coordinates is equivalent to the following system of linear ODEs

$$X_t = U, \tag{3.18a}$$
$$U_t = \frac{1}{2}H - \frac{1}{4}K, \tag{3.18b}$$
$$H_t = 0. \tag{3.18c}$$

Global existence and uniqueness follow by linearity. Since the system is linear, there is no exchange of energy between characteristics. This is in strong contrast to the corresponding Lagrangian formulation of the closely related Camassa-Holm equation [HR07]. Here the resulting Lagrangian system is nonlinear, allowing for energy exchange between characteristics. The explicit solution to (3.18a)-(3.18c) is

$$H(\xi,t) = H(\xi,0), \tag{3.19a}$$
$$U(\xi,t) = \frac{1}{2}(H(\xi,0) - \frac{1}{2}K)t + U(\xi,0), \tag{3.19b}$$
$$X(\xi,t) = \frac{1}{4}(H(\xi,0) - \frac{1}{2}K)t^2 + U(\xi,0)t + X(\xi,0). \tag{3.19c}$$

Everything thus far has been formal. It turns out that this also persists in the general case. In the general case we get an additional complication due to the occurrence of wave breaking. Here we give a brief overview of the Euler-Lagrange formalism, for complete proofs and derivations the reader is referred to [BHR10], [Nor16b] and [HR07]. We augment the integrated Hunter-Saxton equation with a second equation keeping track of the energy density

$$u_t + uu_x = \frac{1}{4}\Big(\int_{-\infty}^{x} d\mu - \int_{x}^{\infty} d\mu\Big), \tag{3.20a}$$
$$\mu_t + (u\mu)_x = 0. \tag{3.20b}$$

Here μ will be a non-negative Radon measure, which in regions where the solution is smooth coincides with the normal kinetic energy density $u_x^2\,dx$. When wave breaking occurs parts of the energy is concentrated on sets of Lebesgue measure zero. That is, energy is transferred from the absolutely continuous part of μ to the singular part. When we here talk about the absolutely continuous part μ_{ac} and the singular part μ_s of μ, it is always with respect to the Lebesgue measure on $\mathbb{R}$. One can continue the solution past wave breaking by various means. One can continue without manipulating the measure μ, resulting in conservative solutions, but one can also remove an α fraction of the concentrated energy from the singular part, leading to an α-dissipative solution. This concept is discussed in [GHR15] and [GN18]. We focus on the

conservative case. Thus in particular when there is a blow-up the energy is transferred from the absolutely continuous part of the measure to the singular part, and after the blow-up it is reinserted into the absolutely continuous part of the measure again.

One can compute conservative solutions to the Hunter-Saxton equation using the method of characteristics, but this only holds under the assumption that the Radon measure μ is purely absolutely continuous, i.e., has no singular part. By Theorem 3.1 we expect wave breaking to occur within finite time, thus the solutions obtained this way will only be valid locally. The Euler-Lagrange formalism is based on transforming from Eulerian to Lagrangian coordinates, and have the main benefits that this change linearizes the Hunter-Saxton equation and turns the measure μ into a function. Hence we can apply a generalization of the method of characteristics, leading to a system of ODEs taking values in a Banach space, which we can solve explicitly. One of the goals of this subsection is to define the function space we seek solutions to (3.18a)-(3.18c) in, and define mappings between Eulerian and Lagrangian coordinates, such that we can map the initial data in Eulerian coordinates to Lagrangian coordinates, solve the ODE system up to time t and then map the solution back to Eulerian coordinates. We will see that this yields a global conservative solution of (3.20a)-(3.20b). We define first an ambient Banach space, which possesses the underlying Banach structure of the space of Lagrangian solutions.

Definition 3.4. Define the following Banach spaces E_1 and E_2 by

$$E_1 := \{f \in L^\infty(\mathbb{R}) : f' \in L^2(\mathbb{R}) \ \& \ \lim_{\xi \to -\infty} f(\xi) = 0\},$$
$$E_2 := \{f \in L^\infty(\mathbb{R}) : f' \in L^2(\mathbb{R})\}.$$

We endow them with the norm

$$\|f\|_{E_j} = \|f\|_{L^\infty(\mathbb{R})} + \|f'\|_{L^2(\mathbb{R})},$$

for $j \in \{1, 2\}$. Moreover define $B = E_2 \times E_2 \times E_1$, which we equip with the following norm

$$\|(f_1, f_2, f_3)\|_B = \|f_1\|_{E_2} + \|f_2\|_{E_2} + \|f_3\|_{E_1},$$

where $f = (f_1, f_2, f_3) \in B$.

The space B is too large and we want to restrict it considerably. In particular we want to restrict it in such a way, that it only contains solutions to the Lagrangian system (3.18a)-(3.18c) and nothing more, this will lead to $\mathcal{F}$. We will observe that in Eulerian coordinates we have two variables (u, μ), and these are transformed into 3 when we go to Lagrangian coordinates. This is due to the simple fact that there are several ways to parameterize the same particle path. Thus one can have two distinct solutions in Lagrangian coordinates that correspond to the same motion, and hence the same solution in Eulerian coordinates.

Definition 3.5 (Eulerian coord.)**.** The set $\mathcal{D}$ consists of pairs (u, μ) such that

1. $u \in E_2$
2. μ is a non-negative finite Radon measure with absolutely continuous part

$$d\mu_{\text{ac}} = u_x^2 \, dx,$$

with respect to the Lebesgue measure.

Notice that in general, the refined Lebesgue decomposition theorem from measure theory, allows us to decompose a non-negative Radon measure μ into an absolutely continuous part, μ_{ac}, a point measure μ_p and a singular continuous part μ_{sc} with respect to the Lebesgue measure on $\mathbb{R}$. That is, we can decompose μ as

$$\mu = \mu_{ac} + \mu_p + \mu_{sc}.$$

We now recall what it means for a measure to be singular and absolutely continuous with respect to another measure, and the particular form a point measure takes.

Recall 3.1. Let $(X, \mathcal{B})$ be a measurable space. We recall the following terminology:

- Singular measure: Let ν, $\mu : \mathcal{B} \to [0, \infty]$ be two positive measures, then we say that ν and μ are mutually singular, denoted by $\nu \perp \mu$, if there is a set $E \in \mathcal{B}$ such that

$$\mu(E) = 0,$$
$$\nu(E^c) = 0.$$

- Absolutely continuous: Let $\nu, \mu : \mathcal{B} \to [0, \infty]$ be two positive measures, we say that ν is absolutely continuous with respect to μ, denoted $\nu << \mu$, if

$$\mu(E) = 0 \implies \nu(E) = 0,$$

  for any set $E \in \mathcal{B}$.

- Point measure: A point measure or a discrete measure on $\mathbb{R}$ takes the following form

$$\mu_p = \sum_{k \in \mathbb{N}} c_k \delta_{x_k},$$

  where $\{x_k\}$ is a countable sequence of points in $\mathbb{R}$ and $\{c_k\}$ is a sequence of real-valued scalars, while δ_{x_k} denotes the Dirac measure for the point x_k.

The intuition behind the notion of two measures being singular with respect to each other, is that they are supported on disjoint sets, so their "support" is disjoint. While the notion of absolute continuity is in some sense the opposite, meaning that the measures are supported on the same sets. In contrast to the notion of singular measures, the notion of absolute continuity is not a symmetric relation. For the peakon example considered in Subsection 3.2, the energy concentrated at a single point, i.e., energy is transferred over to the point measure upon wave breaking.
This refined Lebesgue decomposition is done with respect to the Lebesgue measure on $\mathbb{R}$. Hence $\mu_{ac} << m$ and $\mu_s \perp m$ where m denotes the Lebesgue measure. For the absolutely continuous part we have the Radon-Nikodym theorem at our disposal, and that is what we take advantage of in 2. in Definition 3.5. This theorem allows us to represent the absolutely continuous part with respect to another measure as an integration with weight. We require

$$\mu_{ac}(E)(t) = \int_E u_x^2(y, t) dx,$$

which is written shortly as $d\mu_{ac} = u_x^2 dx$. Next we define the set of Lagrangian coordinates, $\mathcal{F}$.

Definition 3.6 (Lagrangian coord.)**.** The set $\mathcal{F}$ consists of triples $(\eta, U, H) \in B$ such that

1. $(\eta, U, H) \in [W^{1,\infty}(\mathbb{R})]^3$ with $\eta(\xi) = X(\xi) - \xi$
2. $X_\xi \geq 0$, $H_\xi \geq 0$ almost everywhere and

$$X_\xi + H_\xi \geq c > 0,$$

   holds for almost every $\xi \in \mathbb{R}$ and $t \in \mathbb{R}$.

3. $X_\xi H_\xi = U_\xi^2$ almost everywhere.

$\mathcal{F}$ is a normed space with the norm inherited from B, in particular $\mathcal{F} \subseteq B$. $u_x^2\, dx$ is the kinetic energy density in Eulerian coordinates, or the full energy density when solutions are smooth, while $H_\xi d\xi$ is the energy density in Lagrangian variables. To see this, we employ 3. in the definition of $\mathcal{F}$, stating that we have $X_\xi H_\xi = U_\xi^2$ almost everywhere, use the change of variable

$x = X(\xi, t)$ for fixed $t \in \mathbb{R}$ and assume a smooth characteristic such that we have $X^{-1}(\mathbb{R}) = \mathbb{R}$. Together with the chain rule, $U_\xi = (u_x \circ X)X_\xi$, this causes the kinetic energy to transform into

$$\begin{aligned}\int_{\mathbb{R}} u_x^2(y,t)dy &= \int_{\mathbb{R}} u_x^2 \circ X X_\xi d\xi = \int_{\{\xi\in\mathbb{R}: X_\xi(\xi,t)>0\}} \frac{U_\xi^2}{X_\xi} d\xi \\ &= \int_{\{\xi\in\mathbb{R}: X_\xi(\xi,t)>0\}} H_\xi d\xi.\end{aligned}$$

By [Theorem 2.3, [BHR10]] we know that for almost every t we have $X_\xi(\xi, t) > 0$ for almost every $\xi \in \mathbb{R}$. Consequently the set $\{\xi \in \mathbb{R} : X_\xi(\xi, t) > 0\}$ is of full measure. Therefore we have the relation

$$\int_{\mathbb{R}} u_x(y,t)^2 dy = \int_{\mathbb{R}} H_\xi d\xi,$$

for a.e. $t \in \mathbb{R}$ and smooth solutions. Hence it is natural to interpret $H_\xi d\xi$ as the energy density in Lagrangian coordinates.

Time evolution of the Hunter-Saxton equation in Lagrangian coordinates is determined by the system (3.18a)-(3.18c), and in [BHR10] it is shown that the solution of this system remains in $\mathcal{F}$ at all times. We introduce a solution operator $S_t : \mathcal{F} \to \mathcal{F}$ defined by

$$S_t((X_0, U_0, H_0)) = (X(t), U(t), H(t)).$$

This operator takes initial data in $\mathcal{F}$ and solves the Lagrangian system (3.18a)-(3.18c) up till time t, where the solution is given by (3.19a)-(3.19c). In [BHR10] it is shown that the solution operator S_t constitute a C^0-semigroup, where the continuity is with respect to the inherited norm from the ambient space B.

The natural strategy now is, given some initial data $(u_0, \mu_0) \in \mathcal{D}$ we want to transform it to Lagrangian coordinates and apply the solution operator S_t to get a solution to the Lagrangian system at time t. In particular we will define a mapping, L, taking the initial data (u_0, μ_0) to the subspace

$$\mathcal{F}_0 := \{Y = (X, U, H) \in \mathcal{F} \text{ s.t } X + H = I_{\mathcal{F}_0}\},$$

in a rigorous manner, where $I_{\mathcal{F}_0}$ denotes the identity function on $\mathcal{F}_0$.

Definition 3.7. For any $(u, \mu) \in \mathcal{D}$, set

$$X(\xi) = \sup\{x \in \mathbb{R} : \mu((-\infty, x)) + x < \xi\}, \tag{3.21a}$$
$$H(\xi) = \xi - X(\xi), \tag{3.21b}$$
$$U(\xi) = u \circ X(\xi), \tag{3.21c}$$

then $Y = (\eta, U, H) \in \mathcal{F}_0$ with $\eta(\xi) = X(\xi) - \xi$. We denote by $L : \mathcal{D} \to \mathcal{F}_0$ the map that associates to each pair $(u, \mu) \in D$ a triple (η, U, H) via (3.21a)-(3.21c).

After having solved the system of ODEs up to time t we want to map the solution back to Eulerian coordinates again, in order to get a solution to the original formulation of the problem. Here we want to recover a Radon measure from the Lagrangian coordinates. Therefore we will need to use the operation of pushing-forward a measure by a measurable function.

Definition 3.8 (push-forward)**.** Let $f : X \to Y$ be a measurable function between two sets X and Y, and let μ be a measure on X. Then we define the push-forward of μ by the function f as

$$f_\#(\mu)(E) = \mu(f^{-1}(E))$$

for any set $E \subset Y$.

One calls $f_{\#}(\mu)$ a push-forward measure, and one can show that this will be a measure on Y. We will now define a mapping $M : \mathcal{F} \to \mathcal{D}$ which transforms the solution in Lagrangian coordinates to a solution in Eulerian coordinates.

Definition 3.9. Given any element $Y = (X, U, H) \in \mathcal{F}$, we define a pair (u, μ) via

$$u(x,t) = U(\xi,t) \quad \text{for any } \xi \text{ such that } x = X(\xi,t) \tag{3.22a}$$

$$\mu = X_{\#}(H_\xi d\xi) \tag{3.22b}$$

which will belong to $\mathcal{D}$. We denote by $M : \mathcal{F} \to \mathcal{D}$ the map which associates to any triple $(X, U, H) \in \mathcal{F}$ a pair (u, μ) via (3.22a)-(3.22b).

Let E be a Borel measurable set then we can write (3.22b) as

$$\mu(E) = X_{\#}(H_\xi d\xi)(E) = \int_{X^{-1}(E)} H_\xi d\xi.$$

We summarize the key properties of the two mappings L and M introduced thus far. These are stated in [BHR10] and proved in [HR07], they read:

1. L and M are well defined.
2. The following inverse relations holds

$$L \circ M|_{\mathcal{F}_0} = I_{\mathcal{F}_0},$$
$$M \circ L = I_{\mathcal{D}},$$

   here $I_{\mathcal{F}_0}$ and $I_{\mathcal{D}}$ are the identity functions on $\mathcal{F}_0$ and $I_{\mathcal{D}}$, respectively.

Now as mentioned there is an ambiguity. Several solutions in Lagrangian coordinates may corresponds to the same solution in Eulerian coordinates. This is since there exists an additional degree of freedom referred to as relabeling in [BHR10]. Formally there may exist two elements $Y, \bar{Y} \in \mathcal{F}$ such that $\bar{Y} = Y \bullet f$ for some function f. Here $Y \bullet f = (X \circ f, U \circ f, H \circ f)$ is the group action defined below. Let u and $\bar{u}$ be the Eulerian solutions associated to Y and $\bar{Y}$, respectively. These are given by

$$U(\xi) = u \circ X(\xi), \quad \text{and} \quad \bar{U}(\xi) = \bar{u} \circ \bar{X}(\xi).$$

Now if X and $\bar{X}$ are invertible functions, we can solve for u and $\bar{u}$ to get

$$\bar{u} = \bar{U} \circ \bar{X}^{-1} = U \circ f \circ (X \circ f)^{-1} = U \circ X = u, \tag{3.23}$$

hence formally the solutions are identical in Eulerian coordinates, even though they are distinct in Lagrangian coordinates. The next group with associated group action is introduced to identify the Lagrangian elements corresponding to the same Eulerian solution.

Definition 3.10 (G and $\bullet$)**.** Let G be the subgroup of homeomorphism $f : \mathbb{R} \to \mathbb{R}$ such that

1. $f - I_d$, $f^{-1} - I_d \in W^{1,\infty}(\mathbb{R})$,
2. $f_\xi - 1$ belongs to $L^2(\mathbb{R})$.

We endow G with the group action $\bullet : \mathcal{F} \times G \to \mathcal{F}$, referred to as relabeling of Y by f, defined by

$$(Y, f) \to Y \bullet f = (X \circ f, U \circ f, H \circ f).$$

[Proposition 3.4 [HR07]] shows that this map is a true group action. In [Proposition 2.8, [BHR10]] it is shown that one can define an equivalence relation $Y \sim \bar{Y}$, stating that two elements are equivalent if the elements are equal under relabeling. Therefore we can define equivalence classes on $\mathcal{F}$ by

$$[Y] := \{\hat{Y} \in \mathcal{F} : \text{ there exist } g \in G \text{ such that } Y = \hat{Y} \bullet g\}.$$

The next result shows that all elements in the same equivalence class are mapped to the same solution in Eulerian coordinates.

Lemma 3.1. *Let $Y, \bar{Y} \in [Y]$ be two elements from the same equivalence class, then*

$$M(Y) = M(\bar{Y}).$$

Proof. Let $f \in G$ be such that $Y = \bar{Y} \bullet f$ be given and set

$$(u, \mu) = M(Y),$$
$$(\bar{u}, \bar{\mu}) = M(Y \bullet f).$$

One can show that X is surjective, thus given $x \in \mathbb{R}$, one can take $\xi \in \mathbb{R}$ such that $X(\xi) = x$. Now let $f^{-1}(\xi) = \bar{\xi}$. Then we have $X \circ f(\bar{\xi}) = x$ which implies $U \circ f(\bar{\xi}) = \bar{u}(x)$. However on the other hand, we have $f(\bar{\xi}) = \xi$, thus $U \circ f(\bar{\xi}) = U(\xi) = u(x)$. Hence we have $u(x) = \bar{u}(x)$, proving equality of u and $\bar{u}$.
Next we prove equality of the measures. We claim that for any Lipschitz continuous function g and $f \in G$ we have

$$(g \circ f)_\xi = g_\xi \circ f f_\xi. \tag{3.24}$$

To see this define the following sets

$$B_1 := \{\xi : g \text{ is differentiable at } \xi\}$$
$$B_2 := \{\xi : f \text{ and } (g \circ f) \text{ are differentiable at } \xi\}$$

Now since g and f are Lipschitz, so is their composition, and we have by Rademacher theorem that $m(B_i^c) = 0$ for $i \in \{1, 2\}$. Hence both sets are of full Lebesgue measure. Let $\xi \in B_2 \cap f^{-1}(B_1)$ then for $\xi' \neq \xi$ we have

$$\frac{(g \circ f)(\xi) - (g \circ f)(\xi')}{f(\xi) - f(\xi')} \frac{f(\xi) - f(\xi')}{\xi - \xi'} = \frac{(g \circ f)(\xi) - (g \circ f)(\xi')}{\xi - \xi'},$$

using the continuity of f and differentiability of g at ξ we can pass to the limit $\xi' \to \xi$. The left-hand side tends to $g_\xi \circ f f_\xi$, while the right-hand side tends to $(g \circ f)_\xi$. This proves the claim for $B_2 \cap f^{-1}(B_1)$. Since f^{-1} is Lipschitz and bijective by definition of G, we have by Rademacher theorem that $m(f^{-1}(B_1^c)) = 0$, hence (3.24) holds almost everywhere. Using the definition of $M : \mathcal{F} \to \mathcal{D}$, we have that $\mu = X_\#(H_\xi d\xi)$ thus for any $E \subseteq \mathbb{R}$

$$\bar{\mu}(E) = (X \circ f)_\#((H \circ f)_\xi d\xi)(E) = \int_{(X \circ f)^{-1}(E)} (H_\xi \circ f) f_\xi d\xi,$$

here we applied (3.24) to $(H \circ f)_\xi$. As f is invertible and $H_\xi \in L^\infty(\mathbb{R})$ by definition of $\mathcal{F}$, it is in particular in $L^1_{loc}(\mathbb{R})$ (actually $H_\xi \in L^1(\mathbb{R})$). Thus we can apply the change of variable, $\eta = f(\xi)$. This yields

$$\begin{aligned}\int_{(X \circ f)^{-1}(E)} (H_\xi \circ f) f_\xi d\xi &= \int_{f \circ (X \circ f)^{-1}(E)} H_\xi(\eta) d\eta \\ &= \int_{X^{-1}(E)} H_\xi(\eta) d\eta = X_\#(H_\xi d\xi)(E) = \mu(E).\end{aligned}$$

This comes from the fact that $f(\{\xi : X \circ f(\xi) \in E\}) = \{f(\xi) : X \circ f(\xi) \in E\}$. Hence the measures assign to every subset E of $\mathbb{R}$ the same value. Therefore the measures are equivalent on $\mathbb{R}$. □

In particular when one wants to measure the distance between two solutions in Lagrangian or Eulerian coordinates, this ambiguity is important. Then one can define a projection operator from $\mathcal{F}$ to $\mathcal{F}_0$, and one can show that every equivalence class has a unique representative in $\mathcal{F}_0$. In this thesis we are only interested in conservative solutions, and not in measuring the distance between solutions. Therefore we do not need to filter out a unique representative from the equivalence class. Next we define the notion of a conservative solution.

Definition 3.11 (conservative sol.)**.** A pair $(u,\mu)\in\mathcal{D}$ is said to be a weak global conservative solution of the Hunter-Saxton equation if $u\in C([0,\infty);L^\infty(\mathbb{R}))$ and $u_x\in L^\infty([0,\infty);L^2(\mathbb{R}))$. Moreover for all $\phi\in C_0^\infty(\mathbb{R}\times[0,\infty))$ both

$$0=\int_0^\infty\int_{\mathbb{R}}\left(\phi_t u+\frac{1}{2}\phi_x u^2-\frac{1}{4}\phi\left[\int_{-\infty}^{x}d\mu(t)+\int_x^\infty d\mu(t)\right]\right)dx\,dt+\int_{\mathbb{R}}\phi|_{t=0}u|_{t=0}dx,$$

and

$$0=\int_0^\infty\int_{\mathbb{R}}\big(\phi_t+u\phi_x\big)d\mu(t)dt+\int_{\mathbb{R}}\phi|_{t=0}d\mu|_{t=0},$$

hold. In addition one also requires $\mu(\mathbb{R})(t)=\mu|_{t=0}(\mathbb{R})$ for all $t\geq 0$.

Finally we introduce a solution operator $T_t:\mathcal{D}\to\mathcal{D}$, taking the initial data in Eulerian coordinates and evolving the initial data to a solution of the the Hunter-Saxton at time t. This map is defined as the composition of the introduced maps, i.e.,

$$T_t=M\circ S_t\circ L.$$

The main result we are interested in is the next Theorem, which is taken from [BHR10] and [Nor16b].

Theorem 3.2. *The operator $T_t:(u_0,\mu_0)\to(u(t),\mu(t))$, maps the initial data $(u_0,\mu_0)\in\mathcal{D}$ to a global conservative solution of the Cauchy problem for system* (3.20a)-(3.20b).

In [BHR10] a metric is introduced in order to make the flow of the Hunter-Saxton equation Lipschitz, then T_t constitutes a Lipschitz continuous semigroup. A refined Lipschitz metric based on the Wasserstein distance is introduced in [CGH19] which yields an upper bound with quadratic growth in t for the difference between two solutions starting with distinct initial data. For good illustrations about how to apply the Euler-Lagrange formalism to solve Cauchy problems, the reader is referred to [CGH19]. We will now illustrate how to apply this formalism to determine the solution of the example considered in the previous subsection, and later use the formalism in Section 5, Section 6, and Section 7.

Example 3.2. We are given the following initial data in Eulerian coordinates

$$u_0(x)=\begin{cases}0 & \text{for } x<0\\ x & \text{for } 0\leq x<1\\ 2-x & \text{for } 1\leq x\leq 2\\ 0 & \text{for } 2<x\end{cases}.$$

Since no wave breaking occurs initially the initial measure is purely absolutely continuous, and in particular μ and its associated cumulative energy are given by

$$\begin{aligned}\mu_0(x)&=(u_{0,x})^2(x)dx=1_{[0,2]}(x),\\ F_0(x)&=\mu_0((-\infty,x))=x1_{[0,2]}(x)+2\cdot 1_{[2,\infty)}(x).\end{aligned}$$

Next we will apply the operator $L:\mathcal{D}\to\mathcal{F}_0$ in Definition 3.7, to find the initial data in Lagrangian coordinates. $L(u_0,\mu_0)=(X_0,U_0,H_0)=Y_0\in\mathcal{F}$ is given by (3.21a)-(3.21c) leading to the initial characteristic given by

$$X_0(\xi)=\begin{cases}\xi & \text{for } \xi<0\\ \frac{1}{2}\xi & \text{for } 0\leq\xi\leq 4\\ \xi-2 & \text{for } 4<\xi\end{cases},$$

and

$$U_0(\xi) = \begin{cases} 0 & \text{for } \xi < 0 \\ \frac{1}{2}\xi & \text{for } 0 \le \xi < 2 \\ 2 - \frac{1}{2}\xi & \text{for } 2 \le \xi \le 4 \\ 0 & \text{for } 4 < \xi \end{cases},$$

$$H_0(\xi) = \begin{cases} 0 & \text{for } \xi < 0 \\ \frac{1}{2}\xi & \text{for } 0 \le \xi \le 4 \\ 2 & \text{for } 4 < \xi \end{cases}.$$

Then we solve the Lagrangian system (3.18a)-(3.18c) up to time t, by applying the solution operator $S_t : \mathcal{F} \to \mathcal{F}$, i.e., $Y(t) = (X(t), U(t), H(t)) = S_t(Y_0)$. The solution is given through (3.19a)-(3.19c) with $K = 2$ being the total energy, leading to

$$X(\xi,t) = \begin{cases} -\frac{t^2}{4} + \xi & \text{for } \xi < 0 \\ \frac{t^2}{4}(\frac{1}{2}\xi - 1) + \frac{1}{2}\xi(t+1) & \text{for } 0 \le \xi < 2 \\ \frac{t^2}{4}(\frac{1}{2}\xi - 1) + (2 - \frac{1}{2}\xi)t + \frac{1}{2}\xi & \text{for } 2 \le \xi \le 4 \\ \frac{t^2}{4} + \xi - 2 & \text{for } 4 < \xi \end{cases},$$

$$U(\xi,t) = \begin{cases} -\frac{t}{2} & \text{for } \xi < 0 \\ \frac{t}{2}(\frac{1}{2}\xi - 1) + \frac{1}{2}\xi & \text{for } 0 \le \xi < 2 \\ \frac{t}{2}(\frac{1}{2}\xi - 1) + 2 - \frac{1}{2}\xi & \text{for } 2 \le \xi \le 4 \\ \frac{t}{2} & \text{for } 4 < \xi \end{cases},$$

$$H(\xi,t) = H_0(\xi).$$

Finally we want to map this solution back to Eulerian coordinates, by applying $M : \mathcal{F} \to \mathcal{D}$. That is, $(u(t), \mu(t)) = M(Y(t))$ is defined through (3.22a)-(3.22b). Hence we need to solve $x = X(\xi, t)$ in terms of ξ for the various cases. The cases $\xi \in [0, 2)$ and $\xi \in [2, 4]$ lead to

$$\xi = \frac{8(x + \frac{t^2}{4})}{(t+2)^2} \in [0, 2),$$

and

$$\xi = \frac{8(x + \frac{t^2}{4} - 2t)}{(t-2)^2} \in [2, 4].$$

Inserting for these relations we find that the wave profile in Eulerian coordinates becomes

$$u(x,t) = \begin{cases} -\frac{t}{2} & \text{if } x \le -\frac{t^2}{4} \\ \frac{2x-t}{t+2} & \text{if } -\frac{t^2}{4} \le x < t+1 \\ \frac{2x-t-4}{t-2} & \text{if } t+1 \le x \le 2 + \frac{t^2}{4} \\ \frac{t}{2} & \text{if } 2 + \frac{t^2}{4} < x \end{cases}.$$

Observe that $u_x \to -\infty$ as $t \uparrow 2$ at $x = 3$, so the solution breaks, while no such behaviour is observed for the solution to the ODE system in Lagrangian coordinates. The associated measure is given through $\mu = X_{\#}(H_\xi d\xi)$.

4 Weak traveling waves for the Hunter-Saxton Equation

We seek traveling wave solutions of the Hunter-Saxton equation, and will work with the equation on differentiated form, i.e.,

$$(u_t + uu_x)_x = \frac{1}{2}u_x^2. \tag{4.1}$$

That is, we search for solutions of the form $u(x,t) = w(x-st)$ with $s \in \mathbb{R}$ being the wave speed and $w : \mathbb{R} \to \mathbb{R}$ being a continuous and hopefully bounded function. The initial wave profile is given by setting $t = 0$, leading to $u(x,0) = w(x)$, hence such a solution represents the initial wave profile being translated either to the left or right depending on the sign of s. As noticed in Theorem 3.1 from Section 3, smooth solutions will usually admit derivatives that tend to $-\infty$ in finite time, while the solution itself remains bounded. In order to continue the solution past wave breaking we must resort to weak solutions. Thus it seems implausible to search for global classical traveling waves. Instead we want to proceed in a similar fashion to what is done by Grunert and Reigstad in [GR20] for the nonlinear variational wave equation (2.11), and Camassa-Holm equation. Here they patch together local, classical traveling wave solutions in order to produce weak traveling waves that are bounded, and exist globally. This approach allows for discontinuous derivatives at the gluing points. Lenells pointed out in [Len09] that there exists no periodic globally bounded, classical traveling waves for the Hunter-Saxton equation. Moreover in [LL09] the authors mention briefly that there are no bounded traveling waves for the Hunter-Saxton equation. Both these statements agree with our main statement of this section, Theorem 4.1. The main goal of this section is to classify all weak traveling wave solutions for the Hunter-Saxton equation, similarly to that which has been done for the closely related Camassa-Holm equation in [Len05]. We will as we see fit, compare results we obtain to those obtained in [Len05] for the Camassa-Holm equation.

First assume that $w \in C^2(\mathbb{R})$, then we can compute the required partial derivatives of the traveling wave ansatz and insert into the Hunter-Saxton equation. Here $C^2(I)$ means that the function admits continuous first order and second order partial derivatives on the interval I. We set $\xi = x - st$ and let w_ξ denote the derivative of w with respect to ξ. The first few partial derivatives are

$$\begin{aligned} u_t(x,t) &= -sw_\xi(x-st), & u_{xt}(x,t) &= -sw_{\xi\xi}(x-st), \\ u_x(x,t) &= w_\xi(x-st), & u_{xx}(x,t) &= w_{\xi\xi}(x-st). \end{aligned}$$

Inserting into (4.1) and rearranging yields

$$-sw_{\xi\xi} + ww_{\xi\xi} + \frac{1}{2}w_\xi^2 = (w-s)w_{\xi\xi} + \frac{1}{2}w_\xi^2 = 0. \tag{4.2}$$

We search for nontrivial traveling wave solutions, so we exclude the case where $w = \text{const}$ for all ξ. This second order ODE can be rewritten as a system consisting of two first order ODEs. This is done by setting

$$\begin{aligned} w_\xi &= v, \\ v_\xi &= \frac{1}{2}\frac{v^2}{(w-s)}. \end{aligned}$$

We notice that there is a blow up when $w \to s$. Moreover the system admits equilibrium points along the entire w-axis, i.e., the whole line $(w, 0)$ consists of equilibrium points, but this amounts to $w_\xi = 0$ which implies $w = \text{const}$.

Definition 4.1 (Local, classical wave)**.** We say that u is a local, classical traveling wave of the Hunter-Saxton equation if the following holds

1. $u(x,t) = w(x-st)$ for some $w \in C^2(I)$ where $I \subset \mathbb{R}$ is some interval,

2. w satisfies (4.2).

Remark 4.1. Notice that if $u(x,t) = w(x-st) = w(\xi)$ is a traveling wave solution of the Hunter-Saxton equation, then

$$\xi \to -w(-\xi),$$

is also a traveling wave solution with $s \to -s$. In particular this wave has the amplitude reversed, i.e., same magnitude but with opposite sign, and it propagates in the opposite direction. This wave can be interpreted as a reflected wave about the origin.

Another way to phrase the remark is that the ODE (4.2) is invariant under the transform

$$(w(\xi), s) \to (-w(-\xi), -s).$$

A similar symmetry was observed in [Len05] for the Camassa-Holm equation. We can multiply (4.2) by $2w_\xi$, since we search for nontrivial traveling waves we are guaranteed that w_ξ is not identical to the zero function. We can rewrite the resulting equation so it becomes

$$-s(w_\xi^2)_\xi + (ww_\xi^2)_\xi = 0.$$

We integrate and introduce an integration constant k on the right-hand side, yielding

$$-sw_\xi^2 + ww_\xi^2 = (w-s)w_\xi^2 = k. \tag{4.3}$$

We assumed $w \in C^2(I)$ originally, but this expression makes sense for $w \in C^1(I)$. Here s is the wave speed where $s > 0$ represents waves propagating along positive x-direction, while those propagating in negative x-direction have $s < 0$. We can go from a wave traveling to the right, to one traveling to the left by setting $s \to -s$. We now confine our attention to an interval $[\xi_0, \xi_1]$ where we define

$$\begin{aligned} \alpha &= \inf_{\xi \in [\xi_0, \xi_1]} w(\xi), \\ \beta &= \sup_{\xi \in [\xi_0, \xi_1]} w(\xi), \end{aligned} \tag{4.4}$$

in a similar spirit to that in [GR20]. If w is a C^2-function on a compact set, i.e., a closed and bounded interval, then we can replace the infimum and supremum by minimum and maximum, respectively. However stating it this way, it also applies to non-compact sets. If we assume that $s \notin [\alpha, \beta]$, then we can rearrange (4.3) and express it in terms of w_ξ, leading to

$$w_\xi(\xi) = \pm \frac{\sqrt{|k|}}{\sqrt{|w(\xi) - s|}}. \tag{4.5}$$

The right-hand side of (4.5) is bounded and Lipschitz with respect to w when $s \notin [\alpha, \beta]$. Consequently by existence and uniqueness theory for ODEs there exists a unique local solution w which is C^1 and monotone. We also see by (4.5) that the derivative is bounded and the solution w is locally bounded. w is not globally bounded, since if w does not attain the value s anywhere in $\mathbb{R}$, then either $w > s$ or $w < s$ for all ξ. Therefore $|w_\xi| > 0$ for all ξ, and thus $|w|$ will asymptotically tend to infinity. Using separation of variables we can find an explicit solution to the ODE for $s \notin [\alpha, \beta]$. If we choose the plus sign in (4.5) and assume $w(\xi) > s$ for all $\xi \in [\xi_0, \xi_1]$, equivalently $\alpha > s$, then

$$\int_{w(\xi_0)}^{w(\xi)} \sqrt{w-s}\, dw = \int_{\xi_0}^{\xi} \sqrt{|k|}\, d\xi.$$

Integrating yields

$$w(\xi) = s + \left(\frac{3}{2}(\xi - \xi_0)\sqrt{|k|} + (w(\xi_0) - s)^{\frac{3}{2}} \right)^{\frac{2}{3}}.$$

If we have $s > \beta$ we must replace the argument in the square root by $-(w-s)$. The explicit solution then becomes

$$w(\xi) = s - \left((s - w(\xi_0))^{\frac{3}{2}} - \frac{3}{2}\sqrt{|k|}(\xi - \xi_0) \right)^{\frac{2}{3}}.$$

For both these cases we have chosen the plus sign in (4.5), therefore there are two more scenarios to consider. If one chooses the negative sign instead, one can again integrate to find the solutions. One finds that the solutions take similar expressions, but the sign in front of the term involving $\sqrt{|k|}$ has changed.

Now assume that $s \in [\alpha, \beta]$, then the right-hand side of (4.5) is no longer Lipshitz continuous in w. Standard existence and uniqueness results from ODE theory do no longer apply. We want to show that we have Hölder-continuity in this case, in particular with Hölder-exponent $\frac{1}{2}$. For simplicity assume there is only a single point where $w(\xi)$ and s coincide, then there are two scenarios to consider. Either we can have that w and s coincide on one of the endpoints of the interval $[\xi_0, \xi_1] \subset \mathbb{R}$ or there can be a value $\eta \in (\xi_0, \xi_1)$ where they coincide. First assume that either $w(\xi_0) = s$ or $w(\xi_1) = s$, then by integrating and using (4.5) we get

$$\begin{aligned}\int_{\xi_0}^{\xi_1} (w_\xi(\xi))^2 d\xi &= \underbrace{\left| \int_{\xi_0}^{\xi_1} w_\xi(\xi) \frac{\pm\sqrt{|k|}}{\sqrt{|w(\xi) - s|}} d\xi \right|}_{w_\xi d\xi = \frac{dw}{d\xi} d\xi} = \sqrt{|k|} \left| \int_{w(\xi_0)}^{w(\xi_1)} \frac{dw}{\sqrt{|w-s|}} \right| \\ &= 2\sqrt{|k|}\sqrt{|w-s|}|_{w=w(\xi_0)}^{w(\xi_1)},\end{aligned}$$

which is finite. Now the other case to consider is when

$$w(\xi_0) \neq s, \qquad \text{and} \qquad w(\xi_1) \neq s,$$

but there exists a number $\eta \in (\xi_0, \xi_1)$ such that $w(\eta) = s$. Then we can proceed similarly, we just have to split the integral up into two parts, and treat each of them separately. Thus

$$\begin{aligned}\int_{\xi_0}^{\xi_1} w_\xi^2(\xi) d\xi &= \int_{\xi_0}^{\eta} w_\xi^2(\xi) d\xi + \int_{\eta}^{\xi_1} w_\xi^2(\xi) d\xi \\ &= 2\sqrt{|k|}\sqrt{|w-s|}|_{w(\xi_0)}^{w(\eta)} + 2\sqrt{|k|}\sqrt{|w-s|}|_{w(\eta)}^{w(\xi_1)},\end{aligned}$$

which again is finite. Consequently $w_\xi \in L^2(I)$, where $I = [\xi_0, \xi_1]$. In particular if we apply Cauchy-Schwarz inequality we obtain

$$\begin{aligned}|w(\xi_1) - w(\xi_0)| &= \left| \int_{\xi_0}^{\xi_1} w_\xi(\xi) d\xi \right| \leq \left(\int_{\xi_0}^{\xi_1} |w_\xi(\xi)|^2 d\xi \right)^{\frac{1}{2}} \left(\int_{\xi_0}^{\xi_1} d\xi \right)^{\frac{1}{2}} \\ &= \|w_\xi\|_{L^2(I)} \sqrt{|\xi_1 - \xi_0|}.\end{aligned}$$

Therefore w is Hölder continuous with Hölder exponent $\frac{1}{2}$. This will be helpful when the gluing of two local, classical traveling waves is addressed. In particular it therefore makes sense to require continuity of w even at the gluing points.

Our main goal in this section is to determine all possible weak traveling waves of the Hunter-Saxton equation. There are at least two ways to define the concept of weak traveling waves. We can take the approach in [GR20] to define a weak traveling wave in terms of the weak formulation of the underlying PDE. Another way is to use the resulting ODE after inserting the traveling wave ansatz, and define a weak traveling wave in terms of the weak formulation of the resulting ODE. This last approach is taken in [Len05]. We will stick with the approach taken in [GR20]. To derive the weak form of the differentiated Hunter-Saxton equation, first assume

we have a classical solution $u \in C^2(\mathbb{R} \times (0,\infty))$. Then we multiply (4.1) by a test function $\phi \in C_0^\infty(\mathbb{R} \times (0,\infty))$. Here $C_0^\infty(E)$ means the space of smooth functions which are compactly supported on the set E. We will integrate the manipulated equation by parts over $\mathbb{R} \times (0,\infty)$. There are various ways to formulate the resulting expression depending on which terms we integrate by parts, and how many times we integrate the different terms. With our choice we get

$$\begin{aligned} 0 &= \int_0^\infty \int_{\mathbb{R}} \phi[(u_t + uu_x)_x - \frac{1}{2}u_x^2]dxdt \\ &= \int_0^\infty \int_{\mathbb{R}} \left(\phi_{xt}u + \frac{1}{2}\phi_{xx}u^2 - \frac{1}{2}\phi u_x^2\right)dxdt, \end{aligned}$$

which is the same expression as used in [BC05] and [HS91]. Referring to Definition 3.1 which is the definition of a weak solution to the integrated formulation of the Hunter-Saxton equation, we see that with the requirements $u_x \in L^\infty([0,\infty); L^2(\mathbb{R}))$ and $u \in C(\mathbb{R} \times [0,\infty))$, all terms are finite. Due to the compact support of ϕ, the integral is only taken over a compact set. Inserting the traveling wave ansatz $u(x,t) = w(x - st)$ we obtain

$$\int_0^\infty \int_{\mathbb{R}} \left(\phi_{xt}w + \phi_{xx}\frac{1}{2}w^2 - \frac{1}{2}\phi w_\xi^2\right)dxdt. \tag{4.6}$$

Definition 4.2 (Weak traveling wave)**.** A function $u(x,t) = w(x - st)$ with $u \in C(\mathbb{R} \times \mathbb{R}; \mathbb{R})$ and $s \in \mathbb{R}$ is a weak traveling wave solution of (4.1) if

$$\int_0^\infty \int_{\mathbb{R}} \left(\phi_{xt}w + \phi_{xx}\frac{1}{2}w^2 - \frac{1}{2}\phi w_\xi^2\right)dxdt = 0,$$

holds for all test functions $\phi \in C_0^\infty(\mathbb{R} \times (0,\infty))$.

We want to glue together two local, classical traveling waves in order to produce a weak traveling wave. In particular we will derive a lemma, which allows us to glue together two classical traveling waves at points where $w(\xi) = s$, thus yielding a composite weak traveling wave. This composite traveling wave will be a weak solution in a region being the union of the domains of the two local, classical waves. This approach is used to classify all possible weak traveling waves of the Hunter-Saxton equation. First we recall Green's theorem in the plane, which will be used frequently in the coming proof, and the next chapter, to convert "area" integrals to line integrals.

Remark 4.2. Assume Γ is a closed, non-self intersecting curve, lying in a simply connected region, where the functions $P(x,y)$ and $Q(x,y)$ have continuous first order partial derivatives. Then

$$\oint_\Gamma (Pdx + Qdy) = \iint_D \left(\frac{\partial Q}{\partial x} - \frac{\partial P}{\partial y}\right)dxdy,$$

where D is the region enclosed by the curve Γ. This relates the line integral around Γ, to the double integral of its interior.

4.1 The "gluing" lemma

We want to glue together two local, classical traveling waves which generally have different integration constants in (4.5). We assume that the derivatives u_t and u_x have isolated discontinuities that move along a smooth curve Γ which we parameterize in terms of a parameter t. In particular by $\Gamma : x = \sigma(t)$. By isolated discontinuities we mean that u is a classical solution to the Hunter-Saxton equation on either side of the curve Γ, but not on the curve. We assume $\sigma(\cdot)$ is a smooth and strictly increasing function of t, and choose D such that u is a classical solution everywhere inside D except on the curve Γ. Now we will do an argument which is similar

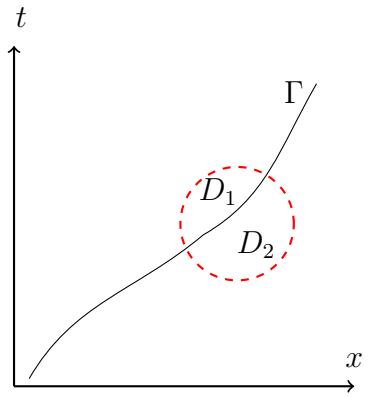

Figure 9: An illustration of a strictly increasing curve $\Gamma : x = \sigma(t)$, and the neighbourhoods D_1 and D_2 used in the setting of the gluing formalism. Here $D = D_1 \cup D_2$.

in nature to that done for Rankine-Hugoniot condition in [HR15], i.e., a Rankine-Hugoniot type argument. Choose a test function ϕ whose support lies within the neighbourhood D, i.e., $\phi \in C_0^\infty(D)$. The neighbourhood D consists of two parts

$$D = D_1 \cup D_2,$$

where D_1 and D_2 are depicted in Figure 9. For any $\epsilon > 0$ we introduce the following sets

$$\begin{aligned} I &:= \{t \in [0,\infty) : (\sigma(t), t) \in D\}, \\ D_i^\epsilon &:= \{(x,t) \in D_i : \operatorname{dist}((x,t), \Gamma) > \epsilon\}, \end{aligned} \tag{4.7}$$

for $i \in \{1,2\}$. I is the set of t-values for which the parameterized curve is inside the region D, while $D_i^\epsilon \subset D_i$, are subsets where all points are more than a distance ϵ away from the curve. In particular u will be a classical solution inside $D_1^\epsilon \cup D_2^\epsilon$, which is the purpose of the decomposition. We have

$$\begin{aligned} &\iint_D \left[\phi_{xt}u + \frac{1}{2}\phi_{xx}u^2 - \frac{1}{2}\phi u_x^2\right] dxdt \\ &\quad = \lim_{\epsilon \to 0^+} \iint_{D_1^\epsilon \cup D_2^\epsilon} \left[\phi_{xt}u + \frac{1}{2}\phi_{xx}u^2 - \frac{1}{2}\phi u_x^2\right] dxdt, \end{aligned} \tag{4.8}$$

and applying usual properties of the Lebesgue integral, we can split this up into one integral over D_1^ϵ and one over D_2^ϵ. We consider the integral over D_1^ϵ first. u is a classical solution in D_1^ϵ, thus we can subtract $(u_{tx} + (uu_x)_x - \frac{1}{2}u_x^2)\phi = 0$ to get

$$\begin{aligned} &\iint_{D_1^\epsilon} \left[\phi_{xt}u + \frac{1}{2}\phi_{xx}u^2 - \frac{1}{2}\phi u_x^2\right] dxdt \\ &\quad = \iint_{D_1^\epsilon} \Big(\phi_{xt}u + \frac{1}{2}\phi_{xx}u^2 - \frac{1}{2}\phi u_x^2 - \phi(u_{tx} + (uu_x)_x - \frac{1}{2}u_x^2)\Big) dxdt. \end{aligned}$$

Notice the terms involving $\frac{1}{2}\phi u_x^2$ cancel. ϕ has compact support inside D, and will therefore vanish everywhere on the boundary ∂D_1^ϵ except on $\Gamma_1^\epsilon := \{(\sigma_1^\epsilon(t), t) : t \in I_1^\epsilon\}$, where we have defined $I_1^\epsilon := \{t \in [0,\infty) : (\sigma_1^\epsilon(t), t) \in D_1\}$ and paramterized the curve Γ_1^ϵ by a parameter t, using a smooth and strictly increasing function of t, $\sigma_1^\epsilon(\cdot)$. That is, Γ_1^ϵ is the part of the boundary of D_1^ϵ which does not coincide with ∂D_1. Now we can integrate the term involving $\phi_{tx}u$ by parts with respect to x and the term $\frac{1}{2}\phi_{xx}u^2$ once with respect to x. This leads to

$$\iint_{D_1^\epsilon} (\phi_{xt}u) dxdt = \int_{I_1^\epsilon} (\phi_t u)(\sigma_1^\epsilon(t), t) dt - \iint_{D_1^\epsilon} \phi_t u_x dxdt,$$

and

$$\iint_{D_1^\epsilon}(\frac{1}{2}\phi_{xx}u^2)dxdt = \int_{I_1^\epsilon}(\frac{1}{2}\phi_x u^2)(\sigma_1^\epsilon(t),t)dt - \iint_{D_1^\epsilon}(\frac{1}{2}\phi_x(u^2)_x)dxdt.$$

Inserting this, we obtain

$$\begin{aligned}&\iint_{D_1^\epsilon}\left[\phi_{xt}u + \frac{1}{2}\phi_{xx}u^2 - \frac{1}{2}\phi u_x^2\right]dxdt\\ &\quad= \iint_{D_1^\epsilon}\left[(-\phi_t u_x - \phi u_{tx}) + (-\frac{1}{2}\phi_x(u^2)_x - \phi(uu_x)_x)\right]dxdt + \int_{I_1^\epsilon}\left(\phi_t u + \frac{1}{2}\phi_x u^2\right)(\sigma_1^\epsilon(t),t)dt.\end{aligned}$$

Now Leibniz's rule can be applied to rewrite this as

$$\begin{aligned}&\iint_{D_1^\epsilon}\left[\phi_{xt}u + \frac{1}{2}\phi_{xx}u^2 - \frac{1}{2}\phi u_x^2\right]dxdt\\ &\quad= -\iint_{D_1^\epsilon}\left((\phi u_x)_t + (\frac{1}{2}\phi(u^2)_x)_x\right)dxdt + \int_{I_1^\epsilon}\left(\phi_t u + \frac{1}{2}\phi_x u^2\right)(\sigma_1^\epsilon(t),t)dt\\ &\quad= -\iint_{D_1^\epsilon}\phi\begin{pmatrix}\frac{\partial}{\partial x} & \frac{\partial}{\partial t}\end{pmatrix}\cdot\begin{pmatrix}\frac{1}{2}(u^2)_x & u_x\end{pmatrix}dxdt + \int_{I_1^\epsilon}\left(\phi_t u + \frac{1}{2}\phi_x u^2\right)(\sigma_1^\epsilon(t),t)dt.\end{aligned}$$

We apply Green's theorem stated in Remark 4.2. This allows us to convert the double integral to an integral over the boundary ∂D_1^ϵ. However ϕ vanishes everywhere on ∂D_1^ϵ except on Γ_1^ϵ. Therefore an application of Green's theorem gives

$$\begin{aligned}&\iint_{D_1^\epsilon}\left[\phi_{xt}u + \frac{1}{2}\phi_{xx}u^2 - \frac{1}{2}\phi u_x^2\right]dxdt\\ &\quad= \int_{\partial D_1^\epsilon}\left(-\frac{1}{2}\phi(u^2)_x dt + \phi u_x dx\right) + \int_{I_1^\epsilon}\left(\phi_t u + \frac{1}{2}\phi_x u^2\right)(\sigma_1^\epsilon(t),t)dt\\ &\quad= \int_{\Gamma_1^\epsilon}\left(-\frac{1}{2}\phi(u^2)_x dt + \phi u_x dx\right) + \int_{I_1^\epsilon}\left(\phi_t u + \frac{1}{2}\phi_x u^2\right)(\sigma_1^\epsilon(t),t)dt\\ &\quad= \int_{I_1^\epsilon}\left(\left[\phi_t u + \frac{1}{2}\phi_x u^2 - \frac{1}{2}\phi(u^2)_x\right](\sigma_1^\epsilon(t),t) + (\phi u_x)(\sigma_1^\epsilon(t),t)\dot{\sigma}_1^\epsilon(t)\right)dt.\end{aligned} \tag{4.9}$$

Here we used that $x = \sigma_1^\epsilon(t)$, such that $dx = \dot{\sigma}_1^\epsilon(t)\,dt$. We can proceed completely similar for D_2^ϵ except now there are two differences. Firstly the line integral is taken clockwise, which leads to the addition of a minus sign in front of the line integral when applying Green's theorem. Secondly the sign in front of the added boundary terms, when we integrate by parts, will now have opposite signs, since D_2^ϵ is to the right of the curve Γ instead of to the left as in the case of D_1^ϵ. We use the notation, Γ_2^ϵ, for the boundary part where ϕ does not vanish. We parameterize Γ_2^ϵ by a parameter t, such that $\Gamma_2^\epsilon := \{(\sigma_2^\epsilon(t),t) : t \in I_2^\epsilon\}$, where $I_2^\epsilon := \{t \in [0,\infty) : (\sigma_2^\epsilon(t),t) \in D_2\}$. As before we assume that $\sigma_2^\epsilon(\cdot)$ is a smooth and strictly increasing function of t. Taking these differences into account, a similar calculation leads to

$$\begin{aligned}&\iint_{D_2^\epsilon}\left[\phi_{xt}u + \frac{1}{2}\phi_{xx}u^2 - \frac{1}{2}\phi u_x^2\right]dxdt\\ &\quad= -\int_{\Gamma_2^\epsilon}\left(-\frac{1}{2}\phi(u^2)_x dt + \phi u_x dx\right) - \int_{I_2^\epsilon}\left(\phi_t u + \frac{1}{2}\phi_x u^2\right)(\sigma_1^\epsilon(t),t)dt\\ &\quad= \int_{I_2^\epsilon}\left(\left[-\phi_t u - \frac{1}{2}\phi_x u^2 + \frac{1}{2}\phi(u^2)_x\right](\sigma_2^\epsilon(t),t) - (\phi u_x)(\sigma_2^\epsilon(t),t)\dot{\sigma}_2^\epsilon(t)\right)dt.\end{aligned} \tag{4.10}$$

The derivation thus far holds for any classical solution u having discontinuities in the derivatives u_t and u_x along a curve Γ, which might be arbitrary. We will now specialize to traveling waves.

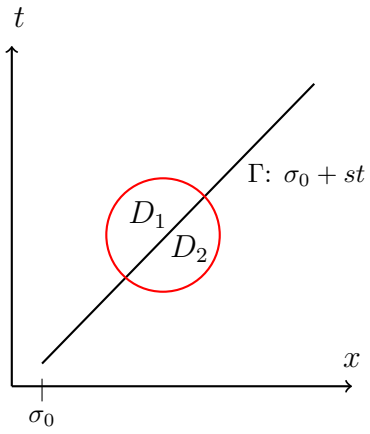

Figure 10: Discontinuities for the travelling wave propagate along a diagonal line, i.e., the curve Γ. Here illustrated in the case of $s > 0$, i.e., for a right-moving wave.

In this case, the curve of discontinuities Γ takes a particular simple form. The discontinuities for a traveling wave move along a diagonal line in the (x,t)-plane with slope s. As a consequence Γ is described by $\sigma(t) = \sigma_0 + st$, as shown in Figure 10. Where the corresponding traveling wave is propagating to the left if $s < 0$ and right for $s > 0$. In Figure 11, a cuspon (defined in Definition 4.3) propagating to the right is depicted. A cuspon and other kinds of traveling waves propagate either to the left or right while preserving their shape. This is typically a phenomenon caused by the balance of dispersive and nonlinear effects of the underlying equation. We summarize the results we obtain in the next lemma.

Lemma 4.1 (Gluing lemma)**.** *Consider two local, classical traveling wave solutions u_1 and u_2 to the Hunter-Saxton equation in D_1 and D_2, respectively. Depicted in Figure 10. We want to patch together these two solutions along a curve $\Gamma : x = \sigma(t) = \sigma_0 + st$, in order to obtain a continuous traveling wave $u(x,t) = w(x - st)$ in D which satisfies*

$$\iint_D \left(w\phi_{xt} + \frac{1}{2}w^2\phi_{xx} - \frac{1}{2}(w_\xi)^2\phi \right) dxdt = 0,$$

for all test functions $\phi \in C_0^\infty(D)$. Here σ_0 is a constant. Let α and β be defined as the infimum and supremum of w in D, respectively.

- *If $s \notin [\alpha, \beta]$ then*

$$w_\xi(\sigma_0^-) = w_\xi(\sigma_0^+), \tag{4.11}$$

  where $w_\xi(\sigma_0^-)$ and $w_\xi(\sigma_0^+)$ denote the left and right limits of w_ξ at σ_0, respectively.

- *If $s \in [\alpha, \beta]$, i.e., the derivative w_ξ is allowed to be unbounded at the curve Γ then*

$$\begin{aligned} \left[\sqrt{|k_1|} \lim_{\xi \uparrow \sigma_0} sign\Big[(s - w(\xi))w_\xi(\xi)\Big] - \sqrt{|k_2|} \lim_{\xi \downarrow \sigma_0} sign\Big[(s - w(\xi))w_\xi(\xi)\Big] \right] \\ \times \sqrt{|w(\sigma_0) - s|} = 0, \end{aligned} \tag{4.12}$$

  where k_1 and k_2 denote the integration constants corresponding to the local, classical solution u_1 and u_2, respectively.

The lemma lets us glue together two classical traveling waves, while still maintaining continuity along the curve which we glue. Thus, in particular it allows us to produce weak traveling waves. We will use this to classify all weak composite traveling waves, and in fact all traveling waves for the Hunter-Saxton equation (4.1).

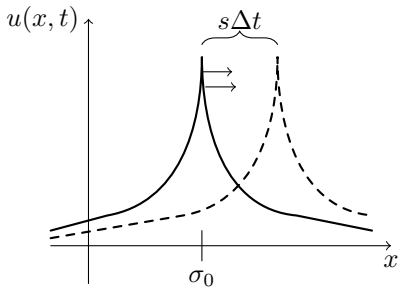

Figure 11: A cuspon traveling towards the right. This is an example where nonlinear effects and dispersion balance each other, therefore the cuspon maintains its shape. Increasing the time from $t \to t + \Delta t$, causes a translation, $s\Delta t$, of the cuspon.

Proof. We consider traveling waves, $u(x,t) = w(x-st)$. We can in this case express the function $\sigma_1^\epsilon(t)$ by

$$\sigma_1^\epsilon(t) := \sigma(t) - \epsilon\sqrt{s^2+1} = \sigma_0 + st - \epsilon\sqrt{s^2+1},$$

here the minus sign indicates that we approach the curve Γ from the left as $\epsilon \downarrow 0$. We have $\dot{\sigma}_1^\epsilon = s$. Plugging in the traveling wave ansatz in the integral involving D_1^ϵ, (4.9), yields

$$\begin{aligned}
&\iint_{D_1^\epsilon} \Big(w\phi_{xt} + \frac{1}{2}w^2\phi_{xx} - \frac{1}{2}(w_\xi)^2\phi \Big) dxdt \\
&\quad = \int_{I_1^\epsilon} \Big(\Big[s - w(\sigma_1^\epsilon(t) - st) \Big] w_\xi(\sigma_1^\epsilon(t) - st)\phi(\sigma_1^\epsilon(t), t) + w(\sigma_1^\epsilon(t) - st)\phi_t(\sigma_1^\epsilon(t), t) \\
&\qquad + \frac{1}{2}w^2(\sigma_1^\epsilon(t) - st)\phi_x(\sigma_1^\epsilon(t), t) \Big) dt.
\end{aligned}$$

We proceed analogously for the part over D_2^ϵ. Now σ_2^ϵ can be expressed as $\sigma_2^\epsilon(t) := \sigma_0 + st + \epsilon\sqrt{s^2+1}$, showing that we approach the curve Γ from the right as $\epsilon \downarrow 0$. Again $\dot{\sigma}_2^\epsilon = s$. We insert the traveling wave ansats into (4.10), resulting in

$$\begin{aligned}
&\iint_{D_2^\epsilon} \Big(w\phi_{xt} + \frac{1}{2}w^2\phi_{xx} - \frac{1}{2}(w_\xi)^2\phi \Big) dxdt \\
&\quad = \int_{I_2^\epsilon} \Big(- \Big[s - w(\sigma_2^\epsilon(t) - st) \Big] w_\xi(\sigma_2^\epsilon(t) - st)\phi(\sigma_2^\epsilon(t), t) - w(\sigma_2^\epsilon(t) - st)\phi_t(\sigma_2^\epsilon(t), t) \\
&\qquad - \frac{1}{2}w^2(\sigma_2^\epsilon(t) - st)\phi_x(\sigma_2^\epsilon(t), t) \Big) dt.
\end{aligned}$$

We consider the two cases, $s \notin [\alpha, \beta]$ and $s \in [\alpha, \beta]$, separately.

- $s \notin [\alpha, \beta]$: Then $w(\xi) \neq s$ for all ξ in D, therefore by (4.5) the derivative w_ξ is bounded at all points in D. We know that w, and ϕ along with all its derivatives are continuous. Moreover a finite product of continuous functions is continuous, thus w^2 is continuous as well. Therefore we can directly pass to the limit $\epsilon \downarrow 0$ in the integral over D_1^ϵ leading to

$$\begin{aligned}
&\lim_{\epsilon \downarrow 0} \iint_{D_1^\epsilon} \Big(w\phi_{xt} + \frac{1}{2}w^2\phi_{xx} - \frac{1}{2}(w_\xi)^2\phi \Big) dxdt \\
&\quad = \int_I \Big(\Big[s - w(\sigma_0) \Big] w_\xi(\sigma_0^-)\phi(\sigma(t), t) + w(\sigma_0)\phi_t(\sigma(t), t) \\
&\qquad + \frac{1}{2}w^2(\sigma_0)\phi_x(\sigma(t), t) \Big) dt,
\end{aligned} \tag{4.13}$$

and similarly for the integral over D_2^ϵ

$$\begin{aligned}
&\lim_{\epsilon\downarrow 0}\iint_{D_2^\epsilon}\Big(w\phi_{xt}+\frac{1}{2}w^2\phi_{xx}-\frac{1}{2}(w_\xi)^2\phi\Big)dxdt\\
&\quad=\int_I\Big(-\Big[s-w(\sigma_0)\Big]w_\xi(\sigma_0^+)\phi(\sigma(t),t)-w(\sigma_0)\phi_t(\sigma(t),t)\\
&\qquad-\frac{1}{2}w^2(\sigma_0)\phi_x(\sigma(t),t)\Big)dt.
\end{aligned}\tag{4.14}$$

We have used that $\sigma_i^\epsilon(t)-st=\sigma_0\pm\epsilon\sqrt{s^2+1}$, which tends to σ_0 in the limit. Moreover we have introduced $w_\xi(\sigma_0^-)$ and $w_\xi(\sigma_0^+)$ as the left and right limits of the derivative w_ξ at σ_0, respectively. Now we combine (4.13) and (4.14). Notice that the terms involving $\frac{1}{2}w^2\phi$ and $w\phi_t$ cancel, as they have opposite signs from the two contributions. Inserting this into (4.8), yields in total

$$\begin{aligned}
&\iint_D\Big(w\phi_{xt}+\frac{1}{2}w^2\phi_{xx}-\frac{1}{2}(w_\xi)^2\phi\Big)dxdt\\
&\quad=\int_I\Big[s-w(\sigma_0)\Big](w_\xi(\sigma_0^-)-w_\xi(\sigma_0^+))\phi(\sigma(t),t)\Big)dt,
\end{aligned}$$

which we require to vanish for all test functions $\phi\in C_0^\infty(D)$ in order for w to be a weak traveling wave. Thus in particular picking a test function which is strictly positive on the interval I and rearranging we get

$$\begin{aligned}
&\int_I\Big[s-w(\sigma_0)\Big](w_\xi(\sigma_0^-)-w_\xi(\sigma_0^+))\phi(\sigma(t),t)\Big)\,dt\\
&\quad=\Big[s-w(\sigma_0)\Big](w_\xi(\sigma_0^-)-w_\xi(\sigma_0^+))\int_I\phi(\sigma(t),t)\,dt\,.
\end{aligned}$$

The integral does not vanish, so this naturally leads to

$$w_\xi(\sigma_0^-)=w_\xi(\sigma_0^+),$$

or $s=w(\sigma_0)$ which we have already excluded by requiring $s\notin[\alpha,\beta]$. This means that the left and right limits of the derivative must coincide, so the wave is C^1 at σ_0.

- $s\in[\alpha,\beta]$: In this case w_ξ may become unbounded on the curve Γ, so we need to eliminate the derivatives of w from the expressions. We still require w to be continuous along the curve Γ. Now since w is classical solution in $\bar{D}_1^\epsilon$, (4.3) holds. That is

$$w_\xi^2(\xi)(w(\xi)-s)=k_1,\tag{4.15}$$

where k_1 is the integration constant taken in D_1. Applying a similar rewriting as in [GR20] we get

$$\begin{aligned}
(w(\xi)-s)w_\xi&=\operatorname{sign}\Big([w(\xi)-s]w_\xi\Big)\sqrt{|w(\xi)-s|}\sqrt{|w(\xi)-s|w_\xi^2}\\
&=\operatorname{sign}\Big([w(\xi)-s]w_\xi\Big)\sqrt{|w(\xi)-s|}\sqrt{|k_1|},
\end{aligned}$$

where we replaced w_ξ by solving (4.15) in terms of w_ξ. Now we can insert this into (4.13), leading to

$$\begin{aligned}
&\lim_{\epsilon\downarrow 0}\iint_{D_1^\epsilon}\Big(w\phi_{xt}+\frac{1}{2}w^2\phi_{xx}-\frac{1}{2}(w_\xi)^2\phi\Big)dxdt\\
&\quad=\int_I\Big(\lim_{\xi\uparrow\sigma_0}\operatorname{sign}\Big[(s-w(\xi))w_\xi(\xi)\Big]\sqrt{|w(\xi)-s|}\sqrt{|k_1|}\phi(\sigma(t),t)\\
&\qquad+w(\sigma_0)\phi_t(\sigma(t),t)+\frac{1}{2}w^2(\sigma_0)\phi_x(\sigma(t),t)\Big)dt.
\end{aligned}$$

We do similarly for D_2^ϵ, but now we have an integration constant k_2 instead, thus

$$\begin{aligned}
&\lim_{\epsilon\downarrow 0}\iint_{D_2^\epsilon}\left(w\phi_{xt}+\frac{1}{2}w^2\phi_{xx}-\frac{1}{2}(w_\xi)^2\phi\right)dxdt\\
&\quad=-\int_I\Bigg(\lim_{\xi\downarrow\sigma_0}\operatorname{sign}\Big[(s-w(\xi))w_\xi(\xi)\Big]\sqrt{|w(\xi)-s|}\sqrt{|k_2|}\phi(\sigma(t),t)\\
&\qquad+w(\sigma_0)\phi_t(\sigma(t),t)+\frac{1}{2}w^2(\sigma_0)\phi_x(\sigma(t),t)\Bigg)dt,
\end{aligned}$$

notice that we have a minus sign in front of the entire expression. Combining the expressions over D_1^ϵ and D_2^ϵ, and using continuity of $w(\cdot)$ we observe that we get the same cancellations as before. The resulting expression becomes

$$\begin{aligned}
&\iint_D\left(w\phi_{xt}+\frac{1}{2}w^2\phi_{xx}-\frac{1}{2}(w_\xi)^2\phi\right)dxdt\\
&\quad=\int_I\Bigg(\Big[\sqrt{|k_1|}\lim_{\xi\uparrow\sigma_0}\operatorname{sign}\Big[(s-w(\xi))w_\xi(\xi)\Big]-\sqrt{|k_2|}\lim_{\xi\downarrow\sigma_0}\operatorname{sign}\Big[(s-w(\xi))w_\xi(\xi)\Big]\Big] \qquad (4.16)\\
&\qquad\times\sqrt{|w(\sigma_0)-s|}\phi(\sigma(t),t)\Bigg)dt.
\end{aligned}$$

In order for w to be a weak solution, we require this to vanish for all test functions $\phi\in C_0^\infty(D)$. Picking a strictly positive test function $\phi>0$, and arguing as before, this leads to

$$\begin{aligned}
&\Big[\sqrt{|k_1|}\lim_{\xi\uparrow\sigma_0}\operatorname{sign}\Big[(s-w(\xi))w_\xi(\xi)\Big]-\sqrt{|k_2|}\lim_{\xi\downarrow\sigma_0}\operatorname{sign}\Big[(s-w(\xi))w_\xi(\xi)\Big]\Big]\\
&\qquad\times\sqrt{|w(\sigma_0)-s|}=0.
\end{aligned}$$

□

4.2 Classification of weak traveling waves

We want to study which local, classical traveling waves that can be glued together. The result is as we will see a composite wave $w:\mathbb{R}\to\mathbb{R}$ that has at least one one-sided unbounded derivative at the gluing points. First we define some traveling wave terminology in agreement with [Len05].

Definition 4.3 (Wave types)**.** We define the following:

- Cuspon: A continuous function w is said to have a cusp at ξ_0 if w is smooth locally on either side of ξ_0 and

  $$\lim_{\xi\uparrow\xi_0}w_\xi(\xi)=-\lim_{\xi\downarrow\xi_0}w_\xi(\xi)=\pm\infty.$$

  A wave profile admitting a cusp singularity is called a cuspon.

- Peakon: A continuous function w is said to have a peak at ξ_0 if w is smooth locally on both sides of ξ_0 and

  $$0\neq\lim_{\xi\uparrow\xi_0}w_\xi(\xi)=-\lim_{\xi\downarrow\xi_0}w_\xi(\xi)\neq\pm\infty,$$

  i.e., the left and right derivatives are of equal finite magnitude, but of opposite sign. A wave profile with peaks is called a peakon.

- Stumpon: If w is obtained by inserting an interval in which w is constant at a cusp, then we say that w has a stump. That is, given some interval $\xi \in [a, b]$ on which w is constant and w is smooth locally to the left of a and right of b but

$$\lim_{\xi \downarrow a} w_\xi(\xi) = -\lim_{\xi \uparrow b} w_\xi(\xi) = \pm\infty,$$

then we say w admits a stump. A wave profile possesing stumps is referred to as a stumpon.

For the case $s \notin [\alpha, \beta]$ the condition (4.11) by Lemma 4.1 forces w and w_ξ to be continuous at the gluing point σ_0, and consequently w will be C^1 along the curve Γ. This is since there is no discontinuity at the starting point σ_0 of the curve Γ. As time evolves the point of the wave profile which initially corresponds to σ_0, will travel along the curve Γ in the (x, t)-plane. w is assumed to be a classical solution everywhere else in D, therefore w coincides with the global solution of

$$w_\xi(\xi) = \pm \frac{\sqrt{|k|}}{\sqrt{|w(\xi) - s|}}, \tag{4.17}$$

for a fixed integration constant $k \in \mathbb{R}$. Consequently no gluing is required at all, and the resulting wave will be monotone and unbounded. Thus, we observe that we need to have $w(\xi) = s$ at some ξ before gluing is required, so we dismiss the case of $s \notin [\alpha, \beta]$. Let $s \in [\alpha, \beta]$, we know by our previous arguments that w_ξ will be in $L^2_{\text{loc}}(\mathbb{R})$. Consider the case where we have one local classical traveling wave w_1 with constant k_1 in D_1 and w_2 in D_2 with constant k_2, which we want to glue together at σ_0. By (4.12) in Lemma 4.1 we require

$$\left[\sqrt{|k_1|} \lim_{\xi \uparrow \sigma_0} \operatorname{sign}\Big[(s - w(\xi))w_\xi(\xi)\Big] - \sqrt{|k_2|} \lim_{\xi \downarrow \sigma_0} \operatorname{sign}\Big[(s - w(\xi))w_\xi(\xi)\Big]\right] \times \sqrt{|w(\sigma_0) - s|} = 0.$$

Remark 4.3. If assume $s \neq w(\sigma_0)$ then this condition reduces to

$$\sqrt{|k_1|}\operatorname{sign}(w_\xi(\sigma_0^-)) - \sqrt{|k_2|}\operatorname{sign}(w_\xi(\sigma_0^+)) = 0,$$

since the left and right derivative at σ_0 are bounded, and by continuity, $(s - w(\xi))$ takes a definite sign in close vicinity of σ_0. In particular two scenarios can play out. Firstly $w_\xi(\sigma_0^-)$ and $w_\xi(\sigma_0^+)$ can have opposite signs, in which case we get

$$\sqrt{|k_1|} + \sqrt{|k_2|} = 0,$$

forcing $k_1 = k_2 = 0$. Secondly they can have the same sign, leading to

$$\sqrt{|k_1|} - \sqrt{|k_2|} = 0,$$

which forces the absolute magnitudes to be the same. In particular this means that the solution w is monotone in the neighbourhood D and is given by (4.17) where k is replaced by k_1. By assumption we have that w is a classical solution in D_1^ϵ and D_2^ϵ, and $s \neq w(\sigma_0)$, so $s \neq w(\xi)$ for all ξ in the entire neighbourhood D. Therefore w is monotone in D and coincides with the local solution of (4.17) in the neighbourhood D.

Remark 4.3 shows that in the case of $s \neq w(\sigma_0)$ we recover the same result as we did when we assumed $s \notin [\alpha, \beta]$. The inevitable conclusion is that gluing at points σ_0 where $s \neq w(\sigma_0)$ does not yield a new solution, rather just a continuation of the same solution.

Corollary 4.1. *Consider two local, classical traveling waves w_1 and w_2 of (4.1) with integration constants k_1 and k_2, respectively. These can only be glued together at a point σ_0 where*

$$w_1(\sigma_0) = w_2(\sigma_0) = s.$$

The corollary states that it is only possible to glue together two traveling wave solutions with different k_i's at a point σ_0 where the amplitudes of the waves are equal to the wave speed. An analogous criterion was derived for cuspons, stumpons and peakons in [Len05] for the Camassa-Holm equation. (4.12) allows both constant and non-constant local, classical traveling waves to be glued together at a point σ_0, provided the resulting composite wave is such that $w(\sigma_0) = s$. We let $u_1(x,t) = w_1(x-st)$ and $u_2(x,t) = w_2(x-st)$ be classical traveling waves in D_1^ϵ and D_2^ϵ, respectively. By our previous considerations, we know that w_1 and w_2 are at least locally Hölder continuous with exponent $\frac{1}{2}$. We require k_1 and k_2 to be finite integration constants, then (4.12) will be satisfied. The derivatives of w_1 and w_2 are given by

$$w_{1,\xi}(\xi) = \pm\frac{\sqrt{|k_1|}}{\sqrt{|w_1(\xi)-s|}}, \qquad \text{and} \qquad w_{2,\xi}(\xi) = \pm\frac{\sqrt{|k_2|}}{\sqrt{|w_2(\xi)-s|}},$$

respectively. Let $w_1(\sigma_0) = w_2(\sigma_0) = s$, and let ξ approach σ_0. We observe that

$$\begin{aligned} w_{1,\xi}(\xi) &\to \pm\infty \quad \text{as } \xi \uparrow \sigma_0, \\ w_{2,\xi}(\xi) &\to \pm\infty \quad \text{as } \xi \downarrow \sigma_0, \end{aligned}$$

i.e., the waves in regions D_1 and D_2, respectively, admit a singularity at the gluing point. That is, their derivatives become unbounded at the gluing point, while the wave profiles themselves remain continuous and bounded at the gluing point. By our previous arguments, we know that a local classical traveling wave of the Hunter-Saxton equation satisfies

$$(w_i(\xi)-s)w_{i,\xi\xi}(\xi) + \frac{1}{2}(w_{i,\xi})^2 = 0, \tag{4.18}$$

in particular the third term is always positive, so the sign of $w_{i,\xi\xi}$ depends only on the sign of $(w_i(\xi)-s)$. Here $w_{i,\xi}$ means the derivative with respect to ξ of w_i with $i \in \{1,2\}$. We observe that

1. If $w_{1,\xi}(\xi) > 0$ in a small neighbourhood of σ_0 with $\xi < \sigma_0$ then $w_1(\xi) < s$ and by (4.18) $w_{1,\xi\xi}(\xi) > 0$.
2. If $w_{1,\xi}(\xi) < 0$ for $\xi < \sigma_0$ but ξ remains close to σ_0 then $w_1(\xi) > s$ and by (4.18) $w_{1,\xi\xi}(\xi) < 0$.
3. If $w_{2,\xi}(\xi) > 0$ in a small neighbourhood of σ_0 with $\xi > \sigma_0$, then $w_2(\xi) > s$ and by (4.18) $w_{2,\xi\xi}(\xi) < 0$.
4. If $w_{2,\xi}(\xi) < 0$ for $\xi > \sigma_0$ but ξ remains close to σ_0 then $w_2(\xi) < s$ and by (4.18) $w_{2,\xi\xi}(\xi) > 0$.

Now we want to study what kinds of traveling waves we can obtain by combining scenarios $1.-4.$ In particular there are four gluing possibilities: 1. and 4., 1. and 3., 2. and 3., and finally 2. and 4. These cases lead either to derivatives that are unbounded or derivatives that are undefined (i.e., left and right derivatives are not equal) with unbounded left and right derivatives at the gluing point. Actually we also have the possibility to glue any of the scenarios $1.-4.$ to a constant value, i.e., one of the waves is the trivial wave equal to s. This leads to one one-sided unbounded derivative at the gluing point.

If we combine 1. and 4. or 2. and 3., then we obtain a cusp at the gluing point σ_0 according to Definition 4.3. This may roughly look similar to that in Figure 13c for 1. and 4., and like Figure 13d for 2. and 3. Notice that the slopes away from the cusp may differ, since w_1 and w_2 may have different k_i's and thus different slopes away from the gluing point σ_0. We also see that (4.18) does not prevent w_1 or w_2 being a constant. Therefore we can combine constant solutions with singular waves. For instance we can have $w_{1,\xi}(\xi) > 0$ for $\xi < \sigma_0$ and $w_2(\sigma_0) = w_2(\xi)$ for $\xi \geq \sigma_0$ as shown in Figure 13e, or we can have that $w_{1,\xi}(\xi) < 0$ for $\xi < \sigma_0$ and $w_2(\sigma_0) = w_2(\xi)$

for $\xi \geq \sigma_0$ as shown in Figure 13f. We can reverse this situation, and let w_1 be constantly equal to $w_1(\sigma_0) = s$, and combine this with either 3. or 4.
Combining 1. and 3., or 2. and 4. we get a traveling wave where the derivative is of the same sign on either side of the gluing point, but the convexity changes. Thus the gluing point is a point of inflection. This exhaust all possibilities where we have a single gluing point.
Moreover we can construct weak traveling waves where we have two gluing points. This can be constructed as follows: combine either 1. or 2. to a constant segment at σ_0, and let $w(\xi) = s$ for $\xi \in [\sigma_0, \sigma_1]$. Then at the second gluing point σ_1 we patch together the constant segment with either 3. or 4. All these scenarios considered here lead to global, unbounded traveling waves, since the non-constant segments are monotone and tend asymptotically to $\pm\infty$. We are however ensured that the resulting wave will be in $L^2(D)$ and is locally Hölder continuous with exponent $\frac{1}{2}$.

In [GR20] the authors take the analysis one step further for the nonlinear variational wave equation, (2.11). They consider how one can combine local, classical traveling waves in order to construct a bounded traveling wave, but this is not possible for the Hunter-Saxton equation. It is not possible to combine the scenarios described in order to get a bounded traveling wave, except from the trivial wave. The derivative of the composite wave, w_ξ, does not change sign any other place than at $w(\xi) = s$ or at $w(\xi) = \pm\infty$. Hence if $w(\cdot)$ consists of an increasing or a decreasing local classical wave on one side of the gluing point σ_0, then at this side $w(\cdot)$ will asymptotically approach $\pm\infty$ as we move away from the gluing point. We can illustrate this by considering gluing scenario 3. and 4. applied to a point σ_0.

(a) A zoom on a glued decreasing part.

(b) A zoom on a glued increasing part.

Figure 12: (a) and (b) show a part of the traveling wave for $\xi > \sigma_0$. $\eta > \sigma_0$ is an arbitrary point where w takes the value a. For (a) we have that $a < s$, while $a > s$ for (b). Here σ_0 is the point where patching takes place. In (a) we have inserted a decreasing segment to the right of σ_0, while in (b) we have inserted an increasing segment.

Consider the case depicted in Figure 12a, where we have glued together a decreasing part to σ_0. In particular we have used scenario 4., thus $\lim_{\xi \downarrow \sigma_0} w_{2,\xi}(\xi) = -\infty$. Consequently w_2 is strictly decreasing and strictly convex for $\xi > \sigma_0$ near σ_0. The derivative is given by

$$w_{2,\xi}(\xi) = -\frac{\sqrt{|k_2|}}{\sqrt{s - w_2(\xi)}}, \tag{4.19}$$

since $w_2(\xi) < s$ for $\xi > \sigma_0$ near σ_0. We observe that this expression is strictly negative, except when w_2 takes the value s in which case it becomes unbounded, and can thus change sign, or $w_2 \to -\infty$. Since $w_2(\xi) < s$ for $\xi > \sigma_0$, the first case is excluded, and the only way this derivative can change sign is if $w_2(\xi) \to -\infty$ in which case $w_{2,\xi} \to 0$. Therefore gluing with a decreasing wave segment leads to a traveling wave which tends asymptotically to $-\infty$.
A similar analysis can be performed for the scenario in Figure 12b, where one glue to σ_0 an increasing part w_2. Then $s < w(\xi)$ for $\sigma_0 < \xi$ and in particular the derivative takes the form

$$w_{2,\xi}(\xi) = \frac{\sqrt{|k_2|}}{\sqrt{w_2(\xi) - s}},$$

which is always positive unless $w_2 = s$ in which case $w_{2,\xi}$ will flip sign while going from $+\infty$ to $-\infty$, or $w_2(\xi) \to +\infty$ in which case $w_{2,\xi}(\xi) \to 0$. Since $w_2(\xi) > s$ for $\xi > \sigma_0$ the former case is

excluded, thus w_2 tends asymptotically to infinity. The next theorem classifies and summarizes what kind of traveling waves that can be obtained by gluing together local classical traveling waves along a curve Γ.

Theorem 4.1 (Glued waves)**.** *Consider a continuous function $w : \mathbb{R} \to \mathbb{R}$ composed of local, classical traveling waves of the Hunter-Saxton equation with wave speed $s \in \mathbb{R}$. Then the following scenarios can play out.*

- *$s \neq w(\xi)$ for any $\xi \in \mathbb{R}$: In this case w is a monotone, classical traveling wave solution which is globally unbounded.*
- *$s = w(\xi)$ for some $\xi \in \mathbb{R}$: Assume σ_0 is such that $w(\sigma_0) = s$. Then the wave w has at least one one-sided unbounded derivative at σ_0, while $w(\cdot)$ remains continuous at σ_0. On either side of this singularity, the wave is a monotone, classical traveling wave solution. The following scenarios are possible:*
  1. *The derivative has the same sign on both sides of σ_0, and the wave has an inflection point at σ_0.*
  2. *The derivative has opposite sign on each side of σ_0 in which case the wave is either concave on both sides or convex on both sides, leading to a cusp singularity at σ_0.*
  3. *The wave can be constant on one side of the singularity and strictly monotone on the other side.*

Moreover the set $\{\xi : w(\xi) = s\}$ consists either of a single point, or a connected segment (interval). In particular this means that there are no weak, bounded traveling waves except from the trivial wave, and there are at most two gluing points.

All possible gluing scenarios described by Theorem 4.1 are depicted in Figure 13. This figure shows what happens locally around the gluing point in the various cases. In particular scenario 1. described by Theorem 4.1 leads to something resembling Figure 13a or Figure 13b, while 2. corresponds to Figures 13c-13d. In particular a traveling wave that looks like that in Figure 13c is called a cuspon according to Definition 4.3, while a traveling wave resembling Figure 13d is called an anti-cuspon. The prefix "anti" refers to the fact that the amplitude is negative and the traveling wave looks like a cuspon reflected about the ξ-axis. Figures 13e-13h correspond to scenario 3. described by Theorem 4.1, here we have only one unbounded one-side derivative, unless we have two gluing points.

A construction that may be of independent interest, is the construction of stumpons. We patch together a monotonically increasing wave segment to a constant segment at σ_0. Let $w(\xi) = s$ for $\xi \in [\sigma_0, \sigma_1]$, where we connect σ_1 to a monotonically decreasing wave segment. This leads to stumpons as defined in Definition 4.3. We can also glue together a monotonically decreasing wave segment to a constant traveling wave at σ_0, and let $w(\xi) = s$ for $\xi \in [\sigma_0, \sigma_1]$. Then we at σ_1 patch the constant segment to an increasing part. This leads to anti-stumpons, where the prefix "anti" again refers to the fact that the wave looks like it has been reflected about the ξ-axis. The outlined constructions lead to something resembling that shown in Figure 14 (a) and Figure 14 (b). That stumpons have to attain the value s at their plateaus was also observed for stumpons of the Camassa-Holm equation in [Len05]. For the Camassa-Holm equation one can however combine countably many wave segments consisting of periodic cuspons, cuspons with decay and constant segments to obtain stumpons, such that it is possible to obtain countably many plateaus. Therefore these stumpons may look much more exotic than those constructed here, since here we can only obtain stumpons with a single plateau. The resulting stumpons for the Hunter-Saxton equation will tend asymptotically to $\pm\infty$, whereas for the Camassa-Holm equation one can construct stumpons that are bounded.

The appearance of a traveling wave shape, and its reflected form, which we observed here several times was to be expected due to the invariance in Remark 4.1. Also observe that there

are two more scenarios that can play out in the case of two gluing points. One can let both wave segments attached to the constant segment be increasing, or deceasing. This exhaust all possible shapes for weak traveling waves of the Hunter-Saxton equation.
Next we will consider an explicit example of a weak traveling wave obtained by gluing together two local, classical traveling waves. The example is taken from [HS91], but adapted in such a way that it is a traveling wave solution. This example can be used to illustrate all gluing scenarios shown in Figure 13.

Example 4.1. Consider the following traveling wave

$$u(x,t) = \begin{cases} s + \alpha(x-st)^{\frac{2}{3}} & \text{if } st \leq x \\ s + \beta(st-x)^{\frac{2}{3}} & \text{if } x < st \end{cases}, \tag{4.20}$$

with $\alpha, \beta \in \mathbb{R}$. To see that this is a weak traveling wave for the Hunter-Saxton equation, introduce $\xi = x - st$, then we can recast this as

$$w(\xi) = \begin{cases} s + \alpha\xi^{\frac{2}{3}} & \text{if } \xi \geq 0 \\ s + \beta(-\xi)^{\frac{2}{3}} & \text{if } \xi < 0 \end{cases}.$$

We can show that this wave consists of two local, classical traveling waves glued together at $\sigma_0 = 0$, equivalently along the curve $x = st$ in the (x,t)-plane. We show only that the expression for $\xi \geq 0$ is a classical traveling wave, the case of $\xi < 0$ is shown similarly. Insert the expression into (4.2), leading to

$$(w-s)w_{\xi\xi} + \frac{1}{2}w_\xi^2 = ([s + a\xi^{\frac{2}{3}}] - s)(-\frac{2a}{9}\xi^{-\frac{4}{3}}) + \frac{1}{2}(\frac{2a}{3}\xi^{-\frac{1}{3}})^2 = 0,$$

so this is indeed a local, classical traveling wave. Observe that at the gluing point, σ_0, we have $w(\sigma_0) = s$ hence (4.12) is satisfied, so this will be a weak traveling wave of the Hunter-Saxton equation. We want to consider how the factor in front of $\sqrt{|w(\sigma_0) - s|}$ in (4.12) looks like in this case. Thus we need to determine the integration constants k_1 and k_2 for the solution. We use (4.3), which in the case of $\xi \geq 0$ reads

$$(w-s)w_\xi^2 = \alpha\xi^{\frac{2}{3}}(\frac{2}{3}\alpha\xi^{-\frac{1}{3}})^2 = \frac{4}{9}\alpha^3 = k_2.$$

The case of $\xi < 0$ is analogous leading to $k_1 = \frac{4}{9}\beta^3$. Thus in particular (4.12) reads

$$\begin{aligned} 0 &= \left[\sqrt{|k_1|}\lim_{\xi\uparrow\sigma_0}\operatorname{sign}\Big[(s-w(\xi))w_\xi(\xi)\Big] - \sqrt{|k_2|}\lim_{\xi\downarrow\sigma_0}\operatorname{sign}\Big[(s-w(\xi))w_\xi(\xi)\Big]\right] \\ &= \sqrt{|\frac{4}{9}\beta^3|}\lim_{\xi\uparrow 0}\operatorname{sign}(-\frac{2}{3}\beta^2(-\xi)^{\frac{1}{3}}) - \sqrt{|\frac{4}{9}\alpha^3|}\lim_{\xi\downarrow 0}\operatorname{sign}(\frac{2}{3}\alpha^2\xi^{\frac{1}{3}}) \\ &= \frac{2}{3}\sqrt{|\beta^3|}\lim_{\xi\uparrow 0}\operatorname{sign}(-(-\xi)^{\frac{1}{3}}) - \frac{2}{3}\sqrt{|\alpha^3|}\lim_{\xi\downarrow 0}\operatorname{sign}(\xi^{\frac{1}{3}}). \\ &= -\frac{2}{3}\Big(\sqrt{|\beta^3|} + \sqrt{|\alpha^3|}\Big). \end{aligned}$$

Thus if w had not been equal to s at the gluing point we would have to force $\alpha = \beta = 0$ in order for this to be a weak traveling wave. The wave (4.20) has a singularity that moves along the line $x = st$, and $u_x(\cdot,t) \in L^2_{\text{loc}}(\mathbb{R})$ at all times, but it does not belong to $L^2(\mathbb{R})$. All scenarios illustrated in Figure 13 can be constructed by this example. Consider for instance Figure 13a, we get something resembling this by setting $\alpha > 0$ and $\beta < 0$, while for Figure 13b we force $\alpha < 0$ and $\beta > 0$. To obtain something like in Figure 13c we set $\alpha, \beta < 0$, while for Figure 13d just revert the sign, $\alpha, \beta > 0$. Scenarios in Figures 13e-13h are all obtained by setting either $\alpha = 0$ or $\beta = 0$ and choosing a sign for the other constant, so to get something resembling Figure 13g, we set $\beta = 0$ and $\alpha > 0$. Setting $\alpha = \beta = 0$ leads to the trivial wave.

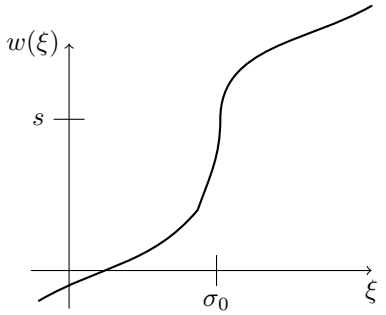

(a) Combining two increasing parts leading to an inflection point at σ_0

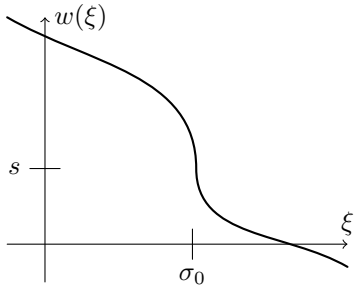

(b) Combining two decreasing parts, leading to an inflection point at σ_0.

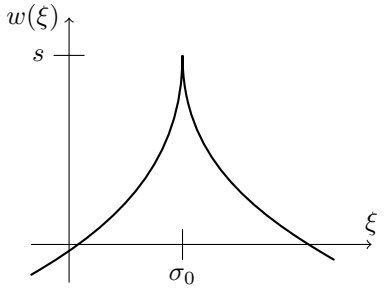

(c) Combining one increasing part with a decreasing part leading to a cusp at σ_0.

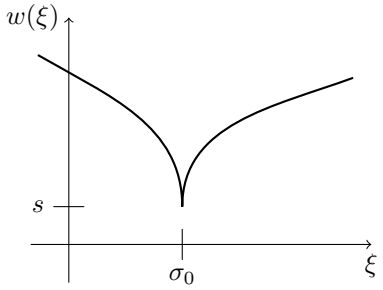

(d) Combining one decreasing part with an increasing part leading to an anti-cusp at σ_0.

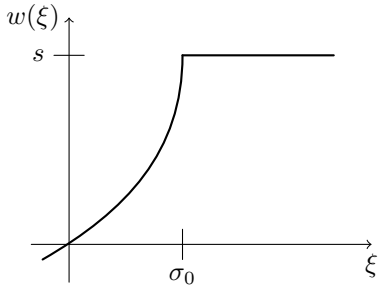

(e) Combining an increasing part with a constant segment.

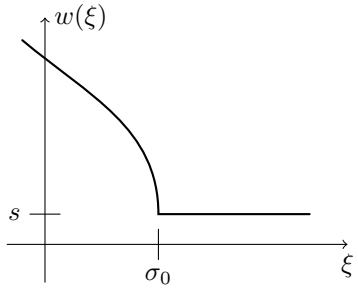

(f) Combining a decreasing part with a constant segment.

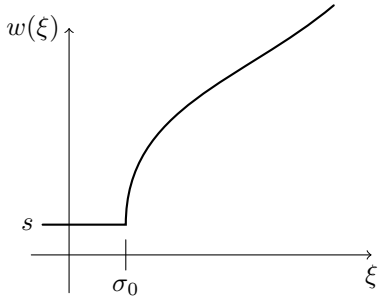

(g) Combining a constant segment with an increasing part at σ_0.

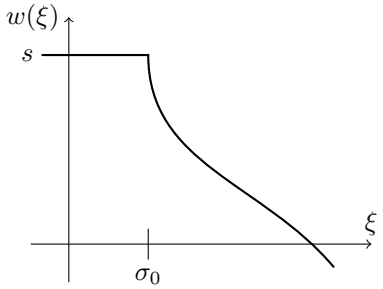

(h) Combining a constant part with a monotonically decreasing part at σ_0.

Figure 13: Illustrates the different possibilities of gluing together two local, classical traveling waves at a single gluing point σ_0.

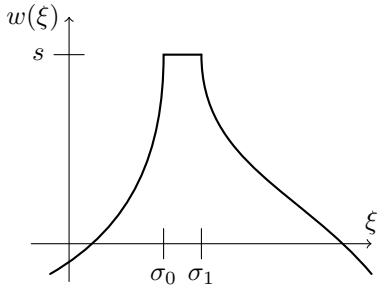

(a) A stumpon. The two gluing points are labeled with σ_0 and σ_1, respectively.

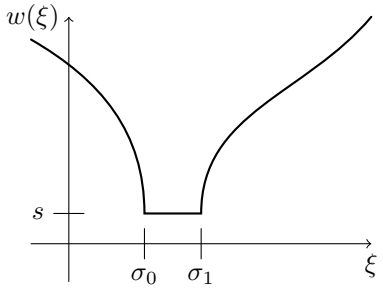

(b) An anti-stumpon. The two gluing points are labeled with σ_0 and σ_1, respectively.

Figure 14: A sketch of a stumpon and an anti-stumpon.

Example 4.2. We can take the previous example one step further, in order to allow for two gluing points. Consider

$$u_0(x) = \begin{cases} s + \alpha(st + c - x)^{\frac{2}{3}} & \text{for } x < st + c \\ s & \text{for } st + c \leq x \leq st + d \\ s + (x - st - d)^{\frac{2}{3}} & \text{for } st + d < x \end{cases},$$

for some $c, d \in \mathbb{R}$ such that $st + c \leq st + d$. This traveling wave is composed of three local, classical traveling waves, in particular the trivial wave at the interval $[st + c, st + d]$, which plays the role of the plateau for stumpons. The first gluing point is $\sigma_0 = c$, while the second gluing point is $\sigma_1 = d$. If $\alpha, \beta < 0$ we get something resembling Figure 14a, while with $\alpha, \beta > 0$ we get something similar to that in Figure 14b. Other choices lead to other kinds of weak traveling waves with two gluing points.

4.3 Multipeakons

Multipeakons are a class of explicitly known soliton-like solutions for the Hunter-Saxton equation. Multipeakons consist of piecewise linear segments, and are solutions on the general form

$$u(x,t) = \begin{cases} u_0(t) & \text{for } x \leq x_1(t) \\ a_n(t)\big[x - x_k(t)\big] + u_n(t) & \text{for } x_k(t) \leq x < x_{k+1}(t) \\ u_N(t) & \text{for } x_N(t) \leq x \end{cases}. \tag{4.21}$$

Here $a_k(t)$ denotes the "amplitude" of the k^{th} linear segment at time t, and $x_k(t)$ is the left endpoint of the k^{th} segment at the same time. The $u_k(t)$'s are the local characteristic wave speeds of the segments. The transition from one linear segment to another is continuous, and the transition points $\{x_k(t)\}$ are called breakpoints.
Such multipeakon solutions can be both conservative and dissipative, depending on how the energy of each linear segment is treated upon wave breaking. We will apply the gluing formalism to multipeakons in Section 7 to show that breakpoints must move along characteristics, and therefore the breakpoints travel at the characteristic velocities. These multipeakons are not traveling waves in the sense that their shape varies with time. In the next chapter we consider the general expression of a conservative multipeakon. Multipeakons are significant for several reason as pointed out in [HZ94], we summarize these observations here

- Solutions to the Hunter-Saxton equation which have derivatives u_x which are compactly supported are limits of multipeakon solutions. Therefore piecwise linear solutions capture the full dynamics of such solutions.
- As $t \to \pm\infty$, any conservative weak solution where u_x has compact spatial support approaches an one-segment linear solution having the same energy as the initial wave

profile. Thus picewise linear solutions describe the long-time asymptotic behaviour. This also applies to dissipative solutions where u_x has compact support, which is shown in [HZ95].

- In Section 2 we saw that the Hunter-Saxton equation could be derived as the high-frequency limit of the Camassa-Holm equation. It turns out that multipeakons are the high-frequency limit of peakon solutions to the Camassa-Holm equation. Numerically it is observed that peakons dominate the long-time asymptotic behaviour of the Camassa-Holm equation. In Section 6 and Section 7 we will consider numerical algorithms based on such multipeakons.

5 Conservative traveling wave solutions

We will now look for conservative traveling waves that satisfy the Hunter-Saxton equation. Therefore we will augment the Hunter-Saxton equation with an additional equation for the energy. Traveling waves are representations of waves with a given shape that translate to the right as time evolves for $s > 0$, and to the left for $s < 0$. Therefore energy cannot concentrate, if the wave is to retain its shape. Moreover since we consider conservative waves, energy cannot dissipate. We still focus on local, classical traveling waves, that are glued together to obtain weak traveling waves. Thus it suffices to augment the Hunter-Saxton equation with (3.3a). The system we consider becomes

$$(u_t + uu_x)_x = \frac{1}{2}u_x^2, \tag{5.1a}$$

$$(u_x^2)_t + (uu_x^2)_x = 0. \tag{5.1b}$$

Inserting the traveling wave ansatz $u(x,t) = w(x - st)$ into the energy equation (5.1b) yields

$$(u_x^2)_t + (uu_x^2)_x = -2sw_\xi w_{\xi\xi} + w_\xi^3 + 2ww_\xi w_{\xi\xi} = 0.$$

Therefore a local, classical conservative traveling wave of the Hunter-Saxton equation must satisfy the following system of second order ODEs

$$(w - s)w_{\xi\xi} + \frac{1}{2}w_\xi^2 = 0, \tag{5.2a}$$

$$2(w - s)w_{\xi\xi}w_\xi + w_\xi^3 = 0. \tag{5.2b}$$

We observe that (5.2b) is $2w_\xi$ multiplied by (5.2a). Therefore applying the chain rule, integrating with respect to ξ, and introducing an integration constant results in

$$w_\xi(\xi)^2(w(\xi) - s) = k, \tag{5.3}$$

which we recognize from Section 4.
We now want to proceed in a similar way as in Section 4. We have already considered (5.1a), so now we proceed first by only considering equation (5.1b). We want to see what requirements the energy equation imposes on two local, classical traveling waves that are glued together. These will be additional requirements to those in Section 4. The weak form of the evolution equation for the energy is obtained by multiplying (5.1b) by a test function $\phi \in C_0^\infty(\mathbb{R} \times (0,\infty))$, and integrating by parts. The result is

$$\int_0^\infty \int_{\mathbb{R}} (u_x^2\phi_t + uu_x^2\phi_x)dxdt = 0,$$

for all test functions supported away from $t = 0$. Otherwise we would get a contribution from the initial data. Inserting the traveling wave ansatz leads to

$$\int_0^\infty \int_{\mathbb{R}} (w_\xi^2\phi_t + ww_\xi^2\phi_x)\,dx\,dt = 0. \tag{5.4}$$

Definition 5.1 (Conservative traveling)**.** We say that $u(x,t) = w(x - st)$ is a conservative traveling wave of the Hunter-Saxton equation if u is a weak traveling wave and in addition

$$\int_0^\infty \int_{\mathbb{R}} (w_\xi^2\phi_t + ww_\xi^2\phi_x)\,dx\,dt = 0,$$

holds for all test functions $\phi \in C_0^\infty(\mathbb{R} \times (0,\infty))$.

We assume that the first partial derivatives, u_t and u_x have isolated discontinuities moving along a curve Γ which we parameterize by $\Gamma : x = \sigma(t)$. The curve may resemble that in Figure 9. We assume that there is a sufficiently small neighbourhood D of Γ, which contains the curve

Γ, such that u is a classical solution on either side of the curve. We make the same assumptions about $\sigma(\cdot)$ as in Section 4, i.e., σ is a smooth and strictly increasing function of t. ϕ is a test function whose support lies within the neighbourhood D, that is, $\phi \in C_0^\infty(D)$. We have

$$\iint_D (u_x^2\phi_t + uu_x^2\phi_x)\,dx\,dt = \lim_{\epsilon\downarrow 0} \iint_{D_1^\epsilon \cup D_2^\epsilon} (u_x^2\phi_t + uu_x^2\phi_x)\,dx\,dt,$$

where as before D_i^ϵ is defined by (4.7). We proceed in a completely analogous fashion to what we did in Section 4, and consider D_1^ϵ first. Since u is a classical solution inside D_1^ϵ we can add $2u_xu_{xt}\phi + (u_x^3 + 2uu_xu_{xx})\phi = 0$. Thus applying Leibniz' rule we obtain

$$\begin{aligned}
&\iint_{D_1^\epsilon} \Big(u_x^2\phi_t + uu_x^2\phi_x + (2u_xu_{xt} + u_x^3 + 2uu_xu_{xx})\phi\Big)\,dx\,dt \\
&\quad = \iint_{D_1^\epsilon} \Big((u_x^2\phi)_t + (uu_x^2\phi)_x\Big)\,dx\,dt \\
&\quad = \int_{\partial D_1^\epsilon} ((uu_x^2\phi)dt - (u_x^2\phi)dx).
\end{aligned}$$

In the last equality we applied Green's theorem, which is stated in Remark 4.2. ϕ vanishes everywhere except on $\Gamma_1^\epsilon := \{(\sigma_1^\epsilon(t), t) : t \in I_1^\epsilon\}$, where as before $I_1^\epsilon := \{t \in [0,\infty) : (\sigma_1^\epsilon(t), t) \in D_1\}$. Therefore this reduces to

$$\begin{aligned}
&\iint_{D_1^\epsilon} (u_x^2\phi_t + uu_x^2\phi_x)\,dx\,dt \\
&\quad = \int_{I_1^\epsilon} \Big((uu_x^2\phi)(\sigma_1^\epsilon(t), t) - (u_x^2\phi)(\sigma_1^\epsilon(t), t)\dot\sigma_1^\epsilon(t)\Big)dt.
\end{aligned} \tag{5.5}$$

We have not assumed anything in particular about the curve, so this holds for a general u admitting discontinuities in its first order partial derivatives in time and space, that move along a curve Γ. We can do precisely the same for D_2^ϵ, where we will get a minus sign in front. This is due to a change in orientation when we apply Green's theorem. The end result reads

$$\begin{aligned}
&\iint_{D_2^\epsilon} (u_x^2\phi_t + uu_x^2\phi_x)\,dx\,dt \\
&\quad = -\int_{I_2^\epsilon} \Big((uu_x^2\phi)(\sigma_2^\epsilon(t), t) - (u_x^2\phi)(\sigma_2^\epsilon(t), t)\dot\sigma_2^\epsilon(t)\Big)\,dt\,.
\end{aligned} \tag{5.6}$$

Now we will again specialize to traveling waves. Then the curve Γ becomes a diagonal line in the (x,t)-plane. The next lemma ensures that gluing to produce weak solutions to the energy equation is possible.

Lemma 5.1. *Consider two local, classical traveling wave solutions u_1 and u_2 to the evolution equation for the energy in D_1 and D_2, respectively. The setting is depicted in Figure 10. We patch the solutions together along a curve $\Gamma : x = \sigma_0 + st$, where σ_0 is a constant, in order to obtain a continuous traveling wave $u(x,t) = w(x - st)$ in the whole region D. That is, a traveling wave w, that satisfies*

$$\iint_D (w_\xi^2\phi_t + ww_\xi^2\phi_x)\,dx\,dt = 0,$$

for all test functions $\phi \in C_0^\infty(D)$. There are two scenarios that may occur:

- *w_ξ is bounded along the curve, in which case*

$$w_\xi^2(\sigma_0^-) = w_\xi^2(\sigma_0^+), \tag{5.7}$$

where $w_\xi^2(\sigma_0^-)$ and $w_\xi^2(\sigma_0^+)$ denote the left and right limits of w_ξ^2 at σ_0, respectively.

- *w_ξ may be unbounded, leading to*

$$\begin{gathered} |k_1| \lim_{\xi\uparrow\sigma_0} sign\Big[(w(\xi)-s)w_\xi^2(\xi)\Big] - |k_2| \lim_{\xi\downarrow\sigma_0} sign\Big[(w(\xi)-s)w_\xi^2(\xi)\Big] = 0, \\ \Updownarrow \\ k_1 - k_2 = 0. \end{gathered} \tag{5.8}$$

Here k_1 and k_2 denote the integration constants corresponding to the local, classical traveling waves u_1 and u_2, respectively.

Proof. We insert the traveling wave ansatz $u(x,t) = w(x-st)$ into (5.5) and (5.6). Then we proceed analogously to what we did in Section 4. We parameterize by $x = \sigma_1^\epsilon(t) = \sigma_0 + st - \epsilon\sqrt{s^2+1}$, thus $\dot{\sigma_1^\epsilon} = s$. As a consequence (5.5) reduces to

$$\begin{aligned} &\iint_{D_1^\epsilon} (w_\xi^2\phi_t + ww_\xi^2\phi_x)\,dx\,dt \\ &\quad = \int_{I_1^\epsilon} \Big(\left[w(\sigma_1^\epsilon(t)-st)-s\right] w_\xi^2(\sigma_1^\epsilon(t)-st)\phi(\sigma_1^\epsilon(t),t)\Big)\,dt\,. \end{aligned} \tag{5.9}$$

Similarly for the neighbourhood D_2^ϵ, where $\sigma_2^\epsilon(t) = \sigma_0 + st + \epsilon\sqrt{s^2+1}$. Thus (5.6) now becomes

$$\begin{aligned} &\iint_{D_2^\epsilon} (w_\xi^2\phi_t + ww_\xi^2\phi_x)\,dx\,dt \\ &\quad = -\int_{I_2^\epsilon} \Big(\left[w\left(\sigma_2^\epsilon(t)-st\right)-s\right] w_\xi^2(\sigma_2^\epsilon(t)-st)\phi(\sigma_2^\epsilon(t),t)\Big)\,dt\,. \end{aligned} \tag{5.10}$$

We here notice that $(w(\sigma_i^\epsilon(t)-st)-s)w_\xi^2(\sigma_i^\epsilon(t)-st)) = k_i$ by (5.3), but we will not substitute this yet. First we assume that w_ξ is bounded. w is always required to be continuous. We can then proceed by taking the limit $\epsilon \downarrow 0$ directly, yielding

$$\begin{aligned} &\iint_D (w_\xi^2\phi_t + ww_\xi^2\phi_x)\,dx\,dt \\ &\quad = \lim_{\epsilon\downarrow 0} \Big(\sum_{k=1}^{2} \iint_{D_k^\epsilon} \Big((w_\xi^2\phi_t + ww_\xi^2\phi_x\Big)\,dx\,dt \\ &\quad = \int_I \Big(\Big[w(\sigma_0)-s\Big](w_\xi^2(\sigma_0^-) - w_\xi^2(\sigma_0^+))\phi(\sigma(t),t)\Big)\,dt\,. \end{aligned} \tag{5.11}$$

Here $w_\xi^2(\sigma_0^+)$ and $w_\xi^2(\sigma_0^-)$ denote the right and left limits of w_ξ^2 at σ_0, respectively. The expression should hold for any $\phi \in C_0^\infty(D)$ in order for w to be a weak traveling wave of the energy equation. Picking a strictly positive test function, $\phi > 0$, we observe

$$\begin{aligned} &\int_I \Big(\Big[w(\sigma_0)-s\Big](w_\xi^2(\sigma_0^-) - w_\xi^2(\sigma^+))\phi(\sigma(t),t)\Big)\,dt \\ &\quad = \Big[w(\sigma_0)-s\Big](w_\xi^2(\sigma_0^-) - w_\xi^2(\sigma^+)) \int_I \phi(\sigma(t),t)\,dt\,. \end{aligned}$$

Hence the pre-factor has to vanish identically, i.e.,

$$\Big[w(\sigma_0)-s\Big](w_\xi^2(\sigma_0^-) - w_\xi^2(\sigma^+)) = 0,$$

this proves (5.7), since the case $w(\sigma_0) = s$ leads to an unbounded derivative, w_ξ.

Now if we allow the derivative w_ξ to be unbounded along the curve Γ, then we need to eliminate w_ξ appearing in (5.9) and (5.10). Since w is a classical traveling wave solution to the energy

equation in D_i^ϵ we have that

$$w_\xi^2 = \frac{k_i}{w-s}, \quad i \in \{1,2\}.$$

Thus we observe that in D_1^ϵ we can write

$$[w(\sigma_1^\epsilon(t)-st)-s]w_\xi^2(\sigma_1^\epsilon(t)-st) = \operatorname{sign}\left[(w(\sigma_1^\epsilon(t)-st)-s)w_\xi^2\right]|k_1|.$$

Similarly for w in D_2^ϵ, but now we may possibly have another integration constant k_2 instead. Therefore we get

$$[w(\sigma_2^\epsilon(t)-st)-s]w_\xi^2(\sigma_2^\epsilon(t)-st) = \operatorname{sign}\left[(w(\sigma_2^\epsilon(t)-st)-s)w_\xi^2\right]|k_2|.$$

We can now proceed by substituting these alternative formulations into (5.9) and (5.10), respectively. Thus

$$\begin{aligned}&\iint_{D_1^\epsilon}(w_\xi^2\phi_t + ww_\xi^2\phi_x)\,dx\,dt\\ &\quad= \int_{I_1^\epsilon}\left(\operatorname{sign}\left[(w(\sigma_1^\epsilon(t)-st)-s)w_\xi^2(\sigma_1^\epsilon(t)-st)\right]|k_1|\phi(\sigma_1^\epsilon(t),t)\right)dt,\end{aligned}$$

and

$$\begin{aligned}&\iint_{D_2^\epsilon}(w_\xi^2\phi_t + ww_\xi^2\phi_x)\,dx\,dt\\ &\quad= -\int_{I_2^\epsilon}\left(\operatorname{sign}\left[(w(\sigma_2^\epsilon(t)-st)-s)w_\xi^2(\sigma_2^\epsilon(t)-st)\right]|k_2|\phi(\sigma_2^\epsilon(t),t)\right)dt\,.\end{aligned}$$

Taking the limit $\epsilon \downarrow 0$ and using continuity of w gives

$$\begin{aligned}&\iint_D(w_\xi^2\phi_t + ww_\xi^2\phi_x)\,dx\,dt\\ &\quad= \int_I\left(|k_1|\lim_{\xi\uparrow\sigma_0}\operatorname{sign}\left[(w(\xi)-s)w_\xi^2(\xi)\right] - |k_2|\lim_{\xi\downarrow\sigma_0}\operatorname{sign}\left[(w(\xi)-s)w_\xi^2(\xi)\right]\right)\phi(\sigma(t),t)\,dt\,.\end{aligned}$$

Picking again a strictly positive test function $\phi > 0$, we get that the factor in front which is independent of t must vanish. This leads to the second condition stated in the lemma. The equivalence follows by observing that w satisfies (5.3). □

We consider what kinds of local, classical traveling waves for the energy equation (5.1b), that can be patched together at a point σ_0. This is illuminating, but we will eventually "couple" (5.1b) with (5.1a) again. Then we already know that we require $w(\sigma_0) = s$ at the gluing point, and that the derivative at σ_0 needs to be unbounded at least on one side of σ_0. Since we have local, classical traveling waves for the energy equation, the derivatives are given by

$$w_{i,\xi}^2(\xi) = \frac{k_i}{w_i(\xi)-s}. \tag{5.12}$$

First assume that the resulting composite wave, w, has a derivative, w_ξ which is bounded at the gluing point, σ_0. Thus $w(\sigma_0) \neq s$ and (5.7) should hold. This yields a total of four combinations

$$\pm w_{1,\xi}(\sigma_0^-) = \pm w_{2,\xi}(\sigma_0^+).$$

The cases of same sign causes w_ξ to be continuous at σ_0. In particular this means that w is a monotone C^1 function, and it coincides with the local solution of the ODE (5.12) in D,

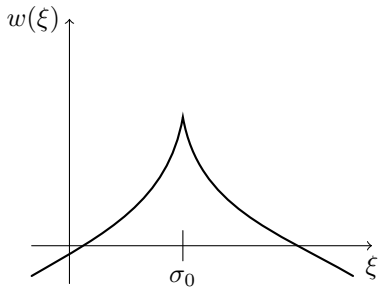

Figure 15: A possible peakon for the energy equation. The slope is the same on either side, except from a difference in sign.

for a fixed integration constant $k_1 \in \mathbb{R}$. Thus, gluing does not yield a new solution, rather a continuation of the local solution. Therefore the two cases of same sign are excluded. We are left with

$$w_{1,\xi}(\sigma_0^-) = -w_{2,\xi}(\sigma_0^+),$$

i.e., the derivatives are of opposite sign, but of the same finite magnitude. We did not observe this for (5.1a), and this allows for the occurrence of peakons according to Definition 4.3. We have by (5.12) that $|k_1| = |k_2|$ in this case. An example of a peakon is shown in Figure 15. However, this case is prohibited when we couple (5.1b) with (5.1a), as already observed, since w is required to have at least one one-sided derivative that is unbounded at the gluing point. Now we consider the case where w_ξ is allowed to be unbounded along Γ, then (5.8) holds. In particular we allow $w = s$ along the curve. Then we require

$$\begin{aligned} |k_1| \lim_{\xi \uparrow \sigma_0} \operatorname{sign}\Big[(w_1(\xi) - s) w_{1,\xi}^2(\xi)\Big] - |k_2| \lim_{\xi \downarrow \sigma_0} \operatorname{sign}\Big[(w_2(\xi) - s) w_{2,\xi}^2(\xi)\Big] \\ = k_1 - k_2 = 0. \end{aligned}$$

In particular if k_1 and k_2 are of opposite signs then this will not become zero, unless $k_1 = k_2 = 0$. This leads to the trivial wave, $w = \text{const}$. The condition enforces $k_1 = k_2$. In particular this means that when we glue together two local classical traveling waves of the energy equation and the derivatives might be unbounded at the gluing point, then the two traveling waves have both to be located at the same side of the line $w(\xi) = s$. This is since we have

$$(w_i - s)^2 w_{i,\xi}^2 = k_i (w_i - s),$$

by multiplying (5.12) with $(w_i - s)^2$ on both sides. The left side is always positive, thus the sign of k_i depends on the sign of $w_i - s$. Therefore if $k_1 = k_2$, we require the two local, classical traveling waves to be located on the same side of $w = s$.
Consequently there are two cases where gluing is adequate for (5.1b). One when the two local, classical traveling waves have derivatives that are finite but of opposite sign, leading to peakons. The other case is when the local, classical traveling waves have the same integration constant, but can posses unbounded derivatives at the gluing point. In particular if the derivatives are bounded this reduces to the peakon case. We observe that condition (5.8) by Lemma 5.1 is not immediately satisfied when $w = s$, so it is an additional requirement that must be satisfied in addition to that found in Section 4 for weak, conservative traveling waves.

5.1 Classification of conservative waves of the Hunter-Saxton Equation

Theorem 5.1 (Conservative traveling waves)**.** *Assume that $w : \mathbb{R} \to \mathbb{R}$ is a conservative traveling wave of the Hunter-Saxton equation according to Definition 5.1. Then there are two possibilities:*

1. *w is composed of two local, classical traveling waves glued together at a point σ_0. The gluing point, σ_0, is a cusp singularity, and w is a cuspon.*

2. *w is the trivial wave.*

Proof. The strategy is to consider all the possible weak traveling waves depicted in Figure 13, and see which of them that satisfy the additional constraint (5.8) imposed by Lemma 5.1.

First consider the case where we glue together two monotonically increasing or two monotonically decreasing classical, traveling waves at a point σ_0. This is described in 1. Theorem 4.1. Thus the gluing point σ_0 is an inflection point. Assume that both local, classical traveling waves are monotonically increasing, resembling that in Figure 13a. The same argument works for the case where both are monotonically decreasing instead, but with a slight modification. We observe that $w_1(\xi) - s < 0$ for $\xi < \sigma_0$ while $w_2(\xi) - s > 0$ for $\xi > \sigma_0$. $w_\xi^2(\xi)$ is finite provided $\xi \neq \sigma_0$, therefore equation (5.8) from Lemma 5.1 reduces to

$$\begin{aligned} 0 &= |k_1| \lim_{\xi \uparrow \sigma_0} \operatorname{sign}\Big[(w(\xi) - s)w_\xi^2(\xi)\Big] - |k_2| \lim_{\xi \downarrow \sigma_0} \operatorname{sign}\Big[(w(\xi) - s)w_\xi^2(\xi)\Big] \\ &= -|k_1| - |k_2|. \end{aligned}$$

Thus in order for this to be a conservative traveling wave, we require $k_1 = k_2 = 0$. This leads to the trivial wave.

Consider 2. from Theorem 4.1. Hence we have a cusp singularity at the gluing point σ_0. We can without loss of generality assume that w_1 is a monotonically increasing, classical traveling wave, while w_2 is a monotonically decreasing, classical traveling wave. Such a scenario is illustrated in Figure 16a. In particular we have that $w_1(\xi) - s < 0$ for $\xi < \sigma_0$, and $w_2(\xi) - s < 0$ for $\xi > \sigma_0$. The term $w_{i,\xi}^2(\xi) > 0$ for $i \in \{1, 2\}$, is finite provided $\xi \neq \sigma_0$. Therefore (5.8) becomes

$$\begin{aligned} 0 &= |k_1| \lim_{\xi \uparrow \sigma_0} \operatorname{sign}\Big[(w(\xi) - s)w_\xi^2(\xi)\Big] - |k_2| \lim_{\xi \downarrow \sigma_0} \operatorname{sign}\Big[(w(\xi) - s)w_\xi^2(\xi)\Big] \\ &= -|k_1| + |k_2|. \end{aligned}$$

This forces the magnitude of the integration constants to be the same. Hence this allows for the existence of nontrivial conservative traveling waves. Possible shapes for conservative cuspons are depicted in Figure 16, the slopes are equal in magnitude but are of opposite sign on either side of the cusp.

The final case to consider is when we glue together one monotonically increasing or monotonically decreasing wave segment to a constant segment, i.e., we have a one-sided unbounded derivative, which corresponds to 3. in Theorem 4.1. Without loss of generality we can assume that w_1 is a monotonically increasing traveling wave with unbounded derivative at the gluing point σ_0, and that $w_2 = s$. All other cases with a one-sided unbounded derivative can be treated similarly. This situation is visualized in Figure 13e. Then (5.8) reduces to

$$\begin{aligned} 0 &= |k_1| \lim_{\xi \uparrow \sigma_0} \operatorname{sign}\Big[(w(\xi) - s)w_\xi^2(\xi)\Big] - |k_2| \lim_{\xi \downarrow \sigma_0} \operatorname{sign}\Big[(w(\xi) - s)w_\xi^2(\xi)\Big] \\ &= |k_1| \lim_{\xi \uparrow \sigma_0} \operatorname{sign}\Big[(w(\xi) - s)w_\xi^2(\xi)\Big] = -|k_1|, \end{aligned}$$

since $w_2(\xi) = s$ for $\xi \geq \sigma_0$ so the derivative $w_{2,\xi}$ is zero. This forces $k_1 = 0$, and thus w_1 to be a constant as well. This also prevents any of the cases of two gluing points to lead to a conservative traveling wave, since then we have to glue together an increasing or decreasing wave segment to a constant segment first, before we glue together a new increasing or decreasing wave segment to the constant segment at a later time. □

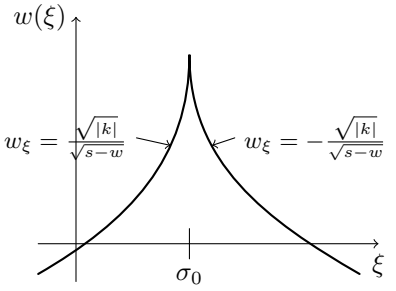

(a) A conservative cuspon, with a cusp singularity at σ_0. The slopes away from the cusp are of equal magnitude, but opposite sign.

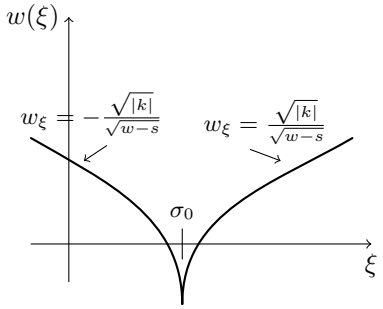

(b) A conservative anti-cuspon, with cusp singularity at σ_0.

Figure 16: The possible conservative traveling waves of the Hunter-Saxton equation, except from the trivial wave.

The theorem states that the only possible conservative traveling waves of the Hunter-Saxton equation, are cuspons. Moreover we have developed an explicit construction procedure, which can be used to construct conservative traveling waves. A formal explanation of why a cuspon is a suitable candidate for a conservative traveling wave for the Hunter-Saxton equation, as opposed to the other cases of weak traveling waves can be given in terms of characteristics. Such an explanation is given in the next subsection. First we present an explicit example of a conservative traveling wave, before we elaborate on conservative multipeakons.

Example 5.1. We consider the traveling wave solution (4.20) from Example 4.1. We want the solution to be a weak conservative traveling wave. The solution under consideration is

$$u(x,t) = \begin{cases} s + \alpha(x-st)^{\frac{2}{3}} & \text{if } st \leq x \\ s + \beta(st-x)^{\frac{2}{3}} & \text{if } x < st. \end{cases}$$

One can directly use the weak formulation of the energy equation (5.4) to verify under what circumstances this is a conservative traveling wave of the Hunter-Saxton equation. Alternatively we know that w_ξ becomes unbounded at the gluing point $\sigma_0 = 0$, since $w_\xi \sim \xi^{-\frac{1}{3}}$. Therefore we can apply Lemma 5.1, and in particular (5.8). This yields

$$\begin{aligned} 0 &= |k_1| \lim_{\xi \uparrow \sigma_0} \operatorname{sign}\Big[(w(\xi)-s)w_\xi^2(\xi)\Big] - |k_2| \lim_{\xi \downarrow \sigma_0} \operatorname{sign}\Big[(w(\xi)-s)w_\xi^2(\xi)\Big] \\ &= |\frac{4}{9}\beta^3| \lim_{\xi \uparrow 0} \operatorname{sign}\Big[\beta(-\xi)^{\frac{2}{3}}(-\frac{2}{3}\beta(-\xi)^{-\frac{1}{3}})^2\Big] - |\frac{4}{9}\alpha^3| \lim_{\xi \downarrow 0} \operatorname{sign}\Big[\alpha\xi^{\frac{2}{3}}(\frac{2}{3}\alpha\xi^{-\frac{1}{3}})^2\Big] \\ &= |\frac{4}{9}\beta^3| \lim_{\xi \uparrow 0} \operatorname{sign}(\frac{4}{9}\beta^3) - |\frac{4}{9}\alpha^3| \lim_{\xi \downarrow 0} \operatorname{sign}(\frac{4}{9}\alpha^3) \\ &= \frac{4}{9}\Big(\beta^3 - \alpha^3\Big). \end{aligned}$$

Hence we require $\alpha = \beta$, and we observe that $\alpha = \beta = 0$ yields the trivial wave, which is a conservative wave. The choice $\alpha < 0$ yields something similar to Figure 16a, and $\alpha > 0$ gives something similar to Figure 16b. We see that the derivative changes sign after it becomes unbounded.

5.2 Conservative multipeakons

Another class of explicitly known conservative soliton-like solutions to the Hunter-Saxton equation are conservative multipeakons as mentioned in Section 4. Applying the Euler-Lagrangian formalism outlined in Subsection 3.3, we can explicitly find the solution for a general conservative multipeakon. Let $\{x_k\}_{k=1}^N$ be a finite strictly increasing sequence in $\mathbb{R}$. We consider the

initial value problem for the Hunter-Saxton equation with

$$u|_{t=0} = \begin{cases} c_0 & \text{if } x < x_1 \\ p_i(x - x_i) + c_i & \text{if } x_i \leq x < x_{i+1} \\ c_N & \text{if } x \geq x_N \end{cases}.$$

Here the p_k's and x_k's are arbitrary, while the constants c_k's are chosen such that $u|_{t=0}$ is continuous. The initial Radon measure is given by

$$d\mu_0(x) = u_{0,x}^2(x)\, dx,$$

provided wave breaking does not occur initially. The solution to the Cauchy problem for the Hunter-Saxton equation is found by applying the solution operator $T_t : \mathcal{D} \to \mathcal{D}$ to the initial data. That is, $T_t(u_0, \mu_0) = (u(t), \mu(t))$ is the solution in Eulerian coordinates. This results in

$$u(x,t) = \begin{cases} -\frac{1}{4}Kt + c_0 & \text{for } x < x_1(t) \\ \frac{p_k}{(1+\frac{1}{2}p_k t)}\left(x - x_k(t)\right) + \frac{1}{2}\left(F_0(x_k) - \frac{1}{2}K\right)t + c_k & \text{for } x_k(t) \leq x < x_{k+1}(t) \\ \frac{1}{4}Kt + c_N & \text{for } x \geq x_N(t) \end{cases},$$

and

$$d\mu_{ac}(x,t) = u_x(x,t)^2\, dx\,.$$

Notice that we can only say something in general for the absolutely continuous part, since energy might concentrate in a single point in Eulerian coordinates for multipeakons, thus we might at a given time also have a contribution from the singular part of μ. Here we have introduced $K = \mu_0(\mathbb{R})$ as the total initial cumulative energy, and $F_0(x_k) = \mu_0((-\infty, x_k])$ as the initial cumulative energy up to the point x_k. We know by the Lagrangian system (3.18a)-(3.18c), that the cumulative energy remains a constant function of time. In particular we also observe, that the solution is again a continuous and piecewise linear function in the spatial variable. The breakpoints travel along characteristics, and therefore their positions are described by

$$x_k(t) = \frac{1}{4}(F_0(x_k) - \frac{1}{2}K)t^2 + c_k t + x_k, \tag{5.13}$$

where $x_k = x_k(0)$ is the starting point of the k^{th} breakpoint. These breakpoints move at the local velocities

$$u_k(t) = c_k + \frac{1}{2}\big(F_0(x_k) - \frac{1}{2}K\big)t.$$

The observation that the breakpoints travel along characteristics in order for this to classify as a weak solution in the first place, is shown in Section 7, and particular in the proof of Lemma 7.1. Thus the breakpoints $x_k(\cdot)$ moves at the local Lagrangian velocity $U(x_k(t), t) = u_k(t)$. The momentum/energy of each segment is conserved even after blow up for conservative multipeakons, since the Lagrangian cumulative energy is constant, i.e., $H(x_{k+1}(t), t) - H(x_k(t), t) = H(x_{k+1}, 0) - H(x_k, 0)$. The breakpoint expression (5.13), was found by the explicit expression we have for the time evolution of the characteristics in Lagrangian coordinates. In particular

$$X(\xi', t) = (\frac{1}{4}H(\xi', 0) - \frac{1}{8}K)t^2 + U(\xi', 0)t + X(\xi', 0),$$

for a characteristic starting at the point ξ'. It is shown formally in [HZ94] that the ordering of the breakpoints is preserved at all times for conservative solutions, that is $x_{k+1}(t) - x_k(t) \geq 0$ at all times. In particular, equality holds only when two breakpoints meet. The focusing of two adjacent breakpoints is how wave breaking manifests itself for such multipeakon solutions. We can apply Theorem 3.1 and in particular the expression for the blow-up time t^*, (3.12), to

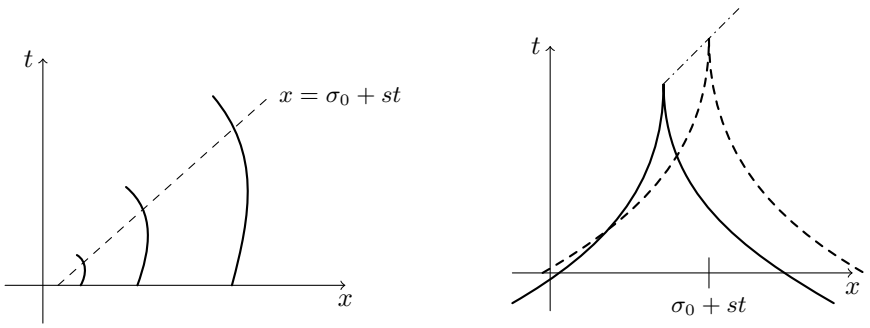

(a) The diagonal line $x = \sigma_0 + st$, and characteristics crossing it.

(b) One conservative cuspon, with the gluing point moving along the diagonal line.

Figure 17: (a) illustrates that different characteristics crosses the diagonal line at different times. (b) shows a conservative cuspon, where the cusp is traveling along the diagonal line $\sigma_0 + st$.

find the blow-up times for the individual linear segments. In particular the n^{th} linear segment shrinks to a singleton when

$$x_n(t) = x_{n+1}(t),$$

which happens at time

$$t_n^* = \frac{2}{\sup_x\{u_0'(x)\}} = -\frac{2}{p_n}.$$

Therefore we have a sequence $\{t_n^*\}_n$ of breaking times for the multipeakon, representing when various linear segments shrink to singletons. Such conservative multipeakons is an essential ingredient in the numerical algorithm presented in Section 6.

5.3 Wave breaking for cuspons

Intuitively one would maybe think that the gluing point moves along a single characteristic with respect to time, but that is not the case. In [Gru16], the author considers a cuspon with exponential decay and non-vanishing asymptotics for the Camassa-Holm equation. Usually wave breaking is associated with energy concentrating on a Lebesgue null set in Eulerian coordinates, which corresponds to wave breaking occurring for a set of positive measure in Lagrangian coordinates. In [Gru16], it is shown that the set of points where wave breaking takes place for the traveling wave consist of a single point in Lagrangian coordinates for each time, and the breaking point is not traveling along a single characteristic as time evolves, but instead it jumps from one characteristic to the next one. We thus expect something similar to occur for the conservative traveling waves to the Hunter-Saxton equation. We know the gluing point, moves along a diagonal line in the (x, t)-plane, this is shown as a dashed line in Figure 17b. We will here only consider the cuspon shown in Figure 17b, although similar considerations can be done for a cuspon of the form shown in Figure 16b.

Wave breaking takes place for any fixed time t for the cuspon. Thus an infinitesimal amount of energy concentrates at any time. The Radon measure discussed in Subsection 3.3 is purely absolutely continuous (with respect to the Lebesgue measure), since the energy accumulation is infinitesimal. Wave breaking presents itself on a new form compared to what one typically expects. Consider the conservative cuspon depicted in Figure 17b we observe that

$$\lim_{\xi\uparrow\sigma_0} w_\xi(\xi) = \infty,$$
$$\lim_{\xi\downarrow\sigma_0} w_\xi(\xi) = -\infty,$$

and hence

$$\lim_{\xi \to \sigma_0} w_\xi^2(\xi) = \infty.$$

This implies that for $u(x,t) = w(x - st)$, the derivative $u_x(x,t)$ is well-defined for all $x \in \mathbb{R} \setminus \{\sigma_0 + st\}$ and we have

$$\lim_{x \to (\sigma_0 + st)} u_x^2(x,t) = \infty. \tag{5.14}$$

Hence, wave breaking occurs along the diagonal line depicted in Figure 17a at all times t. That is, for each fixed time, wave breaking occurs at the single point located on the diagonal line in Eulerian coordinates. We want to turn to Lagrangian coordinates and see how the breaking points present themselves here. In particular we want to show that the cusp singularity jumps from characteristic to characteristic. In order to achieve this we will need to modify the Euler-Lagrange formalism introduced in Subsection 3.3, since now the total energy is infinite. Therefore we can no longer use $-\infty$ as a reference point for the energy. The modification of the formalism takes advantage of some of the properties of the cuspons solutions of the Hunter-Saxton equation. In particular we have a symmetry around the cusp singularity located at σ_0, i.e.,

$$w(\sigma_0 - \delta) = w(\sigma_0 + \delta),$$

for any $\delta > 0$. We also know that the wave height is equal to the wave speed at the cusp singularity. Therefore it makes sense to consider the following initial-boundary value problem

$$u_t + uu_x = \frac{1}{2} \int_{\sigma_0 + st}^{x} u_x^2 dy, \tag{5.15a}$$

$$(u_x^2)_t + (uu_x^2)_x = 0, \tag{5.15b}$$

$$u|_{t=0}(x) = u_0(x), \tag{5.15c}$$

$$u|_{x=\sigma_0+st}(t) = s \quad \text{for all } t \geq 0, \tag{5.15d}$$

since we know that any conservative traveling wave is symmetric about the diagonal line $\sigma_0 + st$. This bears some similarities to that done in [HZ95] where the authors imposed $u|_{x=0} = 0$, except now we know the value of u along a moving reference frame instead. We need to modify the way we initialize the characteristics to account for this new formulation. In particular we modify (3.21a) in Definition 3.7 by instead setting

$$X_0(\xi) = \sup\{x \in \mathbb{R} : \mu((\sigma_0, x)) + x < \xi\}, \tag{5.16}$$

as the initial characteristic in Lagrangian coordinates. Notice here that the use of an open interval (σ_0, x), instead of a half-open interval $(\sigma_0, x]$ or $[\sigma_0, x)$, or a closed interval $[\sigma_0, x]$ does not matter, since the measure is purely absolutely continuous. Hence we use the diagonal line as reference point for the energy, therefore the reference point changes with time. We can now compute the corresponding Lagrangian system with this modification. We proceed in a similar fashion as done in [Nor16a] when the Lagrangian system of the two-component Hunter-Saxton system is motivated. We still have

$$\begin{aligned} X_t(\xi,t) &= U(\xi,t), \\ U(\xi,t) &= u(X(\xi,t)) = w(X(\xi,t) - st). \end{aligned}$$

Since μ is purely absolutely continuous with respect to the Lebesgue measure, we can take any characteristic $X(\xi,t)$ and proceed with the calculations done in [Nor16a]. In this particular case define

$$H(\xi,t) = \mu((\sigma_0 + st, X(\xi,t)), t) = \int_{\sigma_0+st}^{X(\xi,t)} u_x^2(y,t) dy. \tag{5.17}$$

By a direct calculation we find

$$U_t(\xi,t) = u_t(X(\xi,t),t) + X_t(\xi,t)u_x(X(\xi,t)) = \frac{1}{2}H(\xi,t),$$

where we used (5.15a). Taking the time derivative of H is more challenging in this case. We must show that (5.17) can be differentiated. The problem is that u_x^2 is infinite along the diagonal line as shown in (5.14). In particular we want to rewrite the cumulative energy using that we have a conservative solution. A simple manipulation yields for any $\epsilon > 0$,

$$\frac{d}{dt}\int_{\sigma_0+st}^{X(\xi,t)} (u_x^2(y,t))dy = \frac{d}{dt}\bigg(\int_{\sigma_0+st+\epsilon}^{X(\xi,t)} u_x^2(y,t)dy + \int_{\sigma_0+st}^{\sigma_0+st+\epsilon} u_x^2(y,t)dy\bigg).$$

The latter integral is finite, since

$$\begin{aligned}\int_{\sigma_0+st}^{\sigma_0+st+\epsilon} u_x^2(y,t)dy &= \int_{\sigma_0}^{\sigma_0+\epsilon} w_\xi^2(\eta)d\eta = -\int_{\sigma_0}^{\sigma_0+\epsilon} \frac{\sqrt{|k|}}{\sqrt{s-w(\eta)}} w_\xi(\eta)d\eta \\ &= -\sqrt{|k|}\int_{w(\sigma_0)}^{w(\sigma_0+\epsilon)} \frac{dz}{\sqrt{s-z}} \\ &= 2\sqrt{|k|}\sqrt{s-w(\sigma_0+\epsilon)} < \infty.\end{aligned}$$

Moreover because we consider conservative traveling waves and the integral is taken over a region which moves with the same speed as the traveling wave itself, the integral always involves the same part of the wave, thus it will be independent of time. In particular it measures the energy of the wave confined in the interval $[\sigma_0 + st, \sigma_0 + st + \epsilon]$, which is equal to the energy of the initial wave profile in the interval $[\sigma_0, \sigma_0 + \epsilon]$. Therefore we have that

$$\frac{d}{dt}\int_{\sigma_0+st}^{X(\xi,t)} u_x(y,t)^2dy = \frac{d}{dt}\int_{\sigma_0+st+\epsilon}^{X(\xi,t)} u_x(y,t)^2dy.$$

Here we stay a distance ϵ apart from the line $\sigma_0 + st$, i.e., the left boundary. We know that the derivative u_x is continuous everywhere except at the line $\sigma_0 + st$ for the cuspon depicted in Figure 17b. Using this fact, we can compute the governing equation for the Lagrangian cumulative energy H,

$$\begin{aligned}\frac{d}{dt}\int_{\sigma_0+st+\epsilon}^{X(\xi,t)} u_x^2(y,t)dy &= \int_{\sigma_0+st+\epsilon}^{X(\xi,t)} (u_x^2(y,t))_t dy + u_x^2(X(\xi,t),t)X_t(\xi,t) - su_x^2(\sigma_0+st+\epsilon,t) \\ &= -\int_{\sigma_0+st+\epsilon}^{X(\xi,t)} (uu_x^2(y,t))_x dy + uu_x^2(X(\xi,t),t) - su_x^2(\sigma_0+st+\epsilon,t).\end{aligned}$$

Here we inserted for the conservation law (5.15b) describing energy conservation for the wave. We can apply the fundamental theorem of calculus to evaluate the integral, and insert for the traveling wave ansatz $u(x,t) = w(x-st)$. Then this reduces to

$$\begin{aligned}\frac{d}{dt}\int_{\sigma_0+st+\epsilon}^{X(\xi,t)} u_x^2(y,t)dy &= \bigg(- uu_x^2(X(\xi,t)) + uu_x^2(\sigma_0+st+\epsilon,t) + uu_x^2(X(\xi,t)) \\ &\qquad - su_x^2(\sigma_0+st+\epsilon,t)\bigg) \\ &= \big((w-s)w_\xi^2(\sigma_0+st+\epsilon-st)\big) = k.\end{aligned}$$

Here k is the integration constant stemming from (5.12). Hence summing it all up, the Lagrangian system is given by the following system of ODEs

$$X_t(\xi,t) = U(\xi,t), \tag{5.18a}$$

$$U_t(\xi,t) = \frac{1}{2}H(\xi,t), \tag{5.18b}$$

$$H_t(\xi,t) = k. \tag{5.18c}$$

In particular we see that the Lagrangian cumulative energy is now changing with time, due to the fact that the left boundary of our domain also changes with time. The constant $k \in \mathbb{R}$, hints about a qualitative change in behaviour between $k > 0$ and $k < 0$. The value of k yields the rate of change of Lagrangian cumulative energy, and we see that $U_{tt} = \frac{1}{2}H_t(\xi, t)$. Hence it contains information about the second derivative of the velocity of the characteristics.

We want to show that the point $x = \sigma_0$ in Eulerian coordinates is mapped to a single point ξ^* in Lagrangian coordinates. That is, the breaking point at $t = 0$ is mapped to a single point in Lagrangian coordinates. Moreover we can say something about the derivative of the characteristic at this point, this is stated in the next lemma. Let

$$\begin{aligned} u(x, 0) &= w(x) \\ X_0(\xi) &= X(\xi, 0), \end{aligned}$$

be the initial wave profile and characteristic initialized by (5.16), respectively.

Lemma 5.2. *The point $x = \sigma_0$ in Eulerian coordinates is mapped to a single point ξ^* in Lagrangian coordinates. This point satisfies $X_0(\xi^*) = \sigma_0$ and*

$$\{\xi^*\} = \{\xi \in \mathbb{R} : X_{0,\xi}(\xi) = 0\}.$$

Proof. To show the uniqueness of the point in Lagrangian coordinates, we want to show that the mapping (5.16) is injective. Consider the function

$$g(y) = y + \mu((\sigma_0, y)) = y + \int_{\sigma_0}^{y} w_\xi^2(\eta)d\eta, \tag{5.19}$$

which has as pseudoinverse (a nice discussion about pseudoinverses is given in [La 15]) the mapping

$$X_0(\xi) = \sup\{x \in \mathbb{R} : \mu((\sigma_0, x)) + x < \xi\}. \tag{5.20}$$

If we can show that the integral exists for all $y \in (\sigma_0, \infty)$, then g is well-defined, strictly increasing and bijective. As a consequence X_0 will be bijective as well,

$$\begin{aligned} \int_{\sigma_0}^{y} w_\xi^2(\eta)d\eta &= -\int_{\sigma_0}^{y} \frac{\sqrt{|k|}}{\sqrt{s - w(\eta)}} w_\xi(\eta)d\eta \\ &= -\sqrt{|k|}\int_{w(\sigma_0)}^{w(y)} \frac{dz}{\sqrt{s-z}} = +2\sqrt{|k|}\sqrt{s-z}|_{z=s}^{w(y)} < \infty, \end{aligned}$$

provided y is finite. Therefore X_0 is bijective, hence the point σ_0 is mapped to a unique point in Lagrangian coordinates. Denote this point by ξ^*. That is ξ^* is the unique point such that $X_0(\xi^*) = \sigma_0$. Then we observe that

$$\begin{aligned} X_{0,\xi}(\xi) &= \frac{1}{g'(X_0(\xi))} = \frac{1}{1 + w_\xi^2(X_0(\xi))} = \frac{1}{1 + \frac{k}{w(X_0(\xi)) - s}} \\ &= \frac{w(X_0(\xi)) - s}{w(X_0(\xi)) - s + k}, \end{aligned}$$

for all $\xi \in \mathbb{R} \setminus \{\xi^*\}$. Now $w(X_0(\xi)) \leq s$ for all ξ when we consider the cuspon in Figure 17b. Moreover $k < 0$ (notice that for a cuspon having the form depicted in Figure 16b instead, we have that $w(X_0(\xi)) \geq s$ and $k > 0$). Thus in particular $X_{0,\xi}(\xi) > 0$ for all $\xi \in \mathbb{R} \setminus \{\xi^*\}$, so this is a strictly increasing function in ξ when $\xi \neq \xi^*$. We want to see what happens at the point ξ^*. There are several ways to show that $X_{0,\xi}(\xi^*) = 0$. The simplest is to observed that the pseudoinverse (5.19) is antisymmetric around σ_0. In particular since it is the pseudoinverse

of X_0, it means that X_0 is antisymmetric about σ_0. Thus $X_{0,\xi}$ is symmetric about σ_0. In particular this means that the $X_{0,\xi}$ has to be zero at σ_0, i.e.,

$$X_{0,\xi}(\xi^*) = \frac{1}{g'(X_0(\xi^*))} = \frac{1}{g'(\sigma_0)} = 0.$$

□

Next we will prove that X initialized by (5.20) is locally Lipschitz with Lipschitz constant at most one.

Lemma 5.3 (Lipschitz cont.)**.** *Let $X_0(\xi)$ be initialized by* (5.20) *then X_0 is locally Lipschitz continuous. Moreover given ξ, ξ' we have*

$$|X_0(\xi) - X_0(\xi')| \leq |\xi - \xi'|,$$

that is, X_0 is Lipschitz with Lipschitz constant at most one. Consequently X_0 is differentiable almost everywhere with $X_{0,\xi} \leq 1$ for almost all ξ.

Proof. Observe that

$$X_0(\xi) = \sup\{x \in \mathbb{R} : \mu((\sigma_0, x)) + x < \xi\},$$

is increasing since the supremum is taken over larger and larger sets, and μ is a positive Radon measure. Let $\xi < \xi^*$. Take an increasing sequence $\{x_k^*\}$ of real numbers, that converges to $X(\xi^*)$, and let $\{x_k\}$ be a decreasing sequence converging to $X(\xi)$. Then we have

$$\begin{aligned}\mu((\sigma_0, x_k)) + x_k &> \xi,\\ \mu((\sigma_0, x_k^*)) + x_k^* &< \xi^*.\end{aligned}$$

Subtracting the former from the latter yields

$$\mu((\sigma_0, x_k^*)) + x_k^* - (\mu((\sigma_0, x_k)) + x_k) \leq \xi^* - \xi,$$

and then passing to the limit $k \to \infty$ yields the Lipschitz continuity with constant at most one. Consequently

$$|X_0(\xi) - X_0(\xi')| = |\int_{\xi}^{\xi'} X_{0,\xi}(s)ds| \leq \|X_{0,\xi}\|_{L^\infty([\xi,\xi'])}|\xi - \xi^*|,$$

indicating $X_\xi(\xi) \leq 1$ for almost all ξ. □

Now we can give an alternative proof of $X_{0,\xi}(\xi^*) = 0$. This proof follows a similar strategy as used in [Gru16]. Let $\xi > 0$, we observe that

$$\begin{aligned}\xi - \sigma_0 &= \int_{\sigma_0}^{\xi} dy = \int_{\sigma_0}^{\xi} \frac{w_\xi(y)}{w_\xi(y)} dy\\ &= -\int_{\sigma_0}^{\xi} \frac{\sqrt{s - w(y)}}{\sqrt{|k|}} w_\xi(y)dy = -\frac{1}{\sqrt{|k|}} \int_s^{w(\xi)} \sqrt{s - z}dz = \frac{1}{\sqrt{|k|}} \frac{2}{3} \left(s - w(\xi)\right)^{\frac{3}{2}},\end{aligned}$$

which is equivalent to

$$0 \leq s - w(\xi) = w(\sigma_0) - w(\xi) = \left(\sqrt{|k|}\frac{3}{2}\right)^{\frac{2}{3}} (\xi - \sigma_0)^{\frac{2}{3}}.$$

Such an expression was to be expected, as w is continuous. We observe that by making the distance between ξ and σ_0 smaller, the right-hand side becomes smaller, which is what we expect by continuity. By continuity given $\epsilon > 0$ there is a $\delta > 0$ such that

$$|w(\sigma_0) - w(\xi)| < \epsilon \quad \text{whenever} \quad |\sigma_0 - \xi| < \delta.$$

By Lemma 5.3 we know X is Lipschitz continuous, with lipschitz constant at most one. Thus by Rademacher theorem X is differentiable almost everywhere, and

$$|X_0(\xi) - X_0(\xi^*)| \leq |\xi - \xi^*| < \delta \quad \text{whenever} \quad |\xi - \xi^*| < \delta.$$

Using (5.16), we observe by applying the continuity of w that

$$\begin{aligned}
|\xi - \xi^*| &= |X_0(\xi) - X_0(\xi^*)| + \left| \int_{\sigma_0}^{X_0(\xi)} w_\xi^2(\eta) d\eta - \int_{\sigma_0}^{X_0(\xi^*)} w_\xi^2(\eta) d\eta \right| \\
&= |X_0(\xi) - X_0(\xi^*)| + \left| \int_{X_0(\xi)}^{X_0(\xi^*)} w_\xi^2(\eta) d\eta \right| \\
&= |X_0(\xi) - X_0(\xi^*)| + \left| \int_{X_0(\xi)}^{X_0(\xi^*)} \frac{|k|}{|w(\sigma_0) - w(\eta)|} d\eta \right| \\
&\geq |X_0(\xi) - X_0(\xi^*)| + \left| \int_{X_0(\xi)}^{X_0(\xi^*)} \frac{|k|}{\epsilon} d\eta \right| \geq |X_0(\xi) - X_0(\xi^*)| (\frac{\epsilon + |k|}{\epsilon}).
\end{aligned}$$

Hence rearranging, we see that

$$\frac{X_0(\xi^*) - X_0(\xi)}{\xi^* - \xi} \leq \frac{\epsilon}{\epsilon + |k|} \qquad \text{whenever} \qquad |\xi^* - \xi| < \delta,$$

holds for $\epsilon > 0$. Therefore we may choose ϵ equal to zero and

$$X_{0,\xi}(\xi^*) = \lim_{\xi \to \xi^*} \frac{X_0(\xi^*) - X_0(\xi)}{\xi^* - \xi} = 0.$$

This result can be extended to other times $t > 0$, but not in a straight forward way, one would most likely rely on a relabeling argument using the equivalence classes introduced in Subsection 3.3. Hence at all times there is only a single point in Lagrangian coordinates where wave breaking occurs.

Next we want to prove that in Lagrangian coordinates, the gluing point, i.e., the cusp singularity is not traveling along a single characteristic, but as a figure of speak, it jumps from characteristic to characteristic. Let $X(\xi, t)$ be the characteristic at time t with initial position $X_0(\xi)$ given by (5.16). The Lagrangian system takes the following form

$$\begin{aligned}
&X_t(\xi, t) = U(\xi, t) = w(X(\xi, t) - st), \\
&U_t(\xi, t) = (w(X(\xi, t) - st))_t = \frac{1}{2} \int_{\sigma_0}^{X(\xi,t)-st} w_\xi^2(\eta) d\eta = \frac{1}{2} H(\xi, t), \\
&H_t(\xi, t) = k.
\end{aligned}$$

We already hinted about a qualitative change in behaviour for $k > 0$ versus the case of $k < 0$. When we consider a conservative traveling wave of the form as in Figure 16a then $k < 0$, while if we consider one like in Figure 16b then $k > 0$. Now assume $X(\bar{\xi}, t)$ is a characteristic which crosses the diagonal line at some time $T > 0$, i.e., $X(\bar{\xi}, T) = \sigma_0 + sT$. We want to show that

$$X(\bar{\xi}, t) > \sigma_0 + st \quad \text{for } t < T, \tag{5.21}$$

$$X(\bar{\xi}, t) < \sigma_0 + st \quad \text{for } t > T, \tag{5.22}$$

for the case of the cuspon in Figure 17b. The behaviour of the characteristics depends on k. These inequalities state that the diagonal line travels faster than the characteristics in the case of $k < 0$. We start with the latter (5.22) first, i.e., we want to show that the characteristic lies to the left of the diagonal line for all times after T. We will then afterwards show that all

characteristics admit an individual crossing time T. Showing that the characteristic lies to the left of the diagonal line for all $t > T$ is equivalent to showing that

$$F(\xi^*, t) = X(\xi^*, t) - (\sigma_0 + st),$$

is negative for all $t > T$. Computing the derivatives we observe that

$$\begin{aligned} F_t(\bar{\xi}, T) &= U(\bar{\xi}, T) - s = 0, \\ F_{tt}(\bar{\xi}, T) &= U_t(\bar{\xi}, T) = \frac{1}{2} H(\bar{\xi}, T) = 0, \\ F_{ttt}(\bar{\xi}, T) &= U_{tt}(\bar{\xi}, T) = \frac{1}{2} H_t(\bar{\xi}, T) = \frac{1}{2} k. \end{aligned}$$

This follows, since at $t = T$, the characteristic lies on the diagonal line and we have $U = s$ on the diagonal line. Moreover we measure the Lagrangian cumulative energy from the diagonal line, so the Lagrangian cumulative energy along the diagonal line is zero in this case, as the measure is purely absolutely continuous. We see that if $k < 0$, then $U(\bar{\xi}, t)$ has a maximum at $(\bar{\xi}, T)$, seen as a function of time. Therefore the characteristic moves slower than the diagonal line and $X(\bar{\xi}, t) < \sigma_0 + st$ for all $t > T$.

Now we will proceed by proving (5.21). We know there is a unique characteristic variable ξ^* such that $X(\xi^*, 0) = X_0(\xi^*) = \sigma_0$. Therefore for $\bar{\xi} > \xi^*$ we have $X(\bar{\xi}, 0) > \sigma_0$. Keep $\bar{\xi}$ fixed, and define

$$h(\bar{\xi}, t) = X(\bar{\xi}, t) - st.$$

We want to show that there is a time $T > 0$ such that the characteristic emanating from $\bar{\xi}$ crosses the diagonal line. We observe that

$$\begin{aligned} h_t(\bar{\xi}, t) &= \big(X(\bar{\xi}, t) - st\big)_t = U(\bar{\xi}, t) - s \\ &= w(h(\bar{\xi}, t)) - s \leq 0. \end{aligned}$$

Therefore we have that

$$\frac{h_t(\bar{\xi}, t)}{w(h(\bar{\xi}, t)) - s} = 1.$$

This is an ODE in h, which we can solve explicitly by using separation of variables. In particular

$$T = \int_0^T dt = \int_{h(\bar{\xi}, 0)}^{h(\bar{\xi}, T)} \frac{dh}{w(h) - s}.$$

Now we introduce the change of variables $z = s - w(h)$ which leads to

$$dz = -w'(h)dh = -(-\frac{\sqrt{|k|}}{\sqrt{s - w(h)}})dh = \frac{\sqrt{|k|}}{z^{\frac{1}{2}}} dh,$$

as we consider the conservative traveling wave in Figure 17b. Thus we get

$$\begin{aligned} T &= -\frac{1}{\sqrt{|k|}} \int_{s - w(h(\bar{\xi}, 0))}^{s - w(h(\bar{\xi}, T))} \frac{dz}{z^{\frac{1}{2}}} \\ &= -\frac{2}{\sqrt{|k|}} \left(\sqrt{s - w(h(\bar{\xi}, T))} - \sqrt{s - w(X_0(\bar{\xi}))} \right), \end{aligned}$$

which we can solve for the difference $s - w(h(\bar{\xi}, T))$. This results in

$$s - w(h(\bar{\xi}, T)) = \left(\sqrt{s - w(X_0(\bar{\xi}))} - \frac{\sqrt{|k|} T}{2} \right)^2.$$

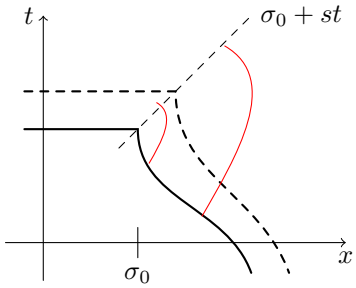

Figure 18: The figure illustrates that the gluing point for a traveling wave with a one-sided unbounded derivative moves along the diagonal line, while characteristics cross the line

In particular we observe that the right-hand side becomes zero at time T given by

$$T = \frac{2}{\sqrt{|k|}}\sqrt{s - w(X_0(\bar{\xi}))}. \tag{5.23}$$

Since we know that w is equal to s only at the diagonal line, it must be the case that the characteristic $X(\bar{\xi}, t)$ hits the diagonal line at time T given by (5.23). By our previous argument we know that $X(\bar{\xi}, t) < \sigma_0 + st$ for all $t > T$. Hence the characteristic only crosses the diagonal line at a single time T. The characteristic was chosen arbitrarily, thus this hold for all characteristics, where the crossing time T is individual for each characteristic. Therefore we have derived the following result.

Lemma 5.4 (Wave breaking)**.** *Let ξ be a characteristic variable and $X(\xi, t)$ the characteristic that emanated from ξ at time $t = 0$. Then there exist some time $T \in \mathbb{R}$ such that*

$$\begin{aligned} X(\xi, t) &> \sigma_0 + st \quad \textit{for } t < T, \\ X(\xi, T) &= \sigma_0 + sT, \\ X(\xi, t) &< \sigma_0 + st \quad \textit{for } t > T. \end{aligned}$$

In particular this lemma states that each characteristic crosses the diagonal line at some time T, and this occurs only once. Since we consider conservative traveling waves, this T may be negative, as we can trace characteristics backward and forward in time for conservative solutions. A negative T means that the crossing has already occurred, while $T > 0$, indicates that a crossing will happen in the future.

We will now use these observations to give a formal/physical explanation about why neither weak traveling waves with a one-sided unbounded derivative, nor those with an inflection point at the gluing point can be conservative traveling waves. This explanation is based on physical intuition, and no rigorous analysis has been conducted. We consider the particular traveling wave depicted in Figure 18. Here the red curves illustrate characteristics that emanate from the traveling wave with $\xi > \sigma_0$. They will at some time T, (individual for each characteristic) cross the diagonal line, i.e., experience wave breaking, and then hit the part of the wave, where it is constant. Each of these characteristics carry along a little amount of energy, but since $w = s$ for $\xi < \sigma_0$, there is no energy here. However since the wave experiences wave breaking at any time, this means that energy is either transferred continuously to the part of the traveling wave, where there initially was no energy or energy is collected on the line. In either case the shape of the wave cannot be preserved while still being a conservative solution.

In the other case, where the gluing point is a point of inflection, we have to consider the Lagrangian system to give an explanation to why this cannot be a conservative traveling wave. We consider the wave depicted in Figure 19a. Now $w(\xi) - s < 0$ for $\xi < \sigma_0$, while $w(\xi) - s > 0$

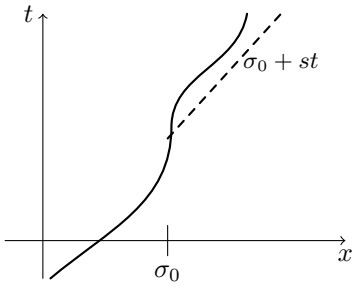

(a) Monotonically increasing wave and the movement of the gluing point shown as a dashed line.

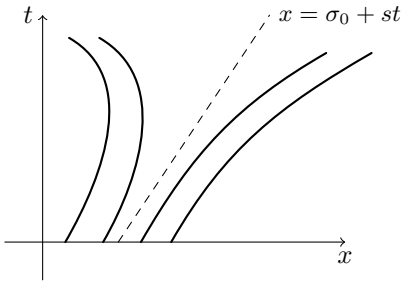

(b) The behaviour of the characteristics in the case of the monotonically increasing wave.

Figure 19: Figure 19a shows the traveling wave under consideration, and the associated rarefaction-like behaviour of the characteristics around the diagonal line is depicted in Figure 19b. The rate at which the characteristics spread away from the dashed line depends on the k_i's.

for $\xi > \sigma_0$, and the derivative is always increasing. Therefore the k_i's are of opposite sign, since we have the following relation

$$w_{i,\xi}^2(\xi)(w_i - \xi)^2 = k_i(w - s).$$

The left side is always positive, therefore the sign of k_i depends on $(w_i - s)$. Now since $(w_1 - s) < 0$ we must have $k_1 < 0$, and $(w_2 - s) > 0$ so $k_2 > 0$. Therefore the diagonal line $\sigma_0 + st$ represents a qualitative change in behaviour for time derivative of the Lagrangian cumulative energy. That is, the part of the wave to the left of the gluing point behaves differently than the part to the right. The expression

$$U_{tt} = \frac{1}{2}H_t = \frac{1}{2}k_i,$$

indicates that for $\xi < \sigma_0$ the velocity attains a maximum at the diagonal line, and the characteristics to the left of the diagonal line move slower than the diagonal line. For $\xi > \sigma_0$ we have that $k_2 > 0$. This means that the diagonal line is a local minimum for the speed of the characteristics, hence the characteristics starting to the right of the diagonal line move faster than the diagonal line. In particular we expect a rarefaction-like behaviour around the diagonal line, based on a comparison to what happens for hyperbolic conservation laws. This is illustrated in Figure 19b. This means that energy is transferred away from either side of the diagonal line along the characteristics, hence the shape cannot be preserved. The rate at which the energy is transferred depends on the k_i's, so the energy can be transferred faster on one side than the other if the magnitudes differ.

Now we can reverse the situation, considering the other possible case as depicted in Figure 20a. Then the case for the k_i's is reversed, so in particular $k_1 > 0$ and $k_2 < 0$ resulting in the characteristics approaching the line $\sigma_0 + st$. Thus we expect a shock-like behaviour as illustrated in Figure 20b. A physical interpretation of this is that energy is transferred from either side of the wave to the line $\sigma_0 + st$. Hence in a sense energy accumulates along this line, which is forbidden for a conservative solution.

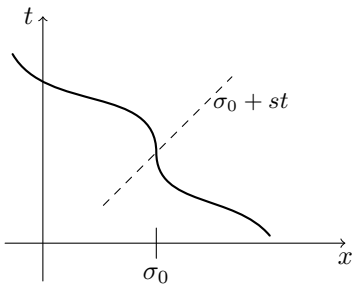

(a) Monotonically decreasing wave and the movement of the gluing point shown as a dashed line.

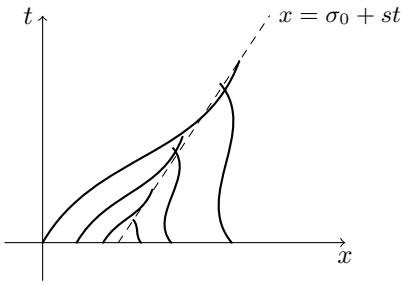

(b) The behaviour of the characteristics in the case of the monotonically decreasing wave.

Figure 20: Figure 20a shows the traveling wave under consideration, and the associated shock-like behaviour of the characteristics around the diagonal line is depicted in 20b. The rate at which the characteristics collide/approach the dashed line depends on the k_i's.

6 Numerical algorithm for conservative solutions

In this section we briefly review some theory about numerical solutions of hyperbolic conservation laws, and then we consider an algorithm for simulating conservative solutions of the Hunter-Saxton equation. The algorithm was introduced in [GNS21]. We will observe that some challenges arise when we want to apply the algorithm to simulate conservative traveling waves. In particular the initial measure μ_0 will not have compact support, and the total cumulative energy is infinite. Therefore the convergence results derived in [GNS21] do not apply.

In [GNS21] a convergent numerical method for conservative solutions of the Hunter-Saxton equation is derived. The method is inspired by Godunov-type methods for conservation laws and based on piecewise linear projections, followed by time evolution of the solution along characteristics forward in time. For finite difference schemes and finite volume methods for hyperbolic conservation laws one need to limit the time step Δt to prevent shocks from arising [LeV02]. A similar time step constraint must be imposed for the Hunter-Saxton equation, but now it is imposed to prevent wave breaking from occurring. The authors in [GNS21] obtain an improved bound on the relation between the time step Δt and step size Δx, compared to the typical CFL-condition one has for hyperbolic conservation laws. In particular the time step Δt has to satisfy a bound of the form

$$\Delta t \leq \frac{\alpha}{2\sqrt{F_\infty}}\sqrt{\Delta x},$$

for $\alpha \in (0, 1]$. This is less restrictive than the typical CFL-condition which states that $\Delta t \leq C\Delta x$, for a constant C depending on the initial data and the particular flux function. However it is not a true CFL-condition in the sense, that characteristics can travel past several grid-cells during a single time step. It is illustrative to consider the origin of the CFL-condition, which is a necessary condition for stability of any finite difference or finite volume scheme applied to conservation laws.

6.1 Interlude: The CFL-condition and Godunov's method

In this subsection we want to discuss the approximation of the true solution $u : \mathbb{R} \times [0, T] \to \mathbb{R}$ to the Cauchy problem of a scalar conservation law

$$\begin{aligned} u_t + f(u)_x &= 0, \\ u|_{t=0} &= u_0, \end{aligned} \tag{6.1}$$

for some given flux function $f : \mathbb{R} \to \mathbb{R}$, initial data $u_0 : \mathbb{R} \to \mathbb{R}$ and for some final time $T > 0$. First we define spatial and temporal grid points by

$$\begin{aligned} t_n &= n\Delta t \quad n \in \mathbb{N} \cup \{0\}, \\ x_j &= j\Delta x \quad j \in \mathbb{Z}, \end{aligned}$$

where $\Delta x = x_{k+1} - x_k$ and $\Delta t = t_{n+1} - t_n$ are independent of $k \in \mathbb{Z}$ and $n \in \mathbb{N} \cup \{0\}$, respectively. Moreover we define $x_{j+\frac{1}{2}} = x_j + \frac{\Delta x}{2}$ and

$$\begin{aligned} I_k &= [x_{k-\frac{1}{2}}, x_{k+\frac{1}{2}}), \\ I_k^n &= I_k \times [t_n, t_{n+1}), \end{aligned}$$

where I_k is the interval between two cell interfaces and I_k^n is a grid cell. Let u_k^n denote an approximation to the cell average of u at time $t = t_n$, that is

$$u_k^n \approx \frac{1}{\Delta x} \int_{I_k} u(x, t_n)\, dx\,.$$

We will here, as is typical for finite volume and finite difference methods define the numerical solution $u_{\Delta t}$ as the piecewise constant function taking the approximate cell averages as values, i.e.,

$$u_{\Delta t}(x,t) = u_j^n \qquad \text{for } (x,t) \in I_j^n.$$

Consider a general conservative three point stencil for hyperbolic conservation laws, which takes the form

$$u_k^{n+1} = u_k^n - \lambda[G(u_k^n, u_{k+1}^n) - G(u_{k-1}^n, u_k^n)]. \tag{6.2}$$

Here G is the numerical flux function, and $\lambda = \frac{\Delta t}{\Delta x}$, is the mesh ratio. Godunov's method is a particular example of such a three point stencil. Being a centered three point stencil, it updates the cell average u_k^{n+1} using the cell average u_k^n and the cell averages in the two adjacent cells, u_{k-1}^n and u_{k+1}^n. Now we will consider the CFL-condition for such a scheme. The CFL condition states that the numerical method must be applied in such a way that information has a chance to propagate at physically correct speeds. In the case of a centered three point stencil, where we use the two nearest adjacent cells to update the new cell average, this means that information must not propagate more than a single grid cell during the time step Δt.

The maximal wave speed for (6.1) is given by $\sup_{u\in\mathbb{R}} |f'(u)|$. Therefore by the CFL-condition, we require for a centered three point stencil that

$$\nu = \frac{\Delta t}{\Delta x} \sup_{u\in\mathbb{R}} |f'(u)| \leq 1,$$

where ν is called the Courant number. ν measures the fraction of a grid cell that information propagates during a single time step Δt. Figure 21 illustrates what goes wrong in the case this condition is not fulfilled. For Figure 21a information propagates less than one grid cell during a time step Δt, and we see the true flux through the cell interface $x_{k-\frac{1}{2}}$ only depends on the value of u_{k-1}^n and u_k^n. For Figure 21b the time step Δt is too large, so the true flux through $x_{k-\frac{1}{2}}$ also relies on the value u_{k-2}^n. Therefore in order for the numerical flux to properly model the true flux, we should use the cell average u_{k-2}^n as well to update u_k^{n+1}.

Another way to phrase the CFL-condition is that a numerical method can only be convergent if its numerical domain of dependence contains the true domain of dependence of the PDE, at least in the limit $\Delta t, \Delta x \to 0$ as the grid is refined. Otherwise, changing the initial data u_0 could effect the true solution u at a point (x,t), while it could leave the numerical approximation unchanged at this point. Clearly if this is the case, we cannot hope for the numerical approximation to converge to the true solution for all choices of initial data. Therefore the method cannot be stable. However it is important to observe that the CFL-condition is only a necessary condition for stability (thus also convergence), but not sufficient. There are schemes which may satisfy the CFL-condition and still be unstable, see [LeV02] for an example.
The numerical method used for producing conservative solution is presented in the next subsection, and is a Godunov-type method, hence it is illuminating to recall Godunov's method for hyperbolic conservation laws first. We here only consider scalar conservation laws. Godunov's method is based on solving Riemann problems forward in time, to determine the local characteristic structure, and use that information to evolve the solution. Godunov's method is a special case of the REA-algorithm [Chp4., [LeV02]], which is summarized in the below pseudocode.

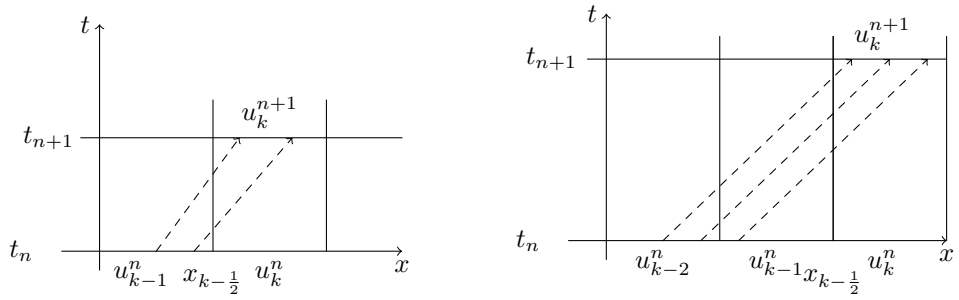

(a) $\nu \leq 1$. **(b)** $\nu \geq 1$.

Figure 21: (a) shows a scenario where the time step is small enough such that the flux at $x = x_{k-\frac{1}{2}}$ only depends on the values of the neighbouring cell u_{k-1}^n and u_k^n. (b) represents a case where the time step is too large and the flux at $x = x_{k-\frac{1}{2}}$ also depends on the cell average u_{k-2}^n.

Pseudocode: REA-Algorithm

1 Initialize the numerical approximation u^0 by computing cell averages from the initial data u_0

$$u_j^0 = \tfrac{1}{\Delta x} \int_{x_{j-\frac{1}{2}}}^{x_{j+\frac{1}{2}}} u_0(x)\, dx$$

2 **for** $n = 0 \dots N$

3 **Reconstruct:** Reconstruct a piecewise polynomial function $\hat{u}(x, t_n)$ defined for all x from the cell averages u_j^n

4 **Evolve:** Evolve the hyperbolic equation exactly or approximately with initial data $\hat{u}(x, t_n)$ to obtain $\hat{u}(x, t_{n+1})$, at a time step Δt later

5 **Average:** Average the solution $\hat{u}(x, t_{n+1})$ over each grid cell to obtain new cell averages

$$u_j^{n+1} = \tfrac{1}{\Delta x} \int_{x_{j-\frac{1}{2}}}^{x_{j+\frac{1}{2}}} \hat{u}(x, t_{n+1})\, dx$$

The three steps involving reconstruction, evolving and averaging (REA) are repeatedly performed until the desired time $T = n\Delta t$ is reached. Godunov's method is based on the particular choice of using piecewise constant reconstructions, that is

$$\hat{u}(x, t_n) = u_j^n \qquad \text{if } x \in I_j.$$

Therefore in particular, we skip the first reconstruction, as $\hat{u}(x, t_0)$ just takes the cell averages, u_j^0, as values. This leads to Riemann problems at each cell interface. That is, one solves

$$u_t + f(u)_x = 0$$
$$u_{t=t_n}(x) = \begin{cases} u_j^n & \text{for } x < x_{j+\frac{1}{2}} \\ u_{j+1}^n & \text{for } x > x_{j+\frac{1}{2}}, \end{cases}$$

at each cell interface, for $j \in \mathbb{Z}$. The Riemann solutions consists of rarefactions, shocks and contact discontinuities propagating at certain speeds, that are all bounded by $f'(u)$. The exact solution to the overall Riemann problem at time t_{n+1}, $\hat{u}(x, t_{n+1})$, can be constructed by patching together the individual Riemann solutions, provided the time step Δt is limited in such a way that the waves from adjacent Riemann problems do not interact. This is illustrated in Figure 22, where we see Δt is so small that the Riemann solutions do not interact. The most natural time step constraint is thus

$$\sup |\frac{\Delta t}{\Delta x} f'(u_j^n)| \leq \frac{1}{2},$$

so that each wave travels at most halfway through the grid cell. Hence if the solution of two adjacent Riemann problems travel directly towards each other, they can only meet at the very

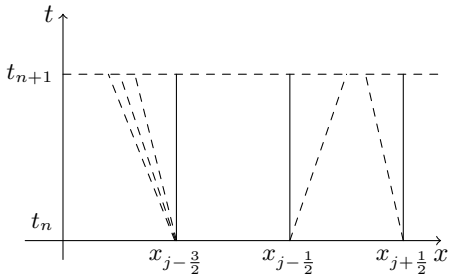

Figure 22: The Riemann problem is solved at each cell interface, and the wave structure is used to find the exact solution a time Δt later. At $x_{j-\frac{3}{2}}$ the Riemann solution is a rarefaction, while at $x_{j+\frac{1}{2}}$ and $x_{j+\frac{3}{2}}$ the solutions are shocks.

end of the time step. After finding the overall Riemann solution, we compute the cell averages to get our numerical approximation at the next time step, u^{n+1}.
One can use the integral formulation of the conservation law to recast Godunov's method as a conservative three point stencil (6.2) where

$$G(u_j^n, u_{j+1}^n) = \frac{1}{\Delta t} \int_{t_n}^{t_{n+1}} f(\hat{u}(x_{j+\frac{1}{2}}, t))\, dt\,.$$

$\hat{u}$ is the Riemann solution and thus remains constant at the cell interface $x_{j+\frac{1}{2}}$, over the time interval. The Riemann problem centered at $x_{j+\frac{1}{2}}$ admits self-similar solutions that are constant along rays $(x - x_{j+\frac{1}{2}})/(t - t_n) = \text{const}$, and considering the particular ray $(x - x_{j+\frac{1}{2}})/t = 0$ yields the value of $\hat{u}(x_{j+\frac{1}{2}}, t)$. Denote this value by $u^*(u_j^n, u_{j+1}^n)$, as it only depends on the value of u at the grid cell on either side of the interface $x = x_{j+\frac{1}{2}}$. Hence the numerical flux G used for Godunov's method reduces to

$$G(u_j^n, u_{j+1}^n) = f(u^*(u_j^n, u_{j+1}^n)).$$

Now as a consequence we can lessen the restriction on the CFL-condition for Godunov's method to

$$\sup |f'(u_j^n)| \frac{\Delta t}{\Delta x} \leq 1. \tag{6.3}$$

With this restriction we allow waves emanating from neighbouring Riemann problems to interact during the time step Δt, but the interactions are entirely confined to stay within a single control volume cell. The true solution to the Riemann problem is then hard to find, but is not needed as we are only interested in the cell averages, and the Riemann solution at the cell interfaces. Since we limit the time step by (6.3), the Riemann solutions are constrained to stay within a single grid cell, so they do not cross the cell interfaces of other Riemann problems, and therefore the Riemann solutions at the cell interfaces are constant. Consequently the Godunov flux is the same as before, and we can update the numerical solution using (6.2).

6.2 An algorithm for conservative solutions

In this subsection we briefly present the numerical scheme developed in [GNS21] for conservative solutions of the Hunter-Saxton equation, and apply it to our example from Subsection 3.2. Moreover we identify some new problems that arise in the case of conservative cuspons, which renders the current formulation of the algorithm unsuitable. From Subsection 3.3 we know that we require two Eulerian variables (u, μ) in order to uniquely describe a solution. We define F to be the cumulative distribution function

$$F(x, t) = \mu((-\infty, x], t),$$

where μ is a finite positive Radon measure on $\mathbb{R}$. As discussed in Subsection 3.3 we introduce the measure to trace the energy density, due to the fact that energy may concentrate on a set of Lebesgue measure zero as time evolves for peakons. For solutions having a cusp singularity on the other hand, wave breaking occurs at all times, but only an infinitesimal amount of energy concentrates, so in this case the measure is purely absolutely continuous. The distribution function F will be an increasing, right-continuous function and thus differentiable almost everywhere. Now we will motivate the equation satisfied by F. We assume that everything is smooth. The conservation law for the energy density reads

$$\mu_t + (u\mu)_x = 0,$$

and

$$\mu_{ac}((a,b],t) = \int_a^b u_x^2(x,t)dx.$$

To motivate the governing equation for the cumulative distribution function, we observe that

$$F_x(x,t) = \frac{d}{dx}\mu_{ac}((-\infty,x],t) = \frac{d}{dx}\int_{-\infty}^x u_x(y,t)^2 dy = u_x^2(x,t),$$

and

$$F_t = \int_{-\infty}^x (u_x^2)_t dy = -\int_{-\infty}^x (uu_x^2)_x dy = -u(x,t)u_x^2(x,t) = -uF_x,$$

provided u vanishes at $-\infty$. This formal computation can be extended to all of $\mathbb{R}\times\mathbb{R}_+$, even though in general $d\mu_{ac} \neq u_x^2 dx$ for the algorithm to be introduced. This is since we introduce an error when we apply a projection operator, so $d\mu_{ac} = (u_x^2 + \rho^2)\,dx$, where ρ^2 denotes the error. Hence μ no longer represents the physical energy density, which is elaborated further upon in the next chapter. Therefore we can write the system in Eulerian coordinates as

$$\begin{aligned} u_t + \frac{1}{2}u_x^2 &= \frac{1}{2}F - \frac{1}{4}F_\infty, \\ F_t + uF_x &= 0. \end{aligned}$$

We recognize this as a reformulation of the two-component Hunter-Saxton system, which generalizes the Hunter-Saxton equation. The two-component Hunter-Saxton equation is discussed in [Nor16a]. It turns out that every conservative solution to the Hunter-Saxton equation can be approximated by smooth solutions of the two-component Hunter-Saxton system. For the numerical approximation to approximate conservative solutions of the Hunter-Saxton equation well, we require them to mimic certain properties of the true solutions. Therefore we want the numerical approximations to be pairs (u,F) that belong to a suitable function space $\mathcal{D}$, not to be confused by the space introduced in Subsection 3.3.

Definition 6.1. The space $\mathcal{D}$ consist of pairs (u,F) such that the following properties are satisfied

1. $u \in L^\infty(\mathbb{R})$ and $u_x \in L^2(\mathbb{R})$
2. $F \in L^\infty(\mathbb{R})$, F is monotonically increasing, and F is right continuous.
3. $\lim_{x\to-\infty} F(x) = 0$
4. $\|F\|_{L^\infty(\mathbb{R})} = F_\infty = \lim_{x\to\infty} F(x)$
5. $\int_a^b (u_x(y))^2 dy \leq \lim_{x\uparrow b} F(x) - \lim_{x\downarrow a} F(x)$

We will exploit that we know exactly how the evolution of the solution looks like for piecewise linear functions. In particular we will project the solution onto the space of piecewise linear continuous functions, and then evolve the solution exactly along the characteristic a time step Δt forward in time. This is the main motivation for introducing the projection operator.

Definition 6.2 (Projection operator)**.** We define a projection operator $P_{\Delta x} : \mathcal{D} \to \mathcal{D}$ so that $(\bar{u}, \bar{F}) = P_{\Delta x}(u, F)$ is given by

$$\begin{aligned} \bar{u}(x_j) &= u(x_j), \\ \bar{F}(x_j) &= F(x_j), \end{aligned}$$

where we use linear interpolation in between grid points $\Delta x\mathbb{Z}$.

This operator evaluates the functions in the spatial grid points, and applies linear interpolation in between grid points. The operator is well-defined as we require F to be right-continuous and hence it can be evaluated pointwise. First we project the initial data, to obtain our first approximation (U^0, F^0). Here U^n is a vector having all the u_k^n's for $k \in \mathbb{Z}$ as components, so it holds all the approximated grid point values at time $t = t_n = n\Delta t$ for $n \in \mathbb{N} \cup \{0\}$, similarly for F^n. Then we apply the solution operator T_t to progress the solution forward a time step Δt exactly, and the resulting solution is projected. The numerical scheme is summarized as

$$\begin{aligned} (U^0, F^0) &= P_{\Delta x}(u_0, F_0), \\ (U^{n+1}, F^{n+1}) &= P_{\Delta x} T_{\Delta t}(U^n, F^n). \end{aligned}$$

If we let $T_t : \mathcal{D} \to \mathcal{D}$ be the solution operator for conservative solutions, then for continuous piecewise linear initial data, this operator takes on a simple form if we restrict Δt in such a way that wave breaking does not occur. The breakpoints of the piecewise linear approximations travel along characteristics according to Lemma 7.1, and the characteristics are given by solving the linear ODE system in Lagrangian coordinates. That is, the breakpoints travel along the curves given by

$$x_j(t) = x_j(0) + u(x_j(0), 0)t + \frac{1}{4}\left(F(x_j(0), 0) - \frac{1}{2}F_\infty\right)t^2, \tag{6.4}$$

where $x_j(\cdot)$ is the characteristic starting at the grid point x_j. Then the solution at time t along these characteristics is given by

$$u(x_j(t), t) = u(x_j(0), 0) + \frac{1}{2}\left(F(x_j(0), 0) - \frac{1}{2}F_\infty\right)t, \tag{6.5a}$$

$$F(x_j(t), t) = F(x_j(0), 0). \tag{6.5b}$$

We apply linear interpolation in between the characteristics to obtain the solution on the entire grid. The two expressions (6.5a)-(6.5b) define implicitly the solution operator T_t, when we have continuous and piecewise linear initial data, which is the case for our numerical method, as we project the initial data before applying T_t. We will use these expressions to progress the solution forward a time Δt, and as initial data we use the projected solution at the previous time step.

We can also determine an expression for the backward characteristics, i.e., the characteristics backwards in time. This is used in [GNS21] where one generalize the Gudonov-type expression for the case where characteristic may move past several grid cells. However we will work with a more restrictive bound, such that we have better control on the characteristics. For completeness we state the expression for the backward characteristics here. We can associate to any grid point (x_k, τ) with τ being a time $\tau \in [t_n, t_{n+1}]$ a unique point which we denote by $(\eta_k^n(\tau), t_n)$. The expression for the point is given implicitly by

$$\eta_k^n(\tau) = x_k - u(\eta_k^n(\tau), t_n)(\tau - t_n) + \frac{1}{4}\left(F(\eta_k^n(\tau), t_n) - \frac{1}{2}F_\infty\right)(\tau - t_n)^2. \tag{6.6}$$

Correspondingly the velocity and cumulative energy, respectively, are given by

$$u(x_j,\tau) = u(\eta_k^n(\tau),\tau) - \frac{1}{2}\left(F(\eta_k^n(\tau),t_n) - \frac{1}{2}F_\infty\right)(\tau - t_n),$$
$$F(x_j,\tau) = F(\eta_j^n(\tau),t_n).$$

Using (6.6) one can determine if the characteristic either came from the right or from the left. This can be used to determine if the value of the numerical solution $u_{\Delta x}$ at (x_k, t_{n+1}) should be updated using information from grid points x_{k-1} and x_k, or x_k and x_{k+1}. Alternatively one can use the forward characteristics to determine which grid cells to use. We will use the forward characteristics.

6.2.1 CFL-condition

As mentioned, we need to restrict the time step to prevent wave breaking from occurring. In [GNS21] a bound of the form $\Delta t = O(\sqrt{\Delta x})$ is introduced, and in particular

$$\Delta t = \frac{1}{2\sqrt{F_\infty}}\sqrt{\Delta x}, \tag{6.7}$$

is used in the proofs. With this choice for Δt, consider the evolution of two characteristics emanating from neighbouring grid points, k and $k+1$, respectively. Then using (6.4) with $t \in [0, \Delta t]$ we find

$$\begin{aligned} x_{k+1}(t) - x_k(t) &= \Delta x + \Big(u(x_{k+1}(0),0) - u(x_k(0),0)\Big)t + \underbrace{\frac{1}{4}\Big(F(x_{k+1}(0),0) - F(x_k(0),0)\Big)t^2}_{\geq 0} \\ &\geq \Delta x + t\int_{x_k}^{x_{k+1}} u_x(y)dy \\ &\geq \Delta x - t\Big(\int_{x_k}^{x_{k+1}} dy\Big)^{\frac{1}{2}}\Big(\int_{x_k}^{x_{k+1}} u_x^2(y)dy\Big)^{\frac{1}{2}} \geq \Delta x - t\sqrt{\Delta x}\sqrt{F(x_{k+1}) - F(x_k)} \\ &\geq \Delta x - \Delta t\sqrt{\Delta x}\sqrt{F_\infty} \geq \frac{1}{2}\Delta x. \end{aligned}$$

Here we have used that F is monotonically increasing, and Cauchy-Schwarz inequality. Moreover we used

$$\int_{x_k}^{x_{k+1}} u_x^2(y,t)dy \leq \mu(([x_k, x_{k+1}),t) = F(x_{k+1},t) - F(x_k,t) \leq F_\infty,$$

being a consequence of 5. in Definition 6.1. Thus characteristics starting from neighbouring grid points, are at least a distance $\frac{1}{2}\Delta x$ apart for all $t \in [0, \Delta t]$. This way we can be sure that wave breaking does not occur, similarly to what we observed in Section 6.1 for Godunov's method. This is however not a true CFL-condition in the sense, that characteristics can move past several grid cells during a single time step. However if we enforce a stricter requirement, we can control the movement of characteristics even better, which we will take advantage of when we want to derive the numerical scheme on a finite difference form.

Remark 6.1. With the choice

$$\Delta t < \frac{\Delta x}{2\left(\|u_0\|_\infty + \frac{1}{8}TF_\infty\right)}, \tag{6.8}$$

characteristics cannot move further than a single grid cell during a time increment, this is precisely like a CFL-condition.

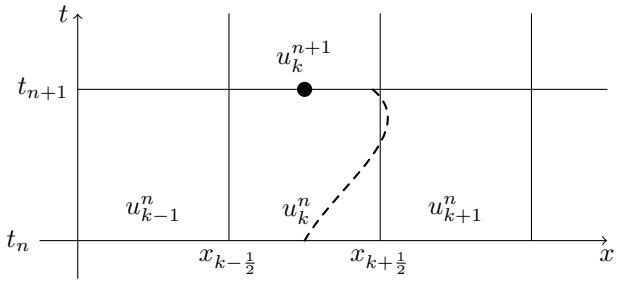

Figure 23: Here the forward characteristic is shown as a dashed line for $u_k^n + \frac{1}{4}(F_k^n - \frac{1}{2}F_\infty)\Delta t > 0$. Hence u_k^{n+1} is determined from linear interpolation based on the solution along characteristics emanating from grid point x_{k-1} and x_k.

To see that the claim in Remark 6.1 is true, we use (6.4) and require the following to hold

$$x_{k-1} + \frac{1}{2}\Delta x < X_k(\Delta t) < x_{k+1} - \frac{1}{2}\Delta x. \tag{6.9}$$

That is, the characteristic emanating from x_k stays a distance $\frac{1}{2}\Delta x$ apart from the neighbouring grid points, or equivalently does not cross the cell interfaces $x_{k\pm\frac{1}{2}}$ after a time step. This is required for all $k \in \mathbb{Z}$. If we rearrange this inequality, using that we have a uniform spatial discretization, i.e., $x_{k-1} = x_k - \Delta x$ and $x_{k+1} = x_k + \Delta x$, then (6.9) becomes

$$x_k - \frac{1}{2}\Delta x < X_k(\Delta t) < x_k + \frac{1}{2}\Delta x. \tag{6.10}$$

Now if we estimate $X_k(\Delta t) - x_k$ from above with $t \in [0, T]$ we get

$$\begin{aligned} |X_k(\Delta t) - x_k| &= \left| u(x_k(0), 0)\Delta t + \frac{1}{4}\left(F(x_k(0), 0) - \frac{1}{2}F_\infty\right)\Delta t^2 \right| \\ &\leq \|u_0\|_\infty \Delta t + \frac{1}{8}TF_\infty \Delta t. \end{aligned}$$

Combining that with (6.10), we observed that we must require

$$\Delta t(\|u_0\|_\infty + \frac{1}{8}TF_\infty) < \frac{1}{2}\Delta x.$$

Solving for Δt we get (6.8). We will stick with this choice for the derivation of the scheme, since this simplifies the considerations, as characteristics cannot move past several grid cells. Therefore a grid value is updated using only its neighbouring grid values at the previous time step.

6.2.2 Derivation of scheme

Consider the situation illustrated in Figure 23, here we observe that the forward characteristic satisfies $X_k^n(\Delta t) > x_k$, i.e., the characteristic emanating from the grid point x_k at time $t = t_n$ is to the right of x_k. Inserting for (6.4) we find

$$x_k < X_k^n(\Delta t) = x_k + u(x_k, t_n)\Delta t + \frac{1}{4}(F(x_k, t_n) - \frac{1}{2}F_\infty)\Delta t^2,$$

where $u(x_k, t_n) = u_k^n$ is the value of the numerical approximation at grid cell (x_k, t_n), similarly for $F(x_k, t_n)$. Rearranging and dividing by Δt, this reduces to

$$u_k^n + \frac{1}{4}(F_k^n - \frac{1}{2}F_\infty)\Delta t > 0.$$

The interpretation of this is that information propagates to the right from grid point x_k^n, where x_k^n denotes the k^{th} grid point at time t_n, but as we use a fixed mesh $x_k^n = x_k$ for all $n \in \mathbb{N} \cup \{0\}$. Hence for the method to be stable the grid values (u_k^{n+1}, F_k^{n+1}) are updated by using linear interpolation on the data emanating from the grid point x_{k-1}^n and x_k^n. In particular we use linear interpolation after evolving the solution exactly along characteristics, thus

$$\begin{aligned} u_k^{n+1} &= u_{k-1}^n(\Delta t) + s(u_k^n(\Delta t) - u_{k-1}^n(\Delta t)), \\ F_k^{n+1} &= F_{k-1}^n(\Delta t) + s(F_k^n(\Delta t) - F_{k-1}^n(\Delta t)), \end{aligned}$$

for some scalar s. Here we use $u_k^n(\Delta t)$ to denote the numerical approximation starting at the value u_k^n, which is evolved a time Δt forward along the characteristic starting at (x_k, t_n). The same applies for $F_k^n(\Delta t)$. We can also use linear interpolation to write the grid point x_k in terms of the characteristic emanating from x_k and x_{k-1} as

$$x_k = X_{k-1}^n(\Delta t) + s\big(X_k^n(\Delta t) - X_{k-1}^n(\Delta t)\big),$$

where capital X is used to denote the characteristics and lower case x is to denote the grid points. Solving this for s and using the expression we have for the time evolution of characteristics (6.4), we obtain

$$\begin{aligned} s &= \frac{x_k - X_{k-1}^n(\Delta t)}{X_k^n(\Delta t) - X_{k-1}^n(\Delta t)} \\ &= \frac{x_k - x_{k-1} - u_{k-1}^n \Delta t - \frac{1}{4}(F_{k-1}^n - \frac{1}{2}F_\infty)\Delta t^2}{\big(x_k + u_k^n \Delta t + \frac{1}{4}(F_k^n - \frac{1}{2}F_\infty)\Delta t^2\big) - \big(x_{k-1} + u_{k-1}^n \Delta t + \frac{1}{4}(F_{k-1}^n - \frac{1}{2}F_\infty)\Delta t^2\big)} \\ &= \frac{\Delta x - u_{k-1}^n \Delta t - \frac{1}{4}(F_{k-1}^n - \frac{1}{2}F_\infty)\Delta t^2}{\Delta x + (u_k^n - u_{k-1}^n)\Delta t + \frac{1}{4}(F_k^n - F_{k-1}^n)\Delta t^2}. \end{aligned}$$

Insert for (6.5a) and (6.5b) as well to get

$$\begin{aligned} u_k^{n+1} &= u_{k-1}^n + \frac{1}{2}(F_{k-1}^n - \frac{1}{2}F_\infty)\Delta t + s\bigg(u_k^n - u_{k-1}^n + \frac{1}{2}(F_k^n - F_{k-1}^n)\Delta t\bigg), \\ F_k^{n+1} &= F_{k-1}^n + s\bigg(F_k^n - F_{k-1}^n\bigg), \end{aligned}$$

as the cumulative energy is conserved along characteristics. This will be the expressions we implement numerically in the case the characteristic at grid point k travel to the right. In the opposite case where it travels to the left, i.e., $X_k(\Delta t) < x_k$ we have by similar reasoning

$$u_k^n + \frac{1}{4}(F_k^n - \frac{1}{2}F_\infty)\Delta t < 0.$$

We must find the new grid values (u_k^{n+1}, F_k^{n+1}) using information from grid points x_k^n and x_{k+1}^n instead. Thus again, using linear interpolation after evolving exactly along the characteristics emanating from the grid points, yields

$$\begin{aligned} u_k^{n+1} &= u_{k+1}^n(\Delta t) + s(u_k^n(\Delta t) - u_{k+1}^n(\Delta t)), \\ F_k^{n+1} &= F_{k+1}^n(\Delta t) + s(F_k^n(\Delta t) - F_{k+1}^n(\Delta t)), \\ x_k &= X_{k+1}^n(\Delta t) + s(X_k^n(\Delta t) - X_{k+1}^n(\Delta t)). \end{aligned}$$

Using the last equation to solve for s we get the following expression

$$\begin{aligned} s &= \frac{x_k - X_{k+1}^n(\Delta t)}{X_k^n(\Delta t) - X_{k+1}^n(\Delta t)} \\ &= \frac{\Delta x + u_{k+1}^n \Delta t + \frac{1}{4}(F_{k+1}^n - \frac{1}{2}F_\infty)\Delta t^2}{\Delta x + (u_{k+1}^n - u_k^n)\Delta t + \frac{1}{4}(F_{k+1}^n - F_k^n)\Delta t^2}. \end{aligned}$$

Similarly, using the expression we have for the solution along the characteristics results in

$$u_k^{n+1} = u_{k+1}^n + \frac{1}{2}(F_{k+1}^n - \frac{1}{2}F_\infty)\Delta t - s\bigg(u_{k+1}^n - u_k^n + \frac{1}{2}(F_{k+1}^n - F_k^n)\Delta t\bigg),$$
$$F_k^{n+1} = F_{k+1}^n - s\bigg(F_{k+1}^n - F_k^n\bigg).$$

It should be noted, that one can weaken the requirement on Δt to (6.7) in which case one updates the grid values (u_i^{n+1}, F_i^{n+1}) using grid points x_j^n and x_{j+1}^n for some index j depending on how far the characteristics move during the time step, and which direction the characteristics come from.

6.2.3 Applying the algorithm to two examples

Next we apply this algorithm to the example considered in Subsection 3.2, and see how well the numerical algorithm approximates the peakon solution.

Example 6.1. We consider

$$u_t + uu_x = \frac{1}{4}\left(\int_{-\infty}^x d\mu(t) - \int_x^\infty d\mu(t)\right),$$
$$F_t + uF_x = 0,$$

with initial data

$$u_0 = \begin{cases} 0 & \text{if } x < 0 \\ x & \text{if } 0 \le x < 1 \\ 2 - x & \text{if } 1 \le x \le 2 \\ 0 & \text{if } 2 < x \end{cases},$$

$$F_0 = \mu_0((-\infty, x)) = \begin{cases} 0 & \text{if } x < 0 \\ x & \text{if } 0 \le x \le 2 \\ 2 & \text{if } 2 \le x \end{cases}.$$

No wave breaking occurs initially, so the measure is purely absolutely continuous at $t = 0$. The initial data is a peakon, consisting of linear segments glued together. The analytical solution is the pair

$$u(x,t) = \begin{cases} -\frac{t}{2} & \text{if } x \le -\frac{t^2}{4} \\ \frac{2x-t}{t+2} & \text{if } -\frac{t^2}{4} \le x \le t+1 \\ \frac{2x-t-4}{t-2} & \text{if } t+1 \le x \le 2 + \frac{t^2}{4} \\ \frac{t}{2} & \text{if } x \ge 2 + \frac{t^2}{4} \end{cases},$$

and

$$F(x,t) = \begin{cases} 0 & \text{if } x \le -\frac{t^2}{4} \\ \frac{4\left(x + \frac{t^2}{4}\right)}{(t+2)^2} & \text{if } -\frac{t^2}{4} \le x \le t+1 \\ \frac{t^2 - 8t + 4x}{(t-2)^2} & \text{if } t+1 \le x \le 2 + \frac{t^2}{4} \\ 2 & \text{if } x \ge 2 + \frac{t^2}{4} \end{cases}.$$

This peakon solution experiences wave breaking at $(x^*, t^*) = (3, 2)$. We observe that F_x and u_x are supported inside $[a(t), b(t)]$ with $a(t) = -\frac{t^2}{4}$ and $b(t) = 2 + \frac{t^2}{4}$. Therefore we want the computational domain to at least contain $[a(t), b(t)]$, such that we catch the spatial variations in the quantities. We apply the algorithm with $\Delta x = \frac{1}{2}10^{-2}$ and one half of (6.8), that is

$$\Delta t = \frac{\Delta x}{2}\frac{1}{2(\|u_0\|_\infty + \frac{1}{8}TF_\infty)} = \frac{\Delta x}{4(1 + \frac{1}{4}T)}.$$

The numerical and analytical solutions are compared for times $t = 1, t = 2$ and $t = 3$, respectively in Figure 24 and Figure 25. The numerical approximation seems to agree reasonably well even when wave breaking occurs at $t = 2$. We observe that there is a jump in the cumulative distribution function, F, at the point where wave breaking occurs, and there is no such jump in $F_{\Delta x}$. It is at the location of this jump the discrepancy between the numerical and analytical solution is the largest. This discrepancy is still visible at $t = 3$ as seen from Figure 25.

In [GNS21] it is shown that provided the initial Radon measure μ_0 is supported on a finite interval, i.e., $\text{supp}(\mu_0) \subseteq [a, b]$, then for all $t \in [0, T]$, $F_{\Delta x,x}(\cdot, t)$ is supported on some interval $[a(t), b(t)]$. In particular this is shown in [Lemma 2.12, [GNS21]] As a consequence $u_{\Delta x}$ will be constant outside $[a(t), b(t)]$. The proof of the statement is based on the bound (6.7), but we can show that it carries over to our choice of time-step used in the example.

Lemma 6.1. *Let $(u_{\Delta x}, F_{\Delta x})$ denote the numerical solution as defined in Definition 7.2 with a chosen mesh size Δx. Moreover let*

$$\Delta t = \frac{1}{2} \frac{\Delta x}{2(\|u_0\|_{L^\infty} + \frac{T}{8} F_\infty)}. \tag{6.11}$$

Fix some $t \geq 0$, then $F_{\Delta x}(\cdot, t)$ is continuous and monotonically increasing. If supp$(\mu_0) \subseteq [a, b]$ then

$$supp F_{\Delta x,x}(\cdot, t) \subseteq [a(t), b(t)],$$

for some smooth curves $a(t), b(t)$.

Proof. $(u_0, F_0) \in \mathcal{D}$ and the first numerical approximation at time $t = 0$ is obtained by $(u^0, F^0) = P_{\Delta x}(u_0, F_0)$. The projection operator $P_{\Delta x}$ preserves monotonicity of F, since it is based on linear interpolation between grid points. Since F_0 is monotonically increasing so is F^0. Moreover F is preserved along characteristics, and the projection operator preserves monotonicity, therefore $F_{\Delta x}$ is monotonically increasing. Continuity is proven in [GNS21] by the observation that characteristics emanating from different grid points stay a distance $\frac{1}{2}\Delta x$ apart at all times when the time step is limited by (6.7). We use a more restrictive bound on the time step, but characteristics are still not allowed to meet, so continuity still holds.

Next we want to prove the support statement, let $\text{supp}(\mu_0) \subseteq [a, b]$. Define

$$\begin{aligned} x^- &: \text{ The closest grid point from below to } a, \\ x^+ &: \text{ The closest grid point from above to } b. \end{aligned}$$

Then initially $F_{\Delta x,x}(\cdot, 0)$ is supported on the interval $[x^-, x^+] \subseteq [a - \Delta x, b + \Delta x]$. Moreover the numerically computed cumulative energy satisfies $F_{\Delta x}(x^-, 0) = 0$ and $F_{\Delta x}(x^+, 0) = F_\infty$. We set $u_{\Delta x}(x^-, 0) = u_l$ and $u_{\Delta x}(x^+, 0) = u_r$. Next we show that $F_{\Delta x,x}(\cdot, \Delta t)$ is also compactly supported. Using (6.4) for the characteristics emanating from x^- and x^+ we get

$$x^-(\Delta t) = x^- + u_l \Delta t - \frac{1}{8} F_\infty \Delta t^2, \tag{6.12a}$$

$$x^+(\Delta t) = x^+ + u_r \Delta t + \frac{1}{8} F_\infty \Delta t^2. \tag{6.12b}$$

Therefore we have that $F_{\Delta x,x}(\cdot, \Delta t)$ is supported on the interval

$$\big[a + u_l \Delta t - \frac{1}{8} F_\infty \Delta t^2 - 2\Delta x, b + u_r \Delta t + \frac{1}{8} F_\infty \Delta t^2 + 2\Delta x\big].$$

We proceed iteratively, we now want to show that $F_{\Delta x,x}(\cdot, k\Delta t)$ is compactly supported for $k \in \mathbb{N}$. To achieve that we consider the movement of x^- and x^+ during that time. Their position

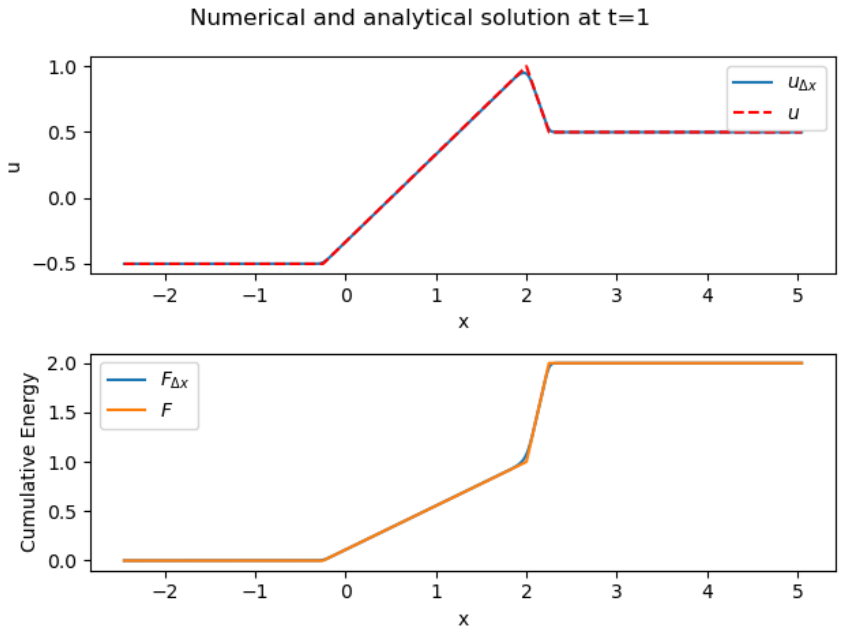

(a) Before wave breaking, $t = 1$.

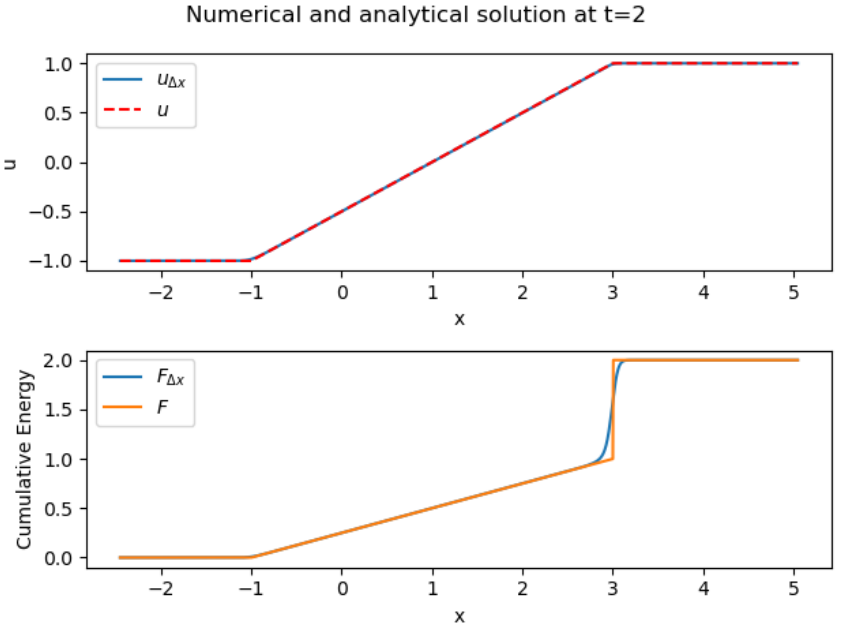

(b) At wave breaking, $t = 2$.

Figure 24: The analytical solution and numerical approximation is compared before (a) and at the moment of wave breaking (b).

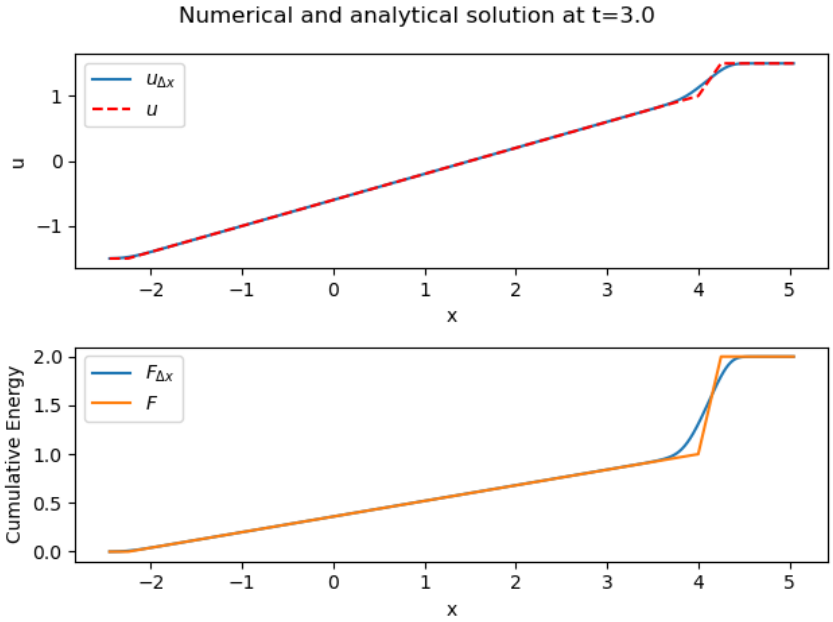

Figure 25: Numerical and analytical solution after wave breaking, $t = 3$.

is still given by (6.12a) and (6.12b), respectively, but with Δt replaced by $k\Delta t$. Therefore $F_{\Delta x,x}(\cdot, k\Delta t)$ is supported on

$$\left[a + u_l k\Delta t - \frac{1}{8}F_\infty(k\Delta t)^2 - (k+1)\Delta x, b + u_r k\Delta t + \frac{1}{8}F_\infty(k\Delta t)^2 + (k+1)\Delta x\right].$$

Using our time step choice (6.11) we can write $(k+1)\Delta x = \Delta x + (4\|u_0\|_\infty + \frac{1}{2}TF_\infty)k\Delta t$. Hence for instance the left side of the interval becomes

$$a + u_l k\Delta t - \frac{1}{8}F_\infty(k\Delta t)^2 - (k+1)\Delta x = a + (u_l - 4\|u_0\|_\infty)k\Delta t - (\frac{1}{8}k\Delta t + \frac{1}{2}T)F_\infty k\Delta t - \Delta x.$$

Using linear interpolation between temporal grid points, $F_{\Delta x,x}(\cdot, t)$ has support on $[a(t), b(t)]$, where

$$a(t) = a + (u_l - 4\|u_0\|_\infty)t - (\frac{1}{8}t + \frac{1}{2}T)F_\infty t - 2\Delta x, \tag{6.13a}$$

$$b(t) = b + (u_r + 4\|u_0\|_\infty)t + (\frac{1}{8}t + \frac{1}{2}T)F_\infty t + 2\Delta x. \tag{6.13b}$$

□

For Example 6.1 we have $\|u_0\|_\infty = 1$, $F_\infty = 2$, $u_l = u_r = 0$ and $[a, b] = [0, 2]$. Inserting that into (6.13a) and (6.13b), respectively, the expressions reduce to

$$a(t) = -4t - 2(\frac{1}{8}t + \frac{1}{2}T)t - 2\Delta x,$$
$$b(t) = 2 + 4t + 2(\frac{1}{8}t + \frac{1}{2}T)t + 2\Delta x.$$

Considering Figure 24 and Figure 25, where $t = T$, the spatial variations in $(u_{\Delta x}, F_{\Delta x})$ seem to be contained inside this interval. Moreover $F_{\Delta x}$ looks continuous, even when wave breaking occurs for the true solution, and is monotonically increasing. Therefore the numerical simulations agree with the expected behaviour.

In [GNS21] it is proven that to any initial data $(u_0, \mu_0) \in \mathcal{D}$ where μ_0 has compact support, the algorithm produces a numerical solution $(u_{\Delta x}, F_{\Delta x})$ which has a convergent subsequence. Therefore we have no troubles for Example 6.1. However when we want to apply the algorithm for conservative traveling waves considered in Section 5 for instance, one immediate problem arises. The initial Radon measure has not compact support. In particular for a cuspon as we observed in Section 4, u_x is monotone but of different sign on either side of the cusp singularity, being convex or concave on both sides. However the derivative decays too slowly such that the resulting cumulative energy is infinite. This will become apparent in the next example. In particular this means that the theorem ensuring the convergence of a subsequence does not carry over. We will consider the initial data used in example 5.1 in Subsection 5.1.

Example 6.2. The initial data for Example 5.1 with $\beta = \alpha$ is given by

$$u_0(x) = \begin{cases} s + \alpha(-x)^{\frac{2}{3}} & \text{for } x < 0 \\ s + \alpha x^{\frac{2}{3}} & \text{for } 0 \leq x \end{cases}.$$

In particular the associated Radon measure will be purely absolutely continuous, but does not have compact support. The cumulative distribution function is not finite if we use $-\infty$ as reference point, i.e., $F_0(x) = \mu((-\infty, x))$ is not defined. In particular assume $x > 0$ (the same conclusion applies for $x < 0$)

$$F_0(x) = \int_{-\infty}^{x} u_{0,x}^2(x)\, dx = \frac{4\alpha^2}{9}\bigg(\int_{-\infty}^{0} (-x)^{\frac{2}{3}}\, dx + \int_0^x y^{-\frac{2}{3}} dy \bigg),$$

which is a simple improper integral. The second integral is convergent, but the first integral satisfies

$$\begin{aligned} \int_{-\infty}^{0} x^{-\frac{2}{3}}\, dx &= \lim_{R\to\infty} \int_{-R}^{0} x(-x)^{-\frac{2}{3}}\, dx \\ &= \lim_{R\to\infty} \int_0^R y^{-\frac{2}{3}} dy \\ &= \lim_{R\to\infty} 3R^{\frac{1}{3}}, \end{aligned}$$

hence is divergent. Therefore $F_0(x)$ is undefined. In order to proceed with the algorithm outlined in the previous subsection, we will have to approximate our initial data, and assume that we have initial data of the form

$$u_0(x) = \begin{cases} s + \alpha|x_l|^{\frac{2}{3}} & \text{for } x \leq x_l \\ s + \alpha|x|^{\frac{2}{3}} & \text{for } x_l < x \leq x_r \\ s + \alpha x_r^{\frac{2}{3}} & \text{for } x_r \leq x \end{cases},$$

instead, for some constants $x_l < 0 < x_r$. That is, we limit ourselves to consider the wave on an interval $[x_l, x_r]$, and say that the wave is constant outside this interval. Then we can calculate the initial cumulative energy using $d\mu = u_{0,x}^2\, dx$ as the measure is purely absolutely continuous, leading to

$$F_0(x) = \begin{cases} 0 & \text{for } x \leq x_l \\ \frac{4}{3}\alpha^2\left(|x_l|^{\frac{1}{3}} - |x|^{\frac{1}{3}}\right) & \text{for } x_l < x \leq 0 \\ \frac{4}{3}\alpha^2\left(|x_l|^{\frac{1}{3}} + |x|^{\frac{1}{3}}\right) & \text{for } 0 < x \leq x_r \\ \frac{4}{3}\alpha^2\left(|x_l|^{\frac{1}{3}} + x_r^{\frac{1}{3}}\right) & \text{for } x_r \leq x_r. \end{cases}$$

The initial data is shown in Figure 26 (a) with the choice $\alpha = 1$, $x_l = -1$ and $x_r = 1$, when the final simulation time $T = \frac{1}{2}$. If we set a larger final simulation time T, we need to include

a larger region where the initial data is constant, in order for the computational domain to contain the parts where the solution vary. We will work with these choice of x_l, x_r, but keep α and s general, to keep the expressions simple. Doing this approximation, we at least hope to approximate the conservative wave locally around the cusp singularity located at $x = st$. We can use the Lagrangian formalism introduced in Subsection 3.3 to solve the Cauchy problem with this truncated initial data exactly. With the choice of x_l and x_r, the initial data now reads

$$u_0(x) = \begin{cases} s+\alpha & \text{for } x < -1 \\ s+\alpha|x|^{\frac{2}{3}} & \text{for } -1 \leq x \leq 1 \\ s+\alpha & \text{for } 1 < x, \end{cases}$$

$$F_0(x) = \begin{cases} 0 & \text{for } x < -1 \\ \frac{4}{3}\alpha^2(1-|x|^{\frac{1}{3}}) & \text{for } -1 \leq x < 0 \\ \frac{4}{3}\alpha^2(1+x^{\frac{1}{3}}) & \text{for } 0 \leq x \leq 1 \\ \frac{8}{3}\alpha^2 & \text{for } 1 < x, \end{cases}$$

which reduces to the cusp-example considered in [GNS21] for $s = 0$ and $\alpha = 1$. We use (3.19a)-(3.19c) to find the solution along characteristics. First we find the characteristics. The characteristic emanating from $X_0(\xi) = -1$ is given by

$$\begin{aligned} x_1(t) = X(\xi,t) &= X_0(\xi) + u_0(X_0(\xi))t + \frac{t^2}{4}(H_0(\xi) - \frac{1}{2}K) \\ &= -1 + t(s+\alpha) - \frac{t^2}{3}\alpha^2. \end{aligned}$$

Similarly one finds the one emanating from $X_0(\xi) = 1$. Now consider $X_0(\xi) \in [0,1]$ and use that $H(\xi,t) = F(X(\xi,t),t)$, then

$$\begin{aligned} X(\xi,t) &= X_0(\xi) + t(s + \alpha X_0^{\frac{2}{3}}(\xi)) + \frac{t^2}{4}(\frac{4}{3}\alpha^2(1+X_0(\xi)^{\frac{1}{3}}) - \frac{1}{2}\frac{8}{3}\alpha^2) \\ &= (X_0(\xi)^{\frac{1}{3}} + \frac{\alpha t}{3})^3 - (\frac{\alpha t}{3})^3 + ts. \end{aligned}$$

Here we completed the cubic factor $(a+b)^3 = a^3 + 3(ab^2 + a^2b) + b^3$ with $a = X_0(\xi)^{\frac{1}{3}}$ and $b = \frac{\alpha t}{3}$. We also determine the value of u along this characteristic

$$\begin{aligned} U(\xi,t) = u(X(\xi,t),t) &= s + \alpha X_0(\xi)^{\frac{2}{3}} + \frac{t}{2}(\frac{4}{3}\alpha^2(1+X_0(\xi)^{\frac{1}{3}}) - \frac{1}{2}\frac{8}{3}\alpha^2) \\ &= \alpha(X_0(\xi)^{\frac{1}{3}} + \frac{\alpha t}{3})^2 - (\frac{\alpha t}{3})^2 + s, \end{aligned}$$

here we completed the square factor $(a+b)^2$ with the same choice of a and b. Now set $x = X(\xi,t)$, solving in terms of $X_0(\xi)^{\frac{1}{3}} + \frac{\alpha t}{3}$ since this appears in the expression for U. This leads to

$$x = X(\xi,t) \qquad \Longleftrightarrow \qquad X_0(\xi)^{\frac{1}{3}} + \frac{\alpha t}{3} = (x + (\frac{\alpha t}{3})^3 - st)^{\frac{1}{3}}.$$

This is inserted into the expression for $U(\xi,t)$ to eliminate $X_0(\xi)$ yielding $u(x,t)$. We do similarly for $X_0(\xi) \in [-1,0)$. The case of $X_0(\xi) < -1$ and $X_0(\xi) > 1$ are even simpler, since u is constant here. Finally we obtain

$$u(x,t) = \begin{cases} s+\alpha-\frac{2}{3}\alpha^2 t & x < -1 + t(s+\alpha) - \frac{t^2}{3}\alpha^2 \\ \alpha\left(x + (\frac{\alpha t}{3})^3 - ts\right)^{\frac{2}{3}} - \alpha^3(\frac{t}{3})^2 + s & -1 + t(s+\alpha) - \frac{t^2}{3}\alpha^2 \leq x \leq 1 + t(s+\alpha) + \frac{t^3}{3}\alpha^2 \\ s+\alpha+\frac{2}{3}\alpha^2 t & 1 + t(s+\alpha) + \frac{t^2}{3}\alpha^2 < x. \end{cases}$$

Now we can also determine the cumulative distribution function

$$F(x,t) = \begin{cases} 0 & x < -1 + t(s+\alpha) - \frac{t^2}{3}\alpha^2 \\ \frac{4}{3}\alpha^2\left(1 - \frac{at}{3} + [x + (\frac{at}{3})^3 - st]^{\frac{1}{3}}\right) & -1 + t(s+\alpha) - \frac{t^2}{3}\alpha^2 \leq x \leq 1 + t(s+\alpha) + \frac{t^2}{3}\alpha^2 \\ \frac{8}{3}\alpha^2 & 1 + t(s+\alpha) + \frac{t^2}{3}\alpha^2 < x. \end{cases}$$

The traveling wave $w(\xi)$ is compared to the analytical solution developed here for the truncated initial data (u, F), and the numerical approximation $(u_{\Delta x}, F_{\Delta x})$, for times $t = \frac{1}{2}$ in Figure 26 (b), $t = 1$ and $t = \frac{3}{2}$ in Figure 27 (a) and (b), respectively. As mentioned the cumulative energy for the traveling wave is infinite, thus it is not shown here. We observe that $(u_{\Delta x}, F_{\Delta x})$ seems to converge to (u, F). At $t = \frac{1}{2}$ the solution with truncated initial data seem to approximate the cusp singularity locally rather reasonably, but as time t evolves the location of the cusp singularity lags behind the true cusp. The differences become larger and larger as time progresses. The qualitative behaviour of the solution with truncated initial data is very different from that of the cuspon, thus this approach is inadequate for simulating conservative cuspons.

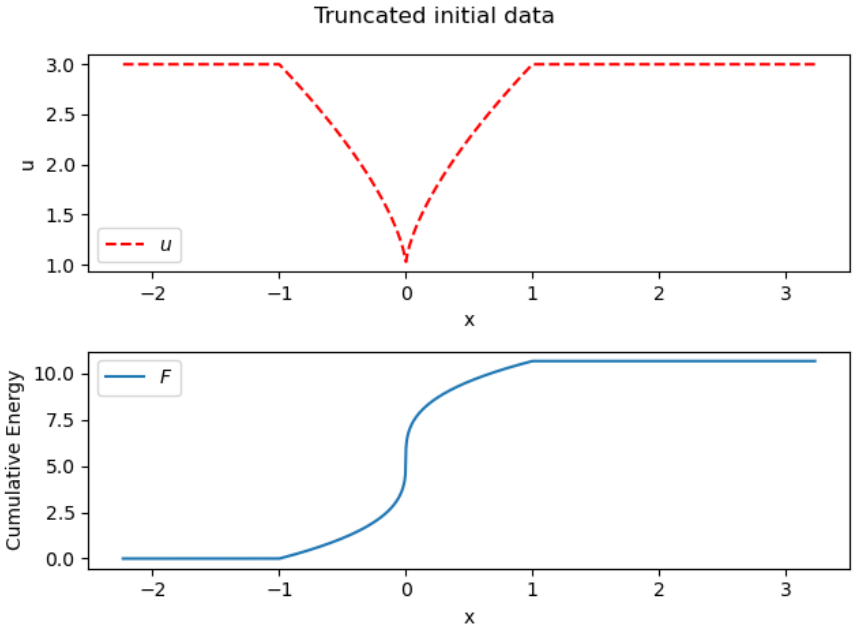

(a) Truncated initial data, $t = 0$.

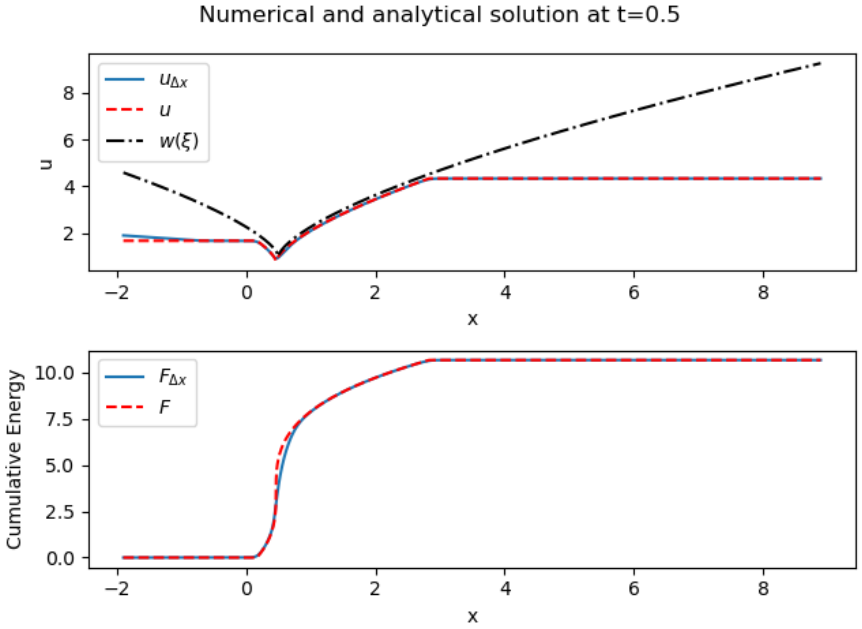

(b) Comparison at $t = \frac{1}{2}$.

Figure 26: The truncated initial data is shown in (a). While the traveling wave, analytical solution with the modified initial data and numerical approximation is compared at $t = \frac{1}{2}$ in (b).

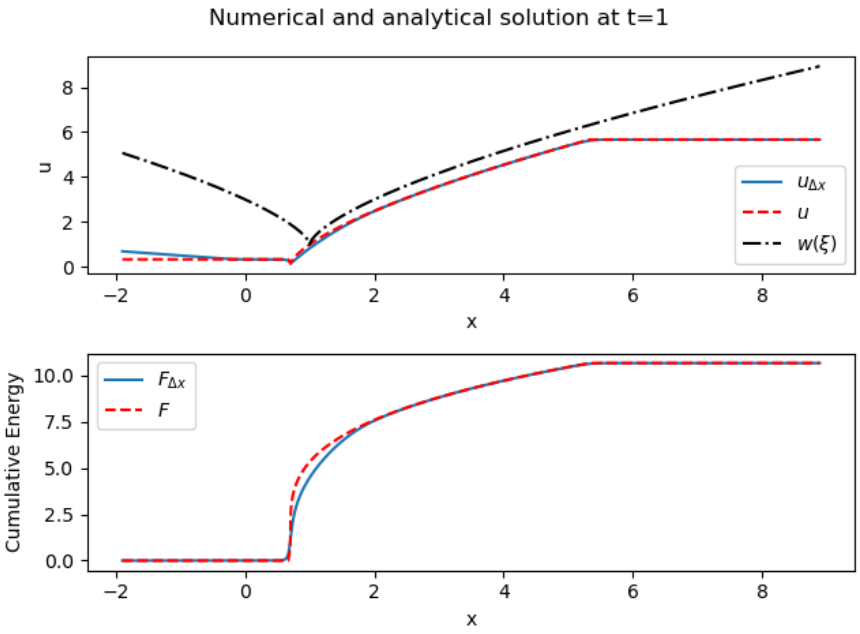

(a) Comparison at $t = 1$.

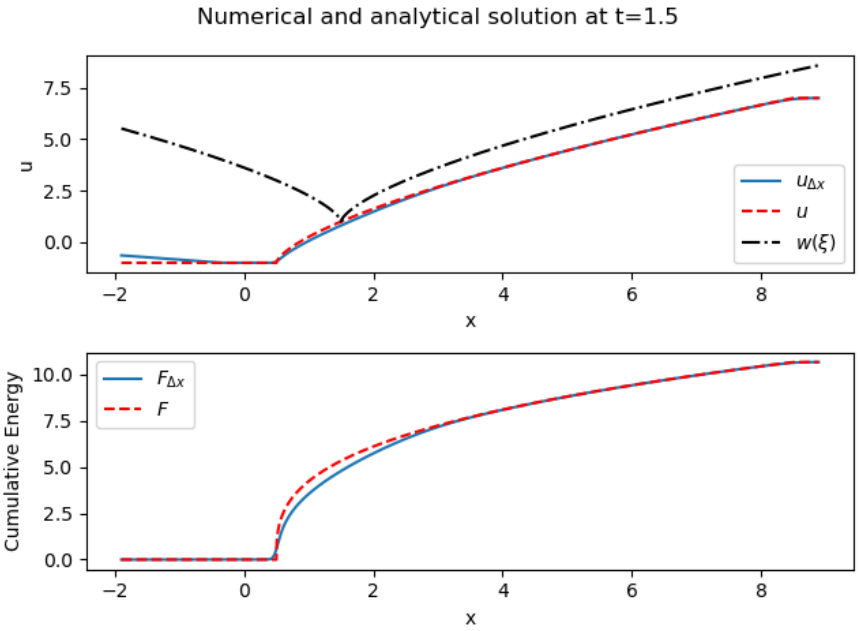

(b) Comparison at $t = \frac{3}{2}$.

Figure 27: The traveling wave $w(\xi)$, analytical solution (u, F) with the modified initial data and numerical approximation $(u_{\Delta x}, F_{\Delta x})$ is compared at $t = 1$ in (a) and $t = \frac{3}{2}$ in (b).

7 A modified algorithm for simulating conservative traveling waves

In this chapter we want to modify the numerical algorithm presented in the previous chapter, with the main goal of simulating weak conservative traveling waves. We noticed that the algorithm developed in [GNS21] is based on the assumption that the initial data is constant outside some finite interval. This is inadequate for the setting of conservative traveling waves. Moreover the algorithm involves the quantity F_∞, which for conservative cuspons is infinite. We want to overcome these obstacles in order to construct an algorithm which is able to approximate conservative traveling cuspons at least locally.

We want the approximation to still rely on continuous piecewise linear solutions, u, that are conservative as in [GNS21], but now we will consider the differentiated form of the Hunter-Saxton equation instead. We can use similar considerations as in Section 4 and Section 5 to show that we can glue together linear solutions to obtain a piecewise linear conservative solution to the Hunter-Saxton equation, provided the gluing points move along characteristics. We want to glue together such continuous piecewise linear functions to approximate the initial data of the Cauchy problem. Then we want to exploit that the gluing points travel along characteristics, to evolve the gluing points exactly a time step Δt forward in time, as well as evolving the solution (u, F) along the gluing points. We project the evolved solution, and then we linearly interpolate in between the grid points to get the approximation $(u_{\Delta x}, F_{\Delta x})$ defined everywhere for a given time step.

We consider the following augmented differentiated formulation of the Hunter-Saxton equation

$$(u_t + uu_x)_x = \frac{1}{2}\mu, \tag{7.1a}$$

$$\mu_t + (u\mu)_x = 0. \tag{7.1b}$$

Here we have added an energy equation. Requiring $d\mu \geq u_x^2\, dx$, then we recognize this as a reformulation of the two-component Hunter-Saxton system, where (7.1a) appears on differentiated form in contrast to the integrated formulation we met in Chapter 6. In particular, $d\mu_{\text{ac}} = (u_x^2 + \rho^2)\, dx$, as we introduce an error when we project the solution after each time step evolution. We will look for local classical solutions on intervals $I_k(t) = [a_k(t), b_k(t)]$ glued together in such a way that the resulting composite function is a solution in $\mathbb{R} \times [0, \infty)$. We will observe that when we derive the associated Lagrangian system, we can avoid having to refer to a quantity F_∞. In general when we construct a computational domain we need to limit ourselves to a bounded interval $[a(t), b(t)]$, in order to have a numerical feasible domain. We want this computational domain to at least contain the line where the cusp singularity moves at all times. We will observe that we need to initialize the mesh on a much larger initial interval $[a, b] \subset \mathbb{R}$, than where we compute the solution. This is due to the fact that we must remove certain grid points from the domain as we evolve the solutions forward in time.

First we want to introduce the notion of a weak conservative solution to the two-component Hunter-Saxton system, (7.1a)-(7.1b). We treat the general case where μ is a positive Radon measure. Take a test function $\phi \in C_0^\infty(\mathbb{R} \times [0, \infty))$ and integrate (7.1a) by parts, to obtain

$$\begin{aligned} 0 &= \int_0^\infty \int_{\mathbb{R}} (u_t + uu_x)_x \phi \, dx \, dt - \frac{1}{2} \int_0^\infty \int_{\mathbb{R}} \phi d\mu(t) dt \\ &= \int_0^\infty \int_{\mathbb{R}} \left(u\phi_{xt} + \frac{1}{2} u^2 \phi_{xx} \right) dx \, dt - \frac{1}{2} \int_0^\infty \int_{\mathbb{R}} \phi d\mu(t) dt + \int_{\mathbb{R}} \phi_x|_{t=0} u_0(x) \, dx \, . \end{aligned}$$

This is well defined even when μ is not a finite measure, since ϕ has compact support. Thus the integrals are only taken over a compact set, and Radon measures on $\mathbb{R}$ assign a finite value to every compact set of $\mathbb{R}$. Similarly we integrate (7.1b) by parts, to transfer the partial derivatives

to the test function. A conservative solution consists of a pair (u, μ) or (u, F) satisfying certain requirements specified in the next definition. Here μ acts as the energy density, although it is no longer the physical energy density since it now also involves a projection error. F is the energy, which is an associated cumulative distribution function of μ, but it is not unique. In particular we have the freedom of choosing a constant when we relate μ and F. Changing this constant, amounts to altering the reference point of the energy.

Definition 7.1 (Conservative sol.)**.** A pair (u, μ) or (u, F) where F is an associated cumulative distribution function of μ, is a conservative solution to (7.1a)-(7.1b) with initial data (u_0, μ_0) if $u \in C^{0,\frac{1}{2}}_{\text{loc}}(\mathbb{R} \times [0, T])$, for all $T > 0$. Moreover for all test functions $\phi \in C_0^\infty(\mathbb{R} \times [0, \infty))$ we have

$$0 = \int_0^\infty \int_{\mathbb{R}} \left(u\phi_{xt} + \frac{1}{2}u^2\phi_{xx} \right) - \frac{1}{2} \int_0^\infty \int_{\mathbb{R}} \phi d\mu(t)dt + \int_{\mathbb{R}} \phi_x|_{t=0} u_0(x)\, dx, \tag{7.2}$$

and

$$\int_0^\infty \int_{\mathbb{R}} \Big(\phi_t + \phi_x u \Big) d\mu(t)\, dt + \int_{\mathbb{R}} \phi|_{t=0}(x) d\mu_0 = 0. \tag{7.3}$$

Here we require u to be Hölder-continuous on compact sets at all times with exponent $\frac{1}{2}$. We observed that this is satisfied for weak traveling waves in Section 4, where we limited ourselves to bounded intervals. Next we will derive some preliminary results which are needed for our algorithm.

7.1 Gluing to obtain multipeakons

Assume we have two classical solutions (u_i, μ_i) for $i \in \{1, 2\}$ in D_1 and D_2, respectively, of the form

$$u_i(x, t) = a_i(t) + b_i(t)x, \tag{7.4a}$$
$$\mu_i(x, t) = \gamma_i(t). \tag{7.4b}$$

We want to glue them together along a curve Γ in order to obtain a new solution (u, μ) which is a composition of the two solutions. In particular u_i and μ_i are linear and constant in space, respectively. Thus we expect u to become a multipeakon. We require u to be continuous at the gluing points, but it will in general posses a derivative which is discontinuous at the gluing points. Therefore we also expect μ to be discontinuous at the gluing points. As a consequence the resulting glued wave is not a classical solution, but rather a weak solution to (7.1a)-(7.1b). Using the gluing formalism presented in Section 4 and Section 5 we can ensure that the composite function pair, (u, μ), is a weak conservative solution of the Hunter-Saxton equation. μ will be spatially piecewise constant, and represents a fictitious energy density, since as mentioned it involves the true energy density in addition to a projection error.

First of all we need to ensure that there exist linear solutions of the form (7.4a)-(7.4b) to the system (7.1a)-(7.1b) in the first place. In order for a pair (u, μ) given by

$$u(x, t) = a(t) + b(t)x,$$
$$\mu(x, t) = \gamma(t),$$

to be a classical solution of the two-component Hunter-Saxton system, (7.1a)-(7.1b), on some interval $I(t)$, we require

$$\dot{b}(t) + (b(t))^2 = \frac{1}{2}\gamma(t),$$
$$\dot{\gamma}(t) + \gamma(t)b(t) = 0,$$

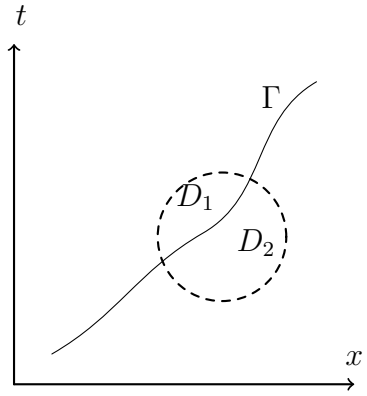

Figure 28: An illustration of an increasing curve Γ which separates the two domains D_1 and D_2.

to hold on $I(t)$. Here we inserted the ansatzed form of (u, μ) into (7.1a)-(7.1b). Thus we have two first order nonlinear coupled ODEs in time which can be solved to obtain a classical solution of the two-component Hunter-Saxton system of the form (7.4a)-(7.4b). The ODE-system describes the time evolution of the functions b and γ. The function $a(t)$ can be determined once we glue together such solutions, as we require continuity at the gluing points. Assume we have N linear solutions which we glue together. The continuity requirement will uniquely determine $N-2$ of the $a_k(\cdot)$'s. We still have some freedom to choose $a_1(\cdot)$, i.e., for the very left linear solution, and $a_N(\cdot)$ for the very right linear solution. That is, the two linear solutions which are not squeezed in between two other linear solutions, but only connected to a linear solution at one side. Moreover as mentioned we also have some freedom when we relate μ and F, since F is determined up to a constant, changing the constant amounts to changing the reference point of the energy.

We recall here the setting outlined in Section 4 and Section 5. We have possible discontinuities in the first order partial derivatives of u that move along a curve Γ which we parameterize as $\Gamma := \{(\sigma(t), t) : t \in \mathbb{R}\}$. μ will typically be piecewise constant, with jumps that travel along the curve Γ. Provided we prevent wave breaking from occurring we may assume that σ is a smooth function of t and strictly increasing, i.e., $\sigma'(t) > 0$. If wave breaking may occur for solutions of the form (7.4a)-(7.4b) smoothness of the curve Γ is in general lost. We assume that (u_1, μ_1) is a classical solution of the form (7.4a)-(7.4b) to (7.1a)-(7.1b) in D_1, except at the part $\partial D_1 \cap \Gamma$, while (u_2, μ_2) is a classical solution in D_2 of the same form, except at $\partial D_2 \cap \Gamma$. The two regions D_1 and D_2 are separated by the curve Γ as illustrated in Figure 28. We want to glue (u_1, μ_1) and (u_2, μ_2) together to obtain a composite pair (u, μ), which is a weak conservative solution in the entire region $D = D_1 \cup D_2$. Therefore we first proceed by considering

$$(u_t + uu_x)_x = \frac{1}{2}\mu,$$

and then we consider

$$\mu_t + (u\mu)_x = 0,$$

leading to requirements that both equations put on our glued pair (u, μ).
Let I and D_i^ϵ be the sets defined in (4.7), that is

$$I := \{t \in [0, \infty) : (\sigma(t), t) \in D\},$$
$$D_i^\epsilon := \{(x, t) \in D_i : \text{dist}((x, t), \Gamma) > \epsilon\},$$

for some $\epsilon > 0$ and $i \in \{1, 2\}$. Using (7.2) with a test function $\phi \in C_0^\infty(D)$ and that μ is now a

piecewise constant function of space and not a measure, we observe that

$$\begin{aligned} 0 &= \iint_D \left(u\phi_{xt} + \frac{1}{2}u^2\phi_{xx} - \frac{1}{2}\mu\phi \right) dx\, dt \\ &= \lim_{\epsilon \downarrow 0} \iint_{D_1^\epsilon \cup D_2^\epsilon} \left(u\phi_{xt} + \frac{1}{2}u^2\phi_{xx} - \frac{1}{2}\mu\phi \right) dx\, dt\,. \end{aligned}$$

Considering the part over D_1^ϵ, performing the same manipulations as in Section 4, we obtain

$$\begin{aligned} &\iint_{D_1^\epsilon} \left(u\phi_{xt} + \frac{1}{2}u^2\phi_{xx} - \frac{1}{2}\mu\phi \right) dx\, dt \\ &\quad = \int_{I_1^\epsilon} \left(\left[u\phi_t + \frac{1}{2}u^2\phi_x - (\frac{u^2}{2})_x\phi \right] (\sigma_1^\epsilon(t), t) + \dot{\sigma}_1^\epsilon(t)(u_x\phi)(\sigma_1^\epsilon(t), t) \right) dx\, dt, \end{aligned} \tag{7.5}$$

where as before $I_1^\epsilon := \{t \in [0,\infty) : (\sigma_1^\epsilon(t), t) \in D_1\}$, and σ_1^ϵ is a function used to parameterize the boundary part of D_1^ϵ which does not coincide with ∂D_1. This is assumed to be a smooth and strictly increasing function. We do the same for D_2^ϵ, where we get an additional minus sign when applying Green's theorem

$$\begin{aligned} &\iint_{D_2^\epsilon} \left(u\phi_{xt} + \frac{1}{2}u^2\phi_{xx} - \frac{1}{2}\mu\phi \right) dx\, dt \\ &\quad = \int_{I_2^\epsilon} \left(- \left[u\phi_t + \frac{1}{2}u^2\phi_x - (\frac{u^2}{2})_x\phi \right] (\sigma_2^\epsilon(t), t) - \dot{\sigma}_2^\epsilon(t)(u_x\phi)(\sigma_2^\epsilon(t), t) \right) dx\, dt\,. \end{aligned} \tag{7.6}$$

Now since we assume that σ_i^ϵ is smooth for $i \in \{1, 2\}$, σ_i^ϵ and its first order derivative, $\dot{\sigma}_i^\epsilon$, tend to σ and $\dot{\sigma}$, respectively, as $\epsilon \downarrow 0$. Moreover we require u to be continuous at the gluing point, thus passing to the limit $\epsilon \downarrow 0$ in (7.5) and (7.6) and adding them up yields

$$\begin{aligned} 0 &= \lim_{\epsilon \downarrow 0} \iint_{D_1^\epsilon \cup D_2^\epsilon} \left(u\phi_{xt} + \frac{1}{2}u^2\phi_{xx} - \frac{1}{2}\mu\phi \right) dx\, dt \\ &= \int_I (\dot{\sigma}(t) - u(\sigma(t), t)) \left[\lim_{x \uparrow \sigma(t)} u_x(x, t) - \lim_{x \downarrow \sigma(t)} u_x(x, t) \right] \phi(\sigma(t), t)\, dt \\ &= \int_I (\dot{\sigma}(t) - u(\sigma(t), t)) \Big[b_1(t) - b_2(t) \Big] \phi(\sigma(t), t)\, dt, \end{aligned}$$

where we inserted for the ansatz (7.4a). This should hold for all test functions $\phi \in C_0^\infty(\mathbb{R} \times (0,\infty))$, hence it must be the case that either $b_1(t) = b_2(t)$ or $u(\sigma(t), t) = \dot{\sigma}(t)$ for a.e. $t \in I$. The former case implies that u is a C^1-function along the curve parameterized by $\sigma(t)$, and no gluing is needed. Alternatively

$$u(\sigma(t), t) = \dot{\sigma}(t), \tag{7.7}$$

which we recognize as the ODE for characteristics, $x = \sigma(t)$. Hence breakpoints, i.e., gluing points where u_x is allowed to be discontinuous have to move along characteristics. Now we want to ensure that the resulting composite wave is conservative as well. Therefore we want (7.3) also to hold, such that the pair (u, μ) classifies as a candidate for a weak conservative solution. That is,

$$\begin{aligned} 0 &= \iint_D (\phi_t + u\phi_x)\, \mu dx dt \\ &= \lim_{\epsilon \downarrow 0} \iint_{D_1^\epsilon \cup D_2^\epsilon} (\phi_t + u\phi_x)\, \mu dx dt. \end{aligned}$$

Proceeding similarly as in Section 5 we assume (u, μ) is a classical solution to the conservation law (7.1b). Hence we can add $\mu_t + (u\mu)_x = 0$ to get

$$\begin{aligned}&\iint_{D_1^\epsilon} \Big(\mu\phi_t + u\mu\phi_x + (\mu_t + (u\mu)_x)\phi\Big)\, dx\, dt \\ &\qquad = \int_{I_1^\epsilon} (u(\sigma_1^\epsilon(t), t) - \dot\sigma_1^\epsilon(t))\, \mu(\sigma_1^\epsilon(t), t)\phi(\sigma_1^\epsilon(t), t)\, dt,\end{aligned}$$

where we applied Liebniz rule and Green's theorem as in Section 5. Proceeding similarly for the region D_2^ϵ we obtain

$$\begin{aligned}&\iint_{D_2^\epsilon} (\mu\phi_t + u\mu\phi_x)\, dx\, dt \\ &= -\int_{I_2^\epsilon} \Big(u(\sigma_2^\epsilon(t), t) - \dot\sigma_2^\epsilon\Big)\mu(\sigma_2^\epsilon(t), t)\phi(\sigma_2^\epsilon(t), t)\, dt,\end{aligned}$$

where the minus sign in front is due to the application of Green's theorem. Passing to the limit $\epsilon \downarrow 0$, using that μ is composed of two constant functions, and adding these two contributions together leads to

$$\begin{aligned}0 &= \iint_D (\phi_t + u\phi_x)\, \mu dx dt \\ &= \int_I (u(\sigma(t), t) - \dot\sigma(t)) \left[\lim_{x\uparrow\sigma(t)} \mu(x, t) - \lim_{x\downarrow\sigma(t)} \mu(x, t)\right] \phi(\sigma(t), t)\, dt \\ &= \int_I (u(\sigma(t), t) - \dot\sigma(t))\, [\gamma_1(t) - \gamma_2(t)]\, \phi(\sigma(t), t)\, dt\,.\end{aligned}$$

This should hold for any test function $\phi \in C_0^\infty(\mathbb{R} \times (0, \infty))$, hence either $\gamma_1(t) = \gamma_2(t)$ for all $t \in I$, in which case μ is continuous along the gluing curve, alternatively $u(\sigma(t), t) = \dot\sigma(t)$, which is the ODE for characteristics. We summarize our findings in the next lemma.

Lemma 7.1 (gluing peakons)**.** *Assume we have two pairs of classical solutions* (u_1, μ_1) *and* (u_2, μ_2) *of the form* (7.4a)-(7.4b) *to* (7.1a)-(7.1b) *in regions* D_1 *and* D_2*, respectively. These can be patched together along a curve* $\Gamma : x = \sigma(t)$ *to form a multipeakon which is a weak conservative solution of* (7.1a)-(7.1b) *in the sense of Definition 7.1 if*

$$\dot\sigma(t) = u(\sigma(t), t),$$

i.e., the gluing point moves along a characteristic.

Remark 7.1. We assumed smoothness of the curve $\Gamma = \{(\sigma(t), t) : t \in t \in \mathbb{R}\}$, this will not hold if wave breaking occurs along the curve. However, for the numerical algorithm which we will apply, the time step Δt is limited in such a way that wave breaking does not occur along any gluing curve. Thus this result remains valid.

Consequently we can glue together many classical solutions of the form (7.4a)-(7.4b) to construct a composite weak conservative solution of (7.1a)-(7.1b), provided all the gluing points move along characteristics. The characteristic between the k^{th} and $(k+1)^{\text{th}}$ is found by solving

$$\dot\sigma_k(t) = a_k(t) + b_k(t)\sigma_k(t),$$

while the solution along this characteristic is given by

$$u(\sigma_k(t), t) = a_k(t) + b_k(t)\sigma_k(t).$$

These equations hold provided no wave breaking does occur for the composite solution u, consisting of the linear solutions patched together. The resulting composite function pair

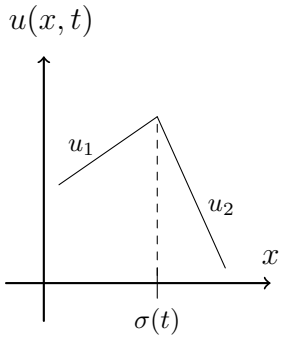

(a) The composite function u locally around the gluing point $\sigma(t)$ for a fixed t.

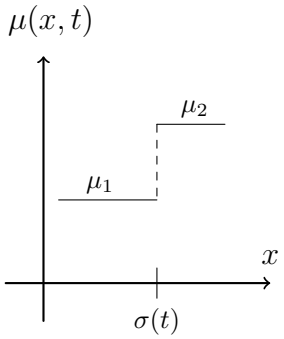

(b) The composite function μ locally around the gluing point $\sigma(t)$ for a fixed t.

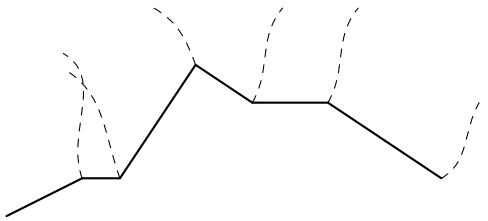

(c) A multipeakon, consiting of several linear solutions patched together.

Figure 29: Figure (a) and (b) illustrate how the resulting composite function pair (u, μ) looks locally around the gluing point. While (c) illustrates a multipeakon u, which is obtained by patching together linear solutions. The breakpoints move along characteristics indicated by dashed curves.

(u, μ) will be a classical solution in between any two gluing points to (7.1a)-(7.1b). Figure 29c illustrates a multipeakon which consists of several linear segments glued together at various points. The gluing points travel along characteristics shown as dashed lines in Figure 29c. The figure also illustrates two characteristics that focus, wave breaking will happen at the time and place where two such characteristics meet. Figure 29a and Figure 29b illustrate how the resulting glued composite functions may look locally around the gluing point.

The next step is to determine how the characteristics evolve as time progresses. We could use the expression we found by the method of characteristics, since we will limit the time step for the numerical algorithm such that wave breaking does not occur. Thus these expressions are valid. However we proceed a little more generally, although not fully rigours. We want to derive the system governing the time evolution of the Lagrangian coordinates, similarly to what we did in Subsection 5.3, except now we want it to be valid for general conservative solutions that do not need to have an energy density which is purely absolutely continuous. To achieve this we will work with the weak formulation introduced in Definition 7.1. We will use Remark 7.2 in the proof sketch. It is a sketch as some of the manipulations performed are not motivated rigorously, and we just assume enough smoothness when needed. We will use some of the machinery developed in Subsection 3.3, even though that was developed for the integrated Hunter-Saxton equation.

Remark 7.2. Let f be a measurable function and μ a measure. A measurable function g is integrable with respect to the push forward measure $f_{\#}\mu$ if and only if the function composition $g \circ f$ is integrable with respect to μ. If this is the case we have

$$\int g d(f_{\#}\mu) = \int (g \circ f) d\mu.$$

Lemma 7.2. *Let (X, U, H) be the characteristic, Lagrangian velocity, and Lagrangian cumula-*

tive energy, respectively. These quantities satisfy the following system of ODEs

$$X_{\xi t} = U_\xi, \tag{7.8a}$$

$$U_{\xi t} = \frac{1}{2} H_\xi, \tag{7.8b}$$

$$H_{\xi t} = 0. \tag{7.8c}$$

Proof. The characteristics are defined by

$$X_t(\xi, t) = u(X(\xi, t), t) = U(\xi, t),$$

hence differentiating both sides with respect to ξ gives (7.8a). To derive (7.8b) we consider (7.2) and apply the change of variables $x = X(\xi, t)$ where t is kept fixed and the new independent variable is ξ. Thus $\frac{dx}{d\xi} = X_\xi(\xi, t)$. For a fixed t, the change of variables $x = X(\xi, t)$, must be performed on the set $\{\xi : X_\xi(\xi, t) > 0\}$, however we observe that if (7.8a)-(7.8c) holds then

$$\frac{d}{dt}(X_\xi H_\xi - U_\xi^2) = 0.$$

Hence if the initial data $Y_0 = (X_0, U_0, H_0)$ satisfies (is in $\mathcal{F}$ as defined in Subsection 3.3)

$$X_{0,\xi} H_{0,\xi} = U_{0,\xi}^2,$$

this relation will hold at all future times. If this is the case, then if $X_\xi = 0$, we have that $U_\xi = 0$. Therefore U_ξ is zero almost everywhere on the complement of $\{\xi : X_\xi(\xi, t) > 0\}$, so we can integrate over $\mathbb{R}$ when we change variables in u. This is provided we assume we have a smooth characteristic such that $X^{-1}(\mathbb{R}) = \mathbb{R}$. Take a test function $\phi \in C_0^\infty(\mathbb{R} \times (0, \infty))$, which is not supported at $t = 0$, then

$$\begin{aligned}
0 &= \int_0^\infty \int_{\mathbb{R}} u\phi_{xt}\, dx\, dt \\
&= \int_0^\infty \int_{X^{-1}(\mathbb{R})} (u\phi_{xt} \circ X) X_\xi d\xi\, dt \\
&= \int_0^\infty \int_{\mathbb{R}} u \circ X \left(\frac{d}{dt}(\phi_x \circ X) - \phi_{xx} \circ X X_t \right) X_\xi d\xi\, dt \\
&= -\int_0^\infty \int_{\mathbb{R}} \frac{d}{dt}(X_\xi u \circ X)\phi_x \circ X d\xi\, dt - \int_0^\infty \int_{\mathbb{R}} (u \circ X)(\phi_{xx} \circ X) X_t X_\xi d\xi\, dt \\
&= -\int_0^\infty \int_{\mathbb{R}} \frac{d}{dt}(X_\xi U)\phi_x \circ X d\xi\, dt + \int_0^\infty \int_{\mathbb{R}} (U^2)_\xi \phi_x \circ X d\xi\, dt\,.
\end{aligned}$$

Here we integrated the first term by parts in time and the last term by parts with respect to ξ, where we exploited that $\phi_x(X(\xi, t), t)_\xi = \phi_{xx} \circ X X_\xi$. We also used $X_t = U$. We treat the first term separately, where we expand by applying the product rule

$$\begin{aligned}
&-\int_0^\infty \int_{\mathbb{R}} \frac{d}{dt}(X_\xi U)\phi_x \circ X d\xi\, dt \\
&\quad = -\int_0^\infty \int_{\mathbb{R}} (X_{\xi t} U + X_\xi U_t)\phi_x \circ X d\xi\, dt \\
&\quad = -\int_0^\infty \int_{\mathbb{R}} U_\xi U \phi_x \circ X d\xi\, dt - \int_0^\infty \int_{\mathbb{R}} X_\xi U_t \phi_x \circ X d\xi\, dt \\
&\quad = -\int_0^\infty \int_{\mathbb{R}} (\frac{U^2}{2})_\xi \phi_x \circ X d\xi\, dt + \int_0^\infty \int_{\mathbb{R}} U_{\xi t} \phi \circ X d\xi\, dt\,.
\end{aligned}$$

Here we used that $X_{\xi t} = U_\xi$. Next we consider the second term in the weak formulation (7.2),

$$\begin{aligned}
\int_0^\infty \int_{\mathbb{R}} \frac{1}{2} u^2 \phi_{xx}\, dx\, dt &= \int_0^\infty \int_{\mathbb{R}} \frac{1}{2} U^2 (\phi_{xx} \circ X) X_\xi d\xi\, dt \\
&= -\int_0^\infty \int_{\mathbb{R}} (\frac{1}{2} U^2)_\xi \phi_x \circ X d\xi\, dt\,.
\end{aligned}$$

Finally we consider the third term in (7.2). Here we will exploit that $\mu = X_{\#}(H_\xi d\xi)$ as observed in Subsection 3.3, and Remark 7.2 to write

$$-\frac{1}{2}\int_0^\infty \int_{\mathbb{R}} \phi d\mu(t)\, dt = -\frac{1}{2}\int_0^\infty \int_{\mathbb{R}} (\phi \circ X) H_\xi d\xi\, dt\,.$$

Adding these contributions together yield

$$\begin{aligned} 0 &= \int_0^\infty \int_{\mathbb{R}} \left(u\phi_{xt} + \frac{1}{2}u^2\phi_{xx} \right) - \frac{1}{2}\int_0^\infty \int_{\mathbb{R}} \phi d\mu(t) dt \\ &= \int_0^\infty \int_{\mathbb{R}} \left[U_{t\xi} - \frac{1}{2}H_\xi \right] (\phi \circ X) d\xi\, dt\,. \end{aligned}$$

For this to vanish identically for all test functions $\phi \in C_0^\infty(\mathbb{R} \times (0,\infty))$ it must be the case that the bracket $[U_{t\xi} - \frac{1}{2}H_\xi]$ vanishes, leading to (7.8b).
To derive (7.8c) we use the weak formulation of the conservation law, (7.3). Again we use $\mu = X_{\#}(H_\xi d\xi)$ thus

$$\begin{aligned} 0 &= \int_0^\infty \int_{\mathbb{R}} \left(\phi_t + u\phi_x \right) d\mu(t)\, dt \\ &= \int_0^\infty \int_{X^{-1}(\mathbb{R})} \left((\phi_t + u\phi_x) \circ X \cdot H_\xi(\xi) \right) d\xi\, dt \\ &= \int_0^\infty \int_{\mathbb{R}} H_\xi(\xi) \frac{d}{dt}(\phi \circ X) d\xi\, dt \\ &= -\int_0^\infty \int_{\mathbb{R}} H_{\xi t}(\xi)(\phi \circ X) d\xi\, dt\,. \end{aligned}$$

If this is to hold for all test functions $\phi \in C_0^\infty(\mathbb{R} \times (0,\infty))$, we must have $H_{\xi t} = 0$. Thus we have formally derived the Lagrangian system. □

Lemma 7.3. *Solutions to the ODE system* (7.8a)-(7.8c) *with initial data* (X_0, U_0, H_0) *are generally given by*

$$\begin{aligned} X(\xi,t) &= X_0(\xi) + tU_0(\xi) + \frac{t^2}{4}H_0(\xi) + \frac{1}{2}\int_0^t \int_0^s \int_0^z K(\eta) d\eta dz ds, \\ &\quad + \int_0^t \int_0^s G(z) dz ds + \int_0^t J(s) ds \\ U(\xi,t) &= U_0(\xi) + \frac{t}{2}H_0(\xi) + \frac{1}{2}\int_0^t \int_0^s K(z) dz ds + \int_0^t G(s) ds, \\ H(\xi,t) &= \int_0^t K(s) ds + H_0(\xi), \end{aligned}$$

where G, K, J *are functions introduced when integrating with respect to* ξ*. In the particular case* $G(\cdot) = K(\cdot) = J(\cdot) = 0$*, we get*

$$X(\xi,t) = X(\xi,0) + tU(\xi,0) + \frac{t^2}{4}H(\xi,0), \tag{7.9a}$$

$$U(\xi,t) = U(\xi,0) + \frac{t}{2}H(\xi,0), \tag{7.9b}$$

$$H(\xi,t) = H(\xi,0). \tag{7.9c}$$

Proof. Integrate (7.8c) with respect to ξ, this leads to an integration constant independent of ξ, i.e., $H_t = K(t)$, we can then integrate from 0 to t, yielding

$$H(\xi,t) = \int_0^t K(s) ds + H_0(\xi).$$

Then using (7.8b) and integrating both sides with respect to ξ we obtain

$$U_t(\xi,t) = \frac{1}{2}H(\xi,t) + G(t),$$

where again $G(t)$ is a new function introduced by integrating with respect to ξ. Yet another integration with respect to time from $t = 0$ to t leads to

$$U(\xi,t) = U_0(\xi) + \frac{t}{2}H_0(\xi) + \frac{1}{2}\int_0^t \int_0^s K(z)dzds + \int_0^t G(s)ds.$$

Finally integrating (7.8a) with respect to both ξ and t we obtain the following solutions for the characteristics

$$\begin{aligned} X(\xi,t) = X_0(\xi) + tU_0(\xi) + \frac{t^2}{4}H_0(\xi) + \frac{1}{2}\int_0^t \int_0^s \int_0^z K(\eta)d\eta dzds \\ + \int_0^t \int_0^s G(z)dz + \int_0^t J(s)ds. \end{aligned}$$

□

In Subsection 5.3 we considered a conservative cuspon, then we had $K(t) = k$, and $G(t) = J(t) = 0$. We observed that the gluing point did not move along a single characteristic, but instead metaphorically speaking jumped from characteristic to characteristic. We have some freedom to choose the integration functions. Based on our experience with the cuspon analysis we want to choose $K(\cdot) = G(\cdot) = J(\cdot) = 0$. The movement of the breakpoints, i.e., gluing points as time progresses are then described by (7.9a), and the solution along the characteristics is described by (7.9b)-(7.9c). There are several reasons for this particular choice. Firstly choosing any of the integration functions nonzero, changes the natural interpretation of the Lagrangian quantities, for instance setting $K(\cdot) \neq 0$, we loose the natural interpretation of $H(\xi,t)$ as the cumulative energy up to characteristic $X(\xi,t)$ at time t. The same holds for the other quantities, for example $G(\cdot) \neq 0$, then $U(\xi,t)$ is no longer the natural velocity of the characteristic, but instead an altered velocity in some sense, and similarly choosing $J(\cdot) \neq 0$ for the characteristics. Moreover as we will observe when we use a moving mesh, with the choice $K(\cdot) = G(\cdot) = J(\cdot) = 0$ the cusp singularity will be located at the same grid point after each time step evolution, if we force the mesh to move at the traveling wave speed s. This is a consequence of the fact that choosing $K(\cdot) = 0$, the energy between characteristics is conserved. Setting $K(\cdot) \neq 0$, induces a time varying energy between characteristics.

7.2 The modified algorithm for a fixed mesh

The algorithm presented here, is based on the one introduced in [GNS21], but there are some differences. We no longer use $-\infty$ as reference point for the cumulative energy F, but instead choose the reference point according to the particular Cauchy problem. This yields more flexibility when we choose the computational domain, which we will take advantage of for traveling waves, where we use a moving mesh. Moreover we no longer need to assume that the initial wave profile u_0, is constant outside some finite interval. In this subsection we consider the case where we use a mesh with fixed grid points as illustrated in Figure 30a. Numerical approximations will consist of pairs $(u_{\Delta x}, F_{\Delta x})$ that are continuous piecewise linear. Where the cumulative energy is given by

$$F(x,t) = \begin{cases} \int_{y(t)}^{x} d\mu(t) & \text{for } y(t) \leq x \\ \int_{x}^{y(t)} d\mu(t) & \text{for } x < y(t) \end{cases}$$

for some chosen reference point $y(t)$. In the particular case of a fixed mesh as described in this subsection it is natural to pick a fixed reference point, such that $y(t) = y$ is independent of time. As μ represents the energy density plus a projection error, we require

$$d\mu(t) \geq (u_x^2 + \rho^2)(t)\, dx,$$

thus μ must be nonnegative. Here $u_x^2\,dx$ is the usual energy density, while $\rho^2\,dx$ represents an error density, introduced by applying the projection operator $P_{\Delta x}$ after evolving exactly along the characteristics. μ will be piecewise constant, i.e., a step function for the numerical approximation so the associated cumulative distribution function is piecewise linear. Let $T_t : \mathcal{D} \to \mathcal{D}$ be the conservative solution operator for the two-component Hunter-Saxton system, as discussed in [Nor16a]. This operator resembles the one introduced in Subsection 3.3. For continuous piecewise linear initial data this operator takes a particular simple form provided no wave breaking occurs. As we saw in Lemma 7.1 breakpoints travel along characteristics and thus the j^{th} breakpoint travels along the curve

$$x_j(t) = x_j(0) + u(x_j(0), 0)t + \frac{t^2}{4}F(x_j(0), 0).$$

The solution (u, F) along this curve is given by

$$\begin{aligned} u(x_j(t), t) &= u(x_j(0), 0) + \frac{t}{2}F(x_j(0), 0), \\ F(x_j(t), t) &= F(x_j(t), t). \end{aligned} \tag{7.10}$$

The solution operator T_t is then implicitly given through the relations (7.10). We project the initial data using the projection operator introduced in Section 6, we recall it below for convenience.

Recall 7.1. Let $P_{\Delta x}$ be the operator defined so that $(\hat{u}, \hat{F}) = P_{\Delta x}(u, F)$ is given by

$$\begin{aligned} \hat{u}(x_k) &= u(x_k), \\ \hat{F}(x_k) &= F(x_k), \end{aligned}$$

where we employ linear interpolation between gridpoints.

After we have projected the initial data, we evolve the solution along the characteristic a time step Δt exactly. After evolving we again project to ensure that the numerical approximation is continuous piecewise linear. This procedure is repeated until the desired final time $t = T$ is reached. Provided Δt is such that wave breaking does not occur, the numerical scheme is given by

$$\begin{aligned} (U^0, F^0) &= P_{\Delta x}(u_0, F_0), \\ (U^{n+1}, F^{n+1}) &= P_{\Delta x} T_{\Delta t}(U^n, F^n). \end{aligned}$$

We will interpret the numerical solution as a function. We define the numerical solution similarly to what is done in [GNS21].

Definition 7.2 (Numerical sol.)**.** The numerical solution $(u_{\Delta x}, F_{\Delta x})$ at a point $(x, t) \in \mathbb{R} \times [0, T]$, where T$> 0$ is some finite time, is defined by

$$(u_{\Delta x}, F_{\Delta x})(x, t) = P_{\Delta x} T_\tau (U^n, F^n)(x),$$

for $t = \tau + t^n$ with $\tau \in [0, \Delta t]$.

The definition states that the numerical solution is given by following the solution along the vertical lines $x = x_j$, from one time step to the next, and then linearly interpolate between these lines.

7.2.1 A CFL-type condition

We want to evolve our approximation a time step Δt forward in time, by considering how the gluing points move exactly and then interpolate linearly in between. In order to achieve this

we need to ensure that characteristics do not meet during the time step Δt, so we derive a CFL-condition in order to prevent wave breaking from occurring just as done in Section 6. If we manage this, then for each time step the numerical solution, $(u_{\Delta x}, F_{\Delta x})$ will be continuous, and piecewise linear. Assume we have a mesh with fixed grid points as shown in Figure 30a, then we can proceed with a similar analysis of characteristics as done in Section 6. Generally for continuous, piecewise linear initial data (u_0, F_0), wave breaking occurs when two characteristics emanating from neighbouring grid points focus, i.e, two breakpoints coincide,

$$x_k(t) = x_{k+1}(t),$$

for some $k \in \mathbb{Z}$ and $t > 0$. The farthest two characteristics can approach each other, is if the characteristic emanating from x_{k+1} moves entirely to the left, and the one from x_k moves entirely to the right. Thus, similarly to the intuition developed for Godunov's method in Subsection 6.1, we must restrict

$$x_{k+1}(t) - x_k(t) > \frac{1}{2}\Delta x, \tag{7.11}$$

for all $t \in [0, \Delta t]$. This is the least restrictive bound for $t \in [0, \Delta t]$ to prevent wave breaking. In particular using (7.9a) and proceeding as in Section 6 this leads to

$$\begin{aligned}
x_{k+1}(t) - x_k(t) &= \Delta x + (u(x_{k+1}, 0) - u(x_k, 0))t + \frac{t^2}{4}(F(x_{k+1}, 0) - F(x_k, 0)) \\
&\geq \Delta x + t \int_{x_k}^{x_{k+1}} u_{0,x}(y)dy \\
&\geq \Delta x - \Delta t\big(\int_{x_k}^{x_{k+1}} dy\big)^{\frac{1}{2}} \big(\int_{x_k}^{x_{k+1}} u_{0,x}^2(y)dy\big)^{\frac{1}{2}} \\
&\geq \Delta x - \Delta t\sqrt{\Delta x}(F(x_{k+1}, 0) - F(x_k, 0)) \\
&\geq \Delta x - \Delta t\sqrt{\Delta x}F_{[a,b]}(0).
\end{aligned}$$

We want this to be larger than $\frac{1}{2}\Delta x$ for all $t \in [0, \Delta t]$ thus in particular we require

$$\Delta t < \frac{\sqrt{\Delta x}}{2F_{[a,b]}(0)},$$

where $F_{[a,b]} = F_{[a,b]}(0) = \mu_0((a, b))$ is the initial total cumulative energy inside the computational domain. However we want to have better control of the movement of the characteristics, since with (7.11), characteristics can move past several grid cells during a single time step Δt. In particular we instead require

$$x_{k-1} + \frac{1}{2}\Delta x \leq X_k(\Delta t) \leq x_{k+1} - \frac{1}{2}\Delta x, \tag{7.12}$$

such that characteristics do not cross the cell interfaces after the end of a time step. This restriction is exemplified in Figure 30b.

Lemma 7.4 (CFL-cond.)**.** *Assume Δt satisfies the bound*

$$\Delta t < \frac{\Delta x}{2(\|u_0\|_{L^\infty([a,b])} + \frac{T}{4}F_{[a,b]})} \tag{7.13}$$

Then wave breaking will not occur during a time increment of $\tau \in [0, \Delta t]$, and characteristics do not move further than half a grid cell away from the grid cell they emanated from during this time increment.

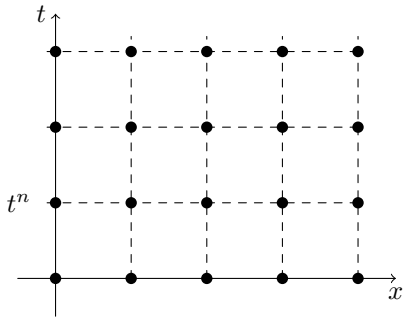

(a) A mesh with fixed grid points.

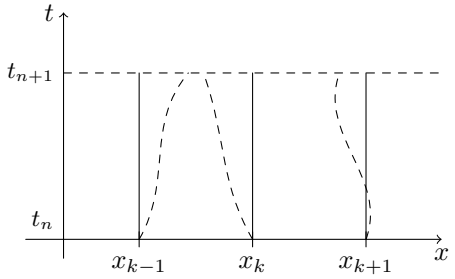

(b) An illustration of characteristics limited by (7.12)

Figure 30: Figure (a) illustrates the fixed mesh, where the dark dots label the grid points. (b) illustrates the time step restriction (7.12), such that characteristics emanating from a grid point must stay $\frac{1}{2}\Delta x$ apart from other grid points during a single time step Δt.

Proof. The proof relies on a similar argument as in Subsection 6.2.1. In particular we use (7.12) and estimate $|X_k(\Delta t) - x_k|$ from above, and require that to be less than $\frac{\Delta x}{2}$. Using (7.9a) we get

$$\begin{aligned} |X_k(\Delta t) - x_k| &= |u(x_k, 0)\Delta t + \frac{\Delta t^2}{4} F(x_k, 0)| \\ &\leq \Delta t(\|u_0\|_{L^\infty([a,b])} + \frac{T}{4} F_{[a,b]}) < \frac{1}{2}\Delta x. \end{aligned}$$

This in particular leads to (7.13). □

7.2.2 Derivation of Godunov-type expression

Now we want to derive the Godunov-expression for our modified numerical algorithm. The idea is the same as in Subsection 6.2.2. Fix a grid point x_k^n. We employ the bound (7.13) in Lemma 7.4, so we only need to consider adjacent grid points to x_k^n, when we want to updated the numerical approximation (u_k^{n+1}, F_k^{n+1}).

First consider the situation where $X_k^n(\Delta t) > x_k$, so the forward characteristic moves to the right. Inserting (7.9a) we get

$$x_k < x_k + u(x_k, t_n)\Delta t + \frac{\Delta t^2}{4} F(x_k, t_n),$$

where as before $u(x_k, t_n) = u_k^n$ and $F(x_k, t_n) = F_k^n$. Hence rearranging and dividing by Δt on both sides this reduces to

$$u_k^n + \frac{\Delta t}{4} F_k^n > 0.$$

When this condition holds information at grid point x_k travels to the right, so we update (u_k^{n+1}, F_k^{n+1}) using information from grid point x_{k-1} and x_k at time $t = t_n$. Similar to what we did in Section 6, we use linear interpolation after we evolve the solution exactly along the characteristics, leading to

$$\begin{aligned} u_k^{n+1} &= u_{k-1}^n(\Delta t) + s(u_k^n(\Delta t) - u_{k-1}^n(\Delta t)), \\ F_k^{n+1} &= F_{k-1}^n(\Delta t) + s(F_k^n(\Delta t) - F_{k-1}^n(\Delta t)). \end{aligned}$$

We can write the line $x = x_k$ using linear interpolation based on the characteristics, leading to

$$x_k = X_{k-1}^n(\Delta t) + s(X_k^n(\Delta t) - X_{k-1}^n(\Delta t)).$$

We will use this latter equation to express the scalar s in terms of known quantities, and then insert this into the expression for u_k^{n+1} and F_k^{n+1}. We find

$$\begin{aligned} s &= \frac{x_k - X_{k-1}^n(\Delta t)}{X_k^n(\Delta t) - X_{k-1}^n(\Delta t)} \\ &= \frac{\Delta x - u_{k-1}^n \Delta t - \frac{1}{4} F_{k-1}^n \Delta t^2}{\Delta x + (u_k^n - u_{k-1}^n)\Delta t + \frac{1}{4}(F_k^n - F_{k-1}^n)\Delta t^2}. \end{aligned}$$

The numerical solution in this case is then updated by

$$\begin{aligned} u_k^{n+1} &= u_{k-1}^n + \frac{\Delta t}{2} F_{k-1}^n + s\bigg(u_k^n - u_{k-1}^n + \frac{\Delta t}{2}(F_k^n - F_{k-1}^n)\bigg), \\ F_k^{n+1} &= F_{k-1}^n + s\bigg(F_k^n + F_{k-1}^n\bigg), \end{aligned}$$

where we have used that the cumulative energy is conserved along characteristics with our choice of integration functions. That is, picking $K(\cdot) = 0$, causes $H_t = 0$, so the energy will be conserved along characteristics. This was discussed in Subsection 7.1.

Next we consider the case where the characteristic travels to the left instead, and we must update (u_k^{n+1}, F_k^{n+1}) using information from the grid points x_k^n and x_{k+1}^n instead. Here we use the notation x_k^n to denote the k^{th} grid point at time $t = t_n$ as before. In particular $X_k^n(\Delta t) < x_k$, leading to

$$u_k^n + \frac{\Delta t}{4} F_k^n < 0.$$

Therefore using linear interpolation after evolving the solution exactly along characteristics gives

$$\begin{aligned} u_k^{n+1} &= u_{k+1}^n(\Delta t) + s(u_k^n(\Delta t) - u_{k+1}^n(\Delta t)), \\ F_k^{n+1} &= F_{k+1}^n(\Delta t) + s(F_k^n(\Delta t) - F_{k+1}^n(\Delta t)). \end{aligned}$$

The grid point x_k can again be written in terms of the characteristics emanating from grid points x_k and x_{k+1} as follows

$$x_k = X_{k+1}^n(\Delta t) + s(X_k^n(\Delta t) - X_{k+1}^n(\Delta t)).$$

Solving for s yields

$$\begin{aligned} s &= \frac{x_k - X_{k+1}^n(\Delta t)}{X_k^n(\Delta t) - X_{k+1}^n(\Delta t)} \\ &= \frac{\Delta x + u_{k+1}^n \Delta t + \frac{\Delta t^2}{4} F_{k+1}^n}{\Delta x + (u_{k+1}^n - u_k^n)\Delta t + \frac{\Delta t^2}{4}(F_{k+1}^n - F_k^n)}. \end{aligned}$$

The numerical approximation is updated using

$$\begin{aligned} u_k^{n+1} &= u_{k+1}^n + \frac{\Delta t}{2} F_{k+1}^n - s\bigg(u_k^{n+1} - u_k^n + \frac{\Delta t}{2}(F_{k+1}^n - F_k^n)\bigg), \\ F_k^{n+1} &= F_{k+1}^n - s\bigg(F_{k+1}^n - F_k^n\bigg). \end{aligned}$$

The resulting algorithm, is summarized in the below pseudocode. The case of $X_k^n(\Delta t) = x_k$ has not been considered, but in this case the characteristic ends up at the same position it emanated from. Hence we update the numerical approximation in this grid point by setting $F_k^n = F_k^{n+1}$ and $u_k^{n+1} = u_k^n$.

MODIFIED GODUNOV-TYPE ALGORITHM FIXED MESH

Discretize in space and time
Initialize $(U^0, F^0) = P_{\Delta x}(u_0, F_0)$
for $t = \Delta t, 2\Delta t \dots n\Delta t \dots T$
    for $k \in \mathbb{Z}$
        if $u_k^n + \frac{1}{4}F_k^n \Delta t > 0$
            $s = \frac{\Delta x - u_{k-1}^n \Delta t - \frac{1}{4}F_{k-1}^n \Delta t^2}{\Delta x + (u_k^n - u_{k-1}^n)\Delta t + \frac{1}{4}(F_k^n - F_{k-1}^n)\Delta t^2}$
            $u_k^{n+1} = u_{k-1}^n + \frac{1}{2}F_{k-1}^n \Delta t + s\big(u_k^n - u_{k-1}^n + \frac{1}{2}(F_k^n - F_{k-1}^n)\Delta t\big)$
            $F_k^{n+1} = F_{k-1}^n + s\big(F_k^n + F_{k-1}^n\big)$
        if $u_k^n + \frac{1}{4}F_k^n \Delta t < 0$
            $s = \frac{\Delta x + u_{k+1}^n \Delta t + \frac{1}{4}F_{k+1}^n \Delta t^2}{\Delta x + (u_{k+1}^n - u_k^n)\Delta t + \frac{1}{4}(F_{k+1}^n - F_k^n)\Delta t^2}$
            $u_k^{n+1} = u_{k+1}^n + \frac{1}{2}F_{k+1}^n \Delta t - s\big(u_{k+1}^n - u_k^n + \frac{1}{2}(F_{k+1}^n - F_k^n)\Delta t\big)$
            $F_k^{n+1} = F_{k+1}^n - s\big(F_{k+1}^n - F_k^n\big)$

7.3 The case of a moving mesh

To simulate conservative traveling waves for the Hunter-Saxton equation we will choose a moving mesh as illustrated in Figure 31a. We will also use a time-varying reference point. In particular as reference point for the cumulative energy distribution we use the line along which the cusp singularity moves. That is

$$F(x,t) = \begin{cases} \int_{\sigma_0+st}^{x} d\mu(t) & \text{for } \sigma_0 + st \le x \\ \int_{x}^{\sigma_0+st} d\mu(t) & \text{for } x < \sigma_0 + st \end{cases}.$$

Assume the cusp singularity starts at $x = \sigma_0$, and that we have a grid point located initially at σ_0. Then using (7.9a) we observe that a characteristic emanating from this grid point satisfies

$$\begin{aligned} x(t) = X(\sigma_0, t) &= \sigma_0 + u(\sigma_0, 0)t + \frac{1}{4}F(\sigma_0, 0)t^2 \\ &= \sigma_0 + st. \end{aligned}$$

Consequently by letting the grid points move with speed s, the cusp singularity is always located at the same particular grid point, the one starting at σ_0. This is a consequence of our choice of integration functions $G = K = J = 0$, with another choice, the characteristic emanating from the grid point located initially at σ_0 would not move along the same line as the cusp singularity. The movement of this grid point is shown by a solid back line in Figure 31a. With a moving mesh, we have for all $k \in \mathbb{Z}$ that the position of the k^{th} grid point at time $t_{n+1} = (n+1)\Delta t$ is given by

$$x_k^{n+1} = x_k^n + s\Delta t = x_k + (n+1)s\Delta t,$$

where x_k is the initial position of the grid point. The expression for the solution along characteristics is the same as before, but the CFL-condition and the Gudonov-type expression change a little. This is to account for the fact that the grid points now move a distance $s\Delta t$ during a single time step.

7.3.1 CFL-condition moving mesh

Since the mesh moves a distance $s\Delta t$ during a time step we have to modify the imposed bound (7.12). It now instead takes the form

$$x_{k-1} + \frac{1}{2}\Delta x + s\Delta t \le X_k(\Delta t) \le x_{k+1} - \frac{1}{2}\Delta x + s\Delta t.$$

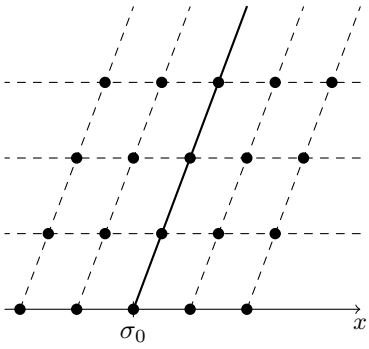

(a) A mesh where the grid points move a distance $s\Delta t$ for each time step, with $s > 0$.

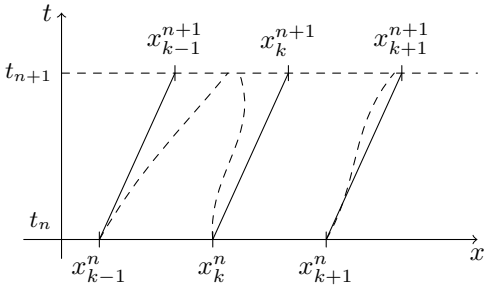

(b) An illustration of the time step limitation (7.14).

Figure 31: Figure (a) illustrates the moving mesh, the solid black line indicates the reference point of the cumulative energy. (b) illustrates the restriction the new CFL-condition puts on the characteristics.

Assuming a uniform discretization in both space and time and using (7.9a) we can write this as

$$-\frac{\Delta x}{2} + s\Delta t \leq u(x_k, 0)\Delta t + \frac{1}{4}F(x_k, 0)\Delta t^2 \leq \frac{\Delta x}{2} + s\Delta t.$$

Rearranging and estimating from above we find

$$\left|\Delta t\left(u(x_k, 0) + \frac{1}{4}F(x_k, 0)\Delta t - s\right)\right| \leq \Delta t\left(\|u_0\|_{L^\infty([a,b])} + \frac{T}{4}F_{[a,b]} + |s|\right) \leq \frac{1}{2}\Delta x,$$

hence we require

$$\Delta t \leq \frac{1}{2}\frac{\Delta x}{(\|u_0\|_{L^\infty([a,b])} + \frac{T}{4}F_{[a,b]} + |s|)}. \tag{7.14}$$

This will be the CFL-condition we use in order to prevent characteristics moving more than half a grid cell, $\frac{1}{2}\Delta x$, away from the grid points they emanated from during a single time step. This is illustrated in Figure 31b.

7.3.2 Godunov-type expression and fictitious boundaries

There are a couple of changes when we derive the Godunov-type expression. In particular the linearization constant which we now label by z in order to avoid confusion with the wave speed s changes, and the if-statements used in the pseudocode in the case of a fixed mesh change. The condition $X_k^n(\Delta t) > x_k^{n+1}$ now reads

$$X_k^n(\Delta t) = x_k^n + u_k^n\Delta t + \frac{1}{4}F_k^n\Delta t^2 > x_k^n + s\Delta t,$$

which simplifies to

$$(u_k^n - s) + \frac{1}{4}F_k^n\Delta t > 0,$$

for characteristics moving to the right, in which case we use the characteristics emanating from grid points x_{k-1}^n and x_k^n to update (u_k^{n+1}, F_k^{n+1}). The case of the characteristic moving to the left is analogous, but with the strict inequality reversed. Assume the characteristic emanating from x_k^n moves to the right, then the linearization constant is determined by

$$x_k^{n+1} = x_k^n + s\Delta t = X_{k-1}^n(\Delta t) + z(X_k^n(\Delta t) - X_{k-1}^n(\Delta t)).$$

Solving in terms of z we find

$$z = \frac{s\Delta t + x_k^n - \left(x_{k-1}^n + u_{k-1}^n \Delta t + \frac{1}{4} F_{k-1}^n \Delta t^2 \right)}{\Delta x + (u_k^n - u_{k-1}^n)\Delta t + \frac{1}{4}(F_k^n - F_{k-1}^n)\Delta t^2}$$
$$= \frac{\Delta x + (s - u_{k-1}^n)\Delta t - \frac{1}{4} F_{k-1}^n \Delta t^2}{\Delta x + (u_k^n - u_{k-1}^n)\Delta t + \frac{1}{4}(F_k^n - F_{k-1}^n)\Delta t^2}.$$

Performing an analogous computation in the case the characteristic emanating from x_k^n instead move to the left we find

$$z = \frac{\Delta x + (u_{k+1}^n - s)\Delta t + \frac{1}{4} F_{k+1}^n \Delta t^2}{\Delta x + (u_{k+1}^n - u_k^n)\Delta t + \frac{1}{4}(F_{k+1}^n - F_k^n)\Delta t^2}.$$

The rest of the Godunov-type expression is unaffected by the change to a moving mesh, and therefore we can use the same expression for (u_k^{n+1}, F_k^{n+1}) as in the pseudocode for the case of a fixed mesh. There is still one thing we need to take into account, and that is the grid cells located at the very ends of our computational domain. Denote the corresponding grid points by x_1 and x_N for the point to the very left and very right, respectively. If

$$(u_1^n - s) + \frac{1}{4} F_1^n \Delta t > 0,$$

then the characteristic emanating from x_1 moves to the right. Hence we must update the numerical solution (u_1^{n+1}, F_1^{n+1}) using linear interpolation based on information from grid points x_0^n and x_1^n, but x_0^n does not exist. To overcome this we simply ignore the solution at x_1^n when this occurs. Similarly when the characteristic from x_N moves to the left, we must update the solution (u_N^{n+1}, F_N^{n+1}) using x_N^n and x_{N+1}^n, but x_{N+1}^n does not exist. Hence to overcome these fictitious boundaries, which are a consequence of the fact that we must use a finite/bounded numerical domain, we just ignore the very left and very right grid cell after each time step evolution. Consequently the computational domain becomes smaller and smaller. Alternatively one could keep the very left grid cell until

$$(u_L^n - s) + \frac{1}{4} F_L^n \Delta t > 0,$$

first arises, where (u_L^n, F_L^n) denotes the numerical solution at the very left grid cell at time t_n. If this occurs then we remove the very left grid cell and continue. Similarly we can keep the very right grid cell until

$$(u_R^n - s) + \frac{1}{4} F_R^n \Delta t < 0,$$

first occurs, where (u_R^n, F_R^n) denotes the numerical solution at the very right grid cell at time t_n. And when this happens we remove the very right grid cell and continue. For simplicity we just remove the very left and the very right grid cell for each time step, such that we remove 2 grid cells for every time step increment. The resulting domain where we compute the solution may then looks something like that illustrated in Figure 32. We must keep the line where the cusp singularity moves inside the shaded region at all times, therefore we must start with an initial computational domain which is much larger than the remaining domain at $t = T$. All these aspects are taken into account in the next pseudocode.

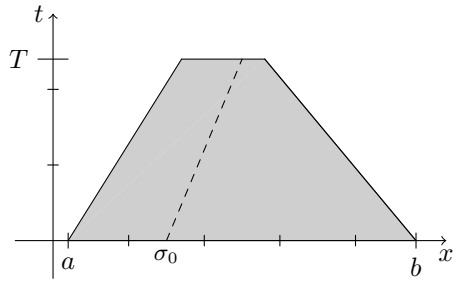

Figure 32: The figure shows the initial computational domain $[a, b]$ and how it shrinks as we progress time. The shaded region, is where we compute the numerical solution, $(u_{\Delta x}, F_{\Delta x})$, and we choose this domain such that it always contains the cusp singularity.

Modified Godunov-Type algorithm moving mesh

Initialize a computational domain $[a, b]$
Initialize $(U^0, F^0) = P_{\Delta x}(u_0, F_0)$
$n = 0$
while $n\Delta t \leq T$
    for $k \in \mathbb{Z}$
        if $(u_k^n - s) + \frac{1}{4}F_k^n \Delta t > 0$
            $z = \frac{\Delta x + (s - u_{k-1}^n)\Delta t - \frac{1}{4}F_{k-1}^n \Delta t^2}{\Delta x + (u_k^n - u_{k-1}^n)\Delta t + \frac{1}{4}(F_{k+1}^n - F_k^n)\Delta t^2}$
            $u_k^{n+1} = u_{k-1}^n + \frac{1}{2}F_{k-1}^n \Delta t + z(u_k^n - u_{k-1}^n + \frac{1}{2}(F_k^n - F_{k-1}^n)\Delta t)$
            $F_k^{n+1} = F_{k-1}^n + z(F_k^n + F_{k-1}^n)$
        if $(u_k^n - s) + \frac{1}{4}F_k^n \Delta t < 0$
            $z = \frac{\Delta x + (u_{k+1}^n - s)\Delta t + \frac{1}{4}F_{k+1}^n \Delta t^2}{\Delta x + (u_{k+1}^n - u_k^n)\Delta t + \frac{1}{4}(F_{k+1}^n - F_k^n)\Delta t^2}$
            $u_k^{n+1} = u_{k+1}^n + \frac{1}{2}F_{k+1}^n \Delta t - z(u_{k+1}^n - u_k^n + \frac{1}{2}(F_{k+1}^n - F_k^n)\Delta t)$
            $F_k^{n+1} = F_{k+1}^n - z(F_{k+1}^n - F_k^n)$
    Remove the very left and very right grid point at this time step
    Translate the grid points a distance $s\Delta t$
    $n = n + 1$

7.4 Testing the algorithm

We want to apply the modified algorithm first to the familiar peakon example considered throughout the thesis, where we can use a fixed mesh and a fixed reference point for F. Then we will go on to use a moving mesh in order to approximate traveling waves.

7.4.1 Peakon-example revisited

Consider the differentiated form (7.1a)-(7.1b) of the Hunter-Saxton equation. As mentioned in Section 3 different formulations admit different explicit solutions. Therefore the analytical solution we had no longer holds. We must find the solution for this Cauchy problem with the

new formulation anew. We consider

$$\begin{aligned}(u_t + uu_x)_x &= \frac{1}{2}\mu,\\ F_t + uF_x &= 0,\\ u_0(x) &= \begin{cases} 0 & \text{for } x < 0\\ x & \text{for } 0 \le x < 1\\ 2-x & \text{for } 1 \le x \le 2\\ 0 & \text{for } 2 < x \end{cases},\\ \mu_0 &= u_{0,x}^2.\end{aligned}$$

We know the breakpoints travel along characteristics by Lemma 7.1. The characteristics and the solution along them are given by (7.9a)-(7.9c), if we make the assumption that the integration constants are zero. Therefore we only need to find the position of the breakpoints and the solution along the breakpoints at time t, and then linearly interpolate to get $u(x,t)$. For instance let $t \to x_0(t)$ and $t \to x_1(t)$ be the characteristics starting at 0 and 1, respectively. Then

$$\begin{aligned}x_0(t) &= 0,\\ x_1(t) &= 1 + t + \frac{t^2}{4}.\end{aligned}$$

The solution $u(x,t)$ for $x \in [x_0(t), x_1(t))$ is given by

$$\begin{aligned}u(x,t) &= u(x_0(t),t) + s(u(x_1(t),t) - u(x_0(t),t)) = su(x_1(t),t),\\ s &= \frac{x - x_0(t)}{x_1(t) - x_0(t)} = \frac{x}{\frac{1}{4}(t+2)^2}.\end{aligned}$$

We do similarly for all the other parts, the result is

$$\begin{aligned}u(x,t) &= \begin{cases} 0 & \text{for } x < 0\\ \frac{2x}{t+2} & \text{for } 0 \le x < 1 + t + \frac{t^2}{4}\\ \frac{2(x-t-2)}{t-2} & \text{for } 1 + t + \frac{t^2}{4} \le x \le 2 + \frac{t^2}{2}\\ t & \text{for } 2 + \frac{t^2}{2} < x \end{cases},\\ F(x,t) &= \begin{cases} 0 & \text{for } x < 0\\ \frac{4}{(t+2)^2}x & \text{for } 0 \le x < 1 + t + \frac{t^2}{4}\\ \frac{4(x-2t)}{(t-2)^2} & \text{for } 1 + t + \frac{t^2}{4} \le x \le 2 + \frac{t^2}{2}\\ 2 & \text{for } 2 + \frac{t^2}{2} < x \end{cases}.\end{aligned} \tag{7.15}$$

We observe that wave breaking occurs at $(x^*, t^*) = (4, 2)$, rather than at $(3, 2)$ as we had for the integrated formulation. Thus we expect a jump in F at $(4, 2)$. We run the numerical algorithm with a fixed mesh (grid points do not move), with $\Delta x = 10^{-2}$ and

$$\Delta t = \frac{1}{2}\frac{\Delta x}{2(\|u_0\|_\infty + \frac{1}{4}TF_{[a,b]})}.$$

Where we use $-\infty$ as reference point for the cumulative energy, since u_0 is constant for $x < 0$. We choose the computational domain such that it contains the interval $[a(t), b(t)]$, with $a(t) = 0$ and $b(t) = 2 + \frac{t^2}{2}$. The numerical approximation $(u_{\Delta x}, F_{\Delta x})$ is compared to the analytical solution (7.15) in Figure 33 and Figure 34 at various times.

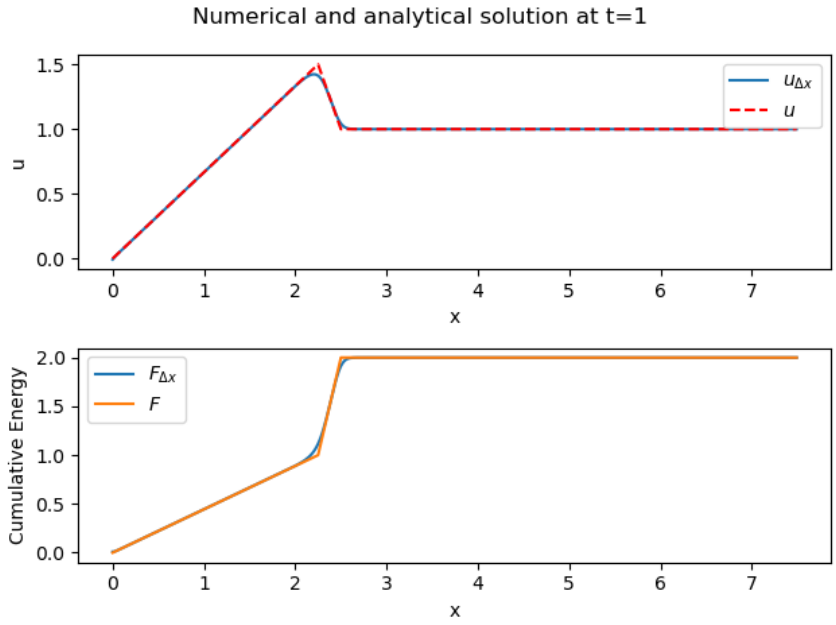

(a) Before wave breaking, $t = 1$.

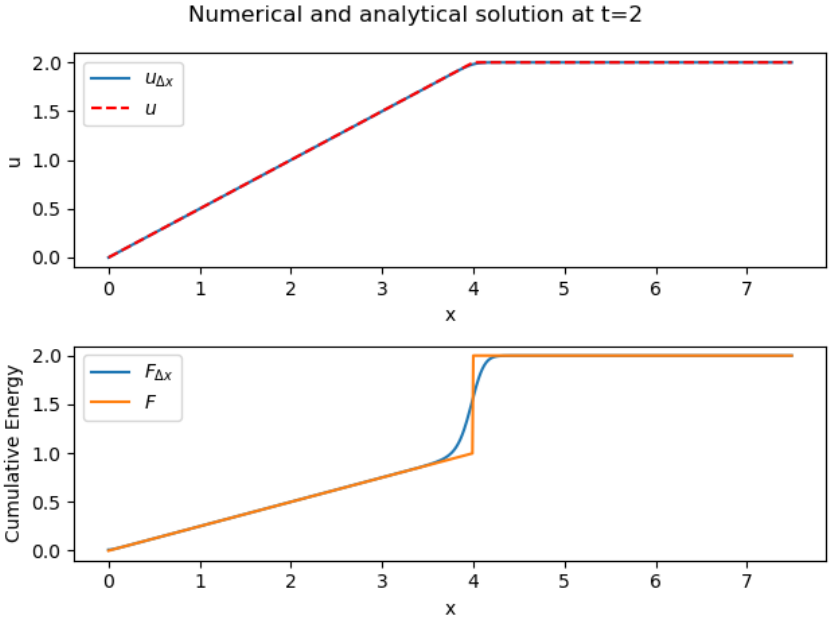

(b) At wave breaking, $t = 2$.

Figure 33: The analytical solution (u, F) in (7.15) is compared to the numerical approximation $(u_{\Delta x}, F_{\Delta x})$ before and at the moment of wave breaking in (a) and (b), respectively.

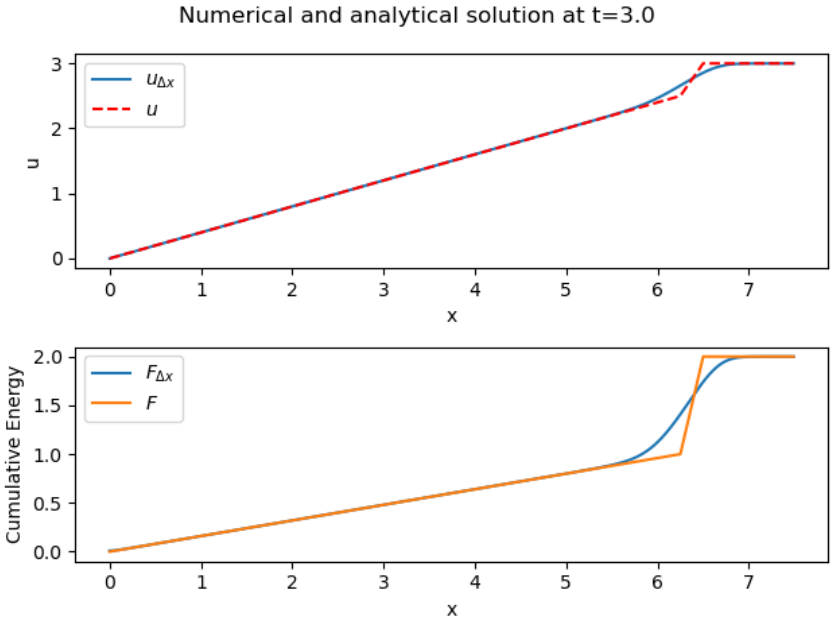

Figure 34: The analytical solution (7.15) is compared to the numerical approximation after wave breaking. In particular at $t = 3$.

7.4.2 Conservative traveling cuspons

We consider the following Cauchy problem

$$\begin{aligned}(u_t + uu_x)_x &= \frac{1}{2}u_x^2,\\ (u_x^2)_t + (uu_x^2)_x &= 0,\\ u_0(x) &= \begin{cases} s + \alpha(-x)^{\frac{2}{3}} & \text{for } x < 0 \\ s + \alpha x^{\frac{2}{3}} & \text{for } 0 \leq x \end{cases}.\end{aligned}$$

We employ the choice of mesh as described in Subsection 7.3.1 and illustrated in Figure 31a. We choose the line $x = st$ as reference point for the cumulative energy. Hence the initial cumulative energy which should be a monotonically increasing function is initialized by

$$F_0(x) = \begin{cases} -\frac{4}{3}\alpha^2|x|^{\frac{1}{3}} & \text{for } x < 0 \\ \frac{4}{3}\alpha^2 x^{\frac{1}{3}} & \text{for } x \geq 0 \end{cases}.$$

As mentioned in Subsection 7.3.2 we remove the very left and very right grid point for each time step such that the computational domain becomes smaller and smaller as time evolves. Hence for the case of $|s| = 1$ and $\alpha = -2$, with a time step $\Delta x = 6.5 \cdot 10^{-2}$, we need the initial computational domain to at least contain the interval $[-15, 15]$ to have some grid points at the final simulation time $T = \frac{1}{4}$. For $T = \frac{1}{2}$ we must choose $[-30, 30]$,$[-135, 135]$ for $T = 1$ and $[-1150, 1150]$ for $T = 2$. Choosing smaller initial computational domains than those specified will cause the resulting computational domain at $t = T$ to be empty or contain very few grid points, since we have removed either all grid points or too many of them. Δx uniquely determines the mesh as we choose Δt by

$$\Delta t = \frac{\Delta x}{2(\|u_0\|_{L^\infty[a,b]} + \frac{T}{4}F_{[a,b]} + |s|)}.$$

The numerical solution $u_{\Delta x}$ computed with the moving reference frame is compared to the analytical solution in Figure 36 in the case of $s = 1$ and $\alpha = -2$ for $T = \frac{1}{4}$, $T = \frac{1}{2}$ $T = 1$ and

$T = 2$ in Figure 36 $(a) - (d)$, respectively. If one zoom closer into the cusp singularity one will observe that there is some discrepancy even at $t = \frac{1}{4}$ between the approximation and the true solution. This difference accumulate and cause a larger and larger deviation at later times.
A comparison between the analytical cuspon solution and the numerical approximation $u_{\Delta x}$, for $a = 2$ and $s = 1$ is shown for $T = \frac{1}{4}$, $T = \frac{1}{2}$, $T = 1$ and $T = 2$ in Figure 37 $(a) - (d)$, respectively. We observe here a similar discrepancy as we observed in the case of a negative α.

7.5 Try of an explanation of discrepancy for cuspon approximations

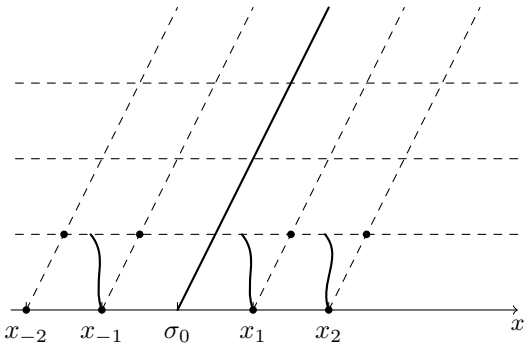

Figure 35: The moving reference frame is shown as the solid line. Here we have focused on characteristics emanating from adjacent grid points to where the cusp singularity is located. Along the solid line the true solution takes the value s. The numerical approximation along x_1 is updated using linear interpolation based on x_1 and x_2.

A plausible explanation to the discrepancy between the numerical approximation $u_{\Delta x}$ and the true cuspon u can be given in terms of the movement of the characteristics. This discussion is motivated by our considerations in Subsection 5.3, where we considered the movement of characteristics for a cuspon. In particular we observed as the cusp singularity is where the true solution u attains its largest value for $a < 0$, which is the case we will focus on here, the cusp singularity moves faster than any characteristic, so characteristics starting to the right of the cusp singularity for $s > 0$ eventually cross it after some time $T > 0$.

Using the language of numerical methods for hyperbolic conservation laws, the numerical experiments performed here indicate that our modified algorithm is not monotone. One possible definition of monotonicity is

$$u_j^n \geq u_{j+1}^n \implies u_j^{n+1} \geq u_{j+1}^{n+1},$$

for all $j \in \mathbb{Z}$. This certainly does not hold according to our numerical simulations in Figure 37 and Figure 36. Initially the largest/smallest (depending on the sign of a) value u_0 attains is s. Figure 36 (d) and Figure 37 (d) show that at $t = 2$ the largest/smallest value is no longer s. Since the method is not monotone, what initially is the point where $u_{\Delta x}$ attains its largest value, i.e., the cusp singularity, will not remain the largest point at later times $t > 0$. Actually the point where $u_{\Delta x}(\cdot, t)$ takes its largest value changes with time, and the value attained also changes with time. We can explain this behaviour by considering the movement of characteristics close to the cusp singularity, which at later times transfer to the new point where $u_{\Delta x}$ attains its maximum.

Figure 35 shows the movement of the nearest characteristics to the line where the cusp moves. In particular we observe that the characteristic emanating from the nearest grid point to the left of the line $\sigma_0 + st$, propagates away from the cusp singularity. Therefore the value $(u_{-1}^{n+1}, F_{-1}^{n+1})$ at the next time step is updated using linear interpolation based on the solution values at grid points x_{-1}^n and x_0^n. Where x_0^n is the grid point where the cusp singularity is located

at time $t = t_n$. Therefore since the update is based on a linear interpolation, it means that $u_{-1}^n \leq s = u_0^n$ and $F_{-1}^n \leq 0 = F_0^n$. Consequently the value of our approximation $u_{\Delta x}$ is less than s for all grid points to the left of the line $\sigma_0 + st$. This argument seems to hold up to $t = 1$, but in Figure 36 (d) we observe that the numerical approximation to the left of the cusp singularity has exceeded the value s.

Consider the characteristic emanating from grid point x_1^0, just to the right of where the cusp is located. This characteristic tends closer to the cusp singularity during a single time step Δt. Therefore (u_1^1, F_1^1) is updated using linear interpolation based on the value of the solution at grid points x_1^0 and x_2^0. F is a monotonically increasing function in space, therefore $F_2^n \geq F_1^n$ for all $n \in \mathbb{N} \cup \{0\}$. As we update F_1^1 using linear interpolation based on the value of F_1^0 and F_2^0, it means that the new value of F along $x_1(t) = x_1 + st$ increases. Since $F(x_1(t), t)$ increases $u(x_1(t), t)$ increases as well. This is due to

$$u(x_1(t + \Delta t), t + \Delta t) = u(x_1(t), t) + \frac{t}{2} F(x_1(t), t).$$

Therefore unfortunately after some time the value of u along $x_1(t)$ exceeds s. Once this happens, $x_1(t)$ is the new location where the solution is the largest. Assume this happens at $t = t_n$. Then the characteristic emanating from the grid point just to the right of x_1^n, i.e., x_2^n will move towards x_1^{n+1}. Therefore the value (u_2^{n+1}, F_2^{n+1}) is updated based on the value of the solution at grid points x_2^n and x_3^n. Again since F is monotonically increasing, $F_2^n \leq F_3^n$ and therefore the same occurs, but this time with the solution along $x_2(t)$. After some time the numerical solution attains its largest value along $x_2(t)$. This pattern is repeated. This will accumulate forward, the larger the simulation time T, the longer this accumulates, and the maximum value $u_{\Delta x}$ attains increases. Hence the part of u to the right of the cusp singularity will be shifted upwards compared to the true cuspon as shown in Figure 36 (c) and (d), and this discrepancy will become larger as T is increased.
A similar explanation can be given in the case where $a > 0$, but in this case the cusp singularity is where the smallest value is attained. Therefore the movement of characteristics will be opposite of that just considered, and we will have a shift downwards of $u_{\Delta x}$ compared to the true solution.

7.6 Application of algorithm to stumpons

As a final application of the algorithm we consider the solution in Example 4.2, but with $\alpha = \beta$, which corresponds to having initial data on the following form

$$u_0(x) = \begin{cases} s + \alpha(\eta - x)^{\frac{2}{3}} & \text{for } x < \eta \\ s & \text{for } \eta \leq x \leq \gamma \\ s + \alpha(x - \gamma)^{\frac{2}{3}} & \text{for } \gamma < x \end{cases},$$

for some real-valued scalars $\eta < \gamma$. We choose the first gluing point located at $x = \eta$ as reference point for the energy. The measure μ is purely absolutely continuous therefore we find the initial cumulative energy

$$F_0(x) = \begin{cases} -\frac{4}{3}\alpha^2(\eta - x)^{\frac{1}{3}} & \text{for } x < \eta \\ 0 & \text{for } \eta \leq x \leq \gamma \\ \frac{4}{3}\alpha^2(x - \gamma)^{\frac{1}{3}} & \text{for } \gamma < x \end{cases}.$$

.
The analytical solution is given by

$$u(x,t) = \begin{cases} s + \alpha(st + \eta - x)^{\frac{2}{3}} & \text{for } x < st + \eta \\ s & \text{for } \eta + st \leq x \leq \gamma + st \\ s + \alpha(x - st - \gamma)^{\frac{2}{3}} & \text{for } \gamma + st < x \end{cases}. \tag{7.16}$$

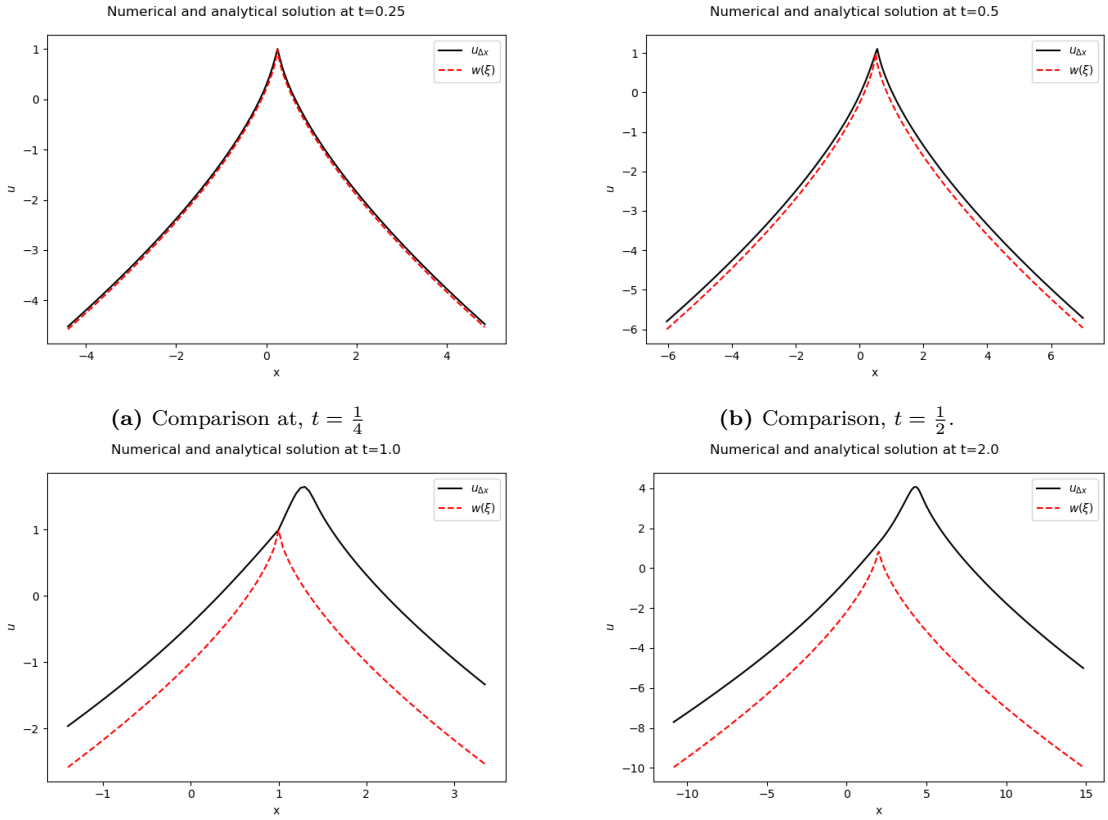

(a) Comparison at, $t = \frac{1}{4}$

(b) Comparison, $t = \frac{1}{2}$.

(c) Comparison, $t = 1$.

(d) Comparison at, $t = 2$.

Figure 36: A comparison of the numerical approximation $u_{\Delta x}$ to the cuspon solution with $a = -2$ and $s = 1$, for $t = \frac{1}{4}$ in (a), $t = \frac{1}{2}$ in (b), $t = 1$ in (c) and finally at $t = 2$ in (d).

We know by our analysis in Section 5 that this is only a weak traveling wave and not a conservative traveling wave. In particular the condition (4.12) in Lemma 4.1 is satisfied as the spatial derivative is unbounded at both gluing points $\eta + st$ and $\gamma + st$, and u is equal to s at the gluing points. However we glue together an increasing part to a constant segment at $x = \eta$ for $\alpha < 0$, and the same constant segment to a decreasing part at $x = \gamma$, so by our proof of Theorem 5.1 this cannot be a conservative traveling wave. However we still want to apply our algorithm and see how it approximates the true solution. Somewhat arbitrarily we choose $\eta = -1$ and $\gamma = 1$, and stick with the choice of $s = 1$ and $\alpha = -2$. Comparisons between the true solution $w(\xi)$ and the numerical approximation $u_{\Delta x}$ are shown in Figure 38 at times $t = \frac{1}{4}$, $t = \frac{1}{2}$, $t = 1$ and finally $t = 2$. The plateau of the stumpon is very well approximated at all times, but even at $t = \frac{1}{2}$ we observe a peak building up at the gluing point $x = \gamma + st$, this peak becomes more and more prominent as time evolves. This resembles in some sense what we observed for the approximation of cuspons, since the part of the numerical approximation to the right of the rightmost gluing point is shifted upwards compared to the true traveling wave.

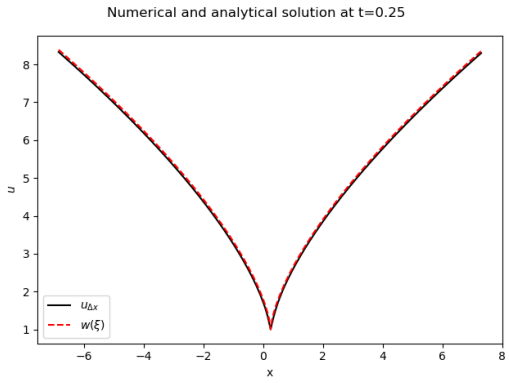

(a) Comparison at, $t = \frac{1}{4}$

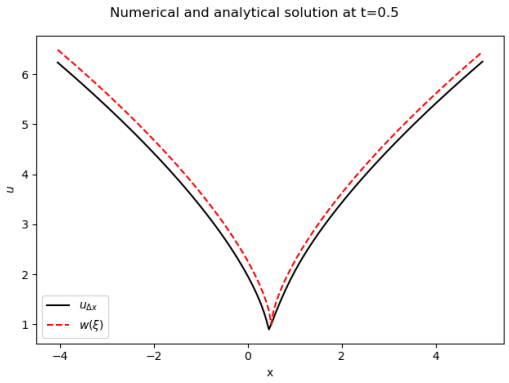

(b) Comparison, $t = \frac{1}{2}$.

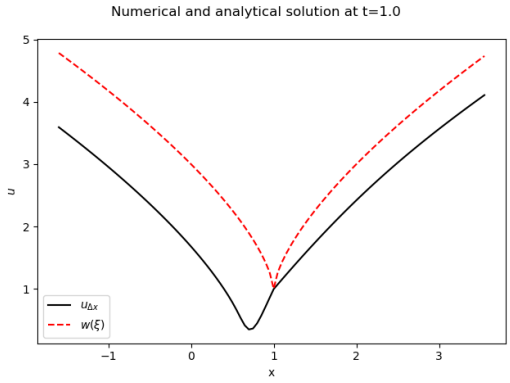

(c) Comparison, $t = 1$.

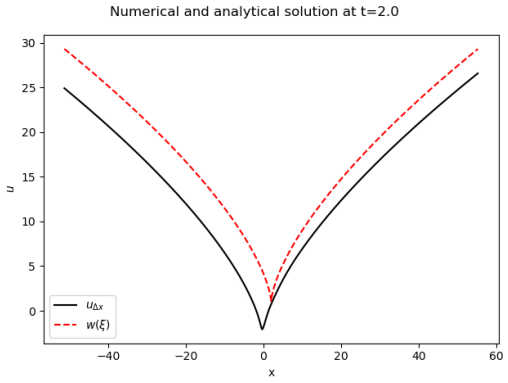

(d) Comparison at, $t = 2$.

Figure 37: A comparison of the numerical approximation $u_{\Delta x}$ to the cuspon solution with $a = 2$ and $s = 1$, for $t = \frac{1}{4}$ in (a), $t = \frac{1}{2}$ in (b), $t = 1$ in (c) and finally at $t = 2$ in (d).

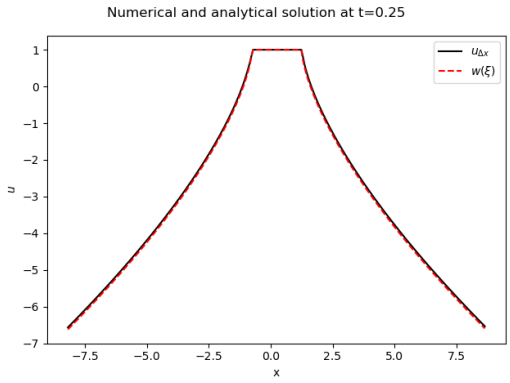

(a) Comparison at, $t = \frac{1}{4}$

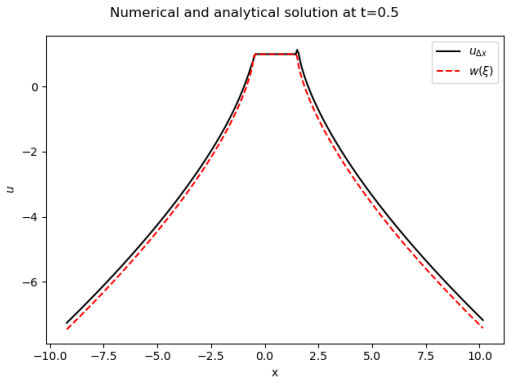

(b) Comparison, $t = \frac{1}{2}$.

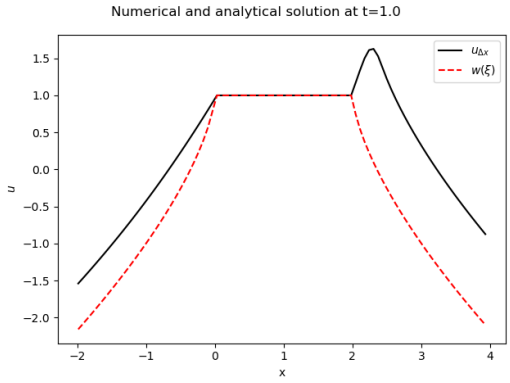

(c) Comparison, $t = 1$.

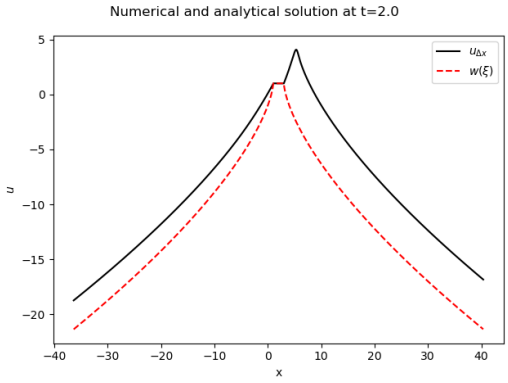

(d) Comparison at, $t = 2$.

Figure 38: A comparison of the numerical approximation $u_{\Delta x}$ to the stumpon solution with $a = -2$ and $s = 1$, for $t = \frac{1}{4}$ in (a), $t = \frac{1}{2}$ in (b), $t = 1$ in (c) and finally at $t = 2$ in (d).

8 Concluding remarks

In this thesis we have studied traveling wave solutions for the Hunter-Saxton equation (4.1). In particular we have used a gluing formalism in order to show the existence of weak traveling waves to the Hunter-Saxton equation. The gluing formalism makes it possible to glue together two local, classical traveling wave solutions provided the composite function admits at least one one-sided unbounded derivative at the gluing point. This result was proved by a Rankine-Hugoniot type argument, assuming the resulting composite wave is continuous at the gluing point and that it is a weak traveling wave solution as defined in Definition 5.1. Based on the derived conditions we could exhaust all possible weak traveling waves, and give a rough sketch of how they have to look locally around the gluing point. Among these we recognized in particular cuspons. We observed that a maximal of two gluing points is allowed, leading to stumpons. Moreover all the weak traveling waves tend asymptotically to $\pm\infty$ as $x \to \pm\infty$.

We then took the analysis one step further and augmented the differentiated Hunter-Saxton equation with an energy equation (5.1b). We applied the gluing formalism and proceeded with a Rankine-Hugoniot type argument isolated for this energy equation. This resulted in an additional requirement, which need to be satisfied for weak conservative traveling waves of the Hunter-Saxton equation. The notion of a weak conservative traveling wave was defined in Definition 5.1. By using the derived condition together with that derived for the Hunter-Saxton equation we were able to filter out cuspons as the only nontrivial, weak, conservative traveling wave solutions of (4.1). Along the way we also gave explicit examples of both weak traveling waves and conservative traveling waves to the Hunter-Saxton equation. Furthermore we discussed soliton-like solutions called multipeakons. These played a central role in the development of the numerical algorithms.

Then we proceeded by analyzing the cuspons in more detail. In particular we derived the Lagrangian system satisfied by cuspons, (5.18a)-(5.18c). This Lagrangian system differs quite a bit from the typical Lagrangian system met in the literature (3.18a)-(3.18c), in particular we observed that the Lagrangian cumulative energy changes with time. Based on the Lagrangian system satisfied by cuspons we were able to show that the cusp singularity jumps from characteristic to characteristic as time evolves. We also showed that wave breaking occurs at the cusp singularity at every time, and that wave breaking occurs at a single point in Eulerian coordinates, and initially a single point in Lagrangian coordinates. Then we gave a plausible intuitive physical explanation to why the other weak traveling waves involving a single gluing point, do not classify as conservative traveling waves.

Next we considered an already existing algorithm for conservative solutions of the Hunter-Saxton equation. We saw that the main obstacles in applying this algorithm in the setting of conservative traveling waves is that it relies on the assumption that the initial measure is compactly supported, and also uses a quantity F_∞ which is infinite for cuspons. To overcome these obstacles we introduced a modified algorithm based on the existing algorithm, but now formulated for the differentiated form of the Hunter-Saxton equation. In particular we adapted a moving reference frame, in order to simulate cuspons. We observed that choosing a moving reference frame lead to some changes. In particular we had to modify the CFL-condition and Godunov-expression, but also due to the introduction of fictitious boundaries we had to remove certain grid points as we evolved the solution along characteristics.

The resulting algorithm was applied to cuspon initial data, where numerical experiments indicate that it at least captures the spatial asymptotic behaviour of cuspons, and gives a reasonable wave profile resembling the true cuspon. Unfortunately the discrepancy between the numerical approximation and the true cuspon grows with increasing simulation time T. The algorithm was also applied to a stumpon example, even though this is not a conservative traveling wave. The initial approximation was reasonable good, but the numerical approximation and the true stumpon started to differ more and more as we increased the simulation time.

It is possible that one may overcome the met difficulties and drawbacks of the modified algorithm if one instead chooses the Lagrangian cumulative energy in such a way that

$$H_t = k,$$

just as we observed for the true cuspon solution in Subsection 5.3. However with such a choice, the interpretation of H would in some sense become blurred, as we would no longer have the natural interpretation of $H(\xi, t)$ being the energy from a chosen reference point up to the characteristic $X(\xi, t)$. The natural interpretation of the other Lagrangian coordinates would also be altered. This would be a natural future starting point, to see if one could overcome the discrepancies observed.

Moreover it would be of interest to perform numerical experiments that could either validate or invalidate the physical explanation we gave to why the other weak traveling waves are not conservative. It would be of interest to see if one observes such rarefaction-like spreading or shock-like gathering of the characteristics around the line where the gluing point moves, in the case the gluing point is a point of inflection. Another topic of interest is that of dissipative traveling wave solutions to the Hunter-Saxton equation. This topic is more intricate, as we want a traveling wave to preserve its form while it translates either to the right or to the left in one spatial dimension. A dissipative solution dissipates away energy, so one would like the energy to decay, while the wave form is still preserved. It could be of interest to apply an algorithm for dissipative solutions, and see if any of the sketched weak traveling waves classify as a candidate for dissipative weak traveling waves.

References

[Aur15] Peder Aursand. "Numerical Solution of the dynamics of director fields in nematic liquid crystals". PhD thesis. Norwegian University of Science and Technology, 2015, pp. 1–53.

[Bal17] J. M. Ball. "Mathematics and liquid crystals". In: *Molecular Crystals and Liquid Crystals* 647.1 (Apr. 2017), pp. 1–27. ISSN: 1563-5287. DOI: 10.1080/15421406.2017.1289425. URL: http://dx.doi.org/10.1080/15421406.2017.1289425.

[BC05] Alberto Bressan and Adrian Constantin. "Global solutions of the Hunter-Saxton equation". In: *SIAM J. Math. Anal.* 37.3 (2005), pp. 996–1026. ISSN: 0036-1410. DOI: 10.1137/050623036. URL: https://doi.org/10.1137/050623036.

[BHR10] Alberto Bressan, Helge Holden, and Xavier Raynaud. "Lipschitz metric for the Hunter-Saxton equation". In: *J. Math. Pures Appl. (9)* 94.1 (2010), pp. 68–92. ISSN: 0021-7824. DOI: 10.1016/j.matpur.2010.02.005. URL: https://doi.org/10.1016/j.matpur.2010.02.005.

[Bre16] Alberto Bressan. "Uniqueness of conservative solutions for nonlinear wave equations via characteristics". In: *Bull. Braz. Math. Soc. (N.S.)* 47.1 (2016), pp. 157–169. ISSN: 1678-7544. DOI: 10.1007/s00574-016-0129-y. URL: https://doi.org/10.1007/s00574-016-0129-y.

[CGH19] José Antonio Carrillo, Katrin Grunert, and Helge Holden. "A Lipschitz metric for the Hunter-Saxton equation". In: *Comm. Partial Differential Equations* 44.4 (2019), pp. 309–334. ISSN: 0360-5302. DOI: 10.1080/03605302.2018.1547744. URL: https://doi.org/10.1080/03605302.2018.1547744.

[Daf11] Constantine M. Dafermos. "Generalized characteristics and the Hunter-Saxton equation". In: *J. Hyperbolic Differ. Equ.* 8.1 (2011), pp. 159–168. ISSN: 0219-8916. DOI: 10.1142/S0219891611002366. URL: https://doi.org/10.1142/S0219891611002366.

[DP98] Hui-Hui Dai and Maxim Pavlov. "Transformations for the Camassa-Holm equation, its high-frequency limit and the Sinh-Gordon equation". In: *J. Phys. Soc. Japan* 67.11 (1998), pp. 3655–3657. ISSN: 0031-9015. DOI: 10.1143/JPSJ.67.3655. URL: https://doi.org/10.1143/JPSJ.67.3655.

[GHR15] Katrin Grunert, Helge Holden, and Xavier Raynaud. "A continuous interpolation between conservative and dissipative solutions for the two-component Camassa-Holm system". In: *Forum Math. Sigma* 3 (2015), Paper No. e1, 73. DOI: 10.1017/fms.2014.29. URL: https://doi.org/10.1017/fms.2014.29.

[GN18] Katrin Grunert and Anders Nordli. "Existence and Lipschitz stability for α-dissipative solutions of the two-component Hunter-Saxton system". In: *J. Hyperbolic Differ. Equ.* 15.3 (2018), pp. 559–597. ISSN: 0219-8916. DOI: 10.1142/S0219891618500182. URL: https://doi.org/10.1142/S0219891618500182.

[GNS21] Katrin Grunert, Anders Nordli, and Susanne Solem. "Numerical conservative solutions of the Hunter–Saxton equation". In: *BIT Numerical Mathematics* 61.2 (Jan. 2021), pp. 441–471. ISSN: 1572-9125. DOI: 10.1007/s10543-020-00835-y. URL: http://dx.doi.org/10.1007/s10543-020-00835-y.

[GR20] Katrin Grunert and Audun Reigstad. *Traveling Waves for the Nonlinear Variational Wave Equation*. 2020. arXiv: 2009.03178 [math.AP].

[Gru16] Katrin Grunert. "Solutions of the Camassa-Holm equation with accumulating breaking times". In: *Dyn. Partial Differ. Equ.* 13.2 (2016), pp. 91–105. ISSN: 1548-159X. DOI: 10.4310/DPDE.2016.v13.n2.a1. URL: https://doi.org/10.4310/DPDE.2016.v13.n2.a1.

[GSP14] Herbert Goldstein, John L. Safko, and Charles P. Poole. *Classical Mechanics*. Vol. 3. Pearson. Pearson, 2014, pp. 34–70. ISBN: 1292026553.

[HP18] Matthias Hieber and Jan W. Prüss. "Modeling and analysis of the Ericksen-Leslie equations for nematic liquid crystal flows". In: *Handbook of mathematical analysis in mechanics of viscous fluids*. Ed. by Yoshikazu Giga and Antonín Novotný. Springer, Cham, 2018, pp. 1075–1134. DOI: https://doi.org/10.1007/978-3-319-13344-7.

[HR07] Helge Holden and Xavier Raynaud. "Global conservative solutions of the Camassa-Holm equation—a Lagrangian point of view". In: *Comm. Partial Differential Equations* 32.10-12 (2007), pp. 1511–1549. ISSN: 0360-5302. DOI: 10.1080/03605300601088674. URL: https://doi.org/10.1080/03605300601088674.

[HR15] Helge Holden and Nils Henrik Risebro. *Front tracking for hyperbolic conservation laws*. Second. Vol. 152. Applied Mathematical Sciences. Springer, Heidelberg, 2015, pp. xiv+515. ISBN: 978-3-662-47507-2. DOI: 10.1007/978-3-662-47507-2. URL: https://doi.org/10.1007/978-3-662-47507-2.

[HS91] John K. Hunter and Ralph Saxton. "Dynamics of director fields". In: *SIAM J. Appl. Math.* 51.6 (1991), pp. 1498–1521. ISSN: 0036-1399. DOI: 10.1137/0151075. URL: https://doi.org/10.1137/0151075.

[HZ94] John K. Hunter and Yu Xi Zheng. "On a completely integrable nonlinear hyperbolic variational equation". In: *Phys. D* 79.2-4 (1994), pp. 361–386. ISSN: 0167-2789. DOI: 10.1016/0167-2789(94)90093-0. URL: https://doi.org/10.1016/0167-2789(94)90093-0.

[HZ95] John K. Hunter and Yu Xi Zheng. "On a nonlinear hyperbolic variational equation. I. Global existence of weak solutions". In: *Arch. Rational Mech. Anal.* 129.4 (1995), pp. 305–353. ISSN: 0003-9527. DOI: 10.1007/BF00379259. URL: https://doi.org/10.1007/BF00379259.

[La 15] Arnaud de La Fortelle. "A study on generalized inverses and increasing functions Part I: generalized inverses". In: (2015), pp. 1–14. DOI: 10.13140/RG.2.1.3020.2082. URL: https://hal-mines-paristech.archives-ouvertes.fr/hal-01255512.

[Len05] Jonatan Lenells. "Traveling wave solutions of the Camassa-Holm equation". In: *J. Differential Equations* 217.2 (2005), pp. 393–430. ISSN: 0022-0396. DOI: 10.1016/j.jde.2004.09.007. URL: https://doi.org/10.1016/j.jde.2004.09.007.

[Len09] Jonatan Lenells. "Periodic solitons of an equation for short capillary-gravity waves". In: *J. Math. Anal. Appl.* 352.2 (2009), pp. 964–966. ISSN: 0022-247X. DOI: 10.1016/j.jmaa.2008.09.070. URL: https://doi.org/10.1016/j.jmaa.2008.09.070.

[Les92] F. M. Leslie. "Continuum theory for nematic liquid crystals". In: *Continuum Mech. Thermodyn* 4 (3 1992), pp. 167–175. ISSN: 1432-0959. DOI: 10.1007/BF01130288. URL: https://doi.org/10.1007/BF01130288.

[LeV02] Randall J. LeVeque. *Finite volume methods for hyperbolic problems*. Cambridge Texts in Applied Mathematics. Cambridge University Press, Cambridge, 2002, pp. xx+558. ISBN: 9780511791253. DOI: 10.1017/CBO9780511791253. URL: https://doi.org/10.1017/CBO9780511791253.

[LL09] J. Lenells and O. Lechtenfeld. "On the N=2 supersymmetric Camassa–Holm and Hunter–Saxton equations". In: *Journal of Mathematical Physics* 50.1 (Jan. 2009), p. 012704. ISSN: 1089-7658. DOI: 10.1063/1.3060125. URL: http://dx.doi.org/10.1063/1.3060125.

[Mar06] Rubens M Marinho. "Noether's theorem in classical mechanics revisited". In: *European Journal of Physics* 28.1 (Oct. 2006), pp. 37–43. DOI: 10.1088/0143-0807/28/1/004. URL: https://doi.org/10.1088/0143-0807/28/1/004.

[Nor16a] Anders Nordli. "A Lipschitz metric for conservative solutions of the two-component Hunter-Saxton system". In: *Methods Appl. Anal.* 23.3 (2016), pp. 215–232. ISSN: 1073-2772. DOI: 10.4310/MAA.2016.v23.n3.a1. URL: https://doi.org/10.4310/MAA.2016.v23.n3.a1.

[Nor16b] Anders Nordli. “On the two-component Hunter–Saxton system”. PhD thesis. Norwegian University of Science and Technology, 2016.

[Ste14] Iain W. Stewart. *Continuum Theory for Liquid Crystals*. "https://strathprints.strath.ac.uk/50654/1/Stewart_Wiley_2015_Continuum_theory_for_liquid.pdf". "Last accessed 2021-05-30. 2014.

[WXL13] Hao Wu, Xiang Xu, and Chun Liu. “On the general Ericksen-Leslie system: Parodi’s relation, well-posedness and stability”. In: *Arch. Ration. Mech. Anal.* 208.1 (2013), pp. 59–107. ISSN: 0003-9527. DOI: 10.1007/s00205-012-0588-2. URL: https://doi.org/10.1007/s00205-012-0588-2.

[ZZ00] Ping Zhang and Yuxi Zheng. “Existence and uniqueness of solutions of an asymptotic equation arising from a variational wave equation with general data”. In: *Arch. Ration. Mech. Anal.* 155.1 (2000), pp. 49–83. ISSN: 0003-9527. DOI: 10.1007/s205-000-8002-2. URL: https://doi.org/10.1007/s205-000-8002-2.

A Appendices

A.1 Python Code - Numerical algorithm for integrated formulation

```
def evolve_data(u0, F0, xl, xr, dx, T, alph):
    """
        The function takes the initial data, and evolves the conservative solution
        up to time T. The algorithm is based on the integrated formulation
        of the Hunter-Saxton equation and the resulting Lagrangian system

        Arguments:
            u0 (array)-> initial value for u
            F0 (array)-> initial value for F
            xl (float)-> left part of computational domain
            xr (float)-> right part of computational domain
            dx (float)-> space step
            T (float)-> final simulation time
            alph (float)-> Between 0 and 1, multiplication factor for CFL-condition
        Returns:
            t (time list), x (list of gridpoint), u (solution at time T)
            F ( cumulative energy distribution at time T)
    """
    x = np.arange(start=xl, stop=xr, step=dx)
    u = u0
    F = F0
    E = F[-1]  # Total energy
    # Time step which satisfied the CFL-type condition

    dt = alph * (dx / (4 * (max(u) + 1/8 * T * E)))
    N = int(T/dt)

    t_arr = np.arange(start=0, stop=T, step=dt)

    # Start the time evolution
    for n in range(N):
       # Temporary arrays used to update to the next time step
       temp_u = np.zeros(len(u))
       temp_F = np.zeros(len(F))

       for k in range(len(x)):
           if u[k] + 0.25 * (F[k] - 0.5*E) * dt > 0:
               # Characteristic move to the right
                if k == 0:  # Missing the grid point (k-1),
                   # Assume the solution is constant outside some bounded interval [a(t), b(t)]
                   temp_u[k] = u[k+1]
                   temp_F[k] = F[k+1]
                else:
                   z = (dx - u[k-1]*dt - \
                                   0.25* (dt**2) * (F[k-1] - 0.5*E))/ (dx + \
                                   (u[k]-u[k-1])*dt + 0.25*(F[k]-F[k-1])*(dt**2))
                   temp_u[k] = u[k-1] + 0.5*(F[k-1] - 0.5*E)*dt + \
                       z * (u[k] - u[k-1] + (dt/2) *(F[k]-F[k-1]))
                   temp_F[k] = F[k-1] + z * (F[k]-F[k-1])
           elif u[k] + 0.25 * (F[k]-0.5*E) * dt < 0:
               # Characteristic move to the left
               if k == len(x)-1:
                   temp_u[k] = u[k-1]
```

```
                    temp_F[k] = F[k-1]
                else:
                    z = (dx + u[k+1]*dt + \
                         0.25 * (dt**2) * (F[k+1]-0.5*E))/(dx + \
                               (u[k+1]-u[k])*dt + 0.25 * (F[k+1]-F[k])*(dt**2))
                    temp_u[k] = u[k+1] + 0.5 *(F[k+1] - 0.5*E)*dt - \
                        z*(u[k+1]-u[k] + (dt/2)*(F[k+1]-F[k]))
                    temp_F[k] = F[k+1] - z * (F[k+1]-F[k])
            else:
                # Characteristic travel vertically aong x = x_k
                 temp_u[k] = u[k]
                 temp_F[k] = F[k]
        u = temp_u.copy()
        F = temp_F.copy()
    return t_arr, x, u, F
```

A.2 Python Code - Numerical algorithm moving reference frame

```
def evolve_data_moving(u0, F0, xl, xr, dx, T, s, a):
    """
        Evolve the initial data up to the solution at time t=T,
        uses a moving reference frame. The algorithm is based on the lagrangian
        system for the differentiated form of the Hunter-Saxton equation, and
        assume the initial data is a conservative traveling wave

    Arguments:
            u0 (array)-> initial value for u
            F0 (array)-> initial value for F
            xl (float)-> left part of computational domain
            xr (float)-> right part of computational domain
            dx (float)-> step size
            T (float)-> final simulation time
            s (float) -> wave speed
            a (float) -> slope of wave profile
        Returns:
            t (time list), x (list of gridpoint that are translated up till T),
            u (solution at time T), F ( cumulative energy distribution at time T)
    """
    x = np.arange(start=xl, stop=xr, step=dx)
    # Initialize the numerical solution
    u = u0
    F = F0
    # Calculate the total cumulative energy
    E = (4/3)* a**2 * ((-xl)**(1/3) + xr**(1/3))
    # Time step which satisfies the CFL-condition
    dt = (dx / (2*(max(abs(u)) + 1/4 * T * E + abs(s))))

    t_arr = np.arange(start=0, stop=T, step=dt)
    N = int(T/dt)

    # Variable keeping count of how many indices which are removed on one side
    indices_rem = 0
    # The grid which we will move forward as we evolve time
    grid = x.copy()

    for n in range(N):
```

```
            # Temporary arrays used to update to the next time step
            temp_u = np.zeros(len(u))
            temp_F = np.zeros(len(F))
            grid = grid + s*dt  # Move the grid points
            # Have not removed indices for the time step yet
            index_removed_step = False
            for k in range(indices_rem, len(x)-indices_rem):
                if u[k] + (dt/4) *F[k] - s > 0:
                    if k == indices_rem and index_removed_step == False:
                        # Missing the grid point (k-1), will remove
                         indices_rem += 1
                         index_removed_step = True
                         temp_u[k] = u[k]
                         temp_F[k] = F[k]
                    else:
                        z = (dx +s*dt - u[k-1]*dt - 0.25 * F[k-1]*(dt**2)) / (dx + \
                                  (u[k] - u[k-1])*dt + 0.25 * (F[k] - F[k-1])*(dt**2))
                        temp_u[k] = u[k-1] + (dt/2) * F[k-1] + \
                            z*(u[k] - u[k-1] + (dt/2) * (F[k] - F[k-1]))
                        temp_F[k] = F[k-1] + z* (F[k] - F[k-1])

                elif u[k] + (dt/4) * F[k] - s < 0:

                    if k == len(x)-1 - indices_rem and index_removed_step == False:
                         indices_rem += 1
                         temp_u[k] = u[k]
                         temp_F[k] = F[k]
                    else:
                        z = (-s*dt + dx + u[k+1]*dt + (dt**2) * 0.25 * F[k+1]) / (dx + \
                                     (u[k+1] - u[k])*dt + 0.25 * (F[k+1] - F[k])*(dt**2))
                        temp_u[k] = u[k+1] + (dt/2)*F[k+1] - \
                            z * (u[k+1] - u[k] + (dt/2) * (F[k+1] - F[k]))
                        temp_F[k] = F[k+1] - z * (F[k+1] - F[k])
                else:
                      temp_u[k] = u[k]
                      temp_F[k] = F[k]
            u = temp_u.copy()
            F = temp_F.copy()
    if len(u) == 0:
        raise ValueError("The initial computational domain is too small, so the final \
                          computational domain is empty")
    else:
        print(f"A total of {2*indices_rem} grid points have been removed.")
        return t_arr, grid, u, F
```